Synthesis of Functionalized Sustainable Polyesters via Controlled Ring-opening Polymerization of *O*-carboxyanhydrides

Xiaoqian Wang

Dissertation submitted to the faculty of the Virginia Polytechnic Institute and State University in partial fulfillment of the requirements for the degree of

Doctor of Philosophy
In
Chemical Engineering

Rong Tong
Chang Lu
Guoliang (Greg) Liu
Aaron S Goldstein

November 29, 2022
Blacksburg, Virginia

Ring-opening polymerization, *O*-carboxyanhydrides, organometallic catalysts, functionalized polyesters, degradation

Synthesis of Functionalized Sustainable Polyesters via Controlled Ring-opening Polymerization of *O*-carboxyanhydrides

Xiaoqian Wang

ABSTRACT

Despite the degradability and biocompatibility of poly(α-hydroxy acids), their utility remains limited because their thermal and mechanical properties are inferior to those of commodity polyolefins, which can be attributed to the lack of side-chain functionality on the polyester backbone. Attempts to synthesize high-molecular-weight functionalized poly(α-hydroxy acids) from *O*-carboxyanhydrides have been hampered by scalability problems arising from the need for an external energy source such as light or electricity. Herein, an operationally simple, scalable method for synthesizing stereoregular, high-molecular-weight (>200 kDa) functionalized polyesters have been developed by means of controlled ring-opening polymerization of *O*-carboxyanhydrides mediated by a highly redox reactive manganese complex and a zinc-alkoxide. Mechanistic studies indicated that the ring-opening process proceeded via the Mn-mediated decarboxylation with alkoxy radical formation (Chapter 2). In addition to the polymerization, a two-step facile chemical recycling strategy for poly(α-hydroxy acids) was developed to achieve closed-loop life cycles (Chapter 3). Moreover, this synthetic strategy is not limited to preparing homopolymers and block copolymers but also to producing stereoblock and gradient copolymers (Chapter 4). In particular, the gradient copolymers exhibited better ductility and toughness than their corresponding homopolymers and block copolymers, highlighting the potential feasibility of

functionalized polyesters as strong and resilient polymeric materials (Chapter 5). Next, an atom-economical, scalable method for block copolymerization of *O*-carboxyanhydrides and epoxides to prepare functionalized poly(ester-*b*-carbonates) with high molecular weights (>200 kDa) was identified, that uses a single Lewis acidic zinc complex at room temperature in the absence of pressurized CO_2 (Chapter 6). Kinetic studies showed that the first stage of the process, ring-opening polymerization of the *O*-carboxyanhydrides, exhibited zero-order kinetics, suggesting that the polymerization rate was independent of monomer concentration, thus allowing for a sharp switch in mechanism without a tapering effect (Chapter 7). The obtained poly(ester-*b*-carbonates) showed better toughness than their corresponding homopolymers and outperformed some commodity polyolefins (Chapter 8). Exploring this new chemical space of poly(ester-*b*-carbonates) via stereosequence-controlled synthetic methods would be a critical step toward improving this promising class of functionalized sustainable polymers (Chapter 9).

Synthesis of Functionalized Sustainable Polyesters via Controlled Ring-opening Polymerization of *O*-carboxyanhydrides

Xiaoqian Wang

GENERAL AUDIENCE ABSTRACT

Poly(α-hydroxy acids) is an environmentally friendly alternative to petrochemical polyolefins due to their excellent degradability and biocompatibility. However, it is difficult to synthesize high-molecular-weight functionalized polyesters on a large scale due to the inefficient catalysts and the need for external energy, such as light and electricity. Herein, a highly reactive Mn/Zn catalytic system for controllable *O*-carboxyanhydrides (OCAs) polymerization has been designed. Compared with the previously reported catalytic system, this method can be used to produce low-cost, large-scale preparation of high molecular weight (>200 kDa) polyesters without the need for external energy sources (Chapter 2). In addition, our synthesized polyesters can be completely degraded under mild conditions, thereby achieving a circular economy in the polyester industry (Chapter 3). More importantly, our operationally simple synthetic method could afford polyesters with different compositions, such as homopolymers, block copolymers, stereoblock copolymers, and gradient copolymers (Chapter 4). In particular, the obtained gradient copolymer is tough and ductile that could compete with commercial polyolefins in terms of mechanical and thermal properties, such as low-density polyethylene (LDPE) (Chapter 5). Next, we developed a single Lewis acidic zinc complex to achieve the copolymerization of OCA and epoxide to synthesize poly(ester-*b*-carbonates), which enriches the class of degradable polymers (Chapter 6). Moreover, this copolymerization showed unique reaction kinetics that enabled the perfectly clean

switching of the polymerization mechanism during chain propagation (Chapter 7). The obtained poly(ester-*b*-carbonates) showed better toughness than their corresponding homopolymers and outperformed some non-degradable plastics (Chapter 8). The exploration of novel degradable polymers by sequence-controlled polymerization to replace non-degradable polyolefin on the market will continue in the near future (Chapter 9).

ACKNOWLEDGEMENTS

I want to start by sincerely thanking my advisor, Dr. Rong Tong, for his invaluable patience and continuous support. He has always provided many valuable suggestions when I encountered difficulties, he made sure that I'm being supported through each step of the way and to regain myself worth and confidence. I feel extremely fortunate to be part of his lab, I could not have imagined having a better advisor and mentor for my Ph.D. study.

Besides my advisor, I would also like to show gratitude to my committee members, including Dr. Chang Lu, Dr. Guoliang Liu, and Dr. Aaron S Goldstein for their encouragement and insightful comments.

I am also grateful to my friends, Ai Lin Chin, Xue Han, and Yunfei Mao, who are always by my side to cheer me up when I break down emotionally. I absolutely appreciate my meal pals, Yan Liu, Xiangrui Wang, Tianyou Mou, Yuanqi Liu, Zechen Zhang, Bohan Zhu, Xiaoyu Xie, Ziyu Huo, Liping Liu, and Lin Liao. I would also like to thank all current and past members of our laboratory for teaching basic experiments and for their valuable friendship.

Most importantly, none of this would happen without my family - my parents, grandma, and sister. Their support has kept my spirits and motivation high during this process. To my nephew and niece – every word you say about loving me is the greatest support I have ever received.

We will all have bright futures, in various ways.

Table of contents

List of Abbreviations

^{13}C NMR	carbon nuclear magnetic resonance
^{1}H NMR	proton nuclear magnetic resonance
σ	fracture strength
ε	fracture strain
BDI	β-diiminate ligands
b	block
BnOH	benzyl alcohol
Conv.	monomer conversion
CHO	cyclohexene oxide
CV	cyclic voltammetry
DOSY	diffusion ordered spectroscopy
Đ	molecular weight distributio
DP	degree of polymerization
DMAP	4-dimethylaminopyridine
DSC	differential scanning calorimetry
DMA	dynamic mechanical analysis
ESI-MS	Electrospray ionization-mass spectrometry
FR	feeding ratio
GPC	gel permeation chromatography
grad	gradient
HMDS	hexamethyldisilazane

HPLC	high-performance liquid chromatography
ICP-MS	inductively coupled plasma mass spectrometry
LA	lactic acid
LDPE	low-density polyethylene
MALDI-MS	matrix-assisted laser desorption/ionization mass spectrum
MW	molecular weight
MW_{cal}	calcluted molecular weight
*M*n	number-average molecular weight
*M*w	weight-average molecular weight
OCAs	*O*-carboxyanhydride(s)
PAHA	poly(α-hydroxy acids)
PLA	poly(lactide acid)
*P*m	probability of *meso* dyad formation
rac	racemic
r	random
ROP	ring-opening polymerization
ROCOP	ring-opening copolymerization
sb	stereoblock
THF	tetrahydrofuran
T_g	glass transition temperature
T_m	melting temperature
TBD	1,5,7-triazabicyclo[4.4.0]dec-5-ene
VCHO	vinyl cyclohexene oxide

CHAPTER 1

Introduction

1.1 Background

Plastic straw lodged in a turtle's throat? Fish trapped in six-pack rings, devoid of freedom and suffocating? Or seagulls found dead on beaches with plastic remnants in their guts? These horrifying images are increasingly prevalent in the media as a consequence of the ever-growing demand for plastic products. [1-3] According to the statistics, more than 300 million metric tons of plastic waste was produced each year, with 4.8 to 12.7 million metric tons going into the ocean and significantly impacting the marine ecosystem;[4] In addition, the landfill disposal of the non-degradable plastic waste would also cause severe environmental consequences as the accumulated waste can persist in ecosystems for hundreds of years. This large-scale production and the environmental consequences linked with the disposal indicate that the earth has reached the limits of our current linear economic model of "take, make, use, and disposal" of resource utilization (**Figure 1.1**). Therefore, considerable research efforts have been devoted to the search for sustainable alternatives to be transformed into commodity plastics.[5-8]

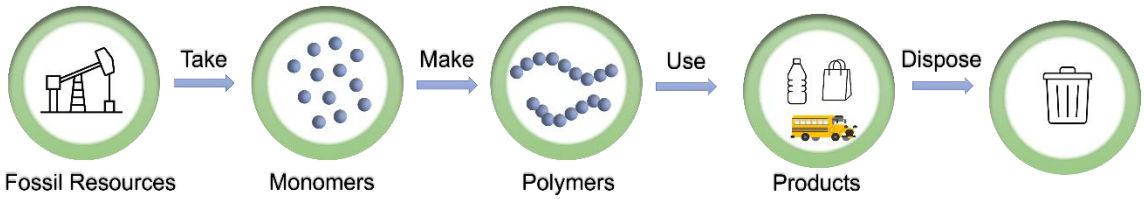

Figure 1.1 Linear material economy frameworks.

Recently, researchers redefined sustainable polymers as "polymers made from renewable sources that are harmless during production and use and may be recycled or disposed of without harming the environment." [9] or "a category of polymers with closed-loop life cycles generated from renewable sources" [4]. The one-way linear framework fails to handle the end-of-life challenges of polymers, not only quickly depletes limited natural resources but also suffers from significant economic loss and produces a serious worldwide environmental impact due to the worsening of plastic pollution. In contrast, the development of sustainable polymers with a closed-loop life cycle offers promising potential to address these serious issues. In the circular economy framework (**Figure 1.2**), research has concentrated not only on the end-of-life options that yield recyclable materials but also on the replacement of fossil raw materials with renewable alternatives, such as biomass from plants.[4, 10]

However, even though the idea of replacing petrochemical-based polymers with renewable and degradable alternatives was pitched in the late 20th century, efforts are still ongoing to improve on current methodologies, to search for sustainable options, and to ultimately generate variants with a simpler strategy that can increase the yield, and reduce the waste. [11-13]

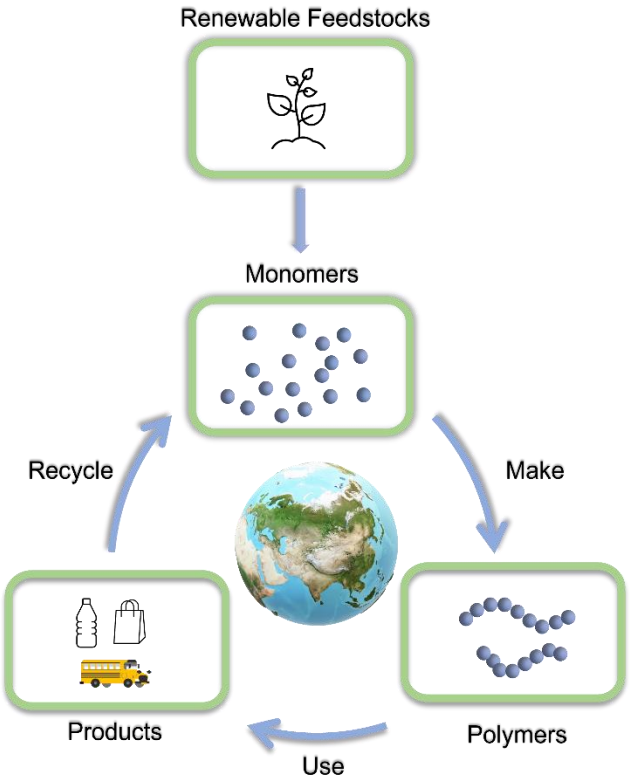

Figure 1.2 The circular material economy framework based on the sustainable polymers with full chemical recyclability.

1.2 Poly(α-hydroxy acids)

Among potential sustainable polymers, poly(α-hydroxy acids) (PAHAs) have been long regarded as a type of industry-applicable, degradable, and biocompatible polymer to replace petrochemical-based polyolefins,[14-16] because they are made from renewable resources, and their chemical or enzymatic degradation products are environmentally benign and can be recycled. They have been widely used in biomedical engineering and food packaging.[17, 18]

Nevertheless, the practical utility of the commercially available polyesters, including poly(α-hydroxy acids), is limited because their thermal and mechanical

properties are inferior to those of commodity non-degradable polyolefins. For example, poly(lactic acid) (PLA) and poly(3-hydroxybutyrate) are brittle and lack toughness (<5% elongation at break)[19]. Additionally, the upper-use temperatures of many aliphatic polyesters are restricted because of their moderate or low glass-transition temperatures (T_g): PLA ($T_g \approx 45$ °C), poly(3-hydroxybutyrate) ($T_g \approx 5$ °C), and polycaprolactone ($T_g \approx -60$ °C). These limitations can be attributed to the lack of functional groups on the aliphatic polyester backbone. Indeed, the incorporation of functional groups on the backbone of polyolefins can alter their processability, adhesion, miscibility, and mechanical strength (**Figure 1.3**). [20, 21]

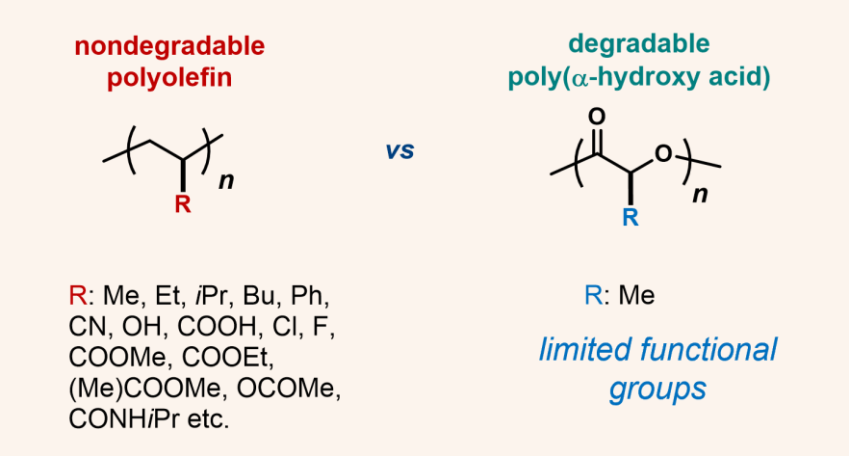

Figure 1.3 Functionalized non-degradable polyolefins and degradable poly(α-hydroxy acids), which have a limited variety of pendant functional groups.

1.2.1 The synthesis of functionalized poly(α-hydroxy acids)

In industry, PAHAs can be synthesized through polycondensation of hydroxy acid (e.g., lactic acid); however, such a method is energy-intensive because a small molecule byproduct, water, or alcohol, is removed at high temperature.[22] In addition, this polymerization usually has a broad molecular weight distribution ($Đ$) of ~2.

Unlike polycondensation, ring-opening polymerization (ROP) of monomers with various side-chain functional groups, including lactides (LAs), dioxolanone, and *O*-carboxyanhydrides (OCAs), are preferred to prepare functional PAHAs (**Figure 1.4**).[23] Among these monomers, the multistep synthesis of functionalized LAs is challenging; monomers are afforded low yields, while the polymerization reactivity significantly drops upon the introduction of pendant groups (**Figure 1.4**, route i).[24-26] These disadvantages limit the use of functionalized LAs as a viable raw material to prepare PAHAs.[26, 27]

Alternative strategies have been developed to access monomers that can be easily synthesized and polymerized. Noticeably, a five-membered heterocycle 1,3-dioxolan-4-one that bears both ester and acetal groups has been recently developed by the groups of Miller[28] and Shaver[29, 30] (**Figure 1.4**, route ii). Either through copolymerization with LAs for acetal retention or ROPs via the deliberation of formaldehyde, this monomer provides an inexpensive strategy to prepare PAHAs. However, the ROP strategy for 1,3-dioxolan-4-one requires further development as the obtained polymers have relatively low molecular weights (MWs; < 20 kDa) due to side reactions; and the ROP procedures demand constant removal of formaldehyde from the reaction solution.[29, 30]

In the quest for practicality, *O*-carboxyanhydrides (OCAs)—which are prepared from amino or hydroxy acids—are perhaps the most ubiquitous class of highly active monomers with pendant functional groups used for ROP to afford functionalized polyesters (**Figure 1.4**, route iii).[14, 31] Pioneered by Bourissou's group[32], OCAs can bear various functional groups[33, 34] (**Figure 1.4**), a promising trait that offers the manipulation of physicochemical, thermal, and mechanical characteristics to the end product. Additionally, the ROP of OCAs offers a facile route to produce PAHAs with various

pendant groups under mild conditions, a stark contrast to methods of polycondensation that entail high temperatures and harsh reaction conditions.[35, 36] The liberation of CO_2 that helps relieve ring strain enables OCA to become more reactive compared to LA.[32] Notably, the initial synthesis of OCAs involves using toxic phosgene or diphosgene. A safe alternative, bis(trichloromethyl) carbonate, has been recently developed for OCA synthesis. Often, activated charcoal and acid scavengers are incorporated to decompose excess phosgene and remove hydrochloric acid that is produced as a byproduct.[37, 38]

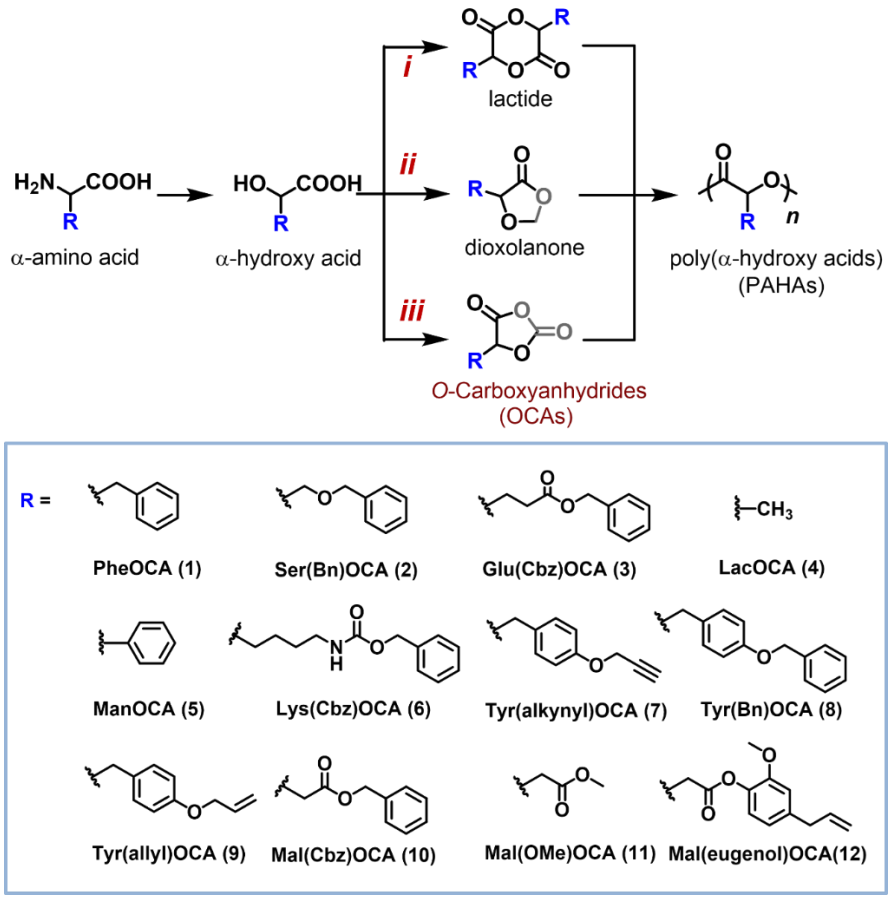

Figure 1.4 Overview of the synthesis of poly(α-hydroxy acids) (PAHAs) from α-amino acids and α-hydroxy acids via different monomer routes. Various *O*-carboxyanhydrides (OCAs) bearing pendant functional groups have been reported for the synthesis of functionalized PAHAs.

1.2.2 Catalysts for ring-opening polymerization of *O*-Carboxyanhydride (OCA)

1.2.2.1 Organocatalysts for *O*-carboxyanhydride polymerization

In 1983, the polymerization of L-LacOCA (L-**4**) was first attempted by the Kricheldorf group with less than satisfactory results.[37] Decades later, the Bourrisou group pioneered efforts towards the ROP of L-**4** and its functionalized derivatives using 4-dimethylaminopyridine (DMAP) in the presence of protic initiators (**Figure 1.5a**).[32] The polymerization of L-**4** only took 5 minutes to complete in the presence of DMAP and *neo*-pentanol at room temperature, while the same catalysts with LA monomer required at least 4 days under heating. In contrast to the noticeable drop in the reactivity of LA when pendant functionalities are introduced,[25, 39-41] OCA demonstrates relatively stable reactivity in the presence of aliphatic and aryl functional groups.

However, in 2011, the occurrence of epimerization in the ROP of L-**10** was uncovered by Pounder et al., as evidenced by the NMR studies.[42] The observed epimerized polymerization is proposed as a result of deprotonation of the acidic methine proton in **10**. Similar epimerization also occurred to the ROP of L-**2**, and L-**5**, all containing acidic α-protons.[43] Lowering the basicity of the organocatalyst was efficient in suppressing the epimerization reaction without negatively affecting the reactivity of the catalyst (**Figure 1.5d**). In 2014, the Davidson group observed that the adduct of mandelic acid and pyridine (Py·MA, **Figure 1.5b**) could allow for the preparation of isotactic poly(L-**5**).[44] Density function theory calculation suggests that the basic activation of OH moiety in MA is energetically favored via hydrogen-bonding for the ring-opening of L-**5**, compared with the pathways involving a direct nucleophilic attack by pyridine moiety.[44] Even so, it still failed to synthesize polyesters with high MWs.

In 2020, Tao, Wang and co-workers[45] described an effective unimolecular anion-binding organocatalyst where 4-(dimethylamino)pyridine was anchored to thiourea for ring-opening polymerization of L-**1** to furnish highly isotactic poly(L-**1**) with molecular weight up to 150.0 kDa (**Figure 1.5c**). This is the first time that organocatalysts have been employed to prepare high-MW PAHAs (> 100 kDa).

Nonetheless, these organocatalysts have traditionally underperformed in the ROP of OCAs: they typically exhibit low activity for the synthesis of high-MW polymers and are incapable of mediating stereoselective ROP of OCAs to produce polyesters with a range of tacticities.

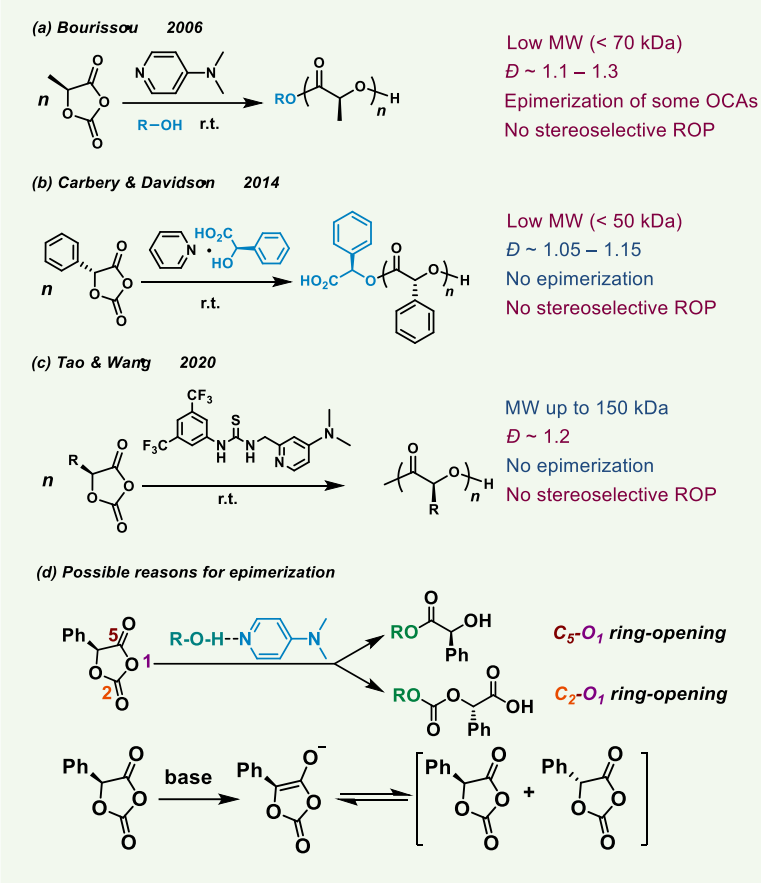

Figure 1.5 (a-c) Representative organocatalysts have been used for the ROP of OCAs, with pros and cons indicated in blue and red type, respectively. (d) The proposed mechanisms of epimerization during the ROP using organocatalysts.

1.2.2.2 Metal catalysts for *O*-carboxyanhydride polymerization

As the progress in developing an organocatalytic system for effective ROP of OCAs was slowly approaching a bottleneck, a pivotal move was made in the early 2010s to deviate towards the incorporation of organometallic catalysts in the polymerization process for elevated catalytic reactivity and improved control. Several organometallic catalysts that promote ROP of lactones or copolymerization of epoxides and CO_2 were tested for ROP of OCAs in early studies, including Sn^{II} Co^{III}, Nd^{III}, Cr^{III}, Al^{III}, Y, and La complexes.[46-49] However, the ROP of OCAs using those metal complexes cannot be achieved in a controlled manner, in which the MW of the obtained polymer is predictably linear to the monomer to catalyst feeding ratios (FRs) with a narrow *Đ*.

The first success was demonstrated by Cheng and Tong's work of using Zn complexes with β-diiminate ligands (**Zn-13)** to achieve well-controlled ROP of various OCAs (L-**1**, L-**2**, L-**4**, L-**5**, L-**7; Figure 1.6a**).[43, 50] No epimerization for poly(L-**2**) and poly(L-**5**) was observed in the homonuclear decoupled ^{1}H NMR spectra, in contrast to similar ROP performed using organocatalysts such as DMAP. **Zn-13** could also achieve one-pot block copolymerization of LAs and OCAs, regardless of the addition sequence (**Figure 1.6a**).

Additionally, as many metal complexes for ROPs of lactones are Lewis acids (e.g., Zn, Mg, and Al complexes), one emerging strategy is to pair those Lewis acids with Lewis bases to form Lewis pairs that initiate ROP via zwitterionic mode.[51-57] Recently, Yang group[58] demonstrated that a Lewis pair catalytic system (**Figure 1.6b**), a primary amine (1-hexyl-NH_2) as a Lewis base and $Zn(C_6F_5)_2$ as a Lewis acid, could mediate the controlled ROP of OCAs. The proposed mechanism involves a Lewis pair-catalyzed

initiation and coordination-insertion chain growth process via a quick transformation of $Zn(C_6F_5)_2$ to Zn-alkoxide. However, its application is limited to the polymerization of L-**1** with FRs < 200 at 50 °C. In continuance to previous findings, Yang and coworkers identified another simple Lewis pair consisting of 1,8-diazabicycloundec-7-ene (DBU) and $Zn(OAc)_2$ to promote the ROP of L-**1** at room temperature (**Figure 1.6b**).[59] However, this catalytic system required alcohol as an initiator and could not yield polymers with MWs over 20 kDa; and epimerization still occurred (P_m = 0.88 for poly(L-**1**)).

It can be seen that though various Zn complexes have been developed for the ROP of OCAs, the polymerization often result in products with low MWs (less than 30 kDa).[43, 60] The inefficient chain propagation in metal-catalyzed ROP of OCAs have been identified as the main problem preventing the synthesis of high-MW PAHAs.[60] It is worth noting that the discovery of efficient synthetic methods to avoid this problem is crucial, since the mechanical properties, thermal properties, and crystallization behavior of polymer is believed to be directly correlated to its MW, as supported by research in PLA.[61, 62]

Aware of substantial studies on metal catalyst-mediated *N*-carboxyanhydrides polymerization,[63, 64] and the emerging use of photoredox catalysts with metal catalysts for decarboxylation,[65, 66] our group in 2017 developed **Ni-1**/ **Zn-1**/ **Ir-1** photoredox catalytic system to mediate controlled photoredox ROP of L-**1**,[67] allowing for the production of PAHAs with MWs up to 140 kDa and narrow *Đ*s (< 1.1; **Figure 1.6c**). This catalytic system could be successfully applied to other OCAs (**2**, **3**, and **4**) as well. It is noted that all components of this catalytic system were necessary for the controlled polymerization results: **Ni**/**Ir** photocatalysts are responsible for decarboxylation to synthesize high-MW

polymers; while Zn-alkoxide at the chain-end is crucial for chain propagation. The oxidative addition of the **Ni^0** complex to the OCA occurs at the O_1-C_5 position regioselectively,[67] which is followed by photoexicted-**Ir-1**-mediated decarboxylation, and transmetalates with Zn-alkoxide for efficient chain propagation. Also, the low-temperature condition is required to avoid a Ni-mediated decarbonylation side reaction that stops chain propagation.

Motivated by the **Ni**/**Zn**/**Ir** photoredox catalytic system, our group investigated a new electrochemical **Co**/**Zn** catalytic system (**Figure 1.6d**).[68] **Co-1** complex can replace **Ni**/**Ir-1** photocatalysts to facilitate highly controlled ROP of OCAs at 0 °C and afford isotactic high-MW PAHAs (> 140 kDa) with narrow MW distributions ($Đ$ < 1.1). During the electrochemical ROP process, the **Co-1**/OCA intermediate forms using anodic oxidation before undergoing cathodic reduction for decarboxylation, followed by transmetalation with the Zn catalyst to produce Zn-alkoxide terminus for productive chain propagation. Notably, no epimerization occurred even for poly(L-**5**). The copolymerization can also be performed by sequential addition of OCA monomers.

Above all, these two catalytic systems offer an efficient opportunity to synthesize high-MW polymers. However, their reliance on an external energy source renders them impractical for large-scale manufacturing, particularly for stereosequence-controlled copolymers. The search for a novel catalytic system capable of dealing with these issues continues.

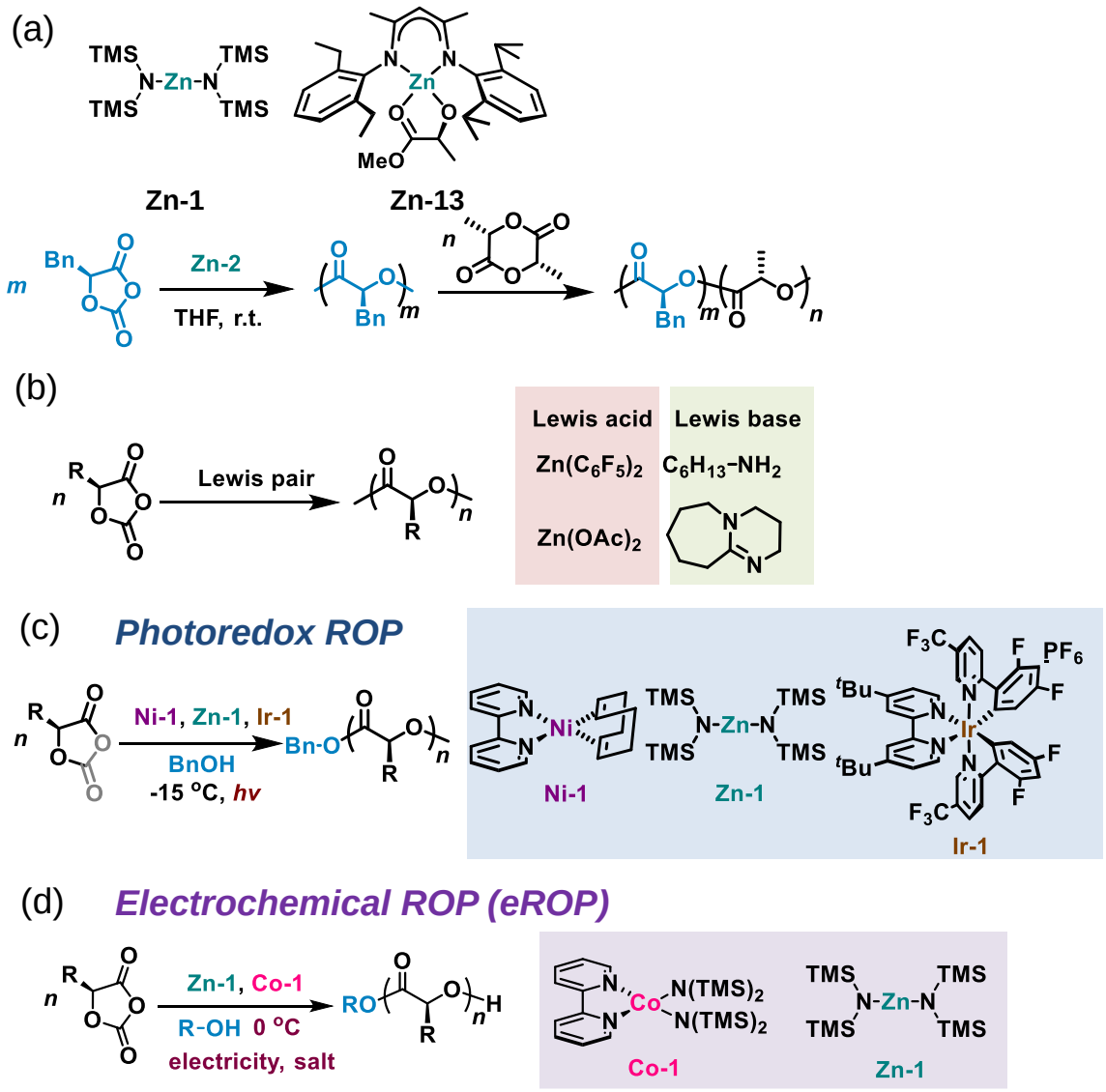

Figure 1.6 The use of metal catalysts for the ROP of OCAs. (a) Zn complexes that can mediate the ROP of lactones have been used for the ROP of OCAs, and the block copolymerization of OCAs and LAs via sequential additions of monomers. (b) The Lewis pair has been used for the ROP of OCAs. (c) Scheme of controlled photoredox ROP of OCAs mediated by **Ni**/**Zn**/**Ir** complexes. (d) Scheme of controlled electrochemical ROP (eROP) of OCAs mediated by **Co**/**Zn** complexes.

1.3 Scope and organization

The easy access to OCA monomers promotes the development of numerous polymerization strategies to prepare functionalized polyesters. However, the following challenges remain:

- More simplified catalytic systems and mild reaction conditions for the synthesis of high MW polyesters without the assistance of external stimuli
- Chemical recycling of synthesized functionalized polyesters to close their life cycle
- Highly stereoselective and sequence-controlled ROP that allows access to functionalized polyesters
- Structure-property relationship of high-MW PAHAs

Based on these challenges, we report a simple method for achieving rapid and controlled OCA polymerization by using highly reactive Mn/Zn complexes without the assistance of an external energy source (**Chapter 2**). The synthesized polyesters are amenable to quantitative chemical recycling under mild conditions (**Chapter 3**). This approach is also used for the large-scale preparation of stereoregular polyesters and stereosequence-controlled copolymers bearing various pendant functional groups (**Chapter 4**). Notably, our scalable Mn/Zn-catalyzed reactions enable us to investigate the stereosequence-structure-property relationship of PAHAs. The obtained gradient copolymers exhibit enhanced ductility and toughness comparable to those of homopolymers and block copolymers and outperform commodity polyolefins such as LDPE in terms of shape recovery resilience (**Chapter 5**).

Moreover, it should be pointed out that the ROP of OCA is driven by reducing the ring-strain and results in releasing a molecule of CO_2 per polymer repeat unit. We discovered that it is feasible to recycle CO_2 using a single Lewis acidic zinc to produce poly(ester-*b*-carbonate) (*b*: block) by facile tandem copolymerization of OCA (CO_2) and epoxide (**Chapter 6**). The kinetic studies showed that the first stage of the process (ROP of OCA) exhibited zero-order kinetics, which is critical for a sharp and clean switch to the second stage (ROCOP of CO_2 and epoxide) without the tapering effect. This new catalytic route could nearly completely recycle the CO_2 released during polyester formation into the subsequent polycarbonate block, achieving the maximum atom economy and sustainable development (**Chapter 7**). The obtained poly(ester-*b*-carbonates) is a new degradable polymer that can combine the benefits of polyester and polycarbonate, and exhibits better material properties than their corresponding homopolymers (**Chapter 8**). The exploration of this new chemical space of poly(ester-*b*-carbonates) via stereosequence-controlled polymerization will continue to enrich the variety of functionalized sustainable polymers (**Chapter 9**).

References

1. Rochman, C. M.; Browne, M. A.; Halpern, B. S.; Hentschel, B. T.; Hoh, E.; Karapanagioti, H. K.; Rios-Mendoza, L. M.; Takada, H.; Teh, S.; Thompson, R. C., Classify plastic waste as hazardous. *Nature* **2013,** *494* (7436), 169-171.
2. Jambeck, J. R.; Geyer, R.; Wilcox, C.; Siegler, T. R.; Perryman, M.; Andrady, A.; Narayan, R.; Law, K. L., Plastic waste inputs from land into the ocean. *Science* **2015,** *347* (6223), 768-771.
3. Wilcox, C.; Van Sebille, E.; Hardesty, B. D., Threat of plastic pollution to seabirds is global, pervasive, and increasing. *Proceedings of the National Academy of Sciences* **2015,** *112* (38), 11899-11904.
4. Zhang, X.; Fevre, M.; Jones, G. O.; Waymouth, R. M., Catalysis as an enabling science for sustainable polymers. *Chemical reviews* **2018,** *118* (2), 839-885.
5. Hillmyer, M. A.; Tolman, W. B., Aliphatic polyester block polymers: renewable, degradable, and sustainable. *Accounts of chemical research* **2014,** *47* (8), 2390-2396.
6. Hong, M.; Chen, E. Y.-X., Chemically recyclable polymers: a circular economy approach to sustainability. *Green Chemistry* **2017,** *19* (16), 3692-3706.
7. Zhu, Y.; Romain, C.; Williams, C. K., Sustainable polymers from renewable resources. *Nature* **2016,** *540* (7633), 354-362.
8. Coates, G. W.; Getzler, Y. D. Y. L., Chemical recycling to monomer for an ideal, circular polymer economy. *Nature Reviews Materials* **2020,** *5* (7), 501-516.
9. Schneiderman, D. K.; Hillmyer, M. A., 50th anniversary perspective: There is a great future in sustainable polymers. *Macromolecules* **2017,** *50* (10), 3733-3749.
10. Hong, M.; Chen, E. Y.-X., Future directions for sustainable polymers. *Trends in Chemistry* **2019,** *1* (2), 148-151.
11. Tang, X.; Chen, E. Y. X., Toward infinitely recyclable plastics derived from renewable cyclic esters. *Chem* **2019,** *5* (2), 284-312.
12. Commission, E. A European strategy for plastics in a circular economy. http://ec.europa.eu/environment/circular-economy/pdf/plastics-strategy-brochure.pdf.
13. Foundation, E. M. The new plastics economy: rethinking the future of plastics & catalysing action. https://www.ellenmacarthurfoundation.org/publications/the-new-plastics-economy-rethinking-the-future-of-plastics-catalysing-action.
14. Yin, Q.; Yin, L.; Wang, H.; Cheng, J., Synthesis and biomedical applications of functional poly (α-hydroxy acids) via ring-opening polymerization of *O*-carboxyanhydrides. *Accounts of Chemical Research* **2015,** *48* (7), 1777-1787.
15. Gilding, D.; Reed, A., Biodegradable polymers for use in surgery—polyglycolic/poly (actic acid) homo-and copolymers: 1. *Polymer* **1979,** *20* (12), 1459-1464.
16. Yamamoto, H.; Kuno, Y.; Sugimoto, S.; Takeuchi, H.; Kawashima, Y., Surface-modified PLGA nanosphere with chitosan improved pulmonary delivery of calcitonin by mucoadhesion and opening of the intercellular tight junctions. *Journal of Controlled Release* **2005,** *102* (2), 373-381.
17. Dechy-Cabaret, O.; Martin-Vaca, B.; Bourissou, D., Controlled ring-opening polymerization of lactide and glycolide. *Chemical Reviews* **2004,** *104* (12), 6147-6176.
18. Zhu, J.-B.; Watson, E. M.; Tang, J.; Chen, E. Y.-X., A synthetic polymer system with repeatable chemical recyclability. *Science* **2018,** *360* (6387), 398-403.

19. Sangroniz, A.; Zhu, J.-B.; Tang, X.; Etxeberria, A.; Chen, E. Y. X.; Sardon, H., Packaging materials with desired mechanical and barrier properties and full chemical recyclability. *Nature Communications* **2019,** *10* (1), 3559.
20. Franssen, N. M. G.; Reek, J. N. H.; de Bruin, B., Synthesis of functional 'polyolefins': state of the art and remaining challenges. *Chemical Society Reviews* **2013,** *42* (13), 5809-5832.
21. Boaen, N. K.; Hillmyer, M. A., Post-polymerization functionalization of polyolefins. *Chemical Society Reviews* **2005,** *34* (3), 267-275.
22. Ajioka, M.; Enomoto, K.; Suzuki, K.; Yamaguchi, A., The basic properties of poly(lactic acid) produced by the direct condensation polymerization of lactic acid. *Journal of Environmental Polymer Degradation* **1995,** *3* (4), 225-234.
23. Cohen-Arazi, N.; Domb, A. J.; Katzhendler, J., New biocompatible polyesters derived from α-amino acids: hydrolytic degradation behavior. *Polymers* **2010,** *2* (4), 418-439.
24. Yin, M.; Baker, G. L., Preparation and characterization of substituted polylactides. *Macromolecules* **1999,** *32* (23), 7711-7718.
25. Simmons, T. L.; Baker, G. L., Poly(phenyllactide): synthesis, characterization, and hydrolytic degradation. *Biomacromolecules* **2001,** *2* (3), 658-663.
26. Chen, X.; Lai, H.; Xiao, C.; Tian, H.; Chen, X.; Tao, Y.; Wang, X., New bio-renewable polyester with rich side amino groups from l-lysine via controlled ring-opening polymerization. *Polymer Chemistry* **2014,** *5* (22), 6495-6502.
27. Tong, R., New chemistry in functional aliphatic polyesters. *Industrial & Engineering Chemistry Research* **2017,** *56* (15), 4207-4219.
28. Martin, R. T.; Camargo, L. P.; Miller, S. A., Marine-degradable polylactic acid. *Green Chemistry* **2014,** *16* (4), 1768-1773.
29. Cairns, S. A.; Schultheiss, A.; Shaver, M. P., A broad scope of aliphatic polyesters prepared by elimination of small molecules from sustainable 1,3-dioxolan-4-ones. *Polymer Chemistry* **2017,** *8* (19), 2990-2996.
30. Xu, Y.; Perry, M. R.; Cairns, S. A.; Shaver, M. P., Understanding the ring-opening polymerisation of dioxolanones. *Polymer Chemistry* **2019,** *10* (23), 3048-3054.
31. Martin Vaca, B.; Bourissou, D., *O*-carboxyanhydrides: useful tools for the preparation of well-defined functionalized polyesters. *ACS Macro Letters* **2015,** *4* (7), 792-798.
32. du Boullay, O. T.; Marchal, E.; Martin-Vaca, B.; Cossio, F. P.; Bourissou, D., An activated equivalent of lactide toward organocatalytic ring-opening polymerization. *Journal of the American Chemical Society* **2006,** *128* (51), 16442-16443.
33. Zhong, Y.; Tong, R., Living ring-opening polymerization of *O*-carboxyanhydrides: the search for catalysts. *Frontiers in Chemistry* **2018,** *6*, 641.
34. Feng, Q.; Zhong, Y.; Xie, L.; Tong, R., Recent advances in ring-opening polymerization of *O*-carboxyanhydrides. *Synlett* **2017,** *28* (15), 1857-1866.
35. Pounder, R. J.; Dove, A. P., Towards poly (ester) nanoparticles: recent advances in the synthesis of functional poly (ester) s by ring-opening polymerization. *Polymer Chemistry* **2010,** *1* (3), 260-271.
36. Basu, A.; Kunduru, K. R.; Katzhendler, J.; Domb, A. J., Poly (α-hydroxy acid) s and poly (α-hydroxy acid-co-α-amino acid) s derived from amino acid. *Advanced Drug Delivery Reviews* **2016,** *107*, 82-96.

37. Kricheldorf, H.; JM, J., New polymer synthesis. VIII: synthesis and polymerization of L-lactic acid *O*-carboxyanhydride (5-methyl-dioxolan-2,4-dione). **1983**.
38. Vandenbossche, C. P.; de Croos, P.; Singh, S. P.; Bakale, R. P.; Wagler, T. R., Formation of (S)-5-cyclohexyl-5-phenyl-1, 3-dioxolane-2, 4-dione: a key intermediate in the synthesis of (S)-oxybutynin hydrochloride. *Organic Process Research & Development* **2010,** *14* (4), 921-925.
39. Gerhardt, W. W.; Noga, D. E.; Hardcastle, K. I.; García, A. J.; Collard, D. M.; Weck, M., Functional lactide monomers: methodology and polymerization. *Biomacromolecules* **2006,** *7* (6), 1735-1742.
40. Kalelkar, P. P.; Alas, G. R.; Collard, D. M., Synthesis of an alkene-containing copolylactide and its facile modification by the addition of thiols. *Macromolecules* **2016,** *49* (7), 2609-2617.
41. Yu, Y.; Zou, J.; Cheng, C., Synthesis and biomedical applications of functional poly([small alpha]-hydroxyl acid)s. *Polymer Chemistry* **2014,** *5* (20), 5854-5872.
42. Pounder, R. J.; Fox, D. J.; Barker, I. A.; Bennison, M. J.; Dove, A. P., Ring-opening polymerization of an *O*-carboxyanhydride monomer derived from L-malic acid. *Polymer Chemistry* **2011,** *2* (10), 2204-2212.
43. Wang, R. B.; Zhang, J. W.; Yin, Q.; Xu, Y. X.; Cheng, J. J.; Tong, R., Controlled ring-opening polymerization of *O*-carboxyanhydrides using a beta-diiminate zinc catalyst. *Angewandte Chemie-International Edition* **2016,** *55* (42), 13010-13014.
44. Buchard, A.; Carbery, D. R.; Davidson, M. G.; Ivanova, P. K.; Jeffery, B. J.; Kociok-Köhn, G. I.; Lowe, J. P., Preparation of stereoregular isotactic poly(mandelic acid) through organocatalytic ring-opening polymerization of a cyclic *O*-carboxyanhydride. *Angewandte Chemie International Edition* **2014,** *53* (50), 13858-13861.
45. Li, M.; Zhang, S.; Zhang, X.; Wang, Y.; Chen, J.; Tao, Y.; Wang, X., Unimolecular Anion-Binding Catalysts for Selective Ring-Opening Polymerization of O-carboxyanhydrides. *Angewandte Chemie International Edition* **2021,** *60* (11), 6003-6012.
46. Zhuang, X. L.; Yu, H. Y.; Tang, Z. H.; Oyaizu, K.; Nishide, H.; Chen, X. S., Polymerization of lactic *O*-carboxylic anhydride using organometallic catalysts. *Chinese Journal of Polymer Science* **2011,** *29* (2), 197-202.
47. He, Z. G.; Jiang, L.; Chuan, Y. M.; Li, H. L.; Yuan, M. L., Ring-opening polymerization of L-lactic acid *O*-carboxyanhydrides initiated by alkoxy rare earth compounds. *Molecules* **2013,** *18* (10), 12768-12776.
48. Jia, F.; Chen, X. Y.; Zheng, Y.; Qin, Y. S.; Tao, Y. H.; Wang, X. H., One-pot atom-efficient synthesis of bio-renewable polyesters and cyclic carbonates through tandem catalysis. *Chemical Communications* **2015,** *51* (40), 8504-8507.
49. Ouyang, H.; Nie, K.; Yuan, D.; Yao, Y. M., Synthesis of amine-bridged bis(phenolate) rare-earth metal aryloxides and their catalytic performances for the ring-opening polymerization of L-lactic acid O-carboxyanhydride and L-lactide. *Dalton Transactions* **2017,** *46* (45), 15928-15938.
50. Yin, Q.; Tong, R.; Xu, Y.; Baek, K.; Dobrucki, L. W.; Fan, T. M.; Cheng, J., Drug-Initiated ring-opening polymerization of *O*-carboxyanhydrides for the preparation of anticancer drug-Poly(*O*-carboxyanhydride) nanoconjugates. *Biomacromolecules* **2013,** *14* (3), 920-929.

51. Brignou, P.; Guillaume, S. M.; Roisnel, T.; Bourissou, D.; Carpentier, J.-F., Discrete cationic zinc and magnesium complexes for dual organic/organometallic-catalyzed ring-opening polymerization of trimethylene carbonate. *Chemistry-A European Journal* **2012,** *18* (30), 9360-9370.
52. Piedra-Arroni, E.; Brignou, P.; Amgoune, A.; Guillaume, S. M.; Carpentier, J.-F.; Bourissou, D., A dual organic/organometallic approach for catalytic ring-opening polymerization. *Chemical Communications* **2011,** *47* (35), 9828-9830.
53. Wang, Q.; Zhao, W.; He, J.; Zhang, Y.; Chen, E. Y. X., Living ring-opening polymerization of lactones by N-heterocyclic olefin/$Al(C_6F_5)_3$ lewis pairs: structures of intermediates, kinetics, and mechanism. *Macromolecules* **2017,** *50* (1), 123-136.
54. Naumann, S.; Scholten, P. B. V.; Wilson, J. A.; Dove, A. P., Dual catalysis for selective ring-opening hydrochloric acid polymerization of lactones: evolution toward simplicity. *Journal of the American Chemical Society* **2015,** *137* (45), 14439-14445.
55. Meisner, J.; Karwounopoulos, J.; Walther, P.; Kästner, J.; Naumann, S., The lewis pair polymerization of lactones using metal halides and N-heterocyclic olefins: theoretical insights. *Molecules* **2018,** *23* (2), 432.
56. Wang, B.; Pan, L.; Ma, Z.; Li, Y., Ring-opening polymerization with lewis pairs and subsequent nucleophilic substitution: a promising strategy to well-defined polyethylene-like polyesters without transesterification. *Macromolecules* **2018,** *51* (3), 836-845.
57. Liu, S.; Bai, T.; Ni, K.; Chen, Y.; Zhao, J.; Ling, J.; Ye, X.; Zhang, G., Biased lewis pairs: a general catalytic approach to ether-ester block copolymers with unlimited ordering of sequences. *Angewandte Chemie International Edition* **2019,** *58* (43), 15478-15487.
58. Nie, Y. Z.; Wang, P.; Du, H. F.; Meng, W.; Yang, J., An efficient strategy for achieving controlled ring-opening polymerization of O-carboxyanhydrides via amine initiation in collaboration with metal-alkoxide catalysis. *Polymer Chemistry* **2018,** *9* (40), 5014-5023.
59. Wang, P.; Liang, J. P.; Yin, T.; Yang, J., Simple lewis pairs of zinc salts and organobases as bifunctional catalysts for controlled ring-opening polymerization of *O*-carboxyanhydrides. *Polymer Chemistry* **2019,** *10* (40), 5498-5506.
60. Feng, Q.; Tong, R., Controlled Photoredox Ring-Opening Polymerization of O-Carboxyanhydrides. *Journal of the American Chemical Society* **2017,** *139* (17), 6177-6182.
61. Garlotta, D., A literature review of poly(lactic acid). *Journal of Polymers and the Environment* **2001,** *9* (2), 63-84.
62. Slomkowski, S.; Penczek, S.; Duda, A., Polylactides-an overview. *Polymers for Advanced Technologies* **2014,** *25* (5), 436-447.
63. Deming, T. J., Facile synthesis of block copolypeptides of defined architecture. *Nature* **1997,** *390* (6658), 386-389.
64. Deming, T. J.; Curtin, S. A., Chain initiation efficiency in cobalt- and nickel-mediated polypeptide synthesis. *Journal of the American Chemical Society* **2000,** *122* (24), 5710-5717.
65. Zuo, Z. W.; Ahneman, D. T.; Chu, L. L.; Terrett, J. A.; Doyle, A. G.; MacMillan, D. W. C., Merging photoredox with nickel catalysis: Coupling of alpha-carboxyl sp(3)-carbons with aryl halides. *Science* **2014,** *345* (6195), 437-440.

66. Twilton, J.; Le, C.; Zhang, P.; Shaw, M. H.; Evans, R. W.; MacMillan, D. W. C., The merger of transition metal and photocatalysis. *Nature Reviews Chemistry* **2017,** *1* (7).
67. Feng, Q. Y.; Tong, R., Controlled photoredox ring-opening polymerization of *O*-carboxyanhydrides. *Journal of the American Chemical Society* **2017,** *139* (17), 6177-6182.
68. Zhong, Y. L.; Feng, Q. Y.; Wang, X. Q.; Chen, J.; Cai, W. J.; Tong, R., Functionalized polyesters via stereoselective electrochemical ring-opening polymerization of *O*-carboxyanhydrides. *ACS Macro Letters* **2020,** *9* (8), 1114-1118.

CHAPTER 2

Mn/Zn complexes for controlled ring-opening polymerization of *O*-carboxyanhydrides

2.1 Introduction

Since 2006, *O*-carboxyanhydrides (OCAs), which can be prepared with a rich variety of side-chain functionalities, have emerged as an alternative class of highly active monomers for polyester polymerization.[1, 2] Unfortunately, current catalytic systems for ring-opening polymerization (ROP) of OCAs, especially those involving organocatalysts, typically present low activity for the synthesis of high-molecular-weight (MW) polymers, and cannot mediate stereoselective ROP of OCAs to form polyesters with various microstructures (**Figure 2.1**). To overcome such challenges, our group recently demonstrated that the combination of light or electricity with organometallic catalysts could produce stereoregular, high-MW polyesters (> 200 kDa) with various tacticities (**Figure 2.1**).[3-5] Despite the efficiency of these reactions, their reliance on an external energy source made them impractical for large-scale synthesis of high-MW polymers, including stereosequence-controlled copolymers. Therefore, a new catalytic system without the assistance of external energy was designed to achieve rapid and controlled OCA polymerization.

Currently, no single metal complex or organocatalyst can efficiently mediate controlled ROP of OCAs to prepare high MW polymers (over 100 kDa) with controls over stereoselectivity and stereosequence. As illustrated in our prior studies, at least two metal complexes were needed to prepare high-MW (>100 kDa) polyesters by ROP of OCAs: (i) a metal-alkoxide (e.g., Zn-alkoxide) for chain propagation and (ii) a metal

complex (Ni/Ir or Co) activated by external energy for OCA decarboxylation, a key step that allowed the metal-alkoxide to engage with OCA and prevented the formation of inactive metal-carbonate complexes.[2, 5] Inspired by this, we hypothesized that a redox-active transition-metal complex could be combined with a Zn-alkoxide catalyst to mediate controlled ROP without the assistance of an external energy source (light or electricity). Recent advances in organometallic chemistry,[6] as well as the wide range of known metalloenzyme-mediated redox reactions,[7] inspired us to attempt to identify a suitable redox-active transition-metal complex. In particular, earth-abundant transition metals were explored because they are less expensive than rare-earth metals and they readily undergo oxidation state changes—that is, lose or gain electrons—to mediate chemical reactions.[8]

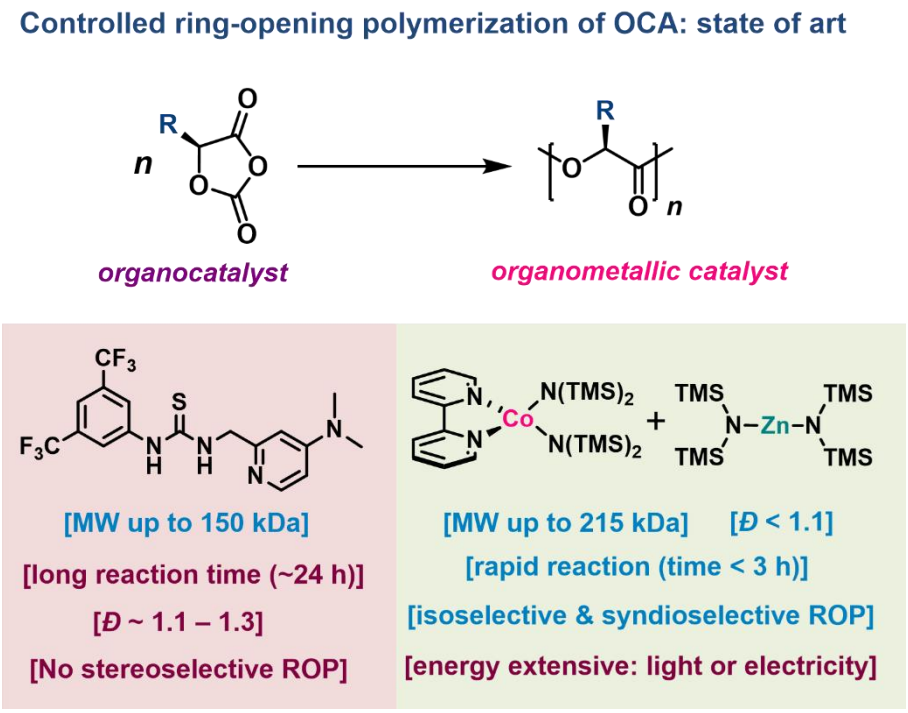

Figure 2.1 Previously reported uses of organocatalysts and organometallic catalysts for ROP of OCAs, with pros and cons indicated in blue and red type, respectively.

2.2 Results and discussions

2.2.1 The discovery of Mn-1 ($Mn[N(SiMe_3)_2]_2$) / Zn-1 ($Zn[N(SiMe_3)_2]_2$) for the controlled ring-opening polymerization without external stimulus

We set about investigating a series of stable low-coordination-number metal (trimethylsilyl)amide complexes (Co, Mn, Fe, Ce, and Y) because these well-characterized redox-active complexes can be easily synthesized in one step on a large scale (**Figure 2.2**).[9-11] Note that none of them has been utilized for decarboxylation without external energy activation.

To test our hypothesis, ROP of L-PheOCA (L-**1**) was performed by using various metal silylamide complexes in the presence of $Zn(HMDS)_2$ (**Zn-1**; HMDS, hexamethyldisilazane) and BnOH ([L-**1**]/[M]/[**Zn-1**]/[BnOH] = 500/1/1/1; **Figure 2.2**). We evaluated the performance of complexes in terms of monomer conversion and the number-average MWs and MW distributions (M_n, and $Đ$, respectively) of the resulting polymers. As shown in **Figure 2.2** and **Table 2.1**, $Ce(HMDS)_3$ and $Y[N(SiHMe_2)_2]_3$ failed to fully polymerize L-**1**. The monomer conversions were 56% and 69% when the [L-**1**]/[**Zn-1**] ratio was 500/1. Additionally, $Fe(HMDS)_2$, $Y(HMDS)_3$ and $Co(HMDS)_2$ could achieve nearly complete monomer conversion, but they could not control polymer's MWs. The obtained MWs (57.2, 50 and 102.4 kDa) were far from our expected MWs (74.1 kDa). However, among the five catalysts, $Mn(HMDS)_2$ (**Mn-1**) could achieve controlled ROP of poly(L-**1**). Monomer conversion was completed within 1 hour at −15 °C, and poly(L-**1**) with a M_n of 83.5 kDa and a $Đ$ of 1.08 was obtained (expected MW, 74.1 kDa). It may because the Mn^{II} complex has the best balance of metal electronegativity and metal–nitrogen bond length among the examined complexes

(**Figure 2.2**). This result is consistent with the fact that the Mn center of some enzymes, including oxalate decarboxylase, can mediate radical decarboxylation reactions.[12]

Then the ROP of L-**1** using various metal alkoxide (Zn, Mg, Y, Hf, and Zr) in the presence of **Mn-1** was investigated to choose the best metal-alkoxide catalyst. As shown in **Table 2.2**, similar with our previous reports,[2, 4, 5] only **Zn-1**/BnOH could achieve the complete monomer conversion even at a higher feeding ratio.

Given that, it could be concluded that the best combination for controlled ROP of OCAs consisted of **Mn-1** and **Zn-1**/BnOH. To the best of our knowledge, there are no reports on using metal silylamides for decarboxylation without external energy activation. Therefore, this operationally simple method provides a new entry for the large-scale synthesis of functionalized poly(α-hydroxy acids).

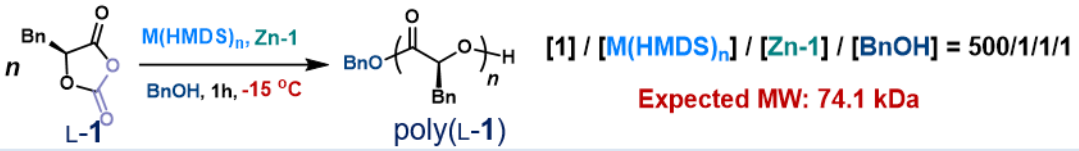

metal silylamides properties	metal electronegativity → / M-N bond length (Å) →				
	$Ce(HMDS)_3$	$Y(N(SiHMe_2)_2)_3$	$Mn(HMDS)_2$	$Fe(HMDS)_2$	$Co(HMDS)_2$
Monomer conversion (%):	56	69	100	96	100
M_n (kDa) / $Đ$:	23.1 / 1.07	48.5 / 1.53	83.5 / 1.08	50.0 / 1.05	102.4 / 1.08

Figure 2.2 Identification of the optimal metal silylamide complex for ring-opening polymerization of OCAs involving redox decarboxylation without an external energy source, on the basis of metal electronegativity and metal–nitrogen bond length.[10] Expected MW: molecular weight calculated based on the feed ratio assuming 100% monomer conversion.

Table 2.1 The discovery of **Mn-1** ($Mn[N(SiMe_3)_2]_2$) / **Zn-1** ($Zn[N(SiMe_3)_2]_2$) for the controlled ring-opening polymerization of L-**1**.

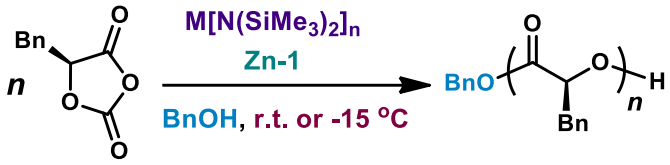

Entry	Metal silylamide	FR	Time (h)	Temp. (°C)	Conv. (%)	M_n (kDa)	MW_{cal} (kDa)	$Đ$
1	$Co[N(SiMe_3)_2]_2$	500	1	r.t.	100	53.2	74.1	1.10
2	$Co[N(SiMe_3)_2]_2$	500	1	−15	100	102.4	74.1	1.08
3	$Co[N(SiMe_3)_2]_2$	700	1	−15	69.0	96.9	71.6	1.06
4	$Fe[N(SiMe_3)_2]_2$	500	1	r.t.	56.8	31.0	42.1	1.14
5	$Fe[N(SiMe_3)_2]_2$	500	1	−15	95.9	50.0	71.1	1.05
6	$Ce[N(SiMe_3)_2]_3$	500	1	r.t.	19.4	6.45	14.5	1.09
7	$Ce[N(SiMe_3)_2]_3$	500	1	−15	55.6	23.1	41.3	1.07
8	$Y[N(SiHMe_2)_2]_3$	500	1	r.t.	53.1	35.2	39.4	1.46
9	$Y[N(SiHMe_2)_2]_3$	500	1	−15	68.9	48.5	51.1	1.53
10	$Y[N(SiMe_3)_2]_3$	500	1	r.t.	61.9	32.7	45.9	1.40
11	$Y[N(SiMe_3)_2]_3$	500	1	−15	100	57.2	74.1	1.63
12	$Mn[N(SiMe_3)_2]_2$	500	1	r.t.	100	69.8	74.1	1.05
13	$Mn[N(SiMe_3)_2]_2$	500	1	−15	100	83.5	74.1	1.08

Table 2.2 The identification of optimal metal alkoxide with **Mn-1** ($Mn[N(SiMe_3)_2]_2$) for the controlled ring-opening polymerization of L-**1**

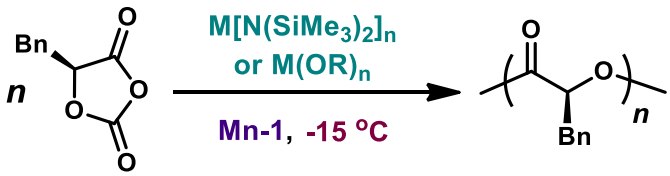

Entry	Metal alkoxide	FR	Time (h)	Conv. (%)	M_n (kDa)	MW_{cal} (kDa)	$Đ$
1	$Zn[N(SiMe_3)_2]_2$ / BnOH	900	1	100	125.5	133.3	1.04
2	$Mg[N(SiMe_3)_2]_2$ / BnOH	300	1	100	38.6	44.5	1.07
3	$Mg[N(SiMe_3)_2]_2$ / BnOH	900	1	26.2	9.12	35.0	1.23
4	$Y[N(SiHMe_2)_2]_3$ / BnOH	300	1	49.3	11.8	22.0	1.16
5	$Y[N(SiMe_3)_2]_3$ / BnOH	300	1	100	31.1	44.5	1.06
6	$Y[N(SiMe_3)_2]_3$ / BnOH	900	1	35.5	20.2	47.4	1.23
7	$Hf(O^iPr)_4$	300	1	38.0	25.9	17.0	1.10
8	$Zr(O^iPr)_4$	300	1	46.1	11.3	20.6	1.04
9	$Hf(O^tBu)_4$	300	1	13.1	9.09	5.92	2.10

2.2.2 Effects of ligands of Mn-1 on controlled ring-opening polymerization

Ligands would affect the metal catalytic activities by electronic effects and/or steric effects.[13] In our previous report, the addition of ligands to $Co(HMDS)_2$ greatly increased M_n values and monomer conversions for photoredox ROP of OCA.[5] However, the addition of ligands to **Mn-1** did not markedly improve its polymerization activity (**Table 2.3**). It seems that the use of ligands in $Co(HMDS)_2$ for photoredox ROP improved the absorption of the photocatalyst, whereas such effect is not required for Mn complex that does not require external energy triggering. On the other hand, the ligands could increase the steric hindrance for the ring-opening process[14], thus they did not markedly improve the polymerization results.

In addition, some commercially available Mn complexes were performed for ROP of OCAs, such as (1*S*,2*S*)-(+)-[1,2-cyclohexanediamino-*N*,*N*'-bis(3,5-di-*t*-butylsalicylidene)]manganese^{III} chloride (**Mn-2**) and bis(cyclopentadienyl)manganese (**Mn-3**). Unfortunately, they were unable to mediate controlled ROP at a high feed ratio (**Table 2.4**).

Table 2.3. Effects of ligands of **Mn-1** on the controlled ring-opening polymerization of L-**1**

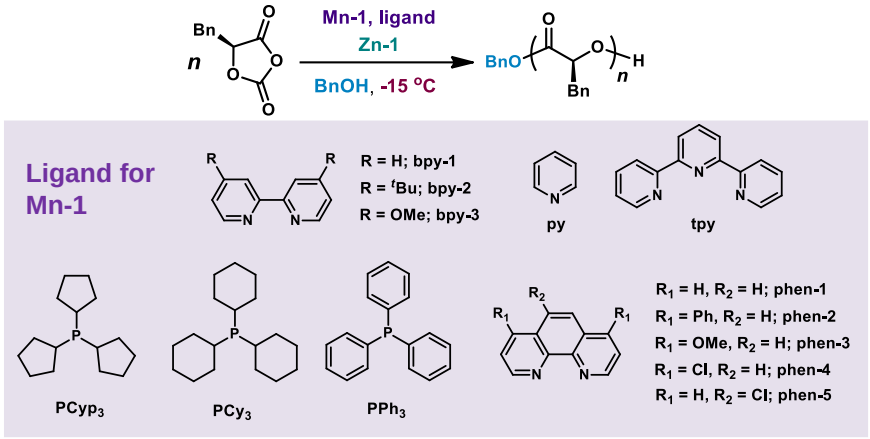

Entry	Ligand	FR	Time (h)	Conv. (%)	M_n (kDa)	MW_{cal} (kDa)	$Đ$
1	-	1100	1.5	100	163.9	162.9	1.02
2	bpy-1	1100	3	49.2	N.D.	80.2	N.D.
3	bpy-2	1100	1.5	100	141.3	162.9	1.06
4	bpy-3	1100	1.5	58.7	N.D.	95.7	N.D.
5	py	900	1	35.8	N.D.	47.7	N.D.
6	tpy	900	1	36.5	N.D.	48.7	N.D.
7	$PCyp_3$	1100	1.5	100	107.1	162.9	1.02
8	PCy_3	1100	1.5	100	91.7	162.9	1.04
9	PPh_3	1100	1.5	100	115.3	162.9	1.07
10	phen-1	1100	2	100	150.8	162.9	1.03
11	phen-2	1100	2	100	147.5	162.9	1.02
12	phen-3	1100	1.5	91.6	122.8	149.2	1.05
13	phen-4	1100	1.5	77.7	121.9	126.6	1.02
14	phen-5	1100	1.5	100	116.6	162.9	1.08

Table 2.4. Examination of other commercially available Mn complexes on the ring-opening polymerization of L-**1**

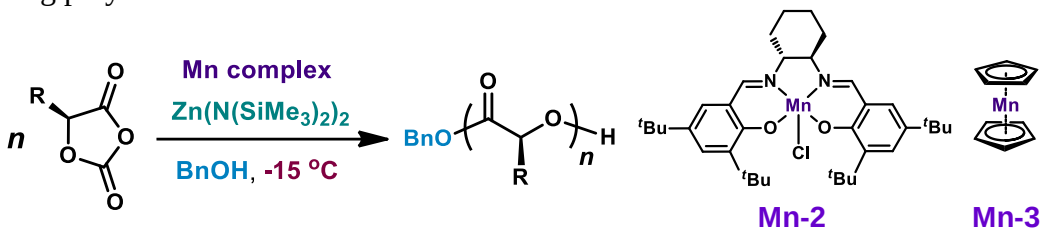

Entry	Catalyst	FR	Time (h)	Conv. (%)	M_n (kDa)	MW_{cal} (kDa)	$Đ$
1	**Mn-2**	300	1	48.6	N.D.	21.7	N.D.
2	**Mn-3**	300	1	100	67.3	44.5	1.15
3	**Mn-3**	900	1.5	95.5	163.1	127.3	1.06
4	**Mn-3**	1300	3	36.2	N.D.	69.8	N.D.

2.2.3 Examining reaction conditions for the redox ring-opening polymerization mediated by Mn-1/Zn-1/BnOH

2.2.3.1 Light

The ROP of L-**1** with or without light was performed separately to confirm whether light offers further assistance for polymerization. As shown in **Figure 2.3**, irradiation with light had a negligible effect on the MW and $Đ$ values of the polymer, indicating that light was not required. It proved our hypothesis that redox-active transition-metal complex could be combined with a Zn-alkoxide catalyst to mediate controlled ROP without the assistance of an external energy source, since they readily undergo oxidation state changes—that is, lose or gain electrons—to mediate chemical reactions.[8]

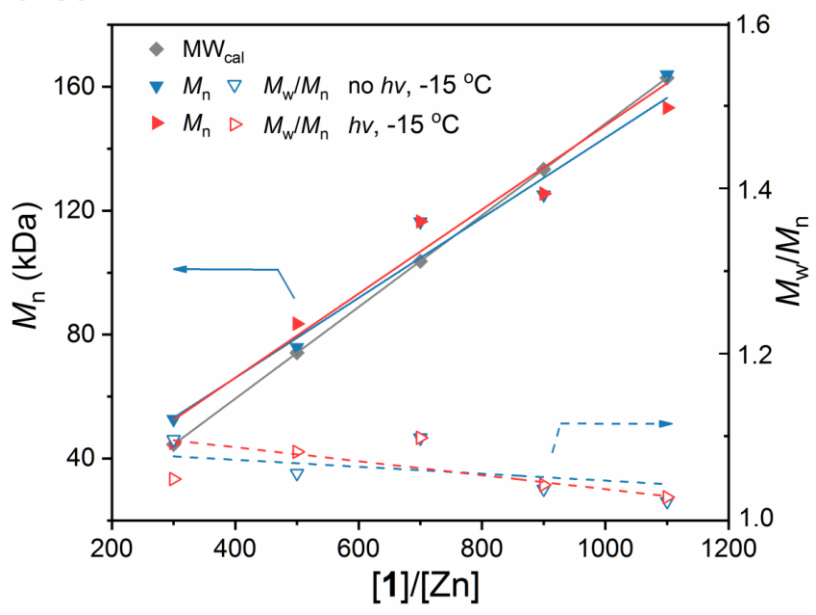

Figure 2.3 Plots of M_n and molecular weight distribution (M_w/M_n) of poly(L-**1**) versus [L-**1**]/[Zn] ratio at -15 °C ([**Mn-1**]/[**Zn-1**]/[BnOH] = 1/1/1), with (red) and without light irradiation (blue).

2.2.3.2 Temperature

The reaction temperature was varied at room temperature, 0 °C, and -15 °C. We observed that monomer conversion was incomplete at higher feeding ratios (FR > 800) when the reaction was performed at room temperature (**Figure 2.4**, blue line). Although the Mn/Zn catalytic system could achieve complete polymerization at 0 °C when the feeding ratios were no higher than 900, the obtained MWs were gradually less than our expected values (**Figure 2.4**, green line). However, lowering the temperature to −15 °C enabled the successful polymerization of L-**1** at a high feeding ratio of 1500 within 2 h to poly(L-**1**) with a MW of 204.7 kDa (**Figure 2.4**, red line). Decarbonylation side reaction at room temperature[2] was previously described in photoredox ROP of OCA, indicating the side reaction existed in our catalytic system as well. However, low temperature (−15

°C) prevented the side reaction that hindered chain propagation from occurring in our catalytic system.

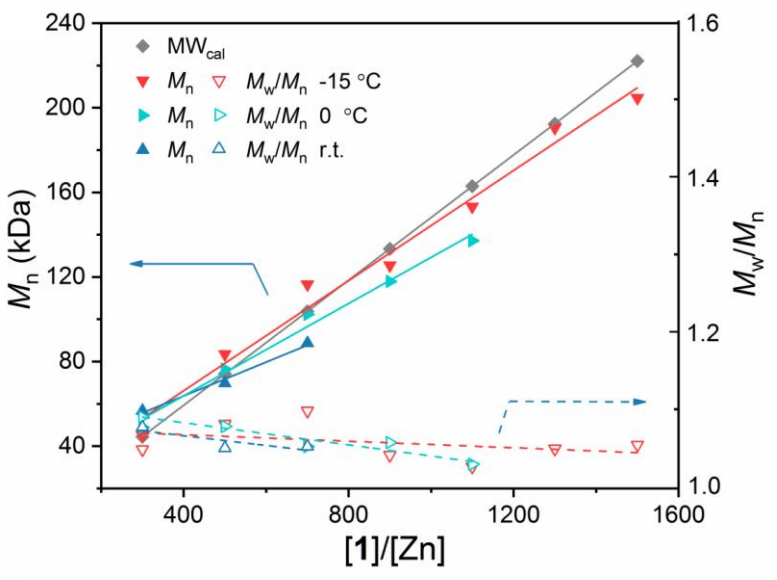

Figure 2.4 Plots of M_n and molecular weight distribution (M_w/M_n) of poly(L-**1**) versus [L-**1**]/[Zn] ratio at different temperature ([**Mn-1**]/[**Zn-1**]/[BnOH] = 1/1/1).

2.2.3.3 The necessity of each of catalytic components

By means of a series of control experiments, we demonstrated the necessity for each of the catalytic components (**Table 2.5**). Without **Mn-1**, the polymerization was uncontrolled with a monomer conversion of 25.7% (entry 2), whereas **Zn-1** was essential for chain propagation (entry 3). In the absence of the initiator, BnOH, the obtained polymer had uncontrolled M_n and $Đ$ values and a low monomer conversion (entry 4). Additionally, electrospray ionization mass spectrometry (ESI-MS) and matrix-assisted laser desorption/ionization (MALDI) analysis of oligo(L-**1**) in **Figure 2.5** confirmed the

attachment of the BnO- group to the oligomer, suggesting that a **Zn**-alkoxide was involved in ring-opening and chain propagation.

Table 2.5. Optimization of conditions for **Zn-1**/**Mn-1**-mediated controlled ring-opening polymerization of L-**1**

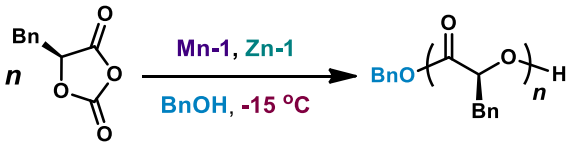

L-**1** poly(L-**1**)

Entry	Conditions	FR	Time (h)	Conv. (%)	M_n (kDa)	MW_{cal} (kDa)	$Đ$
1	As shown	900	1	100	125.5	133.3	1.04
2	No **Mn-1**	900	1	25.7	63.6	34.3	1.14
3	No **Zn-1**	900	1	7.6	9.17	10.2	1.42
4	No BnOH	900	1	21.9	20.0	29.3	1.26
5	Only **Mn-1**	900	1	0	N.D.	0	N.D.
6	Only **Zn-1**	900	1	26.2	62.1	35.0	1.16

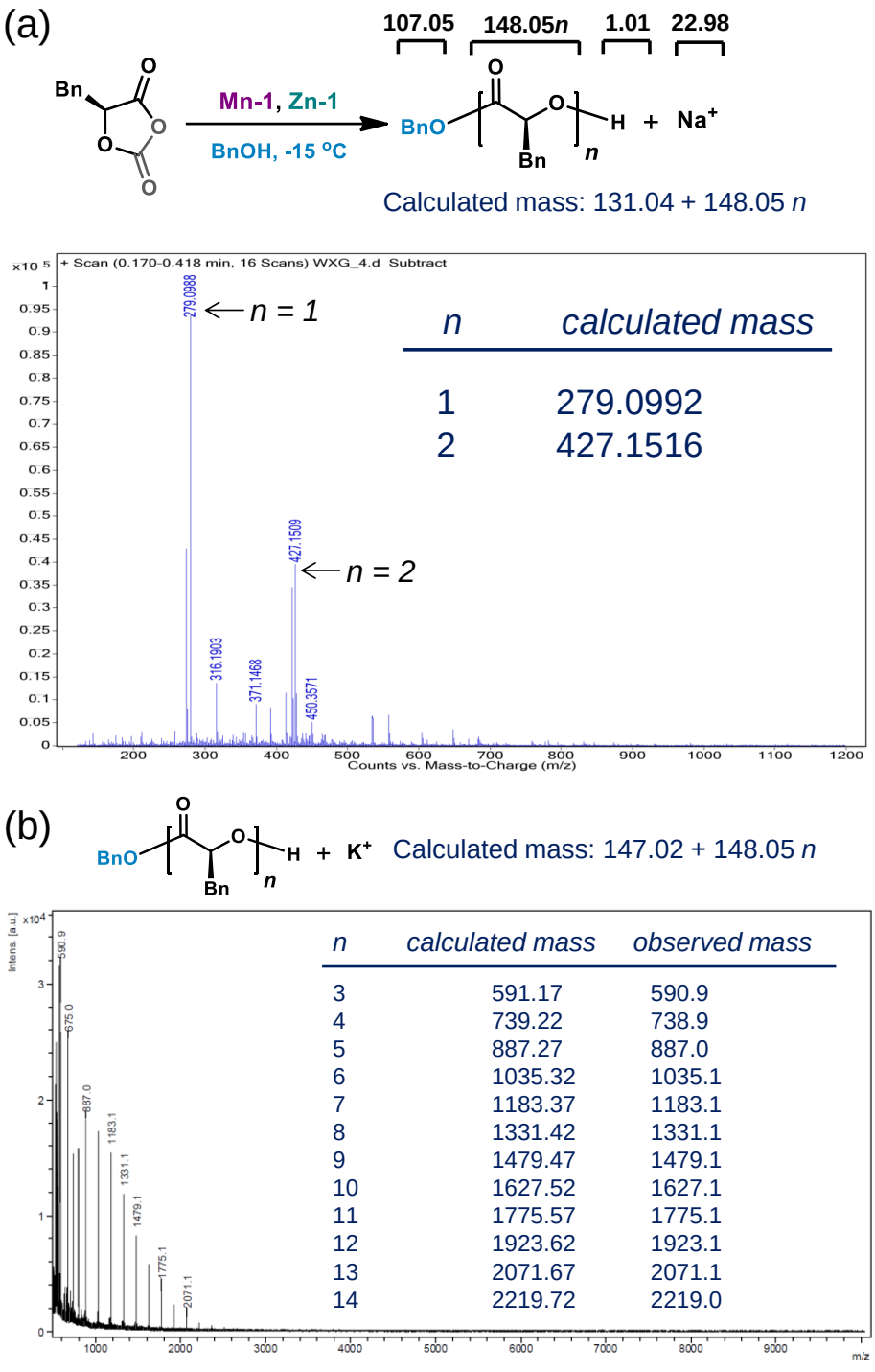

Figure 2.5 Alcohol participated in the Mn/Zn-mediated ROP of L-**1** and was incorporated at the chain end. (a) ESI-MS spectrum of oligo(L-**1**) initiated by BnOH ([L-**1**]/[**Zn-1**]/[**Mn-1**]/[BnOH] = 1/1/1/1, -15 °C). (b) MALDI MS spectrum of oligo(L-**1**) initiated by BnOH ([L-**1**]/[**Zn-1**]/[**Mn-1**]/[BnOH] = 15/1/1/1, -15 °C), together with the raw data of MALDI peaks.

2.2.4 Homopolymerization and copolymerization of OCAs

Using the optimized conditions, we evaluated the effect of the initial [L-**1**]/[Mn]/[Zn] feed ratio on the M_n of the poly(L-**1**) product and found that M_n increased linearly as the feed ratio was increased up to 1500/1/1 (**Figure 2.6**), further indicative of a controlled ROP process. The resultant polyester exhibited unimodal and narrow $Đ$ (**Figure 2.7**) suggesting that chain-breaking reactions did not occur during the polymeirzation[15], and the M_n was very close to our calculated value (**Figure 2.6**). At the FR of 1500, the resulting product had a M_n of 204.7 kDa, which is higher than amy other reported values for the ROP of OCAs.[2, 4, 16] No evidence of epimerization of the α-methine hydrogen was observed in the homodecoupled ^{1}H NMR spectrum (**Figure 2.8**) of a high-MW poly(L-**1**).

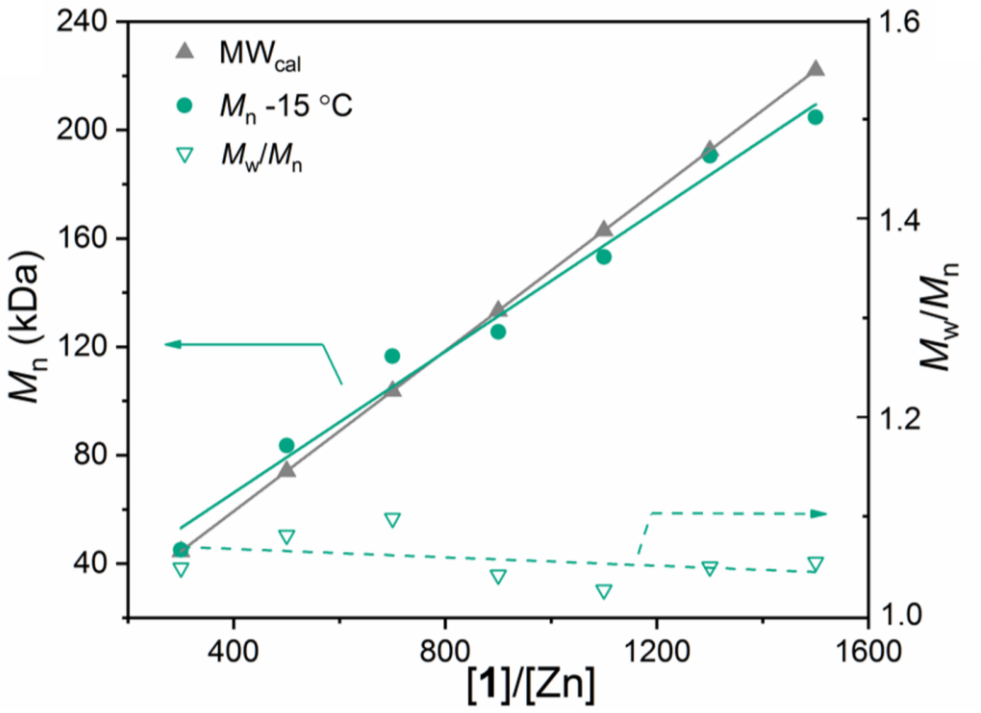

Figure 2.6 Plots of M_n and MW distribution (M_w/M_n) of poly(L-**1**) versus [L-**1**]/[Zn] ratio at −15 °C ([**Mn-1**]/[**Zn-1**]/[BnOH] = 1/1/1).

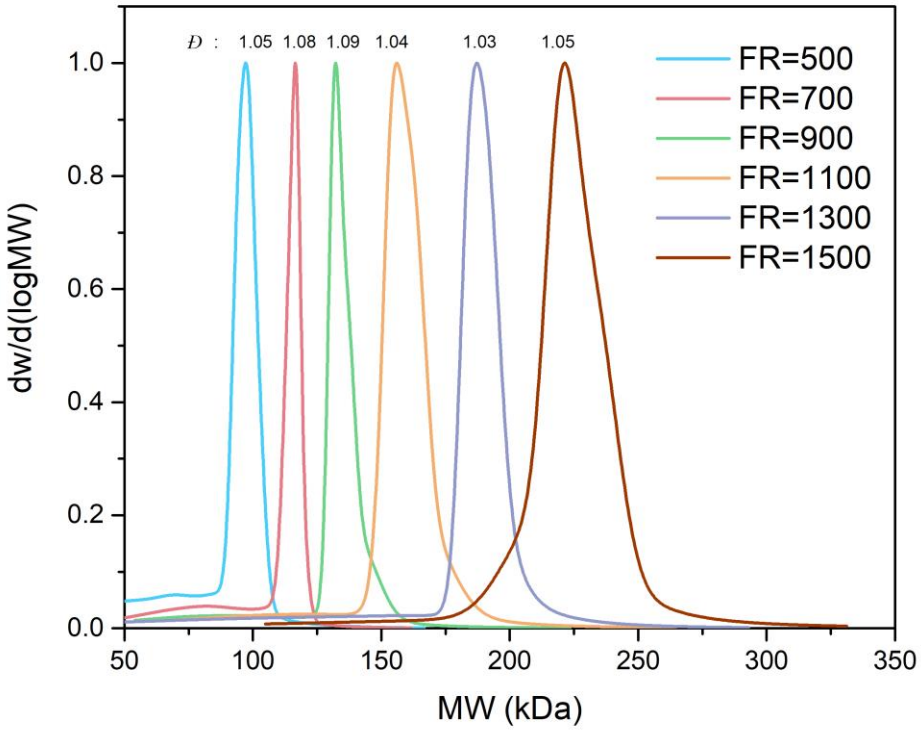

Figure 2.7 GPC overlays of poly(L-**1**) at different feed ratios (FR, [L-**1**]/[**Zn-1**]) as shown in Figure2.6. Note that the y axis is the raw data of dw/dlogM, which is the normalized distribution of molecular weights (MWs) at each time slice and is used for the MW distribution calculation in GPC. The data clearly indicate the narrow MW distribution of the obtained polymers.

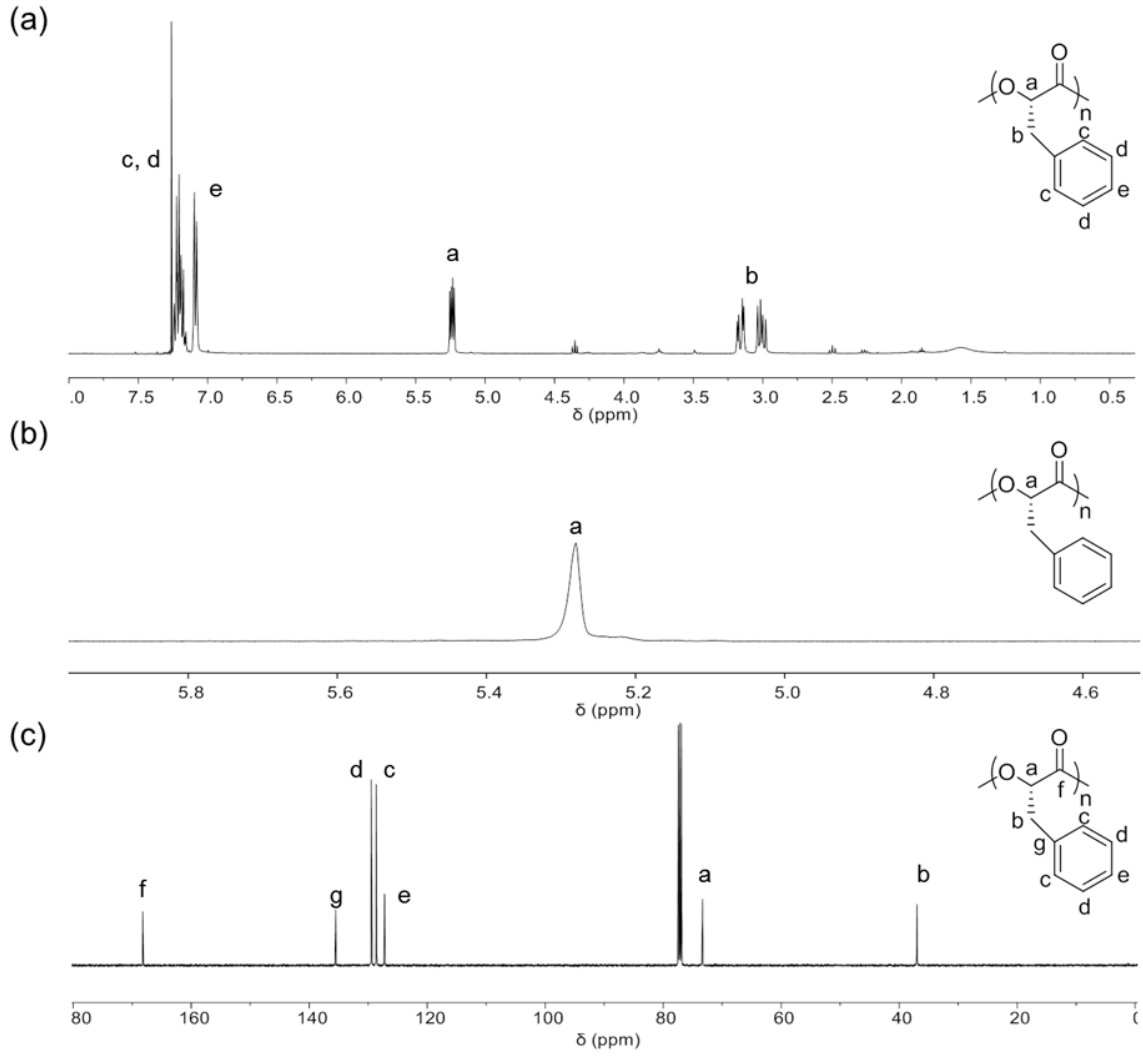

Figure 2.8 NMR spectra of poly(L-**1**) in $CDCl_3$ ([L-**1**]/[**Zn-1**]/[**Mn-1**]/[BnOH] = 1300/1/1/1, M_n = 190.5 kDa, $Đ$ = 1.05). (a) ^{1}H NMR spectrum; (b) Homodecoupling ^{1}H NMR spectrum; (c) ^{13}C NMR spectrum.

In addition, to evaluate the versatility of the redox Mn/Zn catalytic system, the ROP reactions of four other OCA monomers were carried out (see **Figure 1.4** for the structures of **2**–**5**, **Table 2.6** for ROP results). In all cases, polymers were obtained with excellent polymerization control, similar to that for poly(L-**1**). All the M_n values were close to the calculated MWs, and the $Đ$ values were <1.1. Epimerization at the α-methine hydrogen did not occur (**Figures 2.9-2.12**). However, considerable epimerization of L-**5** is often observed when using organocatalysts for ROP.[17]

Furthermore, due to the living polymerizaiton, diblock and triblock copolymers were readily prepared in one pot by sequential addition of the monomers, and remarkable control of the M_n and $Đ$ values were achieved (**Table 2.7**, **Figure 2.13-2.23**). Due to the simplicity of the polymerization process, the polymer production could be easily scaled up to over 5 g, as shown in **Figure 2.24**, allowing for the fabrication of polymer specimens in sufficient quantities to systematically studies their physical properties (*see Chapter 5*).

Table 2.6 Controlled ring-opening polymerization of various *O*-carboxyanhydrides

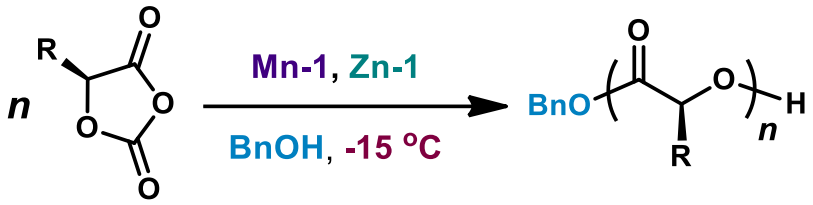

Entry	Monomer	FR	Time (h)	Conv. (%)	M_n (kDa)[c]	MW_{cal} (kDa)	$Đ$
1	L-**2**	400	2	100	66.1	71.3	1.04
2	L-**2**	600	24	100	94.7	106.9	1.01
3	L-**3**	400	1	100	84.0	88.1	1.04
4	L-**3**	700	1	100	133.8	154.3	1.02
5	L-**4**	400	1	100	26.2	28.9	1.07
6	L-**4**	600	1	100	40.6	43.3	1.01
7	L-**5**	400	1	100	54.7	54.1	1.06
8	L-**5**	500	1	100	58.3	67.1	1.01

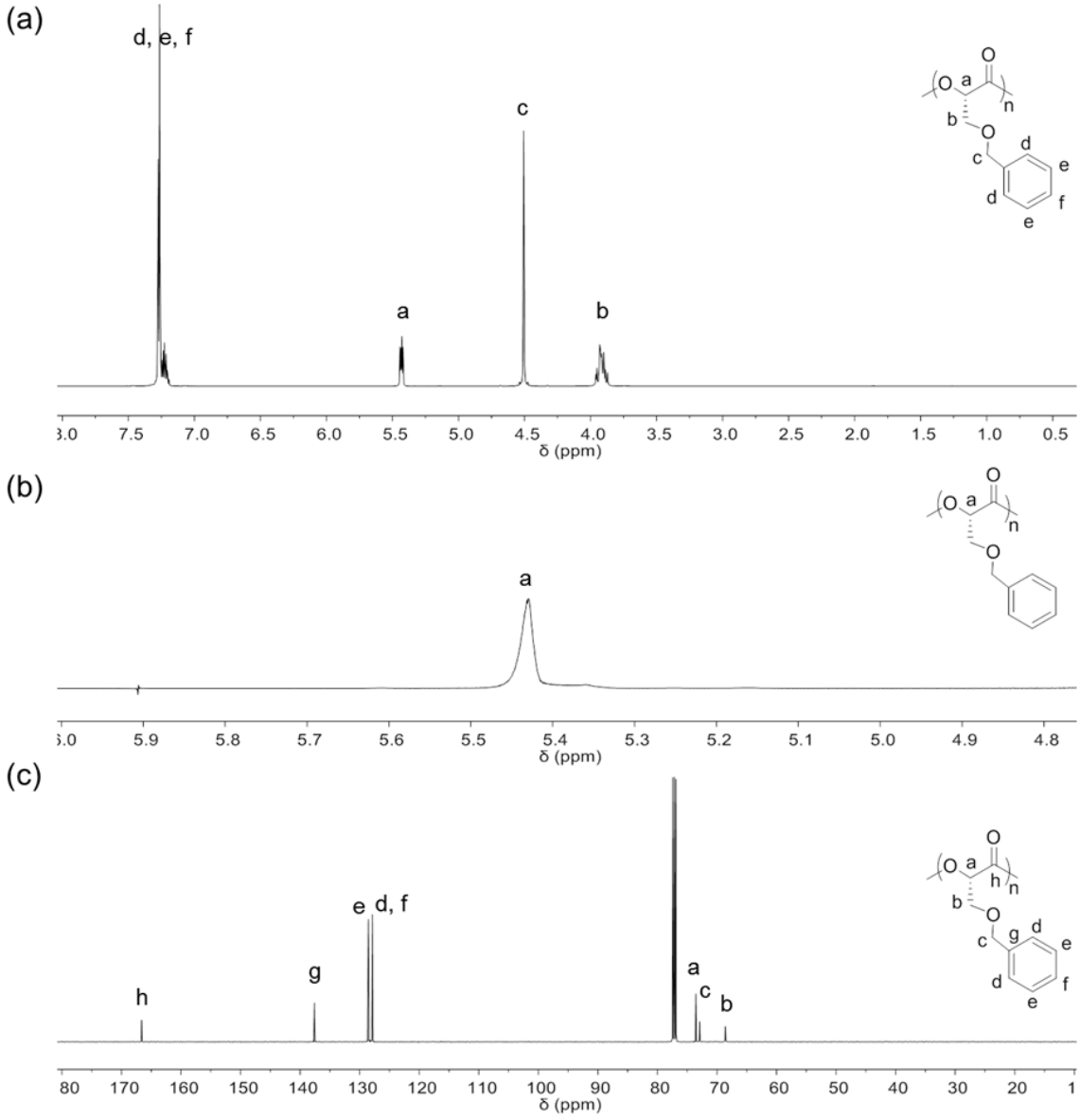

Figure 2.9 NMR spectra of poly(L-**2**) in $CDCl_3$ (Table 2.6, entry 2). (a) ^1H NMR spectrum; (b) Homodecoupling ^1H NMR spectrum; (c) ^{13}C NMR spectrum.

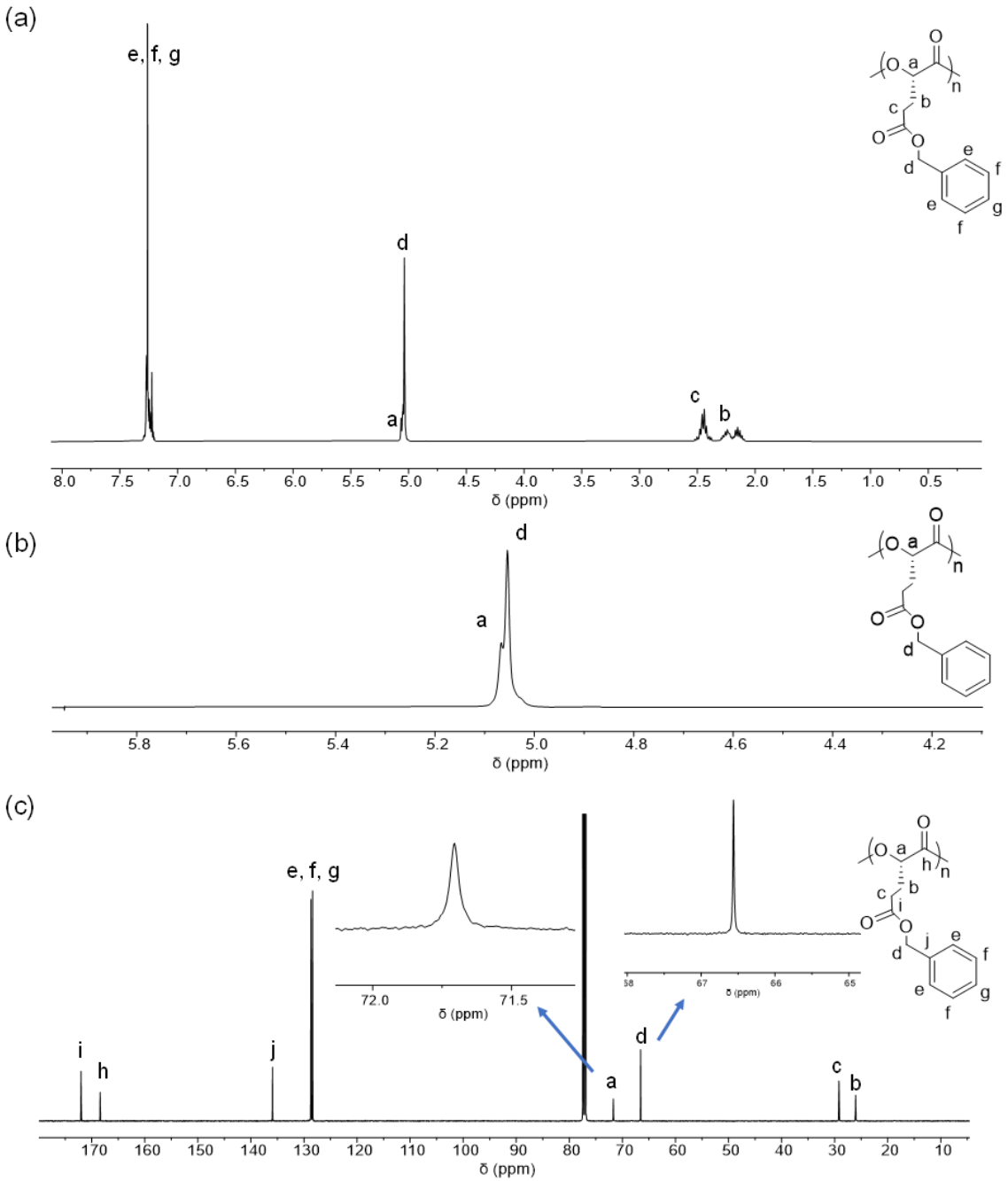

Figure 2.10 NMR spectra of poly(L-**3**) in $CDCl_3$ (Table 2.6, entry 4). (a) ^{1}H NMR spectrum; (b) Homodecoupling ^{1}H NMR spectrum; (c) ^{13}C NMR spectrum**.**

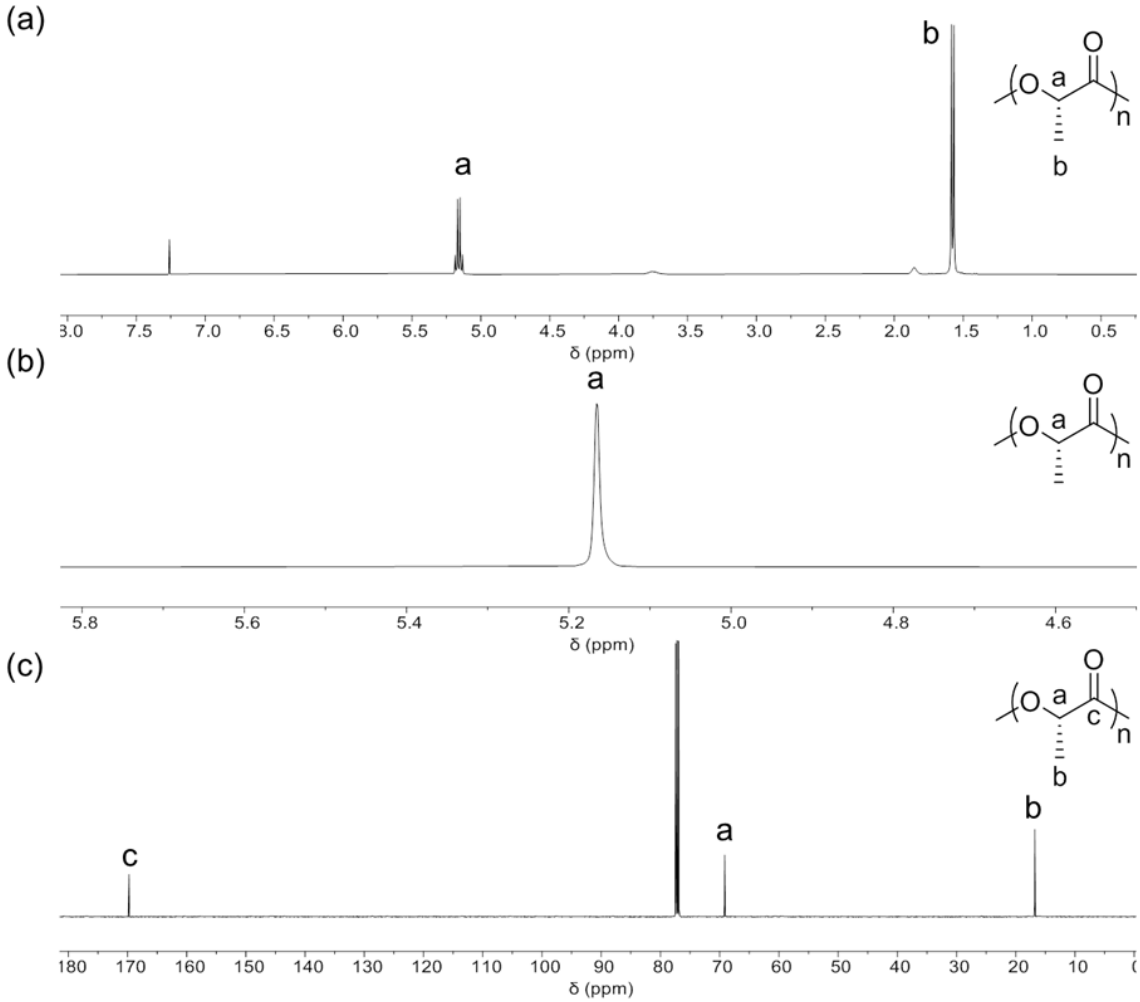

Figure 2.11 NMR spectra of poly(L-**4**) in $CDCl_3$ (Table 2.6, entry 6). (a) ^{1}H NMR spectrum; (b) Homodecoupling ^{1}H NMR spectrum; (c) ^{13}C NMR spectrum.

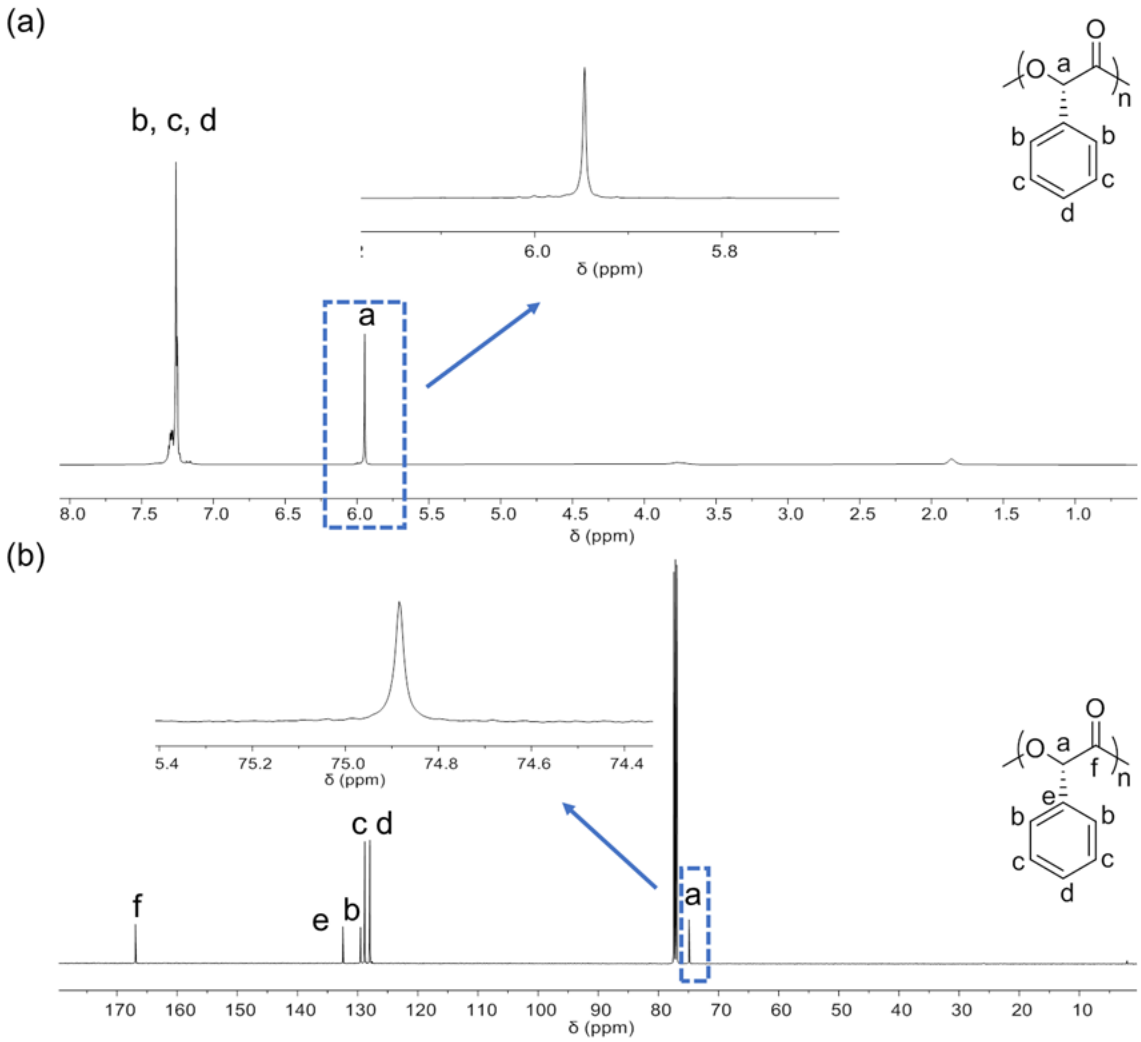

Figure 2.12 NMR spectra of poly(L-**5**) in $CDCl_3$ (Table 2.6, entry 8). (a) ^{1}H NMR spectrum; (b) ^{13}C NMR spectrum.

Table 2.7 Block copolymerization of various *O*-carboxyanhydrides

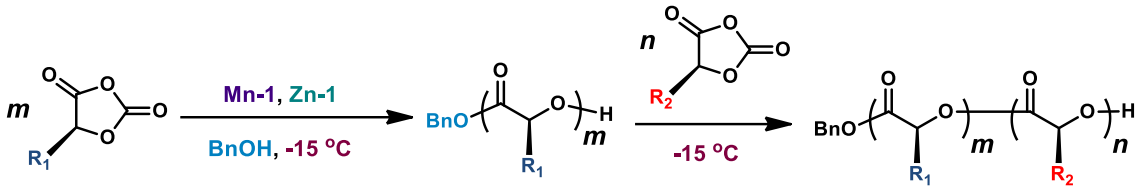

Entry	Monomer	FR	Time (h)	Conv. (%)	M_n (M_n-b1) (kDa)	MW_{cal} (MW_{cal}-b1) (kDa)	$Đ$ ($Đ$-b1)
1	**1/2**	400/200	0.5/1	100	93.0 (68.3)	94.9(59.3)	1.04(1.09)
2	**1/3**	400/200	0.5/1	100	101.7(68.3)	103.4(59.3)	1.07(1.09)
3	**1/4**	400/200	0.5/1	100	74.0 (68.3)	73.7 (59.3)	1.07(1.09)
4	**1/5**	400/200	0.5/96	100	87.3 (68.3)	86.1 (59.3)	1.09(1.09)
5	**1/5**	400/100	0.5/1	100	76.4 (68.3)	72.7 (59.3)	1.08(1.09)
6	**2/3**	200/200	1/1	100	72.2 (33.6)	79.8 (35.7)	1.05(1.07)
7	**2/4**	200/200	2/1	100	51.2 (33.6)	50.2 (35.7)	1.07(1.07)
8	**2/5**	200/200	1/96	100	67.8 (33.6)	62.5 (35.7)	1.09(1.07)
9	**2/5**	200/100	1/1	100	52.3 (33.6)	49.1(35.7)	1.09(1.07)
10	**3/4**	200/200	1/1	100	63.0 (48.8)	58.6 (44.2)	1.09(1.08)
11	**3/5**	200/100	1/1	100	52.8 (48.8)	57.6 (44.2)	1.09(1.08)
12	**5/3**	100/200	1/1	100	51.6 (17.1)	57.6 (13.5)	1.09(1.09)
13	**5/4**	100/200	1/1	100	25.1 (17.1)	27.9 (13.5)	1.06(1.09)
14	**1/3/4**	200/200/200	0.5/1/1	100	87.4 (26.5)	88.2 (29.7)	1.04(1.05)

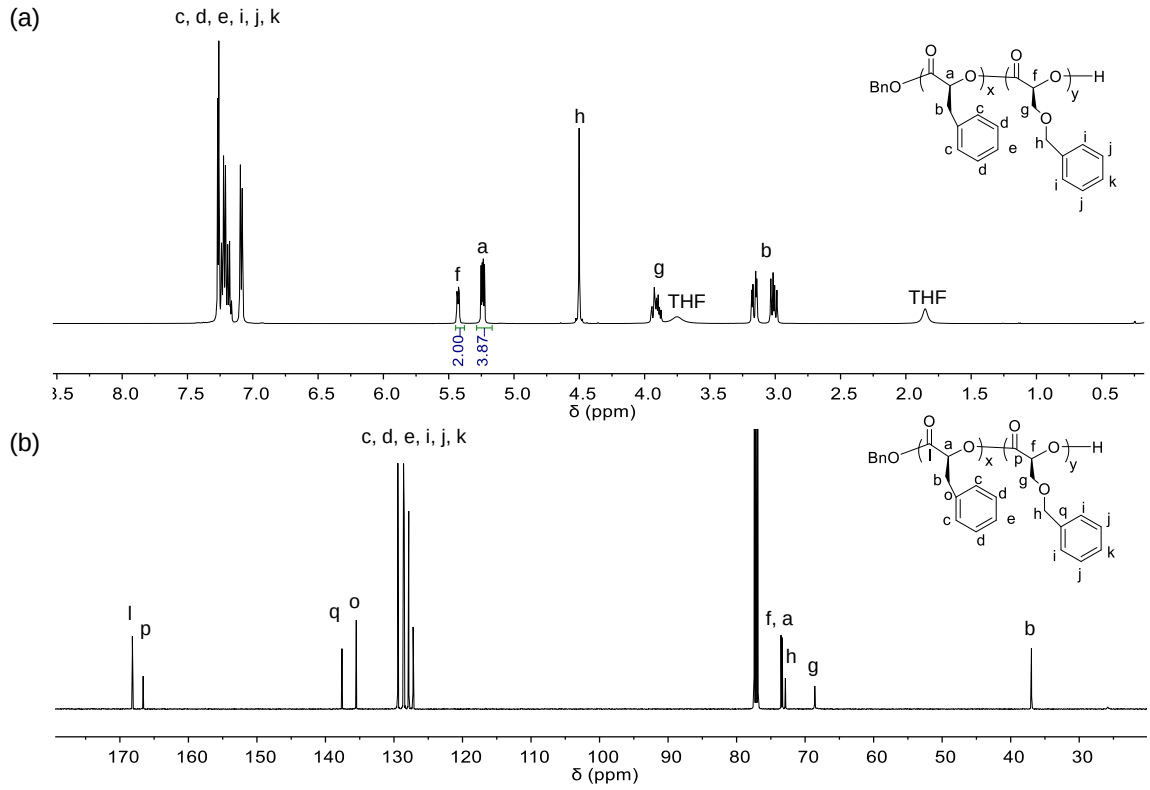

Figure 2.13 NMR spectra of poly(L-**1**-*b*-L-**2**) in $CDCl_3$ (Table 2.7, entry 1). (a) ^{1}H NMR spectrum; (b) ^{13}C NMR spectrum.

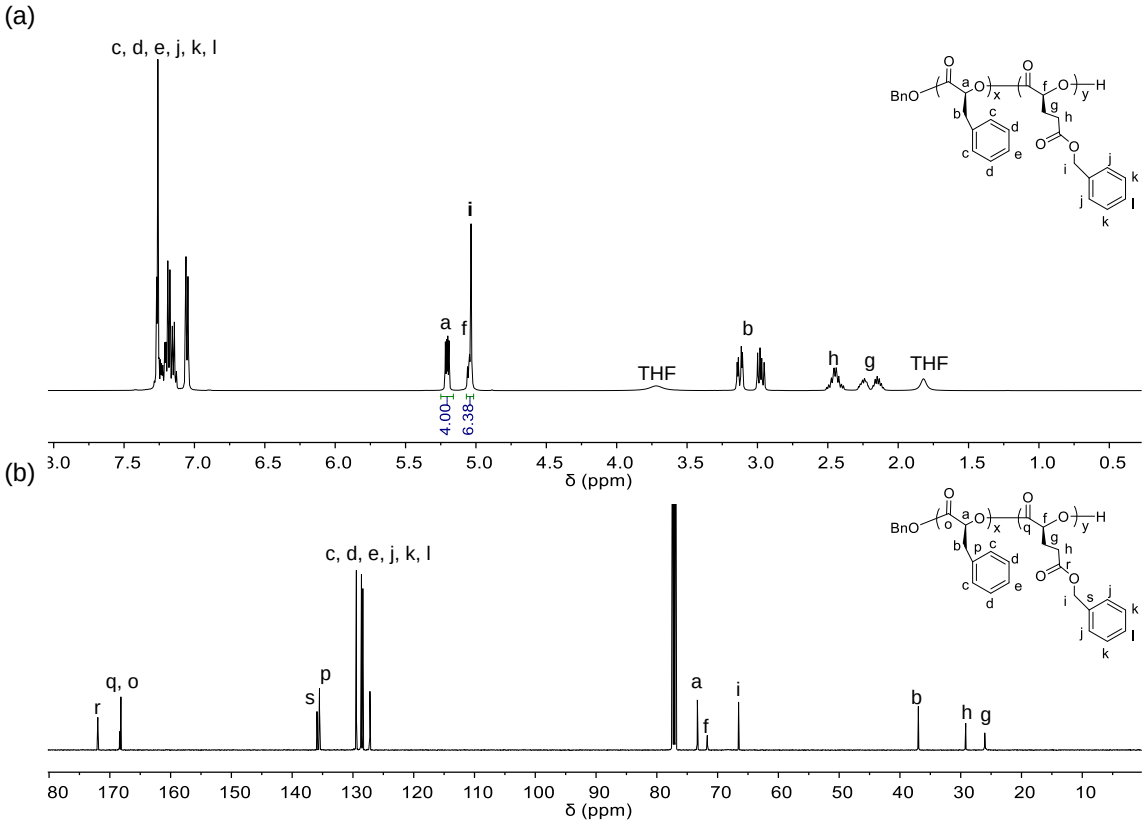

Figure 2.14 NMR spectra of poly(L-**1**-*b*-L-**3**) in $CDCl_3$ (Table 2.7, entry 2). (a) ^{1}H NMR spectrum; (b) ^{13}C NMR spectrum.

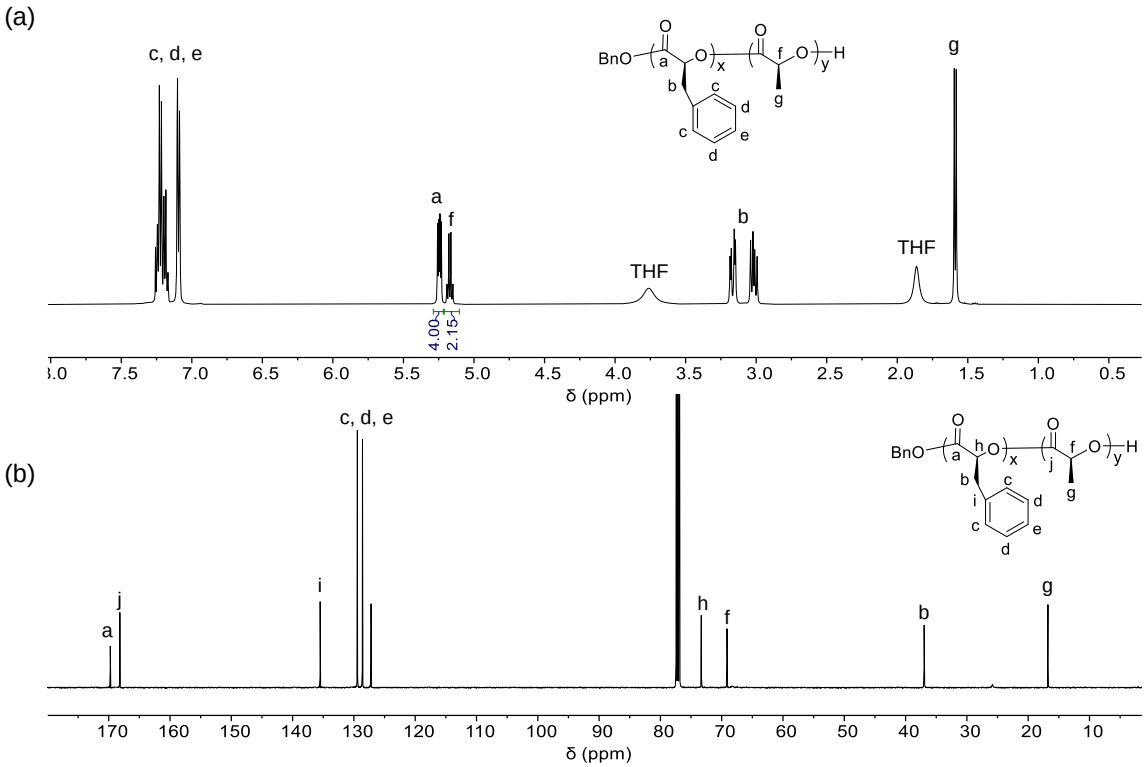

Figure 2.15 NMR spectra of poly(L-**1**-*b*-L-**4**) in $CDCl_3$ (Table 2.7, entry 3). (a) ^{1}H NMR spectrum; (b) ^{13}C NMR spectrum.

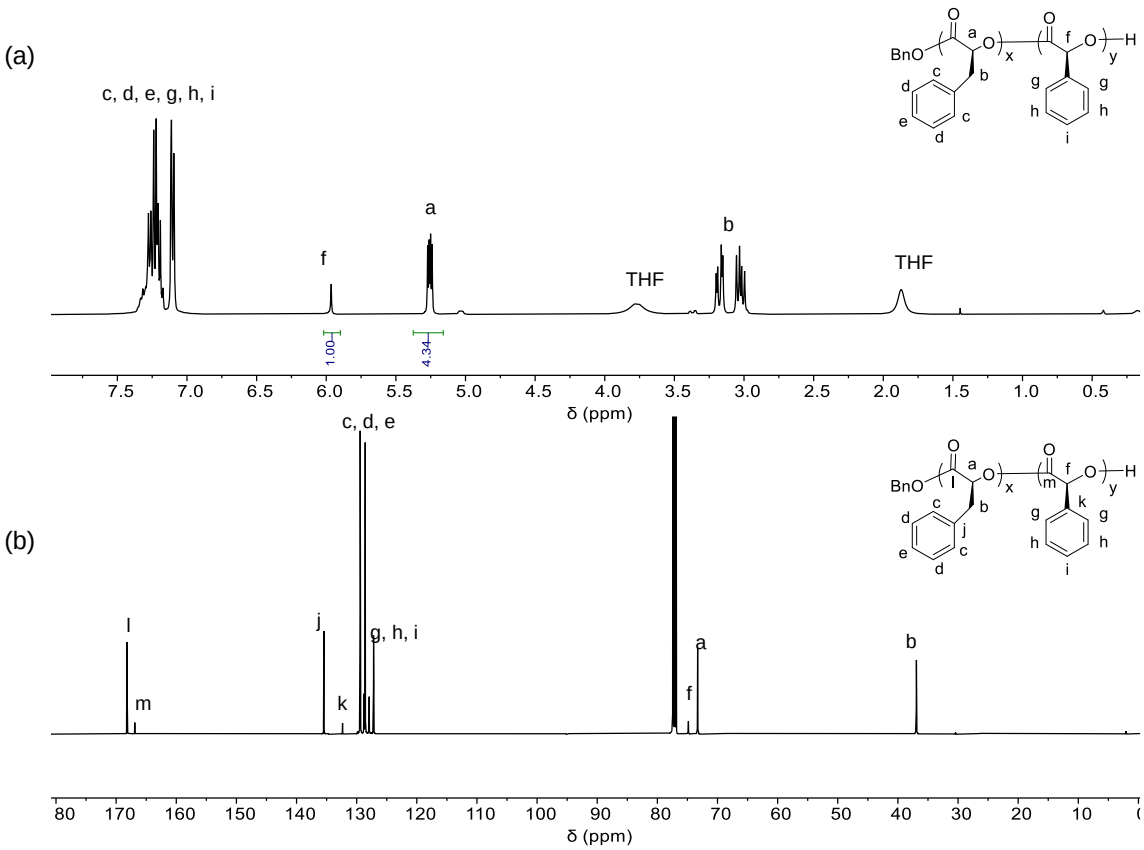

Figure 2.16 NMR spectra of poly(L-**1**$_{400}$-*b*-L-**5**$_{100}$) in $CDCl_3$ (Table 2.7, entry 5). (a) ^1H NMR spectrum; (b) ^{13}C NMR spectrum.

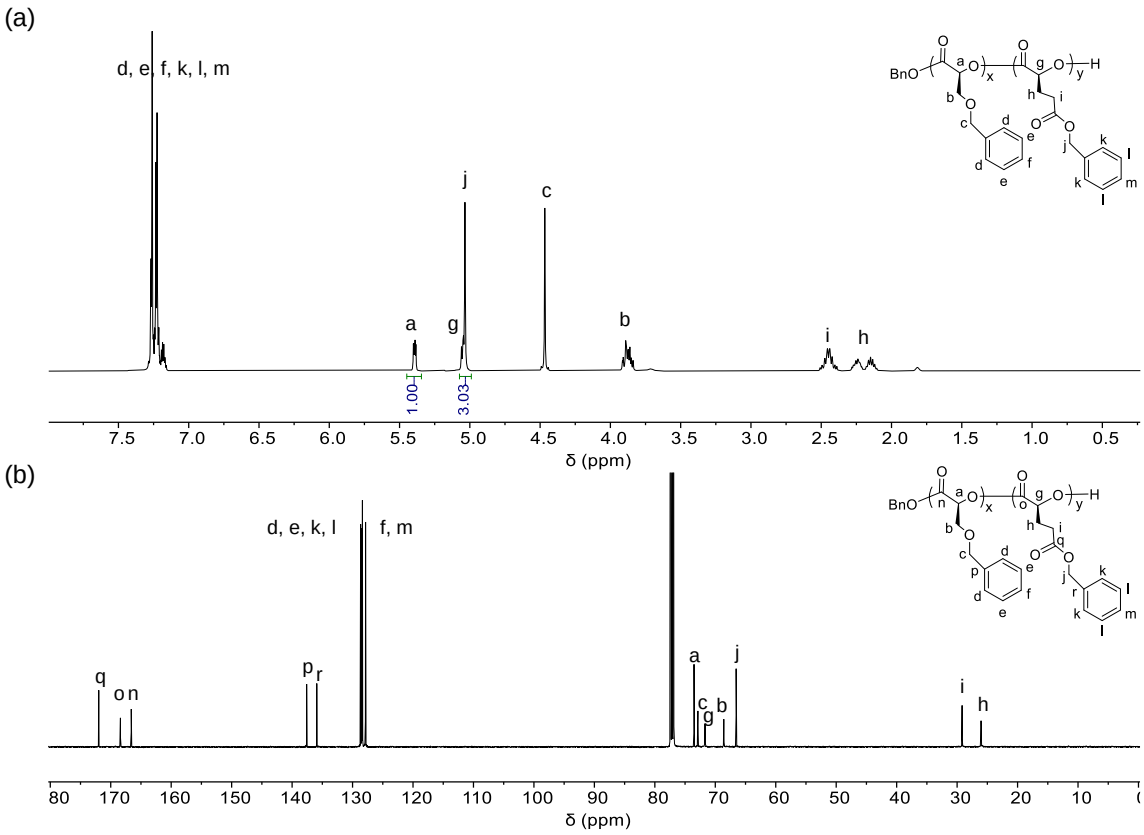

Figure 2.17 NMR spectra of poly(L-**2**-*b*-L-**3**) in $CDCl_3$ (Table 2.7, entry 6). (a) ^{1}H NMR spectrum; (b) ^{13}C NMR spectrum.

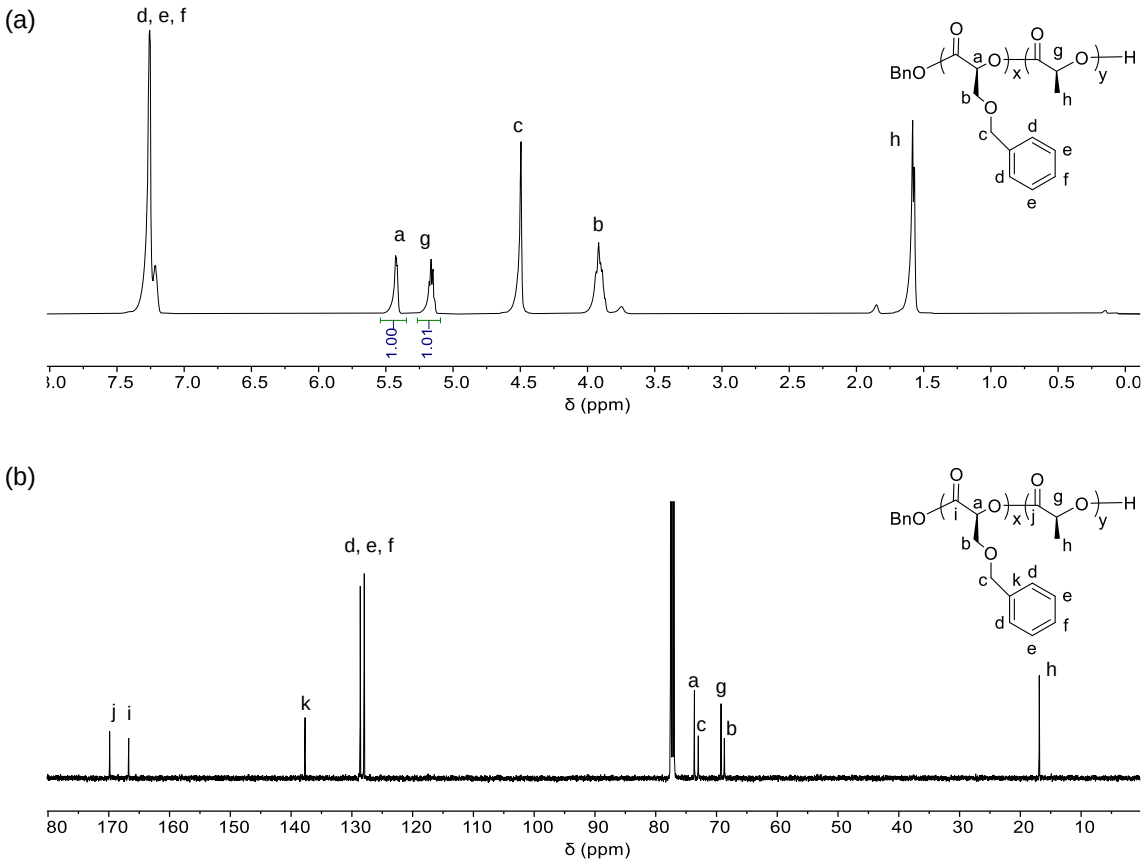

Figure 2.18 NMR spectra of poly(L-**2**-*b*-L-**4**) in $CDCl_3$ (Table 2.7, entry 7). (a) ^1H NMR spectrum; (b) ^{13}C NMR spectrum.

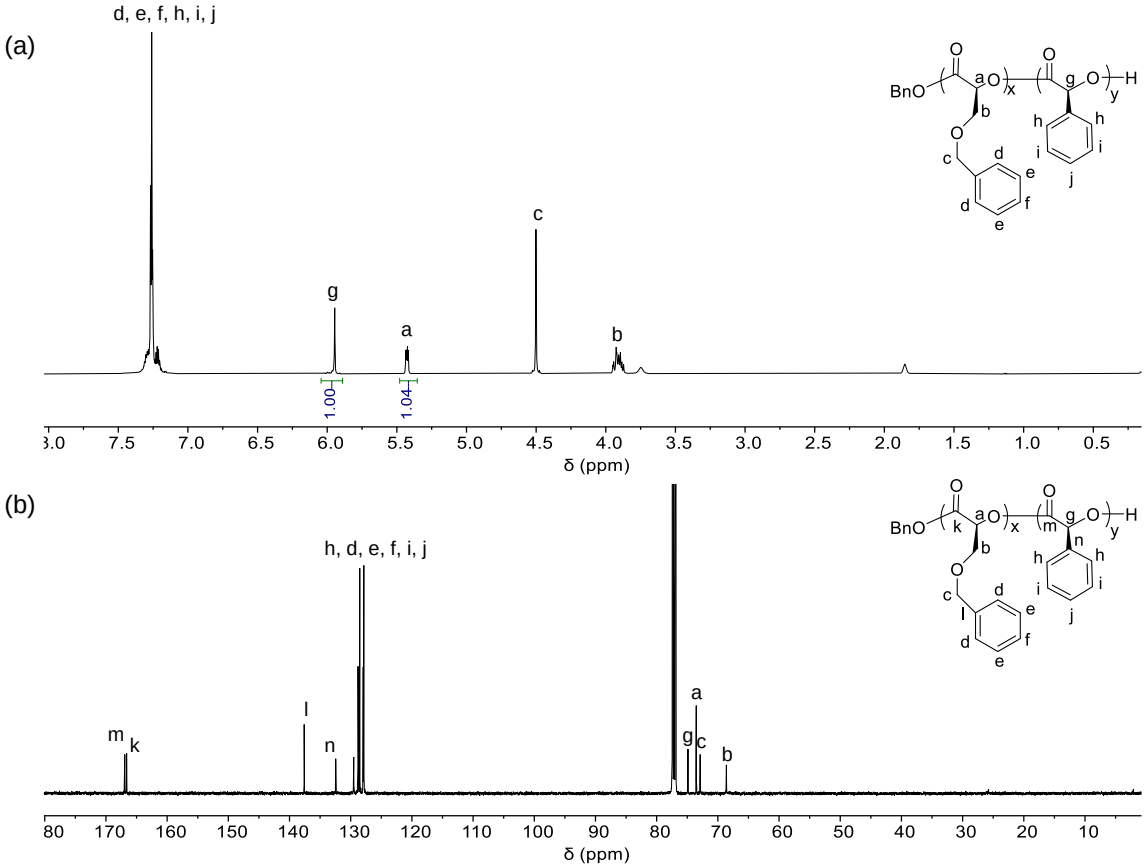

Figure 2.19 NMR spectra of poly(L-**2**-*b*-L-**5**) in $CDCl_3$ (Table 2.7, entry 8). (a) ^{1}H NMR spectrum; (b) ^{13}C NMR spectrum.

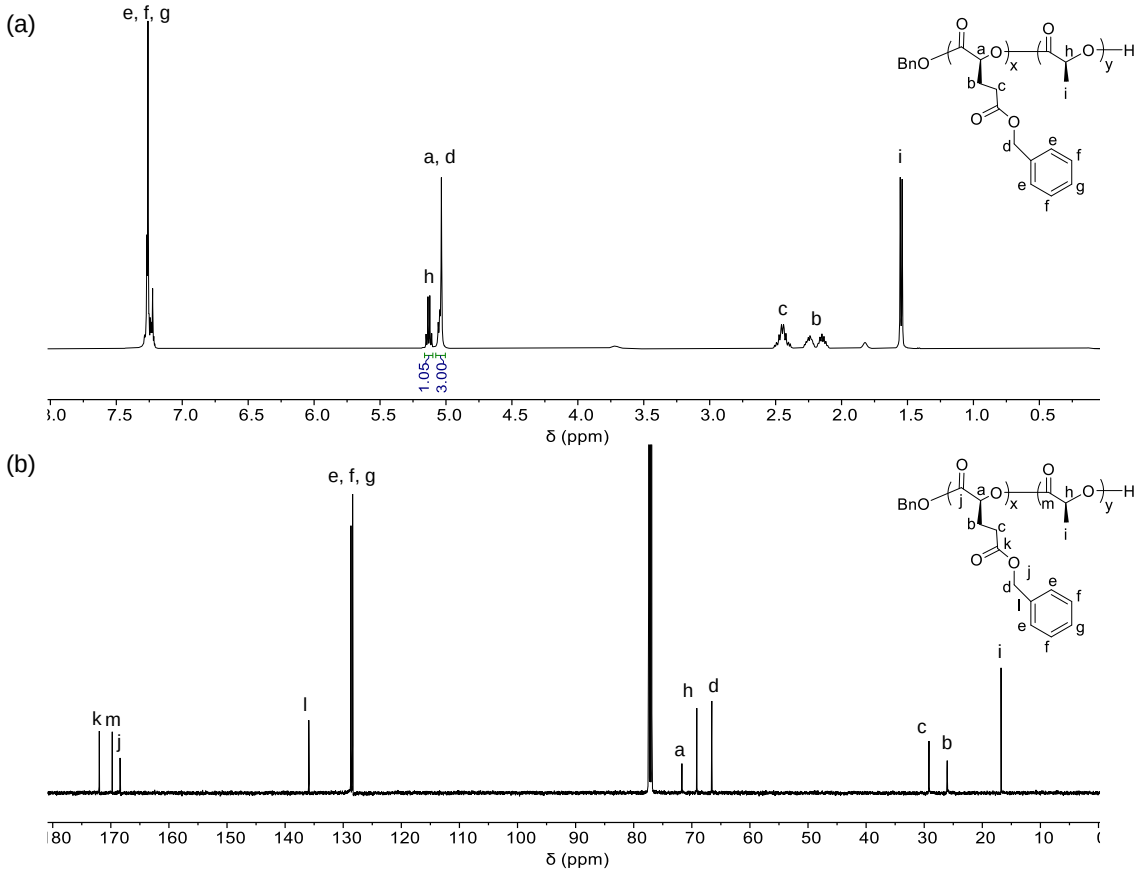

Figure 2.20 NMR spectra of poly(L-**3**-*b*-L-**4**) in $CDCl_3$ (Table 2.7, entry 10). (a) ^{1}H NMR spectrum; (b) ^{13}C NMR spectrum.

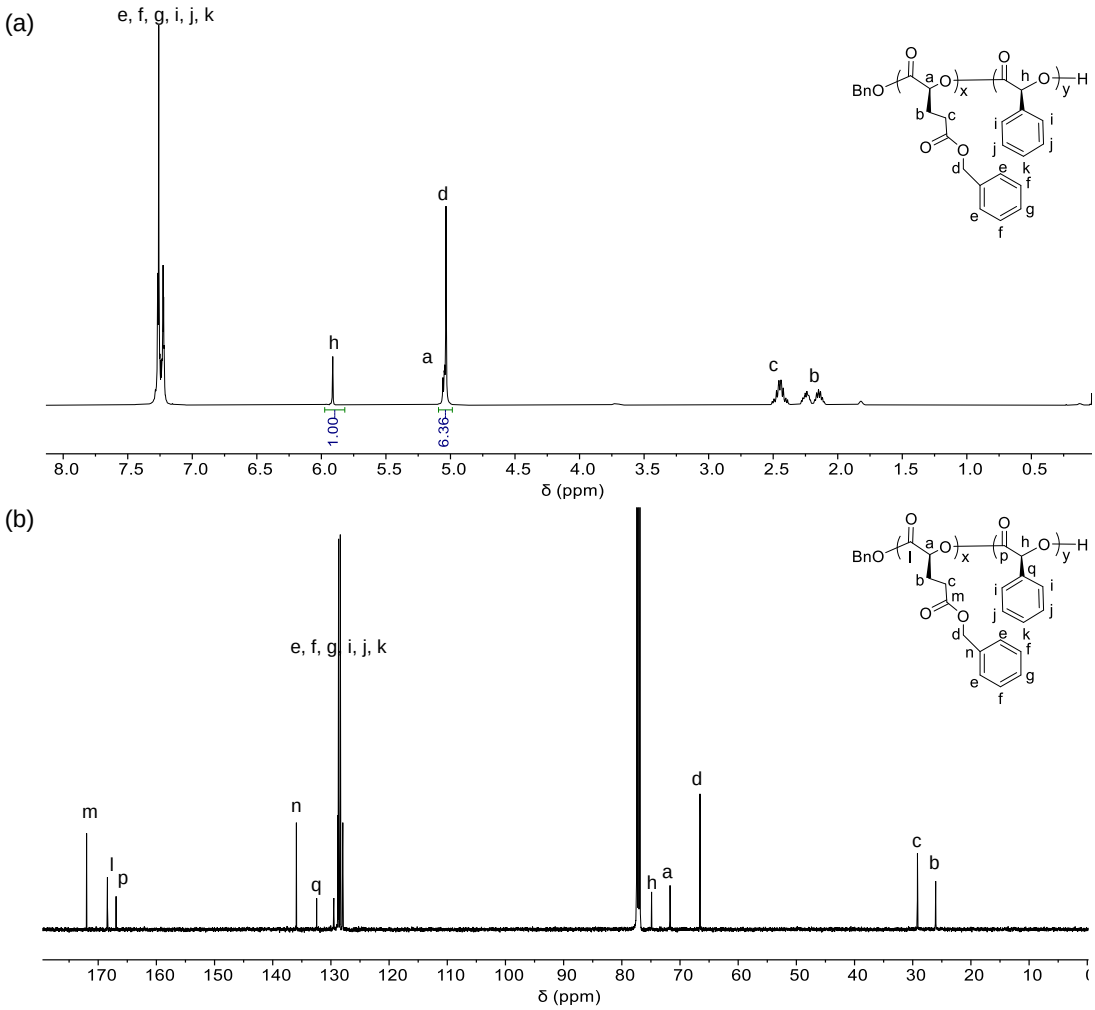

Figure 2.21 NMR spectra of poly(L-**3**-*b*-L-**5**) in $CDCl_3$ (Table 2.7, entry 11). (a) ^{1}H NMR spectrum; (b) ^{13}C NMR spectrum.

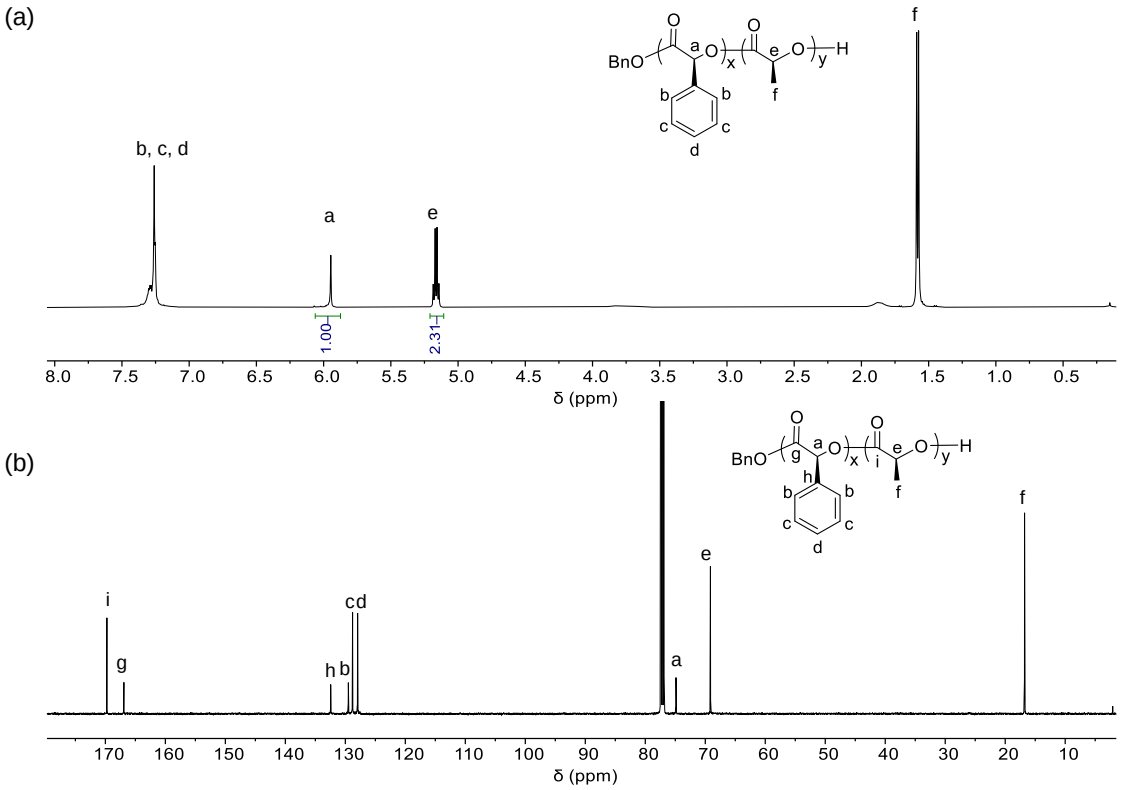

Figure 2.22 NMR spectra of poly(L-**5**-*b*-L-**4**) in $CDCl_3$ (Table 2.7, entry 13). (a) ^{1}H NMR spectrum; (b) ^{13}C NMR spectrum.

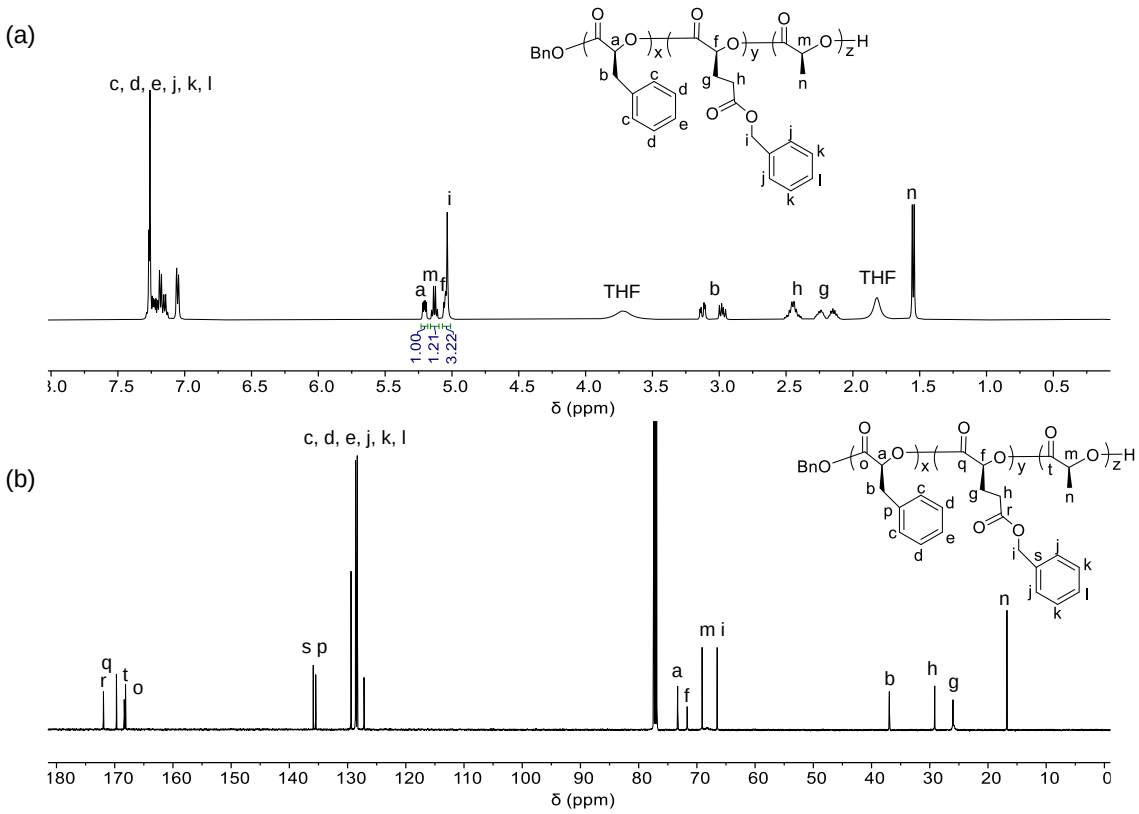

Figure 2.23 NMR spectra of poly(L-**1**-*b*-L-**3**-*b*-L-**4**) in $CDCl_3$ (Table 2.7, entry 14). (a) ^1H NMR spectrum; (b) ^{13}C NMR spectrum.

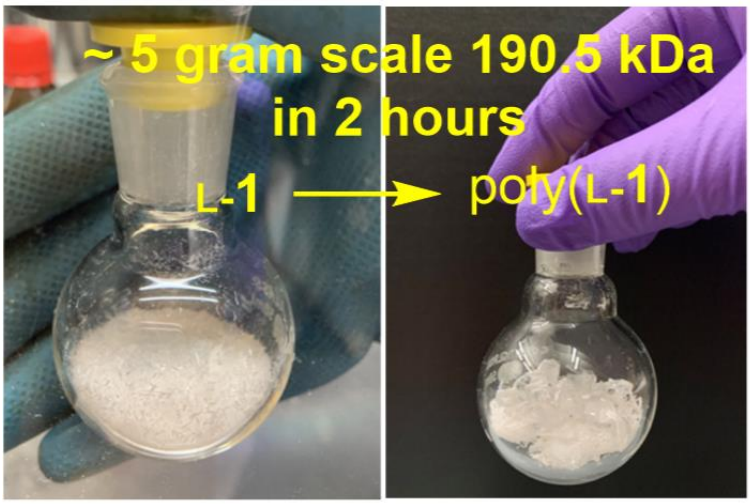

Figure 2.24 Scalable ROP of OCAs to prepare high-molecular-weight polyesters.

2.2.5 Kinetics of ring-opening polymerization of OCA mediated by Mn-1/Zn-1

The kinetics of redox ROP of L-**1** was examined by varying the concentration of each reaction component and monitoring the monomer conversion by Fourier transform infrared (FTIR) spectroscopy. The kinetics is crucial for understanding the mechanism of ring-opening polymerization and making the reaction more controllable. **Figure 2.25** showed that Mn/Zn-mediated ROP of L-**1** at −15 °C exhibited first-order reaction kinetics with a reaction order of 4.60 ± 0.35 (**Figure 2.25b**) at the fixed Mn/Zn ratio of 1/1. The kinetics of ROP was further investigated by varying the concentration of each reaction component (**Figure 2.26**), and we determined that the kinetics of ROP of L-**1** followed an overall kinetic law of the form:

$$-\mathrm{d}[\text{L-}\mathbf{1}]/\mathrm{d}t = k_\mathrm{p}\,[\mathbf{Mn\text{-}1}]^{2.10}[\mathbf{Zn\text{-}1}]^{2.51}[\text{L-}\mathbf{1}]^{1} \qquad (1)$$

where k_p is the rate constant of chain propagation.

It is noted that the reaction order was 4.60 ± 0.35 (R^2 = 0.98) for both **Mn-1** and **Zn-1** catalysts at the same concentration (**Figure 2.25b**). The value is close to the sum of the individual reaction order of **Mn-1** (2.10 ± 0.11, R^2 = 0.99) (**Figure 2.26b**) and **Zn-1** (2.51 ± 0.08, R^2 = 0.99) (**Figure 2.26d**), suggesting there was no complex formed between each of them. **Figure 2.26e** revealed that BnOH did not affect the polymerization rate, which was in accord with the mechanism that BnOH only interacted with Zn to form Zn-alkoxide complex to initiate the ROP.

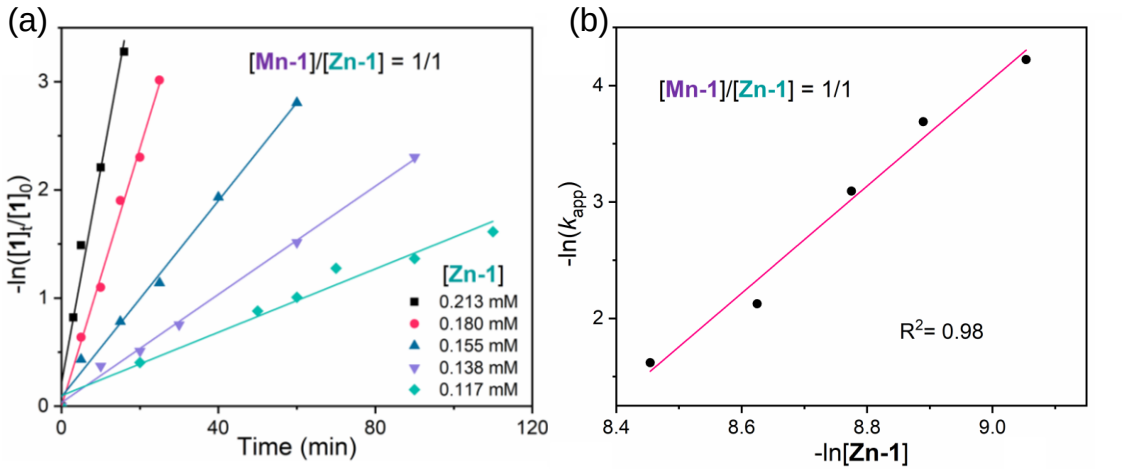

Figure 2.25 (a) Plots of L-**1** conversion versus time at various **Zn-1** concentrations. [L-**1**] = 0.150 M; [**Mn-1**]/[**Zn-1**]/[BnOH] = 1/1/1. (b) Plot of -ln(k_{app}) versus –ln[Zn] for ROP of L-**1**. [L-**1**] = 150.0 mM; [**Mn-1**]/[**Zn-1**]/[BnOH] = 1/1/1.

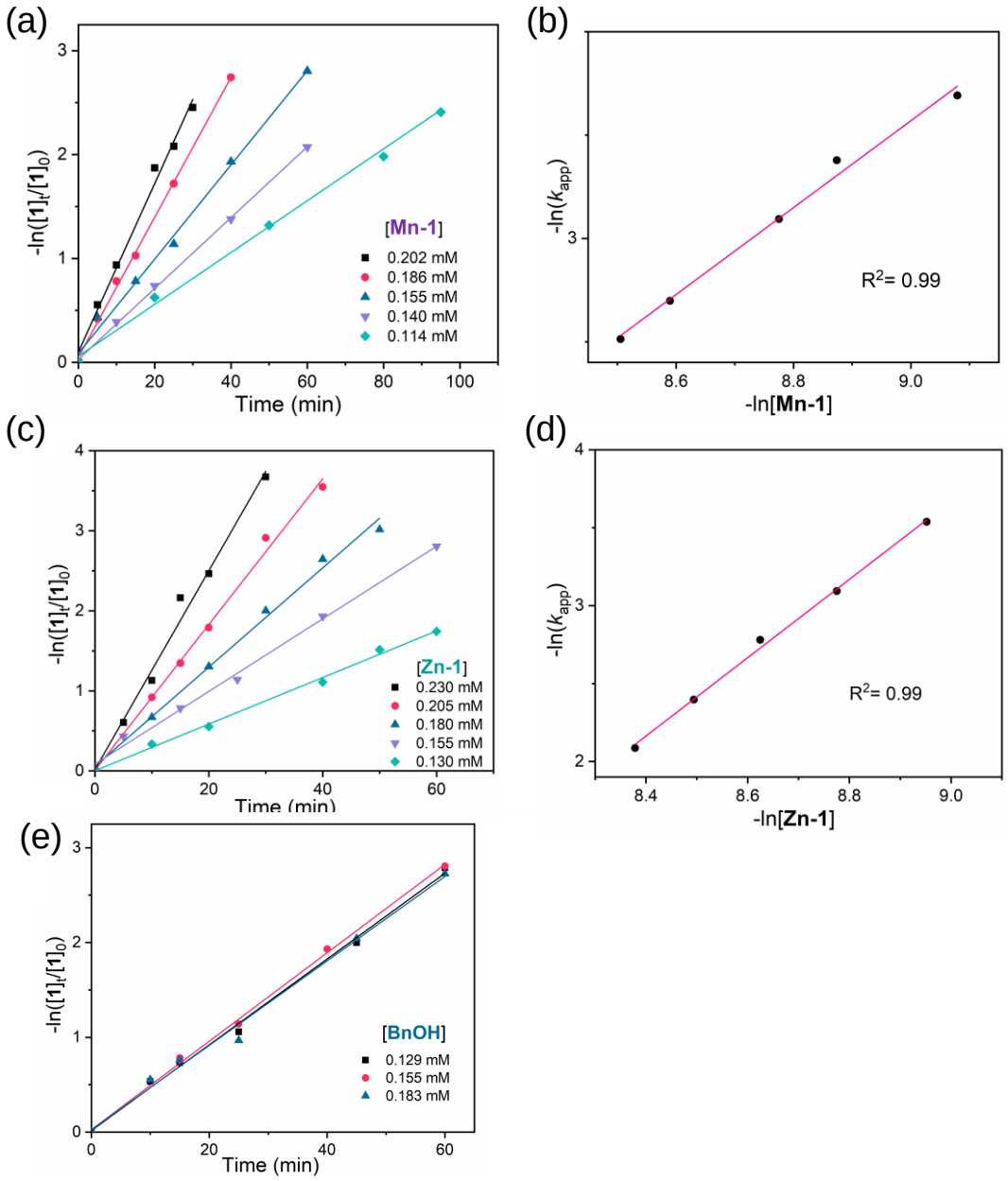

Figure 2.26 (a, c, e) Kinetic plots of the ROP of L-**1** with the variation of the noted catalyst, and the rest catalytical component was fixed at 0.155 mM. [L-**1**] = 150.0 mM. (b, d) Plot of -ln(k_{app}) versus –ln[catalyst] for ROP of L-**1**. The slope of which suggests the reaction order.

2.2.6 Mechanistic Studies

We drew upon our knowledge of the mechanisms of the photoredox ROP[2] and electrochemical ROP by Co/Zn[4] to develop the redox ROP mechanism. The catalytic cycle starts with the oxidative addition of **Mn-1** to the OCA to form the Mn^{IV} species **A** (**Scheme 1**). Unlike the Co complex used in our electrochemical ROP,[4] which exhibited only one reversible redox wave in cyclic voltammetry measurements ($E_{1/2}^{red}[Co^{III}/Co^{II}]$ = 0.77 V vs SCE [saturated calomel electrode], where $E_{1/2}^{red}$ is the redox half-wave potential),[4] **Mn-1** exhibited two quasi-reversible redox waves: $E_{1/2}^{red}[Mn^{III}/Mn^{II}]$ = 0.60 V and $E_{1/2}^{red}[Mn^{IV}/Mn^{III}]$ = 1.15 V versus SCE (**Figure 2.27**). The formation of Mn^{IV} species **A** (**Scheme 1**) was supported by the observation that the $E_{1/2}^{red}[Mn^{III}/Mn^{II}]$ peak had disappeared almost completely within 5 min after the start of the ROP of a L-**1**/**Mn-1**/**Zn-1**/BnOH (1000/1/1/1) mixture at −15 °C, whereas the $E_{1/2}^{red}[Mn^{IV}/Mn^{III}]$ peak (1.22 V) persisted throughout the ROP (**Figure 2.27b**). Given the oxidation potential of amino acid carboxylates (e.g., $E_{1/2}^{red}$ = 0.83 V versus SCE for *N*-(carbobenzyloxy)-L-phenylalanine) and literature reports,[6, 18] the single-electron transfer (Mn^{IV}/Mn^{III}) process is likely to be thermodynamically favored over the two-electron transfer process (Mn^{IV}/Mn^{II}).[19, 20]

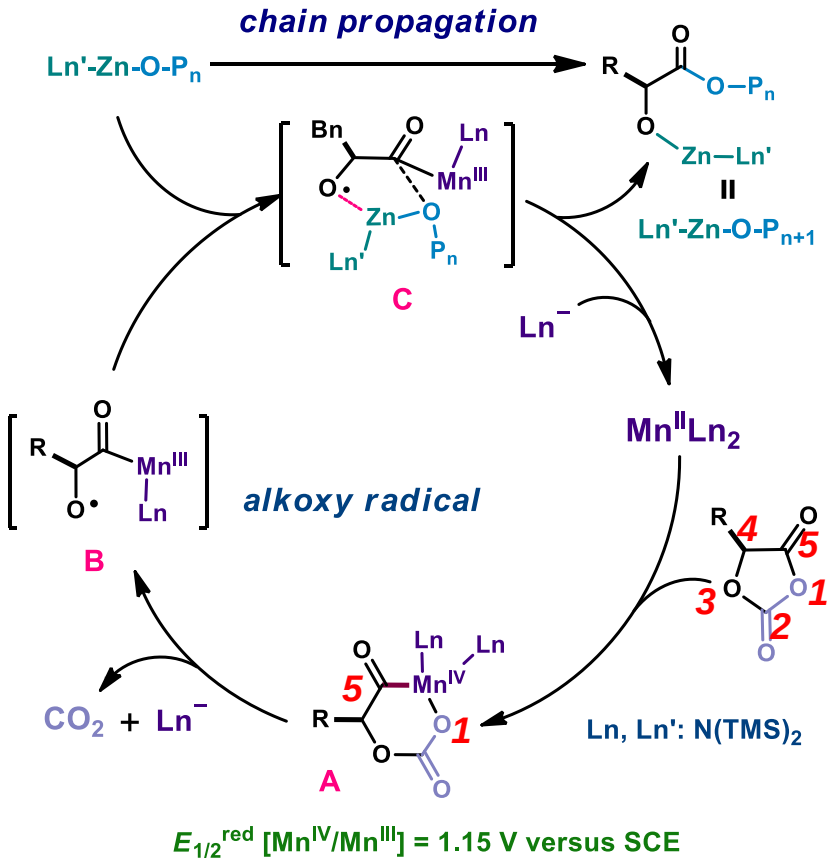

Scheme 1 Proposed Mechanism of Mn/Zn-mediated controlled ring-opening polymerization of *O*-carboxyanhydrides (OCAs)

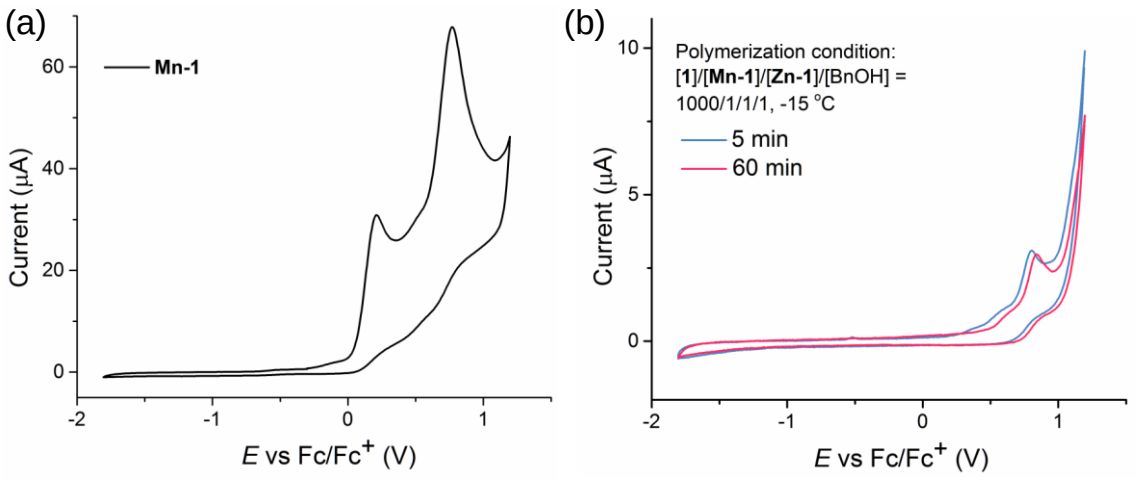

Figure 2.27 Cyclic voltammetry of (a) **Mn-1**, (b) the ring-opening reaction mixtures of L-**1** at -15 °C mediated by **Mn-1**/**Zn-1** ([L-**1**]/[**Mn-1**]/[**Zn-1**]/[BnOH] = 1000/1/1/1). Scan rate: 50 mV/s; solvent: 0.1 M TBAH (tetra-*n*-butylammonium hexafluorophosphate) in THF.

We further investigated the ring-opening process by analyzing the reaction of an L-**1**/**Mn-1**/**Zn-1**/BnOH (1/1/1/1) mixture at −15 °C via ESI-MS (**Figure 2.28a**), which revealed the presence of BnO-terminated oligomers **G1** and **G2**, thus confirming the necessity of Zn-alkoxide for chain propagation. We noted that the Mn complex is paramagnetic and our attempts to study the reaction by NMR were not successful. Moreover, detection of intermediate **H** and its carbonyl complexes **I1–I3**[21] in the mass spectrum (**Figure 2.28a**) indicated that **Mn-1** inserts regioselectively into L-**1**. The absence of epimerization in poly(L-**1**) (**Figure 2.8**) further confirmed that **Mn-1** was unlikely to have been inserted into the C_4–C_5(O) bond. The formation of Mn(CO) complexes **I1–I3** is probably due to the fact that ESI-MS cannot be conducted in completely anhydrous conditions and that Mn complexes undergo carbonylation in an aqueous solution.[22]

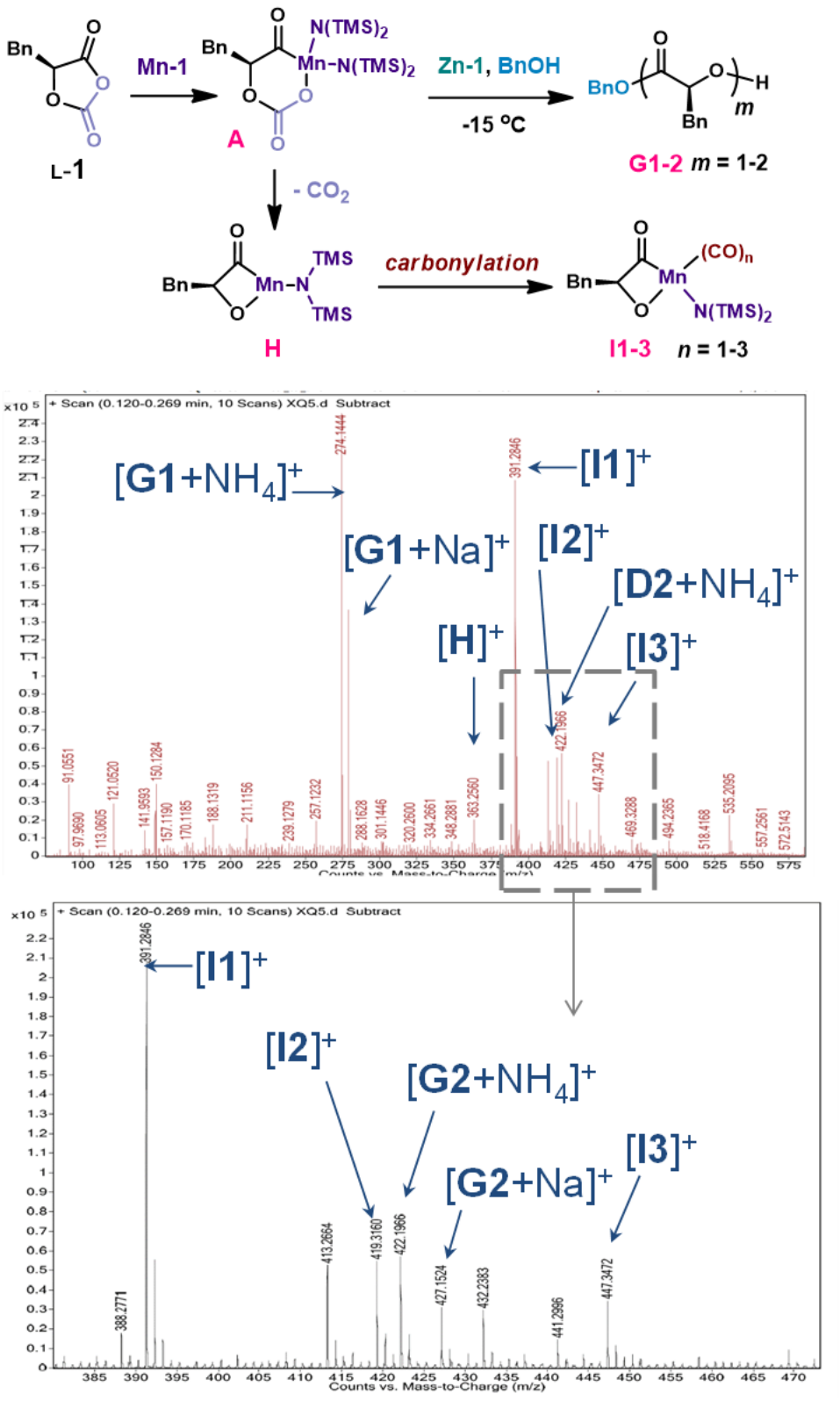

Figure 2.28 The ESI-MS spectrum of the reaction mixture of [L-**1**]/[**Mn-1**]/[**Zn-1**]/[BnOH] = 1/1/1/1/1 (−15 ºC, 30 min).

High-resolution ESI-MS results:

m = 1, [**G1**+NH_4]$^+$ [$C_{16}H_{20}O_3N$]$^+$ calculated: 274.1443; found: 274.1444

[**G1**+Na]$^+$ [$C_{16}H_{16}O_3Na$]$^+$ calculated: 279.0997; found: 279.1570

m = 2, [**G2**+NH_4]$^+$ [$C_{25}H_{28}O_5N$]$^+$ calculated: 422.1967; found: 422.1966

[**G2**+Na]$^+$ [$C_{25}H_{24}O_5Na$]$^+$ calculated: 427.1521; found: 427.1524

[**H**]$^+$ [$C_{15}H_{26}NO_2Si_2Mn$]$^+$ calculated: 363.0883; found: 363.2560

n = 1, [**I1**]$^+$ [$C_{16}H_{26}NO_3Si_2Mn$]$^+$ calculated: 391.0832; found: 391.2846

n = 2, [**I2**]$^+$ [$C_{17}H_{26}NO_4Si_2Mn$]$^+$ calculated: 419.0781; found: 419.3160

n = 3, [**I3**]$^+$ [$C_{18}H_{26}NO_5Si_2Mn$]$^+$ calculated: 447.0730; found: 447.3472

Decarboxylation of **A** furnishes a radical species (**Scheme 1**), as confirmed by our finding that the addition of the radical scavenger 2,2-di(4-*tert*-octylphenyl)-1-picrylhydrazyl (DPPH) markedly inhibited the ROP (**Table 2.8**, entry 2), in a manner similar to that observed for single-electron-transfer reactions involving Ni/Ir photocatalysts.[2, 6, 23] On the basis of our prior studies[2] and literature reports,[23-25] we reasoned that Mn-mediated decarboxylation could result in either alkoxy radical **B** or acyl radical **E** (two corresponding radical reaction pathways in **Figure 2.29a**). Since these putative intermediates would be highly reactive, we added an alkene with an electron-withdrawing group to a reaction mixture containing L-**1**/**Mn-1**/**Zn-1**/BnOH (1/1/1/1) at −15 °C with the goal of capturing and identifying the radical species (**Figure 2.29b**).[26] Monitoring the reaction by ESI-MS (**Figure 2.29c**) revealed the formation of **D**, instead of **F**, indicating that decarboxylation generates an alkoxy radical (**B** in **Scheme 1**).

The alkoxy radical is reportedly difficult to detect by electron paramagnetic resonance spectroscopy (EPR).[27] While the paramagnetic **Mn-1** showed signals in the X-band continuous wave EPR spectrum at 77 K (**Figure 2.30a**), no obvious peaks were found in the mixture of either L-**1**/**Mn-1** (1/1) or L-**1**/**Mn-1**/**Zn-1**/BnOH (1/1/1/1, **Figure 2.30b-c**), likely due to the short-lived alkoxy radical species. To verify the existence of such radical species, the radical scavenger DPPH (2,2-di(4-*tert*-octylphenyl)-1-picrylhydrazyl)—that shows hyperfine splitting peaks in the EPR spectrum at room temperature—was added to the reaction mixture of and L-**1**/**Mn-1**(1/1); the intensity of the splitting peaks from DPPH significantly decreased, suggesting that the alkoxy radical reacted with unpaired-electron-containing DPPH (**Figure 2.31**). Furthermore, the addition of DPPH to the mixture L-**1**/**Mn-1**/**Zn-1**/BnOH (1/1/1/1) led to substantially decreased peaks in EPR, confirming the presence of alkoxy radical species (**Figure 2.31**). In this model (Scheme 1), the alkoxy radical is then rapidly intercepted by the Zn complex to generate a reactive Zn-alkoxide terminus, thereby enabling regeneration of the Mn^{II} catalyst (**Scheme 1**).

Table 2.8 The addition of radical scavenger for **Zn-1**/**Mn-1**-mediated controlled ring-opening polymerization of L-**1**

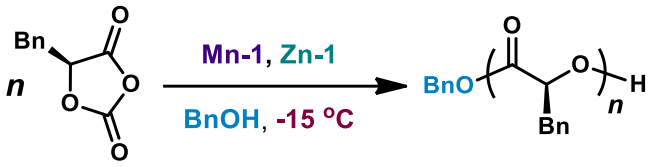

L-**1** poly(L-**1**)

Entry	Conditions	FR	Time (h)	Conv. (%)	M_n (kDa)	MW_{cal} (kDa)	$Đ$
1	+ TEMPO (10 equiv.)	900	1.5	71.1	80.1	94.8	1.06
2	+ DPPH (10 equiv.)	900	1.5	10.1	18.1	13.6	1.24

TEMPO, 2,2,6,6-tetramethylpiperidyl-1-oxyl; DPPH, 2,2-di(4-*tert*-octylphenyl)-1-picrylhydrazyl. Polymerization conditions: [**Mn-1**] = [**Zn-1**] = [BnOH] at −15 °C in a glove box.

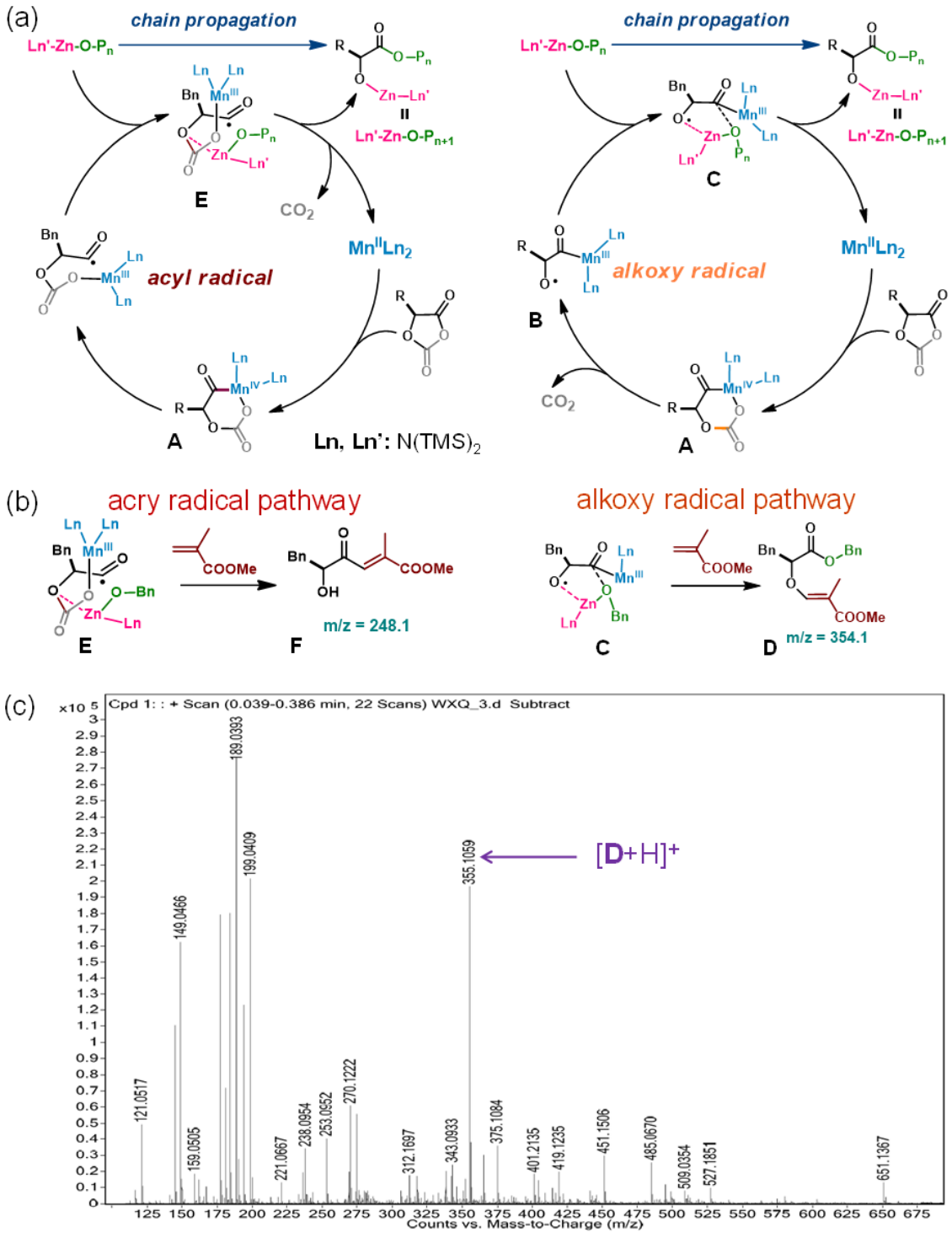

High-resolution ESI-MS results:

$[\mathbf{D}+H]^+$ $[C_{21}H_{23}O_5]^+$ calculated: 354.1545; found: 355.1059

Figure 2.29 Mechanistic studies to identify the putative reaction pathway as shown in Scheme 1. (a) Proposed radical reaction pathways via acyl (left) or alkoxy (right) radical. (b) The proposed use of methacrylate to capture the radical species in the ring-opening process, which was expected to generate the product with distinguishable mass in the ESI-MS measurement. (c) The ESI-MS spectrum of reaction mixture of [L-**1**]/[**Mn-1**]/[**Zn-1**]/[BnOH]/[acrylate] = 1/1/1/1/1 (−15 °C), showing the peak of [**D**+H]$^+$, which corresponded to the alkoxy radical pathway. Note that the reaction solution was dried and briefly washed by hexane to remove metal complexes for ESI-MS studies.

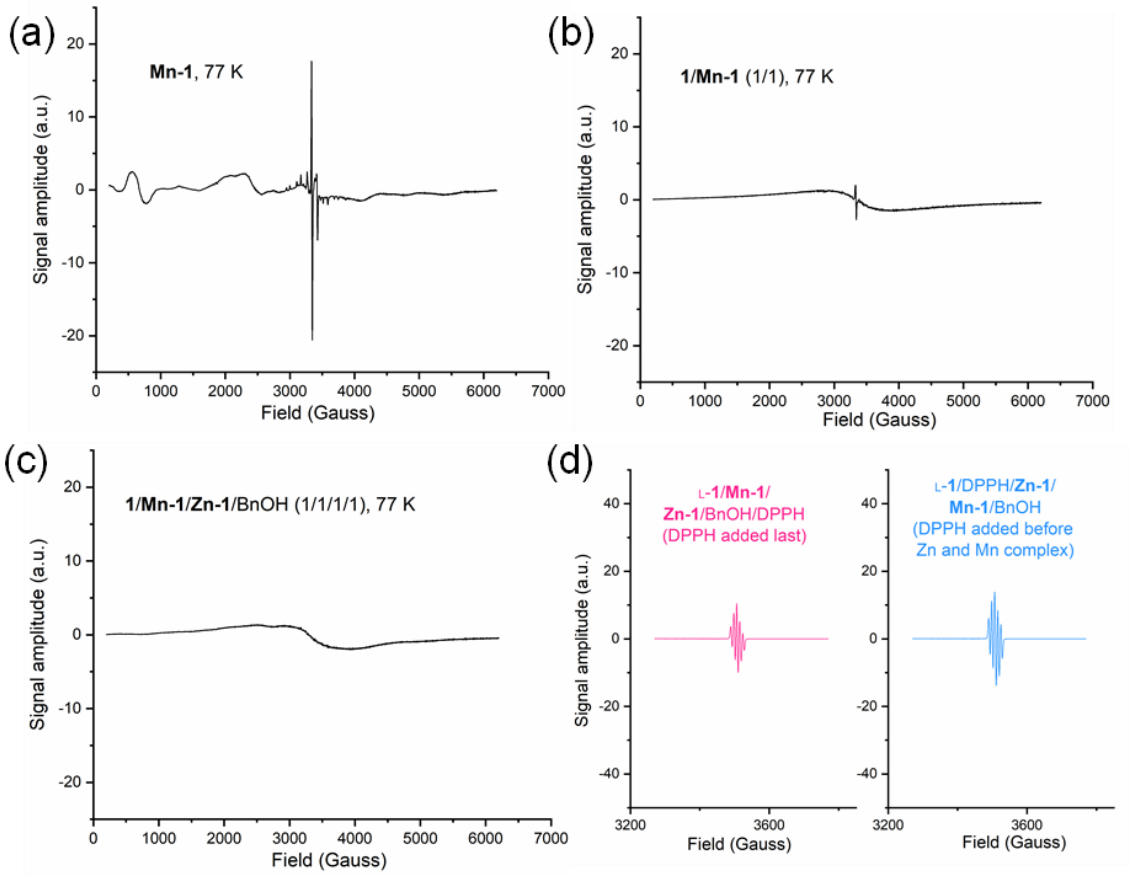

Figure 2.30 EPR spectra of (a) **Mn-1**, (b) the mixture of L-**1**/**Mn-1** (1/1), (c) the mixture of L-**1**/**Mn-1**/**Zn-1**/BnOH (1/1/1/1), and (d) L-**1**/**Mn-1**/**Zn-1**/BnOH/DPPH (1/1/1/1/1). (a-c) were recorded at 77 K cyrogenic condition as it is difficult to observe electron spin peaks of **Mn-1** in EPR at room temperature. (d) was recorded at 298 K (the same as in Figure 4). Reaction condition: [DPPH] = [**Mn-1**] = [**Zn-1**] = [BnOH] = [L-**1**] = 9.05 mM in toluene at -15 °C in a glove box for 30 minutes for all reactions.

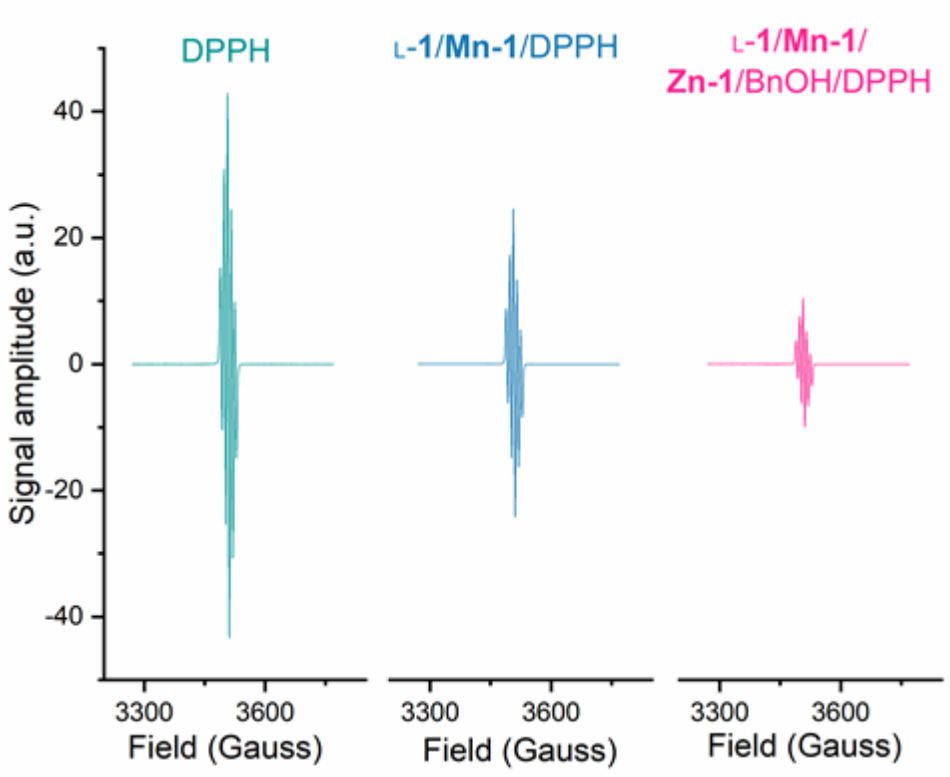

Figure 2.31 Electron paramagnetic resonance (EPR) study of using DPPH (2,2-di(4-*tert*-octylphenyl)-1-picrylhydrazyl) to quench radical species in Mn/Zn-mediated ring-opening reaction of L-**1** (298 K). Reaction condition: [DPPH] = [**Mn-1**] = [**Zn-1**] = [BnOH] = [L-**1**] = 9.05 mM in toluene at -15 °C for all reactions.

2.3 Materials and methods

2.3.1 General

2,2'-bipyridine (bpy), $Hf(O^iPr)_4$, $Hf(O^tBu)_4$, $Zr(O^iPr)_4$, bis(cyclopentadienyl) manganese and (1*S*,2*S*)-(+)-[1,2-cyclohexanediamino-*N*,*N*'-bis(3,5-di-*t*-butylsalicylidene)]manganese^{III} chloride were purchased from Strem Chemicals (Newbury port, MA). *O*-benzyl-L-serine, *O*-benzyl-D-serine, L-glutamic acid-γ-benzyl ester, D-glutamic acid-γ-benzyl ester, S-(+)-mandelic acid and R-(-)-mandelic acid were purchased from Chem-Impex (Wood Dale, IL). L-phenylalanine and D-phenylalanine were purchased from Alfa Aesar (Haverhill, MA). Anhydrous tetrahydrofuran (THF) was dried by alumina columns and stored with 4Å molecular sieve in the dark bottle in the glove box (MBraun, Labstar Pro, < 1 ppm oxygen and moisture). Anhydrous THF-d_8, benzyl alcohol, hexane, benzene, toluene, diethyl ether, diisopropyl ether, pyridine and dichloromethane were dried and stored by 4Å molecular sieves in the glove box. All other chemicals were purchased from Sigma-Aldrich (St. Louis, MO) unless otherwise noted. All metal catalysts were synthesized in the glove box, characterized by NMR, and stored in the glove box freezer (−30 °C).

2.3.2 OCA monomers

L-PheOCA (L-**1**) and D-PheOCA (D-**1**),[28] L-Ser(Bn)OCA (L-**2**) and D-Ser(Bn)OCA (D-**2**),[29] L-Glu(Cbz)OCA (L-**3**) and D-Glu(Cbz)OCA (D-**3**),[30] L-LacOCA (L-**4**) and D-LacOCA (D-**4**),[1] and L-ManOCA (L-**5**) and D-ManOCA (D-**5**),[17] were synthesized and recrystallized according to the literature. All OCA monomers were recrystallized three times and stored in -30 °C freezer in the glove box.

2.3.3 Metal silylamide complexes

$Zn(HMDS)_2$ (**Zn-1**) was prepared and distilled according to the literature.[31] $Y(N(SiMe_3)_2)_3$ and $Mg(N(SiMe_3)_2)_2$ were purchased from Sigma-Aldrich. $Mn(N(SiMe_3)_2)_2$ (**Mn-1**),[9] $Fe(N(SiMe_3)_2)_2$,[9] $Co(N(SiMe_3)_2)_2$[4], $Ce(N(SiMe_3)_2)_3$,[32] $Y(N(SiHMe_2)_2)_3$,[33] and Hf complexes[34] were prepared and recrystallized according to the literature, and were stored in the glove box freezer.

2.3.4 Instrument and characterization

2.3.4.1 NMR spectroscopy

All room temperature NMR and homodecoupling ^1H NMR spectra were recorded on Agilent U4-DD2 (400 MHz) or Bruker Avance II (500 MHz). Low temperature ^1H and ^{13}C NMR spectra were measured on Bruker Avance III (600 MHz) after the inner temperature of the NMR machine reached −20 °C for 20 min. The samples were kept at −15 °C ± 5 °C with a dry ice/ethylene glycol bath before the low-temperature NMR acquisition. All ^{13}C NMR spectra are proton decoupled.

2.3.4.2 FTIR spectroscopy

Fourier-transform infrared spectra were recorded on an Agilent Cary 630 FTIR spectrometer (Agilent Technologies Inc., Santa Clara, CA, USA) equipped with Diamond ATR and transmission sampling accessory.

Monomer conversion measurement:

A small aliquot of polymer solution (20 μL) was removed out of the glove box and quenched with 5% acetic acid / THF solution (20 μL). The mixture (~10 μL) was immediately dropped onto the FTIR-ATR diamond sampler and formed a film within 10-

20 seconds for the spectra measurement. The peak at 1800 cm^{-1} is assigned as the anhydride bond stretch in OCA; the peak at 1760 cm^{-1} corresponds to the formation of the ester bond in the polymer. The monomer conversion was determined by the intensity ratio between 1760 cm^{-1} and 1800 cm^{-1}: conversion% = I_{1760} / (I_{1760}+ I_{1800}).

2.3.4.3 Gel permeation chromatography (GPC)

GPC experiments were performed on a system equipped with an isocratic pump with degasser (Agilent 1260 series, Agilent Technologies, Santa Clara, CA, USA), Wyatt DAWN HELEOS multiangle laser light scattering (MALS) detector (GaAs 30 mW laser at λ=690nm), and an Wyatt Optilab rEX differential refractive index (DRI) detector with a 690 nm light source (Wyatt Technology, Santa Barbara, CA, USA). Separations were performed using serially connected size exclusion columns (100 Å, 500 Å, 10^3 Å, and 10^4 Å Phenogel columns, 5 μm, 300 × 4.6 mm, Phenomenex, Torrance, CA, USA) at 35 °C using THF as the mobile phase with a flow rate of 0.35 mL/min. The polymer molecular weight (MW) and molecular weight distribution (*Đ*) were determined using Zimm model fit of MALS-DRI data by ASTRA software (Version 6.1, Wyatt Technology). Data collection interval: 0.5 sec.

The refractive index increment dn/dc value was determined by the Wyatt Optilab rEX refractive index detector using ASTRA software dn/dc template (Version 6.1, Wyatt Technology). Five polymer / THF solutions with different concentrations were sequentially injected into the refractive index detector and the refractive index values were plotted versus concentration in ASTRA software. The slope of the linear fitting data is the dn/dc value.

The dn/dc values: poly(L-**1**), 0.1670; poly(L-**2**), 0.1377; poly(L-**3**), 0.1057; poly(L-**4**), 0.042; poly(L-**5**), 0.084.

2.3.4.4 Electrospray ionization mass spectrometry (ESI-MS)

The ESI-MS analysis of air-sensitive samples followed the literature.[35] In brief, in a glove box, a 100 μL aliquote of the sample containing air-sensitive Mn / Zn complexes was taken up into the 250 μL Hamilton gastight syringe. The syringe was punched into a 1 mL LC sampler vial capped with rubber septum to avoid contact between needle and air, and was sealed in a zip bag. The zip bag was removed from the glove box and immediately analyzed by ESI-MS (Agilent 6220 Accurate-Mass Time-of-Flight LC/MS).

2.3.4.5 Matrix-assisted laser desorption ionization mass spectrometry (MALDI-MS)

MALDI mass spectrometry was carried out on a Bruker Daltonics UltrafleXtreme MALDI set to positive ion reflectron mode. Samples were dissolved in THF at 10 mg/mL. α-Cyano-4-hydroxycinnamic acid (10 mg/mL in THF) or *trans*-2-[3-(4-*tert*-butylphenyl)-2-methyl-2-propenylidene] malononitrile (DCTB, 10 mg/mL in THF) were used as matrix. Potassium trifluoroacetate (KTFA, 10 mg/mL in THF) was used as a salt. The components were mixed in the ratio of 1:1:1 (polymer:KTFA:matrix), spotted onto a plate and allowed to dry completely before MALDI analysis.

2.3.4.6 Cyclic voltammetry (CV)

CVs were performed in a three-electrode measurement setup in a glove box with a Gamry Interface 1010 potentiostat/galvanostat at a potential sweep rate of 50 mV/s (the setup was previously described).[4] The measurements were carried out in a 20 mL Gamry

Dr. Bob's electrochemical cell with approximately 1 mM concentration of Mn complex in 0.1 M tetra-*n*-butylammonium hexafluorophosphate (TBAH) in anhydrous THF, fitted with a glassy carbon working electrode (3 mm in diameter, Gamry), a $Ag/AgNO_3$ reference electrode (a silver wire in 0.01 M $AgNO_3$ and 0.1 M TBAH in anhydrous acetonitrile), and a platinum wire (Gamry) counter electrode. Ferrocene (Fc) was measured as an internal standard,[36] and all potentials versus Fc^+/Fc were subsequently referenced to SCE (adding 380 mV) based on the reported method.[37]

2.3.4.7 Electron Paramagnetic Resonance (EPR)

EPR spectrometry was performed in the EPR Laboratory, Department of Chemistry, University of Illinois. Samples for EPR were prepared in a glove box. The sample solutions in anhydrous toluene were then transferred into standard 4 mm o.d. EPR quartz tubes. EPR experiments were performed using Bruker 10" EMXPlus X-band Continuous Wave EPR. The acquisition parameters were fixed to 20 dB (2mW) microwave power, 60 dB receiver gain, and 100 kHz modulation frequency. The amplitude modulation was varied to resolve the hyperfine coupling constants. Cryogenic temperature (77 K) was achieved by using liquid nitrogen cryostat. The signal intensity was determined by double integration after linear baseline correction. The evaluation of the total spin concentration for each scan was done by comparison to a TEMPO concentration calibration scale in toluene. Source data for all EPR spectra was attached with the manuscript.

2.3.5 Polymerization Procedures

2.3.5.1 The polymerization of L-1 mediated by Mn-1 / Zn-1 / BnOH

In a glove box, prior to the polymerization, all reagents were cooled in the cold trap equipped with a thermometer at -20 ^{o}C, which was cooled by the liquid nitrogen and ethanol in a dewar. The monomer **1** (15 mg, 150 μL of 100 mg/mL in THF, 0.078 mmol, 700 equiv.) was mixed with **Mn-1** (10.5 μL of 4.0 mg/mL in THF, 0.112 μmol, 1 equiv.), **Zn-1** (10.3 μL of 4.2 mg/mL in THF, 0.112 μmol, 1 equiv.), and BnOH (3.3 μL of 3.7 mg/mL in THF, 0.112 μmol, 1 equiv.) in a 7-mL glass vial equipped with a magnetic stir bar. The solution was stirred at -15 ± 5 ^{o}C (with a cooling fan to keep the reaction temperature) over 1-2 hours. The OCA monomer conversion was monitored by FTIR (see 2.3.4.2). The resulted polymer's MW and *Đ* were directly measured by GPC after the polymerization.

2.3.5.2 Block copolymerization of of L-1 and L-2 mediated by Mn-1 / Zn-1 / BnOH

In a glove box, L-**1** (15 mg, 150 μL of 100 mg/mL in THF, 0.078 mmol, 400 equiv.) was mixed with **Mn-1** (18.3 μL of 4.0 mg/mL in THF, 0.195 μmol,, 1 equiv.), **Zn-1** (23.6 μL of 3.2 mg/mL in THF, 0.195 μmol, 1 equiv.), and BnOH (13.2 μL of 1.6 mg/mL in THF, 0.195 μmol, 1 equiv.) in a 7-mL glass vial equipped with a magnetic stir bar at room temperature. The solution was stirred around -15 ^{o}C ± 5 ^{o}C (with a cooling fan to keep the reaction temperature) for 30 min. Upon the quantitative conversion of **1** was achieved, measured by FTIR, an aliquot of poly(L-**1**) solution (50 μL) was taken out of the box for GPC characterization. The monomer L-**2** (65.5 μL of 100 mg/mL in THF, 0.0295 mmol, 200 equiv.) was added into the remaining mixture and stirred at -15 ^{o}C ± 5 ^{o}C over another 1-3 hours. The monomer conversion was measured by FTIR. The obtained copolymer's MW and *Đ* were measured by GPC, and ^{1}H NMR. The

copolymer's MW from NMR was calculated based on the integration ratio between α-proton of two OCAs and the M_n of poly(**1**) obtained from GPC.

2.3.5.3 Kinetic study of Mn/Zn-mediated polymerization of OCA

In a glove box, the monomer L-**1** (10 mg, 100 μL of 100 mg/mL in THF, 52.1 μmol, 1000 equiv.) was mixed with **Mn-1** (3.9 μL of 5.0 mg/mL in THF, 52.1 nmol, 1 equiv.), **Zn-1** (4.4 μL of 4.6 mg/mL in THF, 52.1 nmol, 1 equiv.), and BnOH (1.8 μL of 3.1 mg/mL in THF, 52.1 nmol, 1 equiv.) in a 7-mL glass vial equipped with a magnetic stir bar. The mixture was stirred at -15 °C ± 5 °C in a manner similar to that in **2.3.5.1**. At the predetermined time point, 20 μL of the polymer solution was taken out and immediately analyzed by FTIR.

All the catalysts' concentrations were varied, and the semi-logarithmic plots were drawn to calculate the kinetic constants and reaction orders according to the kinetic laws:

$$-d[\mathbf{1}]/dt = k_{app}\cdot[\mathbf{1}] \qquad (2)$$

where k_{app} is the apparent first-order rate constant. For eq.7 it equals to

$$\ln[\mathbf{1}]_0/\ln[\mathbf{1}]_t = k_{app}\cdot t + C \qquad (3)$$

thus $\ln[\mathbf{1}]_0/\ln[\mathbf{1}]_t$ versus t was plotted.

2.4 Conclusions

Herein, a **Mn-1**/**Zn-1**/BnOH redox catalytic system was developed to mediate controlled ring-opening polymerization of OCAs, allowing for the production of poly(α-hydroxy acids) with molecular weights up to 200 kDa and narrow molecular weight distributions. Notably, this synthetic method is operationally simple and does not require external energy triggers compared to our previously reported methods. It provides a new entry to scale up functionalized poly(α-hydroxy acids) with high molecular weights. A plausible redox ROP mechanism was proposed based on kinetic studies, ESI-MS, EPR, and CV results: the oxidative addition of **Mn-1** to the OCA occurs at the O_1-C_5 position regioselectively to form the Mn^{IV} species, followed by decarboxylation to generate an alkoxy radical, which is rapidly intercepted by the Zn complex to generate a reactive Zn-alkoxide terminus for chain propagation.

References

1. du Boullay, O. T.; Marchal, E.; Martin-Vaca, B.; Cossio, F. P.; Bourissou, D., An activated equivalent of lactide toward organocatalytic ring-opening polymerization. *Journal of the American Chemical Society* **2006,** *128* (51), 16442-16443.
2. Feng, Q.; Tong, R., Controlled Photoredox Ring-Opening Polymerization of O-Carboxyanhydrides. *Journal of the American Chemical Society* **2017,** *139* (17), 6177-6182.
3. Feng, Q.; Yang, L.; Zhong, Y.; Guo, D.; Liu, G.; Xie, L.; Huang, W.; Tong, R., Stereoselective photoredox ring-opening polymerization of O-carboxyanhydrides. *Nature Communications* **2018,** *9* (1), 1559.
4. Zhong, Y.; Feng, Q.; Wang, X.; Chen, J.; Cai, W.; Tong, R., Functionalized Polyesters via Stereoselective Electrochemical Ring-Opening Polymerization of O-Carboxyanhydrides. *ACS Macro Letters* **2020,** *9* (8), 1114-1118.
5. Zhong, Y.; Feng, Q.; Wang, X.; Yang, L.; Korovich, A. G.; Madsen, L. A.; Tong, R., Photocatalyst-independent photoredox ring-opening polymerization of O-carboxyanhydrides: stereocontrol and mechanism. *Chemical Science* **2021,** *12*, 3702-3712.
6. Zuo, Z. W.; Ahneman, D. T.; Chu, L. L.; Terrett, J. A.; Doyle, A. G.; MacMillan, D. W. C., Merging photoredox with nickel catalysis: Coupling of alpha-carboxyl sp(3)-carbons with aryl halides. *Science* **2014,** *345* (6195), 437-440.
7. Yu, Y.; Liu, X.; Wang, J., Expansion of Redox Chemistry in Designer Metalloenzymes. *Accounts of Chemical Research* **2019,** *52* (3), 557-565.
8. Bullock, R. M., *Catalysis without Precious Metals*. Wiley-VCH Weinheim, Germany, 2010.
9. Andersen, R. A.; Faegri, K.; Green, J. C.; Haaland, A.; Lappert, M. F.; Leung, W. P.; Rypdal, K., Synthesis of bis[bis(trimethylsilyl)amido]iron(II). Structure and bonding in M[N(SiMe3)2]2 (M = manganese, iron, cobalt): two-coordinate transition-metal amides. *Inorganic Chemistry* **1988,** *27* (10), 1782-1786.
10. Power, P. P., Stable Two-Coordinate, Open-Shell (d1–d9) Transition Metal Complexes. *Chemical Reviews* **2012,** *112* (6), 3482-3507.
11. Hu, A.; Guo, J.-J.; Pan, H.; Zuo, Z., Selective functionalization of methane, ethane, and higher alkanes by cerium photocatalysis. *Science* **2018,** *361* (6403), 668-672.
12. Walsh, C. T., Biologically generated carbon dioxide: nature's versatile chemical strategies for carboxy lyases. *Natural Product Reports* **2020,** *37* (1), 100-135.
13. Song, D.-P.; Shi, X.-C.; Wang, Y.-X.; Yang, J.-X.; Li, Y.-S., Ligand steric and electronic effects on β-ketiminato neutral nickel (ii) olefin polymerization catalysts. *Organometallics* **2012,** *31* (3), 966-975.
14. Crivello, J. V.; Liu, S., Photoinitiated cationic polymerization of epoxy alcohol monomers. *Journal of Polymer Science Part A: Polymer Chemistry* **2000,** *38* (3), 389-401.
15. Webster, O. W., Living Polymerization Methods. *Science* **1991,** *251* (4996), 887-893.
16. Li, M.; Zhang, S.; Zhang, X.; Wang, Y.; Chen, J.; Tao, Y.; Wang, X., Unimolecular Anion-Binding Catalysts for Selective Ring-Opening Polymerization of O-carboxyanhydrides. *Angewandte Chemie International Edition* **2021,** *60* (11), 6003-6012.

17. Buchard, A.; Carbery, D. R.; Davidson, M. G.; Ivanova, P. K.; Jeffery, B. J.; Kociok-Köhn, G. I.; Lowe, J. P., Preparation of stereoregular isotactic poly(mandelic acid) through organocatalytic ring-opening polymerization of a cyclic *O*-carboxyanhydride. *Angewandte Chemie International Edition* **2014,** *53* (50), 13858-13861.
18. Zuo, Z.; MacMillan, D. W. C., Decarboxylative Arylation of α-Amino Acids via Photoredox Catalysis: A One-Step Conversion of Biomass to Drug Pharmacophore. *Journal of the American Chemical Society* **2014,** *136* (14), 5257-5260.
19. Lynch, M. W.; Hendrickson, D. N.; Fitzgerald, B. J.; Pierpont, C. G., Intramolecular two-electron transfer between manganese(II) and semiquinone ligands. Synthesis and characterization of manganese 3,5-di-tert-butylquinone complexes and their relationship to the photosynthetic water oxidation system. *Journal of the American Chemical Society* **1984,** *106* (7), 2041-2049.
20. Romero, I.; Collomb, M.-N.; Deronzier, A.; Llobet, A.; Perret, E.; Pécaut, J.; Le Pape, L.; Latour, J.-M., A Novel Dimanganese(II) Complex with Two Chloride Bridges − A Two-Electron Oxidation System. *European Journal of Inorganic Chemistry* **2001,** *2001* (1), 69-72.
21. Steinlechner, C.; Roesel, A. F.; Oberem, E.; Päpcke, A.; Rockstroh, N.; Gloaguen, F.; Lochbrunner, S.; Ludwig, R.; Spannenberg, A.; Junge, H.; Francke, R.; Beller, M., Selective Earth-Abundant System for CO2 Reduction: Comparing Photo- and Electrocatalytic Processes. *ACS Catalysis* **2019,** *9* (3), 2091-2100.
22. Walsh, J. J.; Neri, G.; Smith, C. L.; Cowan, A. J., Water-Soluble Manganese Complex for Selective Electrocatalytic CO2 Reduction to CO. *Organometallics* **2019,** *38* (6), 1224-1229.
23. Le, C.; MacMillan, D. W. C., Fragment Couplings via CO2 Extrusion-Recombination: Expansion of a Classic Bond-Forming Strategy via Metallaphotoredox. *Journal of the American Chemical Society* **2015,** *137* (37), 11938-11941.
24. Dong, S.; Wu, G.; Yuan, X.; Zou, C.; Ye, J., Visible-light photoredox catalyzed hydroacylation of electron-deficient alkenes: carboxylic anhydride as an acyl radical source. *Organic Chemistry Frontiers* **2017,** *4* (11), 2230-2234.
25. Zhang, J.; Li, Y.; Zhang, F.; Hu, C.; Chen, Y., Generation of Alkoxyl Radicals by Photoredox Catalysis Enables Selective C(sp3)−H Functionalization under Mild Reaction Conditions. *Angewandte Chemie International Edition* **2016,** *55* (5), 1872-1875.
26. Barthelemy, A.-L.; Tuccio, B.; Magnier, E.; Dagousset, G., Alkoxyl Radicals Generated under Photoredox Catalysis: A Strategy for anti-Markovnikov Alkoxylation Reactions. *Angewandte Chemie International Edition* **2018,** *57* (42), 13790-13794.
27. Paul, H.; Small, R. D.; Scaiano, J. C., Hydrogen abstraction by tert-butoxy radicals. A laser photolysis and electron spin resonance study. *Journal of the American Chemical Society* **1978,** *100* (14), 4520-4527.
28. Yin, Q.; Tong, R.; Xu, Y.; Baek, K.; Dobrucki, L. W.; Fan, T. M.; Cheng, J., Drug-Initiated ring-opening polymerization of *O*-carboxyanhydrides for the preparation of anticancer drug-Poly(*O*-carboxyanhydride) nanoconjugates. *Biomacromolecules* **2013,** *14* (3), 920-929.
29. Lu, Y.; Yin, L.; Zhang, Y.; Zhang, Z.; Xu, Y.; Tong, R.; Cheng, J., Synthesis of water-soluble poly (α-hydroxy acids) from living ring-opening polymerization of *O*-benzyl-l-serine carboxyanhydrides. *ACS Macro Letters* **2012,** *1* (4), 441-444.

30. du Boullay, O. T.; Bonduelle, C.; Martin-Vaca, B.; Bourissou, D., Functionalized polyesters from organocatalyzed ROP of gluOCA, the *O*-carboxyanhydride derived from glutamic acid. *Chemical Communications* **2008,** (15), 1786-1788.
31. Lee, D.-Y.; Hartwig, J. F., Zinc trimethylsilylamide as a mild ammonia equivalent and base for the amination of aryl halides and triflates. *Organic letters* **2005,** *7* (6), 1169-1172.
32. Bradley, D. C.; Ghotra, J. S.; Hart, F. A., Low co-ordination numbers in lanthanide and actinide compounds. Part I. The preparation and characterization of tris {bis (trimethylsilyl)-amido} lanthanides. *Journal of the Chemical Society, Dalton Transactions* **1973,** (10), 1021-1023.
33. Smith, A. R.; Livinghouse, T., Rapid and Efficient Procedure for the Synthesis of Group 3 Metal Tris [bis (dimethylsilyl) amide] THF Complexes. *Organometallics* **2013,** *32* (5), 1528-1530.
34. Chmura, A. J.; Davidson, M. G.; Frankis, C. J.; Jones, M. D.; Lunn, M. D., Highly active and stereoselective zirconium and hafnium alkoxide initiators for solvent-free ring-opening polymerization of rac-lactide. *Chemical communications* **2008,** (11), 1293-1295.
35. Evans, W. J.; Johnston, M. A.; Fujimoto, C. H.; Greaves, J., Utility of Electrospray Mass Spectrometry for the Characterization of Air-Sensitive Organolanthanides and Related Species1. *Organometallics* **2000,** *19* (21), 4258-4265.
36. Gagne, R. R.; Koval, C. A.; Lisensky, G. C., Ferrocene as an internal standard for electrochemical measurements. *Inorganic Chemistry* **1980,** *19* (9), 2854-2855.
37. Pavlishchuk, V. V.; Addison, A. W., Conversion constants for redox potentials measured versus different reference electrodes in acetonitrile solutions at 25 C. *Inorganica Chimica Acta* **2000,** *298* (1), 97-102.

CHAPTER 3

Chemical recycling of functionalized poly(α-hydroxy acids)

3.1 Introduction

The past few decades have seen the rapid development of synthetic polymers. Still, these studies have almost focused on performance and durability, with little attention to the degradability and recyclability of synthetic polymers, which has resulted in the tremendous accumulation of polymer wastes and the significant reduction of finite raw materials.[1-3] To address these issues, recycling is one of the most important end-of-use options for reducing the environmental impacts and resource depletion of plastics. Achieving a closed-loop life cycle of plastics consistent with the principles of circular economy[4] and industrial ecology[5] is necessary, in which there are no wastes but only products.[6]

Currently, three major types of recycling processes for polymers exist as shown in **Figure 3.1**.[6] The shortest path to achieve the recycling of plastics is mechanical recycling (route 1), which involves sorting, washing, and drying postconsumer polymer before melt processing to produce a new product. However, due to the complexity of the separation of different types of plastics and the contaminations of non-plastic materials, only clear polyethylene terephthalate (PET) and high-density polyethylene (HDPE) bottles are routinely recycled, and most into low-grade materials.[7, 8] Another strategy developed is biological recycling (route 3). The degradation of plastics by natural or engineered microorganisms generates primarily CO_2 and H_2O (sometimes CH_4) as end-products, which can return to the life cycle via photosynthesis. However, this process is economically inefficient; none of the material's value is typically recovered.[3, 6] Chemical

recycling process (route 2) includes the selective depolymerization of plastic into its monomers or monomer derivatives, which provide feedstocks for repolymerization to the original products or the transformation to other chemicals for repurposing.[9] Compared with the two former recycling methods, chemical recycling offers an attractive option to recover product values. It could not only solve the end-of-life issue of polymers and provide a direct approach to establish a circular materials economy, but also reduce the demand for finite raw materials.[10-12]

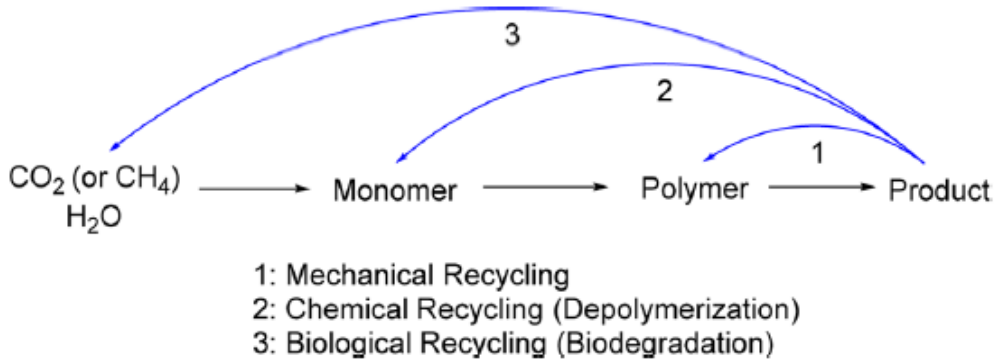

Figure 3.1 Different routes of recycling. (Reproduced from *Chem. Rev.* **2018**, 118, 839−885)

To date, there has been little discussion about the controlled degradation of poly(α-hydroxy acids) to close their life cycle. Most of the work has only focused on poly(lactic acid) (poly(L-**4**)). Chemical recycling of poly(L-**4**) occurs via three possible routes: thermolysis,[13, 14] hydrolysis[15], and alcoholysis (transesterification)[16, 17]. However, the first two methods require high temperatures (200 − 400 °C), which lead to increased operating costs and the difficulty of possible scalability issues. Alcoholysis can be achieved under mild conditions, making it more economically and environmentally

feasible at industrial scales. Recent research has shown the degradation of poly(L-**4**) into methyl lactate by some Zn(II) complex with methanol.[16-18] As shown in **Figure 3.2**, it enabled the formation of lactate esters, which can be transformed back into lactide, thereby closing the loop in the circular economy. However, it has remained challenging to degrade other poly(α-hydroxy acids) with functional groups, such as poly(L-**5**). Given that, a versatile two-step degradation approach for functionalized poly(α-hydroxy acids) has been designed under mild conditions. It comprises the degradation of functionalized poly(α-hydroxy acids) into corresponding methyl esters, and the transformation of methyl ester into hydroxyl acid, thus closing their end-life cycle (**Figure 3.3**).

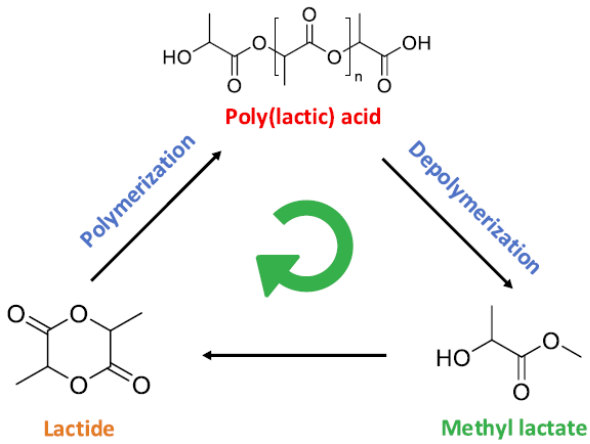

Figure 3.2 Circular economy in the chemical recycling of poly(lactic acid) into methyl lactate. (Reproduced from *Ind. Eng. Chem. Res.* **2020**, 59, 11149−11156)

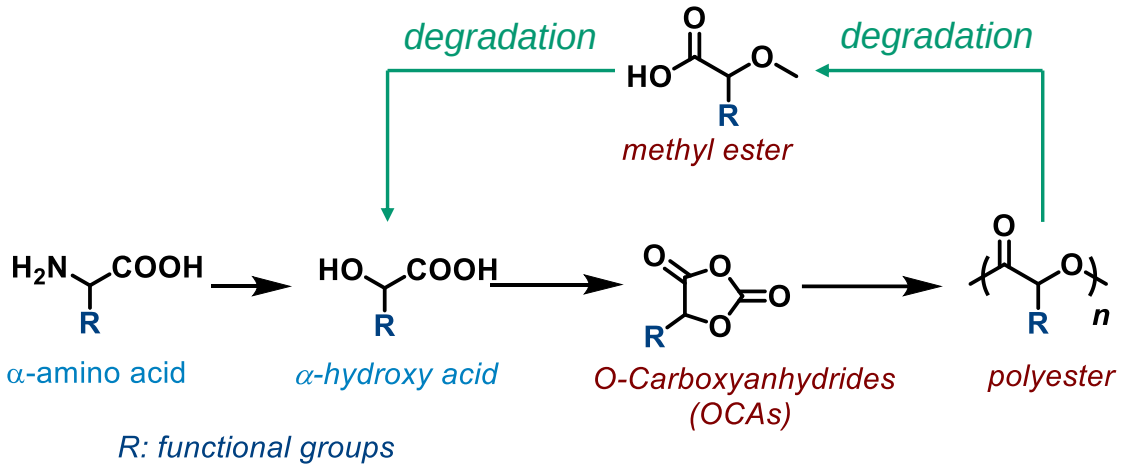

Figure 3.3 General degradation framework in the chemical recycling of functionalized poly(α-hydroxy acids) to achieve circular economy.

3.2 Results and discussions

3.2.1 The first step: efficient degradation of poly(α-hydroxy acids) to corresponding methyl esters

The Wang group reported that **Zn-1** was an excellent catalyst with high yields and chemoselectivity for the depolymerization of poly(L-**4**).[18] Therefore, the degradation of poly(L-**1**) by treatment with **Zn-1** (10 wt%) in MeOH (**Figure 3.4**) was initially attempted at room temperature. Still, the peaks of polymer and methyl ester were both found in the ^{1}H NMR (**Figure 3.5a**) after 1 week, suggesting the incomplete degradation of the polymer. Then the temperature was increased to 50 ^{o}C. Fortunately, we determined that poly(L-**1**) could be fully degraded and yielded pure methyl ester within 12 h, as indicated by the ^{1}H NMR (**Figure 3.5b**) and ESI-MS spectra (**Figure 3.6**) of the degradation reaction solution.

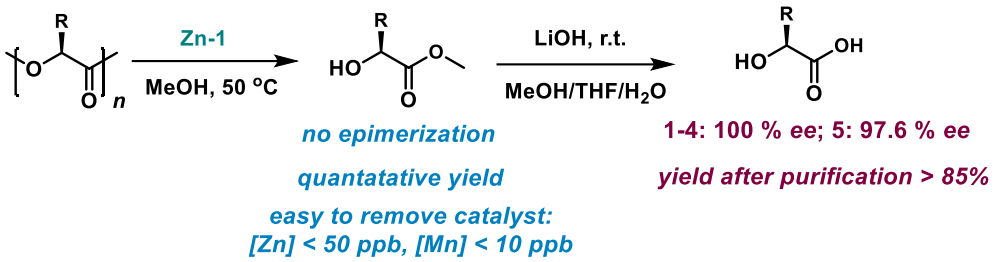

Figure 3.4 Degradation of poly(α-hydroxy acids) to α-hydroxy acid by our work, fulfilling the recycling circle.

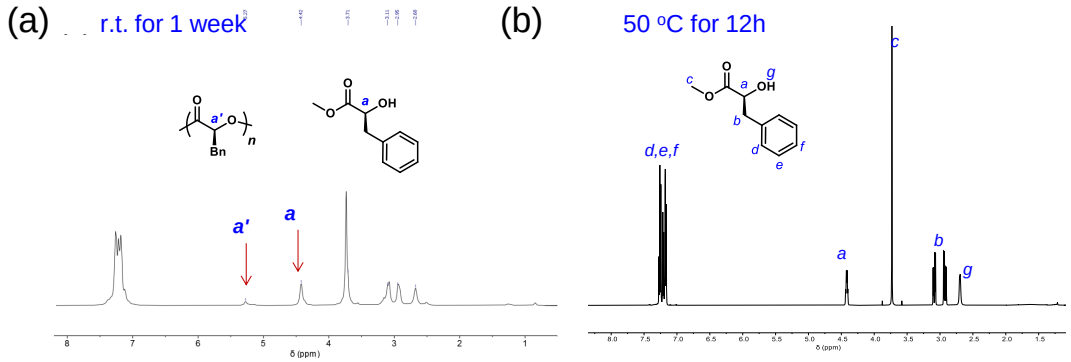

Figure 3.5 Degradation of poly(L-**1**) by **Zn-1**/MeOH: ^{1}H spectra of the degradation reaction solution for (a) 1 week at room temperature or (b) 12 h at 50 °C. (No purification, only solvent evaporation and dissolve in $CDCl_3$ for NMR analysis)

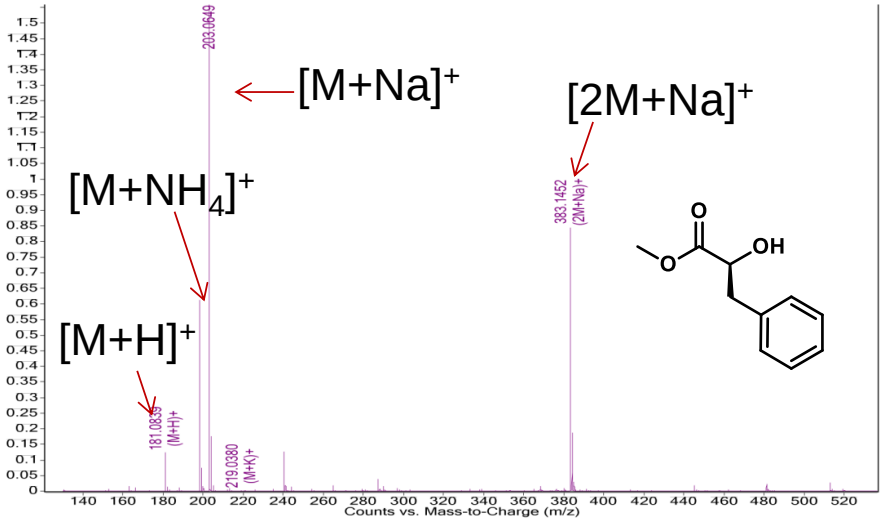

Figure 3.6 ESI-MS spectrum of the degradation reaction solution for poly(L-**1**) degradation by **Zn-1**/MeOH.

As shown in **Figure 3.7**, the Zn-alkoxide complex was insoluble in MeOH solution [18] and could be easily removed by filtration through silica gel. Then the methyl ester with a high yield of 89.7 % was recovered by evaporation of the filtrate. In addition, enantiopure methyl ester forms were measured by chiral HPLC (**Figure 3.8**), showing no epimerization of the chiral centers.

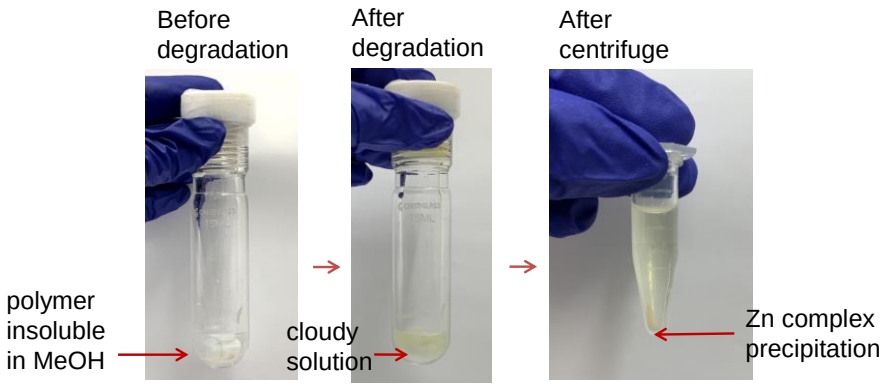

Figure 3.7 Degradation process of the first step, where the Zn catalyst can be easily separated from the degradation product by centrifugation.

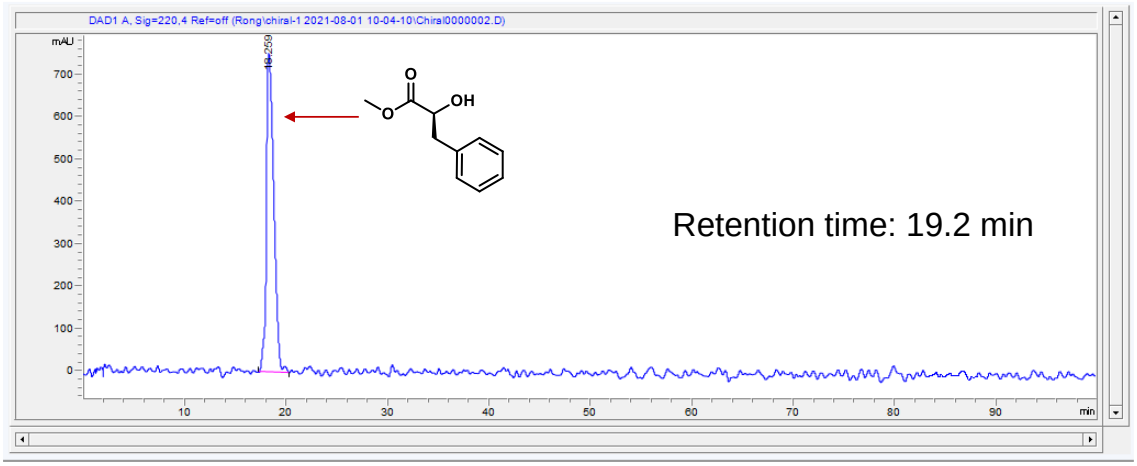

Figure 3.8 Chiral HPLC spectrum of the methyl ester obtained from the first step. HPLC condition: 85% 2 mM $CuSO_4$ aqueous solution / 15% acetonitrile for 100 min, measured at 220 nm.

The two-step degradation method could also be extended to OCA monomers **2**–**5**, all of which could be completely degraded to their corresponding methyl ester forms, as shown in the ^{1}H NMR spectrum and ESI-MS spectra (**Figure 3.9-3.12**). The chiral HPLC analysis (**Figure 3.9c and 3.10c**) confirmed that these methyl ester forms were all enantiopure, indicating that **Zn-1** does not change the product chirality. Note that there are no absorbances from degraded methyl esters of **3** and **4** as they did not bind to Cu^{II}; however, the obtained hydroxy acid in the second step could bind to Cu^{II} and exhibit UV signals which could be measured by the HPLC detector and had the same retention time as the standard hydroxy acid (obtained from Sigma-Aldrich) (**Figure 3.15 and 3.16**), confirming no epimerization occurred during the degradation. Using inductively coupled plasma mass spectrometry, we confirmed that the filtrates contain negligible Zn ([Zn] < 50 ppb, **Table 3.1**).

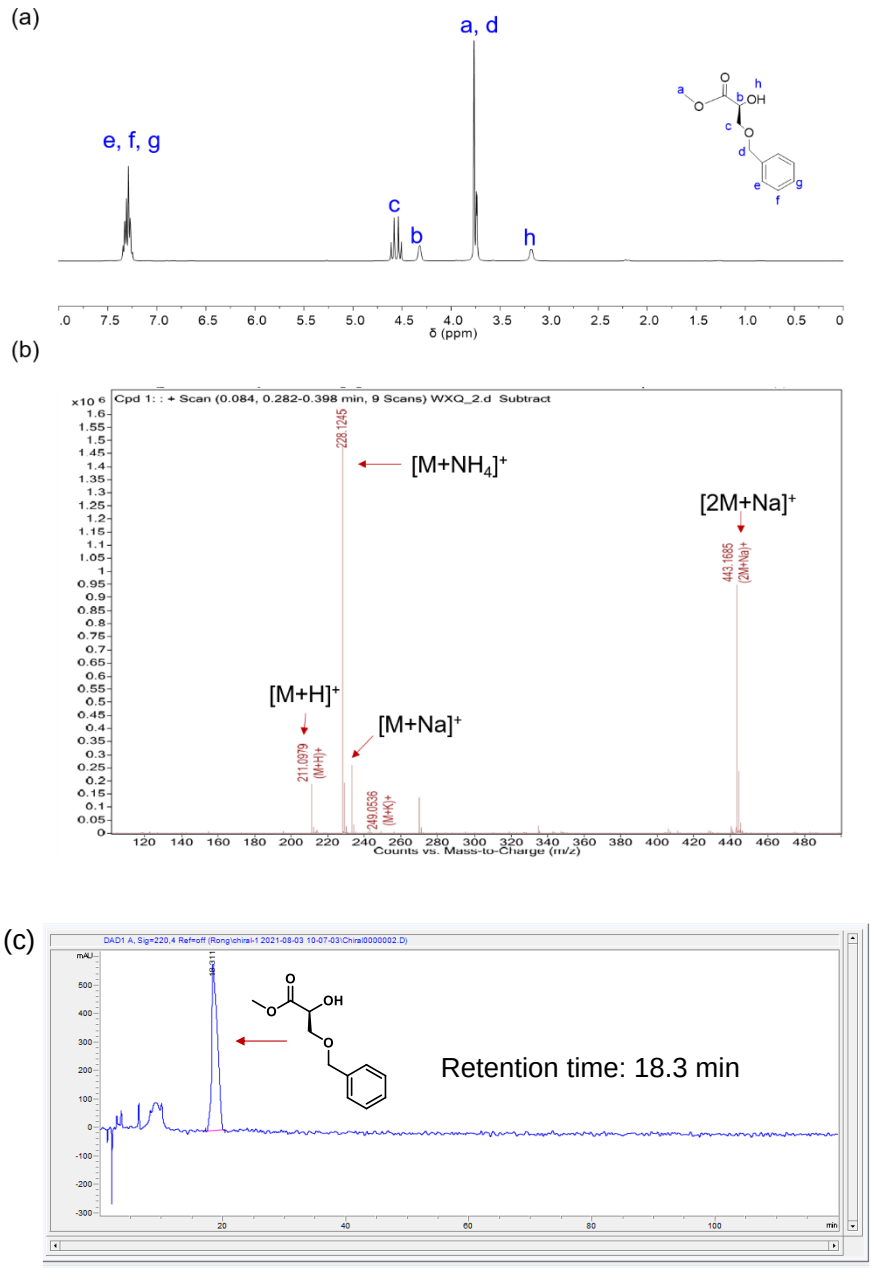

Figure 3.9 Degradation of poly(L-**2**) by **Zn-1**/MeOH, (a) ^{1}H NMR, and (b) ESI-MS spectra of the degradation reaction solution for 12 hours (no purification, only solvent evaporation, and dissolve in $CDCl_3$ for NMR analysis). (c) Chiral HPLC spectrum of the methyl ester obtained from the first step. HPLC condition: 85% 2 mM $CuSO_4$ aqueous solution / 15% acetonitrile for 120 min, measured at 220 nm.

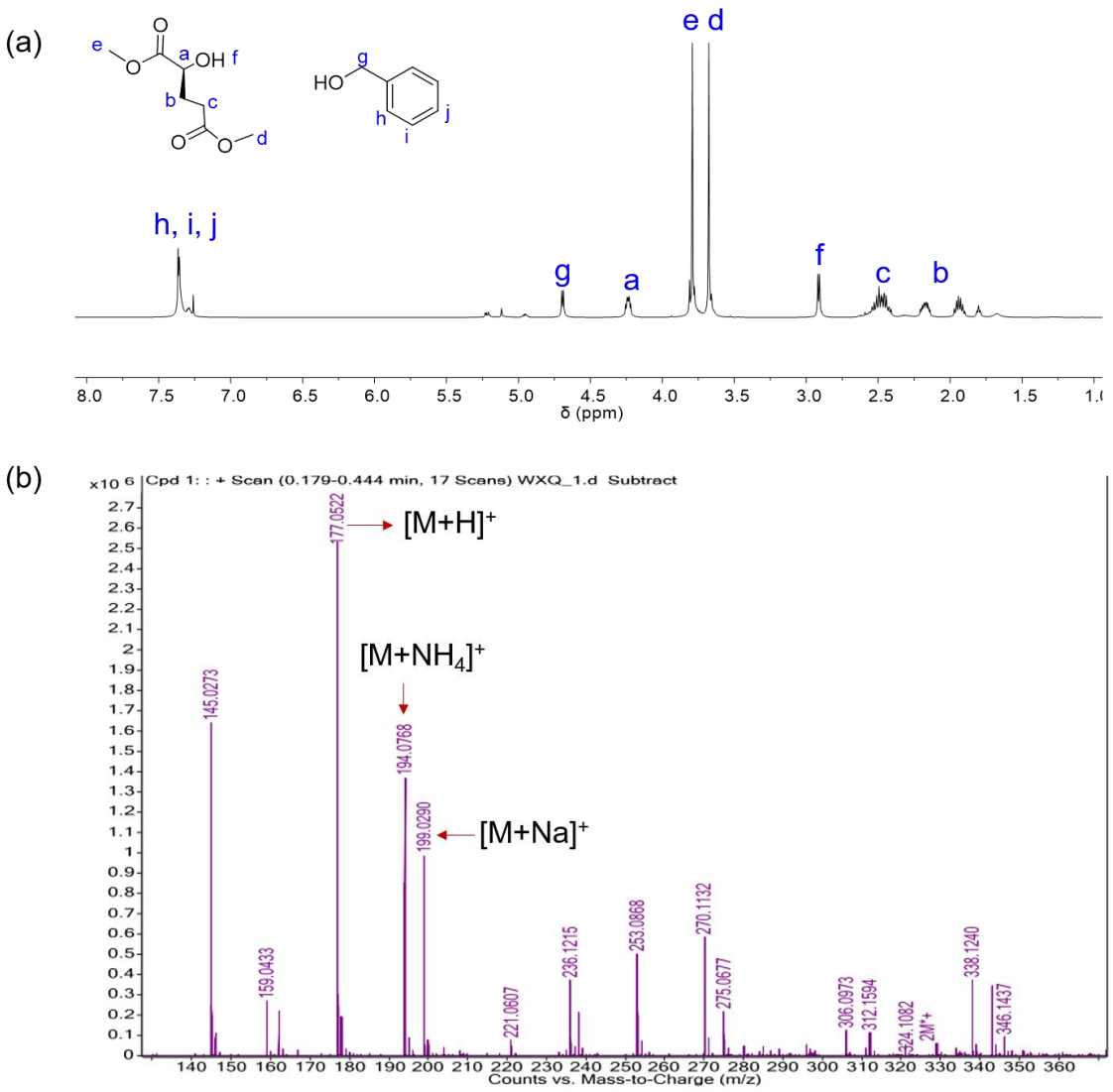

Figure 3.10 Degradation of poly(L-**3**) by **Zn-1**/MeOH, (a) ^{1}H NMR, and (b) ESI-MS spectra of the degradation reaction solution for 12 hours (no purification, only solvent evaporation, and dissolve in $CDCl_3$ for NMR analysis).

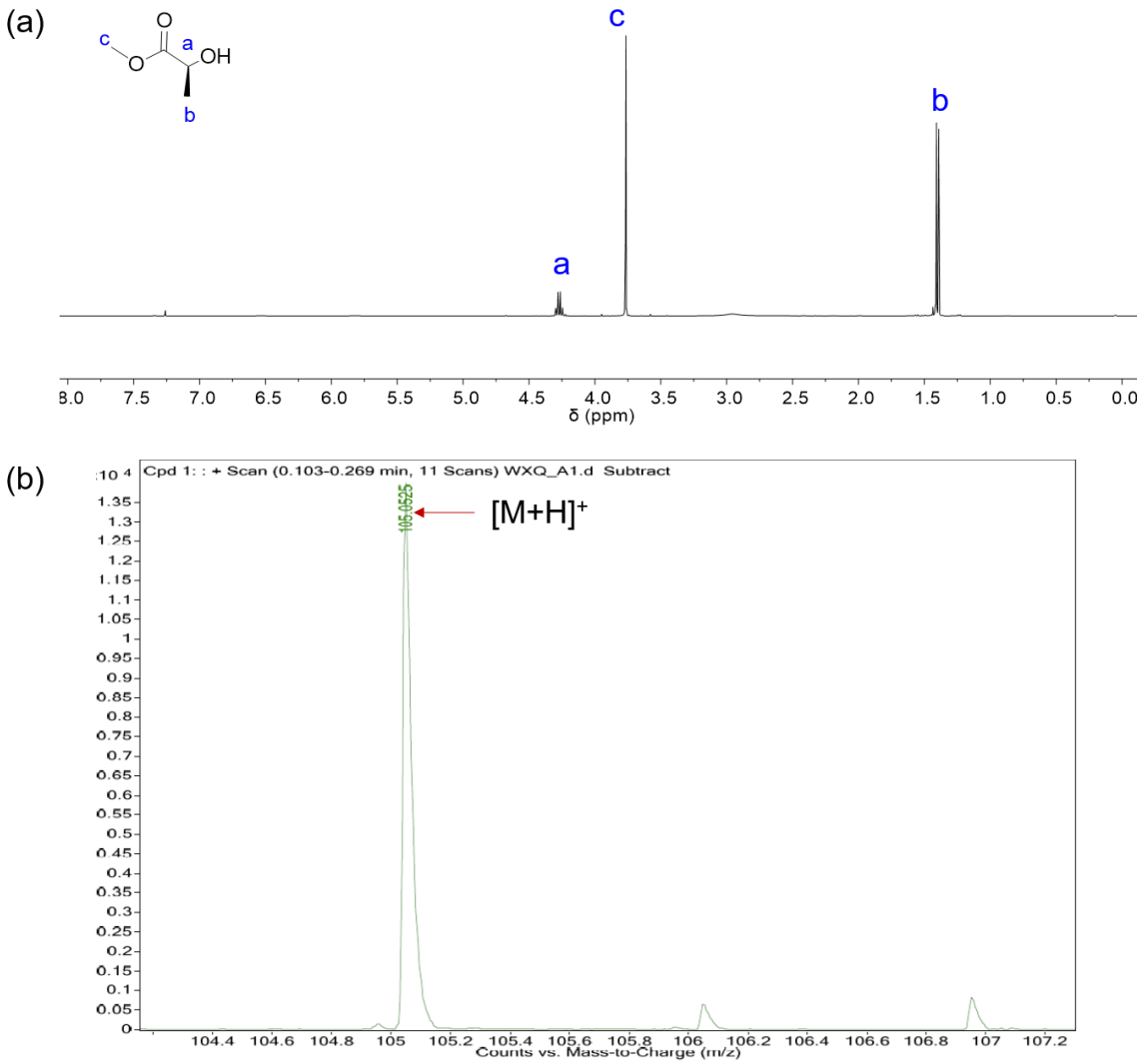

Figure 3.11 Degradation of poly(L-**4**) by **Zn-1**/MeOH, (a) ^{1}H NMR, and (b) ESI-MS spectra of the degradation reaction solution for 12 hours (no purification, only solvent evaporation and dissolve in $CDCl_3$ for NMR analysis).

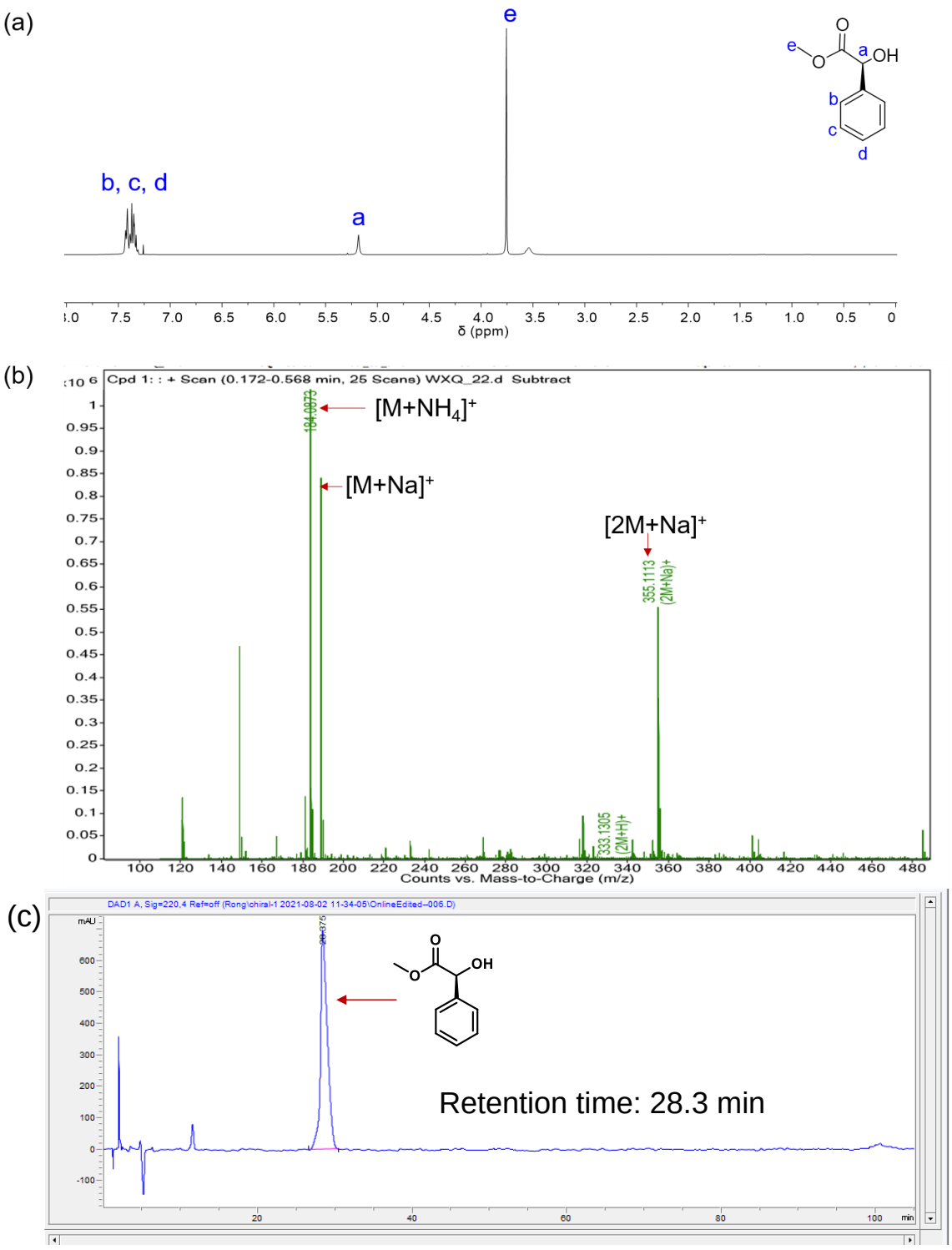

Figure 3.12 Degradation of poly(L-**5**) by **Zn-1**/MeOH, (a) ^{1}H NMR, and (b) ESI-MS spectra of the degradation reaction solution for 12 hours (no purification, only solvent evaporation, and dissolve in $CDCl_3$ for NMR analysis). (c) Chiral HPLC spectrum of the methyl ester of L-**5** obtained from the first step. HPLC condition: 85% 2 mM $CuSO_4$ aqueous solution / 15% acetonitrile for 120 min, measured at 220 nm.

Table 3.1 Measurement of residue metal concentrations in purified polymers and degradation products by inductively coupled plasma mass spectrometry (ICP-MS).

	[Mn] (ppb)	[Zn] (ppb)
10% HNO_3 (v/v)	4.0	43.3
Degradation product of poly(L-**1**) (mediated by **Zn-1**)	5.8	39.4

3.2.2 The second step: transformation of methyl ester into hydroxyl acid

The obtained methyl esters are value-added chemicals,[19] and can be rapidly transformed to hydroxy acids by reacting with LiOH at room temperature within 4 hours (**Figure 3.4**).[20] No epimerization occurred in the obtained hydroxy acids degraded from all polymers synthesized from L-**1** to L-**4** (**Figures 3.13-3.16**), and only slight epimerization appeared for L-**5** (97.6 % *ee*), determined by chiral HPLC (**Figure 3.17**).

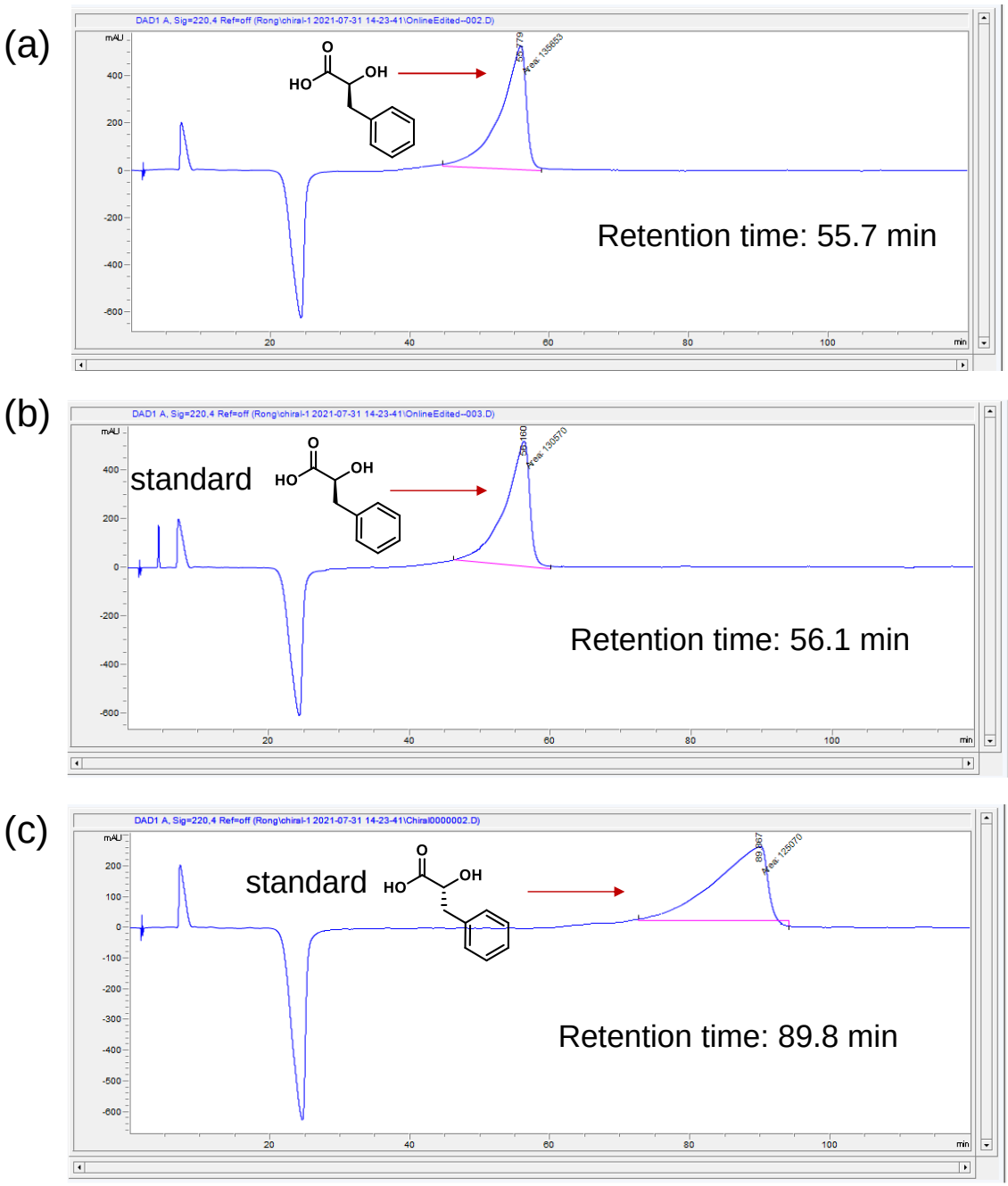

Figure 3.13 (a) Chiral HPLC of hydroxy acid of L-**1** obtained from the degradation of methyl ester (after extraction, no purification). HPLC condition: 85% 1 mM $Cu(OAc)_2$ and 0.05 mM NH_4OAc aqueous solution / 15% isopropanol for 120 min, measured at 220 nm. (b, c) Chiral HPLC spectra of standard hydroxy acids of L-**1** and D-**1**, respectively. HPLC condition was the same as that in (a). The chiral HPLC results confirmed that no epimerization occurred in the degradation reactions in poly(L-**1**).

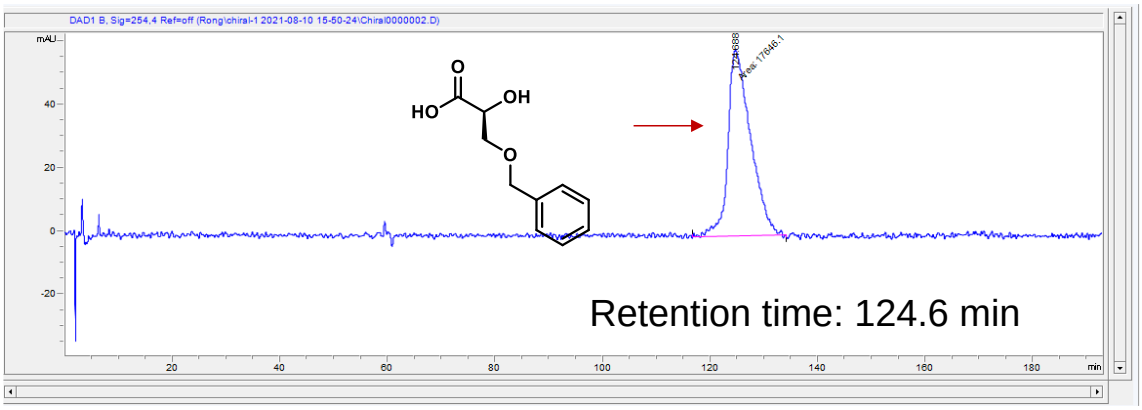

Figure 3.14 Chiral HPLC spectrum of the obtained hydroxy acid of L-**2** from the second step (after extraction, no purification). HPLC condition: 85% 2 mM $CuSO_4$ aqueous solution / 15% acetonitrile for 200 min, measured at 254 nm. The results suggested that the polymer was fully degraded to hydroxy acid of L-**2** without epimerization.

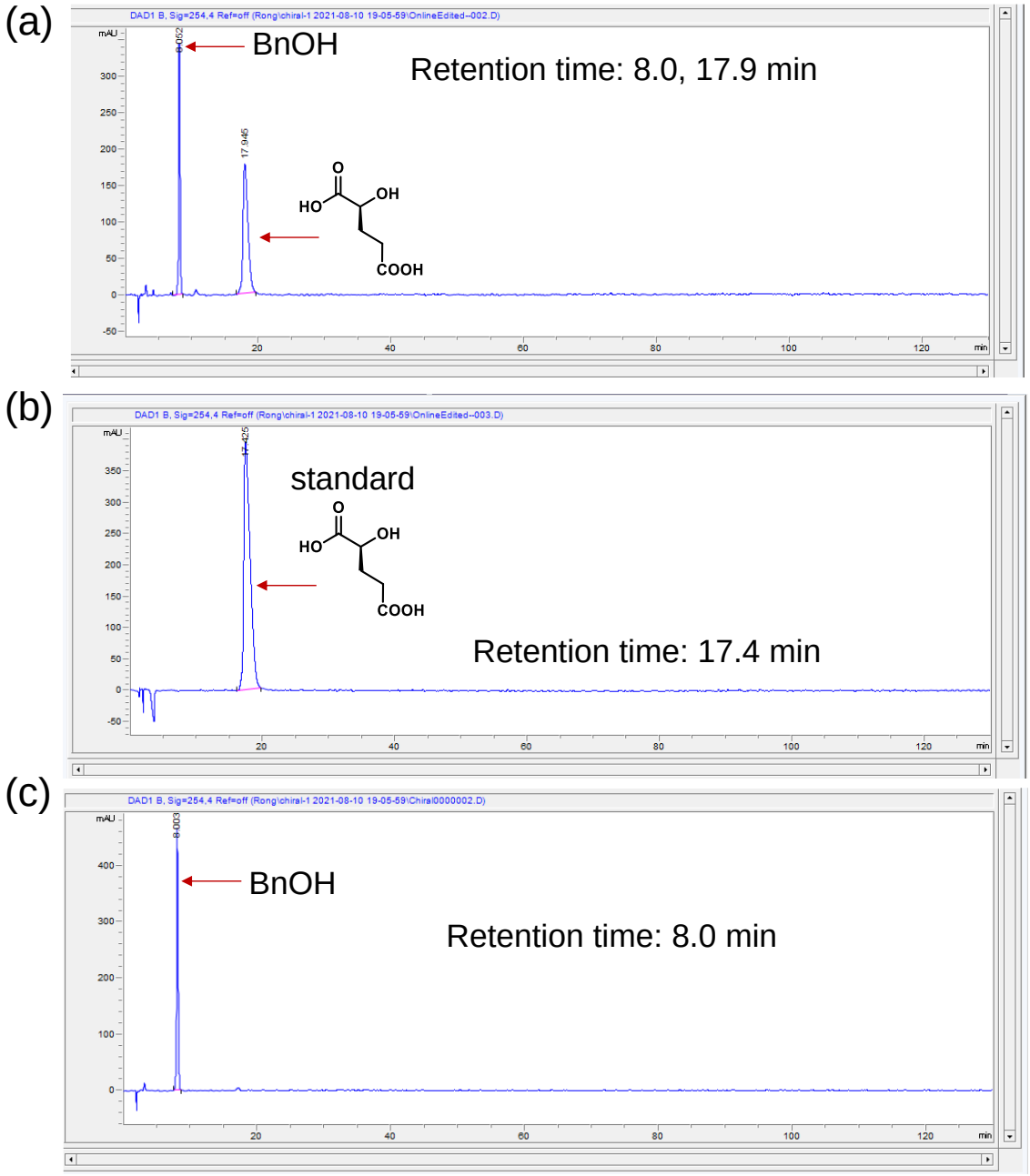

Figure 3.15 (a) Chiral HPLC spectrum of the obtained hydroxy acid of L-**3** from the second step (after extraction, no purification). HPLC condition: 85% 2 mM $CuSO_4$ aqueous solution / 15% acetonitrile for 130 min, measured at 254 nm. (b-c) Chiral HPLC spectra of the standard samples of hydroxy acid of **3** and BnOH (deprotected by **Zn-1**), respectively. The HPLC condition is the same as that in (a). The results suggested that the polymer was fully degraded. Note that the benzyl alcohol was cleaved from the side chain (Cbz protection group) from L-**3**, and it could be measured in HPLC after two degradation steps as we did not purify the samples by columns.

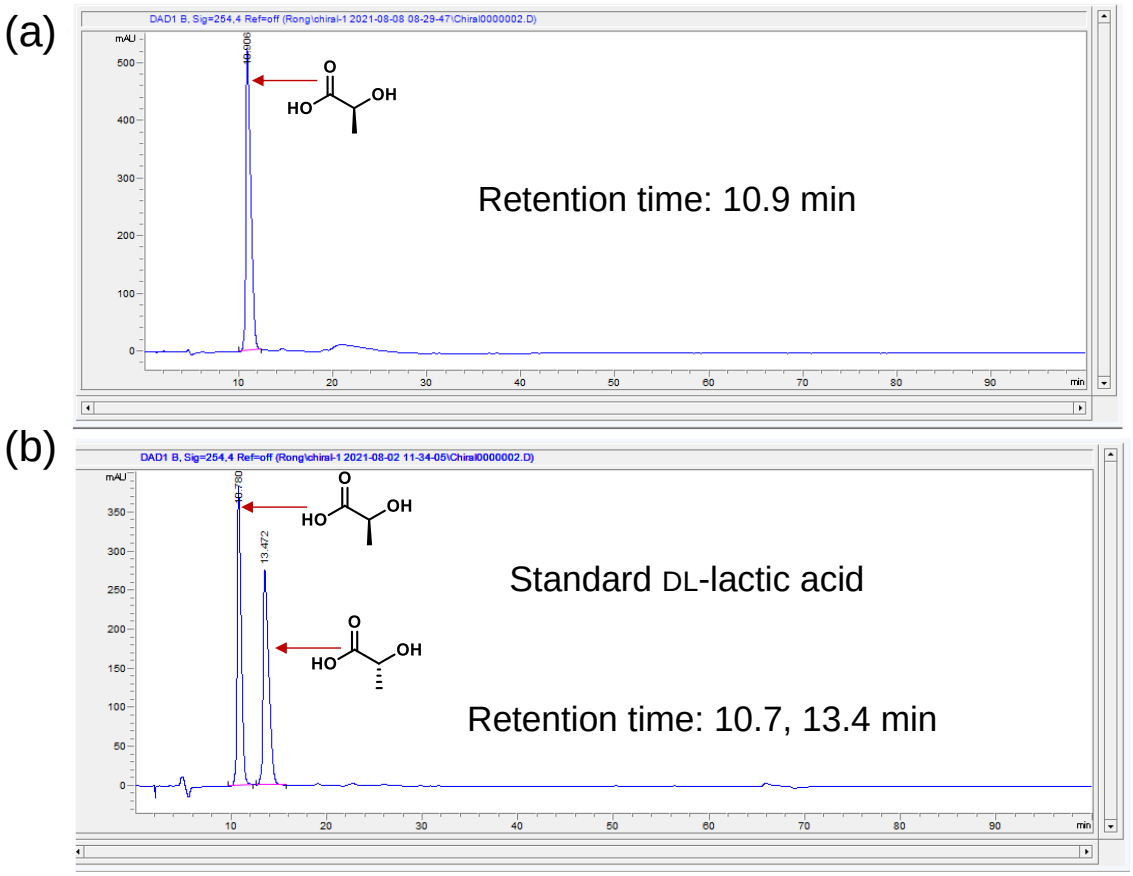

Figure 3.16 (a) Chiral HPLC spectrum of obtained hydroxy acid of L-**4** from the second step (after extraction, no purification). HPLC condition: 95% 2 mM $CuSO_4$ aqueous solution / 5% acetonitrile for 100 min, measured at 254 nm. (b) Chiral HPLC spectrum of standard DL-lactic acid (from Sigma-Aldrich), using the same HPLC condition as that in (a). The results confirmed that there was no epimerization in the degradation.

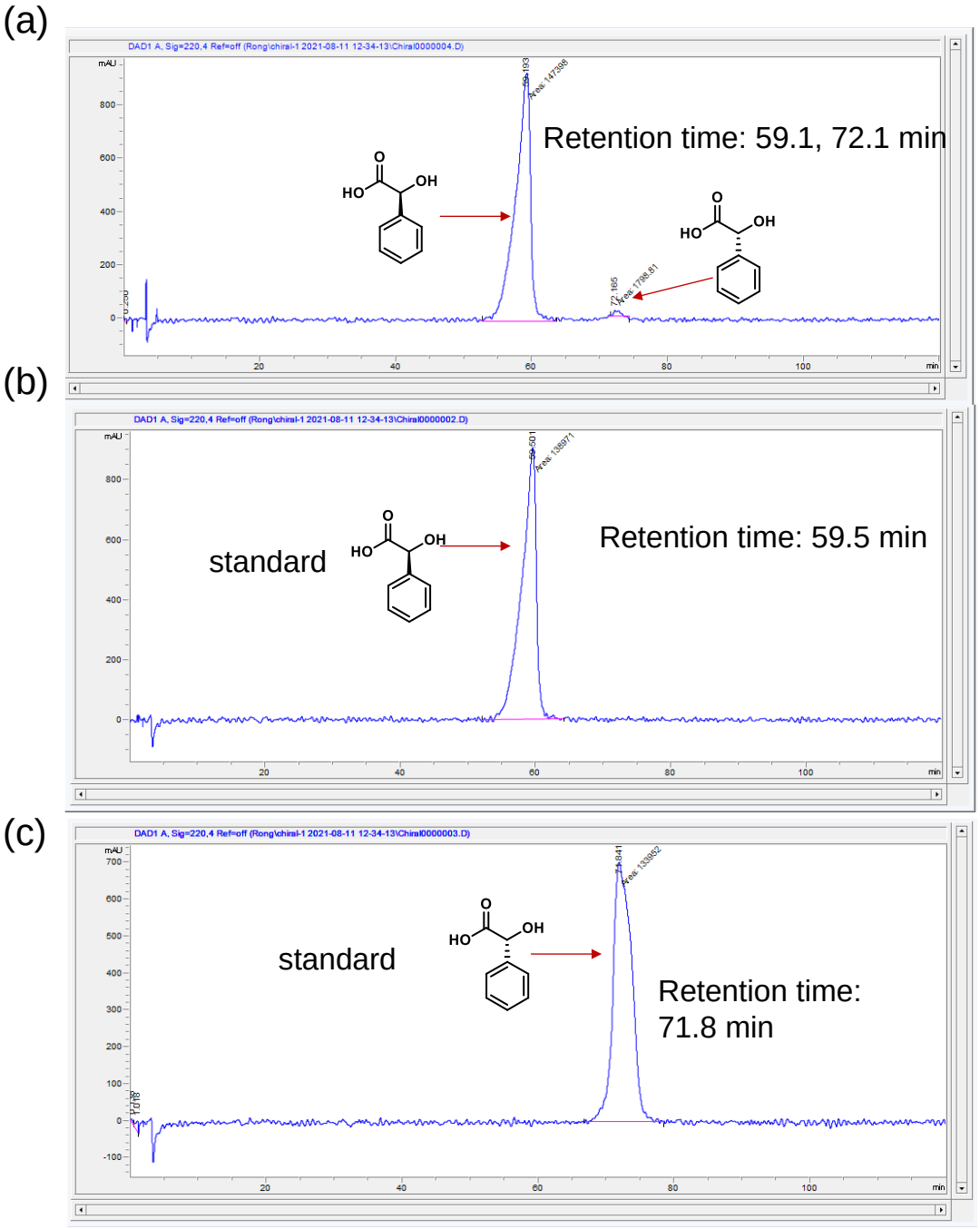

Figure 3.17 (a) Chiral HPLC spectrum obtained hydroxy acid of L-**5** from the second step (after extraction, no purification). A small peak of D-**5** (72 min) was found in the mixture. The calculated *ee* is based on chiral HPLC peak areas: 97.6 % *ee*. HPLC condition: 85% 2 mM $CuSO_4$ aqueous solution / 15% acetonitrile for 120 min, measured at 220 nm. (b, c) Chiral HPLC spectra of the standard L-**5** and D-**5** hydroxy acids, respectively, using the same HPLC condition as that in (a). The results suggested that the polymer was fully degraded to L-**5** hydroxy acid, with minimal epimerization during the second step of degradation using LiOH.

3.2.3 Benchmark against conventional methods

In comparison, we found that the conventional degradation methods (including using different bases and documented metal complexes) did not work for poly(L-**1**) (**Table 3.2, Figure 3.18**).[21-23] Firstly, entry 2 and **Figure 3.18a** showed that the methanol solution without **Zn-1** at 50 °C did not generate any degradation of poly(L-**1**). The conventional hydrolysis method at basic pH (entry 3 and **Figure 3.18b**)[23, 24] and using Zn salts at high temperature (entry 4 and 5; **Figure 3.18c-d**)[21] resulted in slight degradation of poly(L-**1**). However, the use of a strong organic base (TBD, pKa = 21 in THF) (entry 6 and **Figure 3.18e**) led to significant degradation of the polymer, but the final yield was still lower than our method (comparing with NMR spectra in **Figure 3.5b**). The functional group on the polyesters likely has steric effects of slowing down the degradation for those conventional degradation methods. Note that the separation of TBD from the resulting methyl ester using chromatography is still required after degradation, whereas the use of **Zn-1** as catalyst allows for a simple centrifugation and filtration method to remove the degradation catalyst. Our method is thus advantageous when benchmarked against conventional degradation methods, which typically require high temperature, prolonged reaction time, and extra steps for separating catalysts from depolymerized products,[25] in addition to suffering from side reactions that generate substantial epimerized products.[26]

Table 3.2 Degradation of poly(L-1) by Zn-1/MeOH benchmarked against conventional methods.

Entry	Condition	Solvent	Temp. (°C)	Time (h)	Conv. (%)
1	10 wt% **Zn-1**	MeOH	50	12	100
2	/	MeOH	50	12	0
3	1 M NaOH [23]	Water	50	12	9.2
4	10 wt% $ZnCl_2$	MeOH	50	12	0
5	2 mol% $ZnCl_2$ [21]	Toluene	120	24	0
6	10 wt% TBD [22]	MeOH	50	12	86.1

Abbreviation: TBD, 1,5,7-triazabicyclo[4.4.0]dec-5-ene.

(a) poly(L-**1**) in MeOH at 50 °C for 12 hr

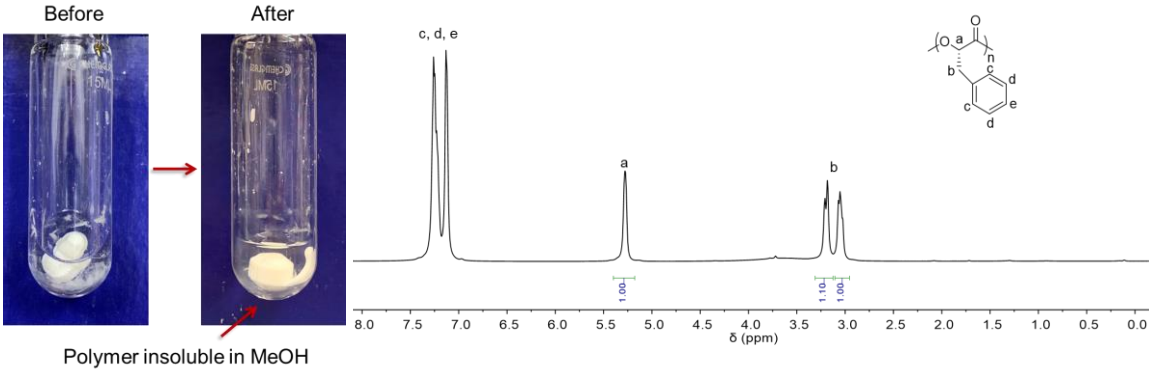

(b) poly(L-**1**) in NaOH (1 M aqueous solution) at 50 °C for 12 hr

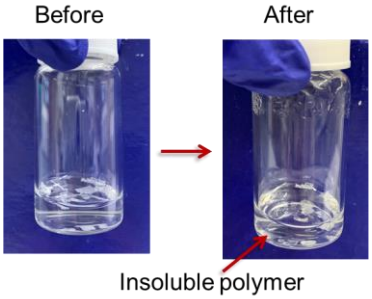

(c) poly(L-**1**) in 10 wt% $ZnCl_2$ solution at 50 °C for 12 hr

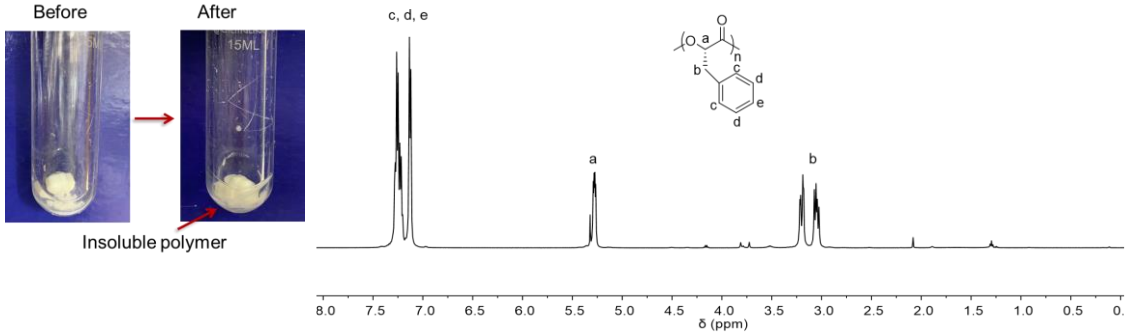

(d) poly(L-**1**) in 2 mol% $ZnCl_2$ toluene solution at 120 °C for 24 hr

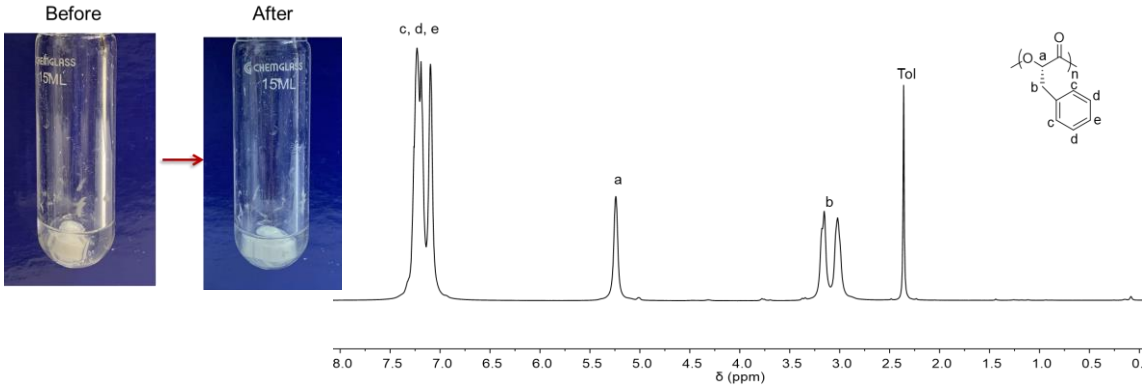

(e) poly(L-**1**) in 10 wt% TBD methanol solution at 50 °C for 12 hr

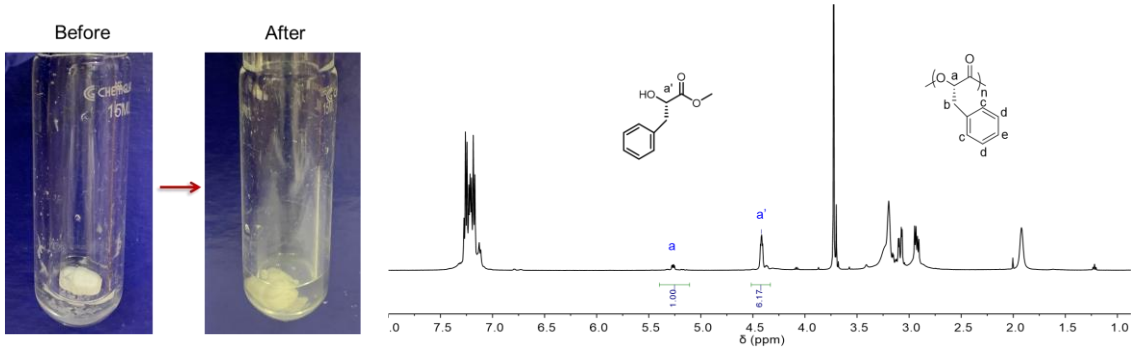

Figure 3.18 Degradation of poly(L-**1**) using conventional degradation methods (each panel corresponding to Table 3.2, entries 2-6).

3.3 Materials and methods

3.3.1 General

1,5,7-triazabicyclo[4.4.0]dec-5-ene (TBD), $ZnCl_2$, NaOH and lithium hydroxide monohydrate, copper sulfate, copper(II) acetate and ammonium acetate were purchased from Sigma-Aldrich (St. Louis, MO). *O*-benzyl-L-serine, *O*-benzyl-D-serine, L-glutamic acid-γ-benzyl ester, D-glutamic acid-γ-benzyl ester, *S*-(+)-mandelic acid and *R*-(-)-mandelic acid were purchased from Chem-Impex (Wood Dale, IL). L-phenylalanine and D-phenylalanine were purchased from Alfa Aesar (Haverhill, MA). Anhydrous tetrahydrofuran (THF) was dried by alumina columns and stored with 4Å molecular sieve in the dark bottle in the glove box (MBraun, Labstar Pro, < 1 ppm oxygen and moisture). Benzyl alcohol, and anhydrous MeOH were dried and stored by 4Å molecular sieves in the glove box. All other chemicals were purchased from Sigma-Aldrich (St. Louis, MO) unless otherwise noted.

3.3.2 Instrument and characterization

3.3.2.1 Electrospray ionization mass spectrometry (ESI-MS)

The ESI-MS analysis of air-sensitive samples followed the literature.[27] In brief, in a glove box, a 100 μL aliquote of the sample was taken up into the 250 μL Hamilton gastight syringe. The syringe was punched into a 1 mL LC sampler vial capped with a rubber septum to avoid the contact between needle and air and was sealed in a zip bag. The zip bag was removed from the glove box and immediately analyzed by ESI-MS (Agilent 6220 Accurate-Mass Time-of-Flight LC/MS).

3.3.2.2 NMR spectroscopy

All room temperature NMR and homodecoupling ^{1}H NMR spectra were recorded on Agilent U4-DD2 (400 MHz) or Bruker Avance II (500 MHz). Low temperature ^{1}H and ^{13}C NMR spectra were measured on Bruker Avance III (600 MHz) after the inner temperature of the NMR machine reached −20 °C for 20 min. The samples were kept at −15 °C ± 5 °C with a dry ice/ethylene glycol bath before the low-temperature NMR acquisition. All ^{13}C NMR spectra are proton decoupled.

3.3.2.3 Chiral high-performance liquid chromatography (HPLC)

Chiral HPLC analysis was performed on an Agilent series 1260 Infinity HPLC with the 1260 multiwavelength diode array detector (Agilent, Santa Clara, CA) equipped with an analytical Chirex 3126 (D)-penicillamine chiral HPLC column (50 x 4.6 mm, 5 μm, Phenomenex, Torrance, CA, catalog # 00F-3126-E0), eluted with the mixture of $CuSO_4$ aqueous solution (2 mM) and acetonitrile. The UV wavelength for detecting hydroxyl acid and methyl ester analysis was set at 220 nm or 254 nm.

3.3.3 Degradation procedures

3.3.3.1 Degradation of polyesters by Zn-1/MeOH

In a glove box, poly(L-**1**) (30 mg) and **Zn-1** (10 wt%, 3 mg) were sequentially added in anhydrous methanol (1 mL) in a flask with a stir bar. The polymer was insoluble in MeOH (see Figure 3.7). The flask was sealed and was moved out of the glove box and was stirred at 50 degree for 12 hours. During the degradation, the polymer was gradually dissolved in the methanol solution, forming a cloudy solution. After the reaction, yellow precipitates (presumably Zn-alkoxide) were observed upon quick centrifugation (see Figure 3.7). The resulted mixture was quickly filtered through a short silica chromatography to remove Zn precipitates. The filtrate was evaporated for NMR and ESI-MS analysis that confirmed the complete degradation of polymers with quantitative yield, and ICP-MS analysis that confirmed that metal concentrations were below 100 ppb levels (see Table 3.1). The chirality of the obtained methyl ester was determined by chiral HPLC (see 3.3.2.3) and no epimerization was found in the reaction.

3.3.3.2 Conversion of methyl ester to hydroxy acid

The methyl ester (1.0 mmol) obtained in 3.3.3.1 was mixed with LiOH (3 mmol, 71.9 mg), water (1.0 mL), MeOH (1.0 mL) and THF (0.5 mL) according to the literature.[20] The reaction was quenched with 1 M HCl (4 mL) and was extracted with EtOAC (5 mL × 3). The combined organic layer was dried over Na_2SO_4 and concentrated for chiral HPLC analysis, which indicated minimal epimerization (100 *ee*% for **1-4**, and 97.6 *ee*% for **5**). For all reactions, the yield was over 85%, consistent with the literature report.[20] We note that for the degradation of poly(L-**3**), 6 mmol LiOH was used for 1.0 mmol methyl esters, as the side chain in the monomer **3** also becomes methyl ester.

3.4 Conclusions

The chemical recycling of poly(α-hydroxy acids) under mild conditions was studied experimentally. It consisted of two steps, degradation to the corresponding methyl ester and then transformation into hydroxy acid, which served as the starting material for monomer synthesis, thereby closing the life cycle loop. This degradation method outperforms other conventional degradation methods, which tend to require high temperatures, prolonged reaction time, and additional steps for separating catalysts from depolymerized products, in addition to generating epimerized products due to side reactions. We believe that the current results represent significant progress in understanding the process of polyester alcoholysis mediated by metal complexes. It will be helpful in designing new catalysts for the depolymerization of polyesters into the corresponding monomer or monomer derivatives.

References

1. Jambeck, J. R.; Geyer, R.; Wilcox, C.; Siegler, T. R.; Perryman, M.; Andrady, A.; Narayan, R.; Law, K. L., Plastic waste inputs from land into the ocean. *Science* **2015,** *347* (6223), 768-771.
2. Moore, C. J., Synthetic polymers in the marine environment: a rapidly increasing, long-term threat. *Environmental research* **2008,** *108* (2), 131-139.
3. Hong, M.; Chen, E. Y.-X., Chemically recyclable polymers: a circular economy approach to sustainability. *Green Chemistry* **2017,** *19* (16), 3692-3706.
4. Clark, J. H.; Farmer, T. J.; Herrero-Davila, L.; Sherwood, J., Circular economy design considerations for research and process development in the chemical sciences. *Green Chemistry* **2016,** *18* (14), 3914-3934.
5. Jelinski, L. W.; Graedel, T. E.; Laudise, R. A.; McCall, D. W.; Patel, C. K., Industrial ecology: concepts and approaches. *Proceedings of the National Academy of Sciences* **1992,** *89* (3), 793-797.
6. Zhang, X.; Fevre, M.; Jones, G. O.; Waymouth, R. M., Catalysis as an enabling science for sustainable polymers. *Chemical reviews* **2018,** *118* (2), 839-885.
7. Hopewell, J.; Dvorak, R.; Kosior, E., Plastics recycling: challenges and opportunities. *Philosophical Transactions of the Royal Society B: Biological Sciences* **2009,** *364* (1526), 2115-2126.
8. Shen, L.; Worrell, E.; Patel, M. K., Open-loop recycling: A LCA case study of PET bottle-to-fibre recycling. *Resources, conservation and recycling* **2010,** *55* (1), 34-52.
9. Majgaonkar, P.; Hanich, R.; Malz, F.; Brüll, R., Chemical Recycling of Post-Consumer PLA Waste for Sustainable Production of Ethyl Lactate. *Chemical Engineering Journal* **2021**, 129952.
10. Tang, X.; Chen, E. Y.-X., Toward infinitely recyclable plastics derived from renewable cyclic esters. *Chem* **2019,** *5* (2), 284-312.
11. Beromi, M. M.; Kennedy, C. R.; Younker, J. M.; Carpenter, A. E.; Mattler, S. J.; Throckmorton, J. A.; Chirik, P. J., Iron-catalysed synthesis and chemical recycling of telechelic 1, 3-enchained oligocyclobutanes. *Nature chemistry* **2021,** *13* (2), 156-162.
12. Hong, M.; Chen, E. Y.-X., Future directions for sustainable polymers. *Trends in Chemistry* **2019,** *1* (2), 148-151.
13. Herrera-Kao, W.; Loría-Bastarrachea, M.; Pérez-Padilla, Y.; Cauich-Rodríguez, J.; Vázquez-Torres, H.; Cervantes-Uc, J. M., Thermal degradation of poly (caprolactone), poly (lactic acid), and poly (hydroxybutyrate) studied by TGA/FTIR and other analytical techniques. *Polymer Bulletin* **2018,** *75* (9), 4191-4205.
14. Liu, L.; Zachariah, M. R.; Stoliarov, S. I.; Li, J., Enhanced thermal decomposition kinetics of poly (lactic acid) sacrificial polymer catalyzed by metal oxide nanoparticles. *RSC advances* **2015,** *5* (123), 101745-101750.
15. Piemonte, V.; Gironi, F., Kinetics of hydrolytic degradation of PLA. *Journal of Polymers and the Environment* **2013,** *21* (2), 313-318.
16. Román-Ramírez, L. A.; Mckeown, P.; Jones, M. D.; Wood, J., Poly (lactic acid) degradation into methyl lactate catalyzed by a well-defined Zn (II) complex. *ACS Catalysis* **2018,** *9* (1), 409-416.
17. Román-Ramírez, L. A.; McKeown, P.; Shah, C.; Abraham, J.; Jones, M. D.; Wood, J., Chemical degradation of end-of-life poly (lactic acid) into methyl lactate by a

Zn (II) complex. *Industrial & engineering chemistry research* **2020,** *59* (24), 11149-11156.
18. Yang, R.; Xu, G.; Lv, C.; Dong, B.; Zhou, L.; Wang, Q., Zn(HMDS)2 as a Versatile Transesterification Catalyst for Polyesters Synthesis and Degradation toward a Circular Materials Economy Approach. *ACS Sustainable Chemistry & Engineering* **2020,** *8* (50), 18347-18353.
19. Planer, S.; Jana, A.; Grela, K., Ethyl Lactate: A Green Solvent for Olefin Metathesis. *ChemSusChem* **2019,** *12* (20), 4655-4661.
20. Koshikari, Y.; Sakakura, A.; Ishihara, K., N,N-Diarylammonium Pyrosulfate as a Highly Effective Reverse Micelle-Type Catalyst for Hydrolysis of Esters. *Organic Letters* **2012,** *14* (12), 3194-3197.
21. Zhu, J.-B.; Watson, E. M.; Tang, J.; Chen, E. Y.-X., A synthetic polymer system with repeatable chemical recyclability. *Science* **2018,** *360* (6387), 398-403.
22. Leibfarth, F. A.; Moreno, N.; Hawker, A. P.; Shand, J. D., Transforming polylactide into value-added materials. *Journal of Polymer Science Part A: Polymer Chemistry* **2012,** *50* (23), 4814-4822.
23. Codari, F.; Lazzari, S.; Soos, M.; Storti, G.; Morbidelli, M.; Moscatelli, D., Kinetics of the hydrolytic degradation of poly(lactic acid). *Polymer Degradation and Stability* **2012,** *97* (11), 2460-2466.
24. de Jong, S. J.; Arias, E. R.; Rijkers, D. T. S.; van Nostrum, C. F.; Kettenes-van den Bosch, J. J.; Hennink, W. E., New insights into the hydrolytic degradation of poly(lactic acid): participation of the alcohol terminus. *Polymer* **2001,** *42* (7), 2795-2802.
25. Fukushima, K.; Coulembier, O.; Lecuyer, J. M.; Almegren, H. A.; Alabdulrahman, A. M.; Alsewailem, F. D.; Mcneil, M. A.; Dubois, P.; Waymouth, R. M.; Horn, H. W.; Rice, J. E.; Hedrick, J. L., Organocatalytic depolymerization of poly(ethylene terephthalate). *Journal of Polymer Science Part A: Polymer Chemistry* **2011,** *49* (5), 1273-1281.
26. Nishida, H.; Mori, T.; Hoshihara, S.; Fan, Y.; Shirai, Y.; Endo, T., Effect of tin on poly(l-lactic acid) pyrolysis. *Polymer Degradation and Stability* **2003,** *81* (3), 515-523.
27. Evans, W. J.; Johnston, M. A.; Fujimoto, C. H.; Greaves, J., Utility of Electrospray Mass Spectrometry for the Characterization of Air-Sensitive Organolanthanides and Related Species1. *Organometallics* **2000,** *19* (21), 4258-4265.

CHAPTER 4

Stereoselective polymerization of racemic *O*-carboxyanhydrides

4.1 Introduction

While a transition to degradable polymers can address the plastic pollution problem, their commercialization is hampered by competition with commodity non-degradable polyolefins. Compared with non-degradable polyolefins, degradable polymers do not have more favorable material properties, such as thermal resistance and mechanical strength.[1] Apart from functional groups on the side-chain of aliphatic polyesters, another significant determinant of the polymer's physical and mechanical properties is its tacticity, that is, the regularity of the configurations of adjacent stereocenters along the polymer chain.[2] There are two types of ordered structures: isotactic structures, in which the configurations of neighboring stereocenters are the same, and syndiotactic structures, in which neighboring stereocenters have alternating configurations (**Figure 4.1**). Polymers with isotactic or syndiotactic microstructures referred to as stereoregular polymers, usually are crystalline and have improved thermal and mechanical properties relative to those of atactic polymers. For example, syndiotactic polystyrene is a highly crystalline material with a T_m of 270 ℃, whereas atactic polystyrene is amorphous.[3] Therefore, the search for a new catalytic system capable of precisely controlling the stereosequence of copolymers is crucial.

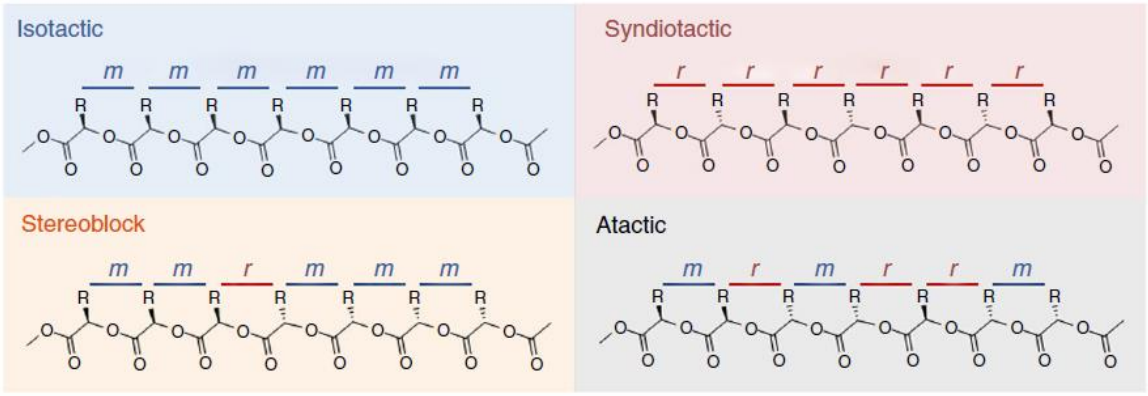

Figure 4.1 Stereoselective ring-opening polymerization of *O*-carboxyanhydrides (OCAs). (Reproduced from *Nat. Commun.* **2018**, 9, 1159)

Despite efforts devoted to the synthesis of stereoregular polyesters by stereoselective ring-opening polymerization of racemic lactide and lactones,[4-13] relatively few well-defined metal catalysts are available for stereoselective polymerization of racemic OCA monomers. For isoselective ROP of OCAs, the Wu group[14] demonstrated that a Zn complex with a dipyrrin ligand (**L-TMP-Zn**, **Figure 4.2**) could mediate isoselective ROP of *rac*-**1**, *rac*-**4**, and *rac*-**8** via a chain-end-control mechanism, with P_m values ranging from 0.95–0.97 at -70 °C. However, it should be noted that significant epimerization was observed during the ROP process for L-**5**. Similar isoselectivity results of aminobisphenolate Zn complex (**L^{1}Zn + 3-F-Py**) were also reported by Wu's group[15] (**Figure 4.2**), which could mediate isoselective ROP of *rac*-**5** with a high P_m of 0.92 at -50 °C. However, both catalysts need extremely low reaction temperatures (-50 °C or -70 °C) to complete the polymerization, and the obtained MWs of stereoblock polyesters were either less than 10 kDa or with broad molecular weight distributions ($Đ$ > 1.4).

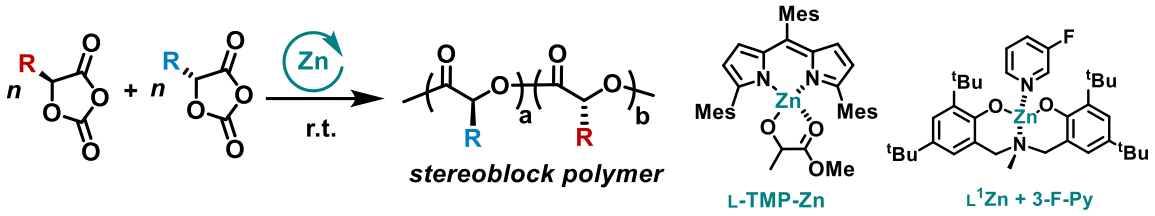

Figure 4.2 Isoselective ROP of OCAs mediated by Zn complexes.

A breakthrough for syndioselective ROP of OCAs was Wu group described Zr or Hf-alkoxides with aminotris (phenolate) ligands to control syndioselective ROP of *rac*-**4** in 2017 (**Figure 4.3**)[16]. The Hf-alkoxide complex afforded syndiotactic polyesters at room temperature with high P_r values of 0.80–0.95 (P_r, the maximum probability of racemic dyad formation). This particular catalytic system could also produce alternated poly(D-**1**-*alt*-L-**8**) and poly(L-**1**-*alt*-D-**4**) with high alternation percentage (~95% alternation). However, such a syndioselective catalytic system was still unable to synthesize stereoselective polymers with high MWs (only 10 kDa). Wu and coworkers further reported another Hf alkoxide complex with bulky adamantyl groups that exhibited excellent syndioselectivity for *rac*-**4** with a P_r of 0.91, but a poor syndioselectivity for *rac*-**11** with a P_r of 0.46.[17] Intriguingly, when the copolymerization of D-**4** and L-**11** was carried out at room temperature, alternating poly(D-**4**-*alt*-L-**11**) was successfully produced with an alternation level of 86%. However, in all cases, these alternating polymers had low MWs (< 10 kDa).

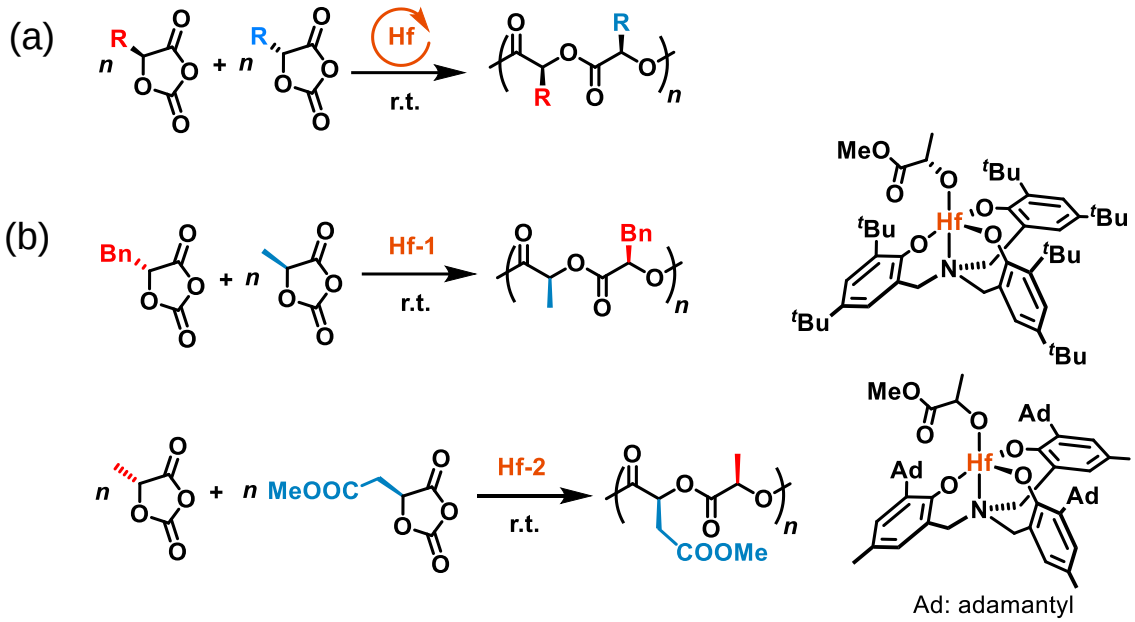

Figure 4.3 Syndioselective ROP of OCAs mediated by Hf complexes. (a) The development of two Hf complexes for syndioselective ROP of OCAs. (b) Alternating copolymerization of two OCA monomers with opposite chirality, mediated by different Hf complexes.

To address these challenges, our group has examined stereoselective polymerization of OCAs by using Ni/Zn/Ir-mediated photoredox ROP method[2], and Co/Zn-mediated electrochemical ROP (*e*ROP) of OCAs[18], which all result in high MW functionalized polyesters with narrow MW distributions ($Đ$ < 1.1). A less bulky tridentate Schiff base ligand was screened to form **Zn-4** complex (**Figure 4.4a**), which could combine with Ni and Ir complex to synthesize highly stereoblock (*sb*) poly(*sb*-**1**) with high MWs (78 kDa). It also enabled the synthesis of a series of gradient polymers in one pot (**Figure 4.4b**). Moreover, our group recently disclosed a new electrochemical pathway to achieve the stereoselective ROP of *rac*-OCAs in 2020 (**Figure 4.4c**).[18] When a current is applied, the **Co-1**/**Zn-3** catalytic system offered stereoblock poly(*sb*-**1**) with a MW of 67.6 kDa and a high P_m value of 0.95. Moreover, the **Co-2**/**Zn-10** catalytic system generated syndiotactic poly(*sd*-**1**) (*sd*, syndiotactic) with a MW of 46.2 kDa and a

P_r value of 0.79. It was observed that aside from the ligand of the metal complex, the side-chain functionalities of OCA monomers also influenced stereoselectivity during the electrochemical polymerization process.

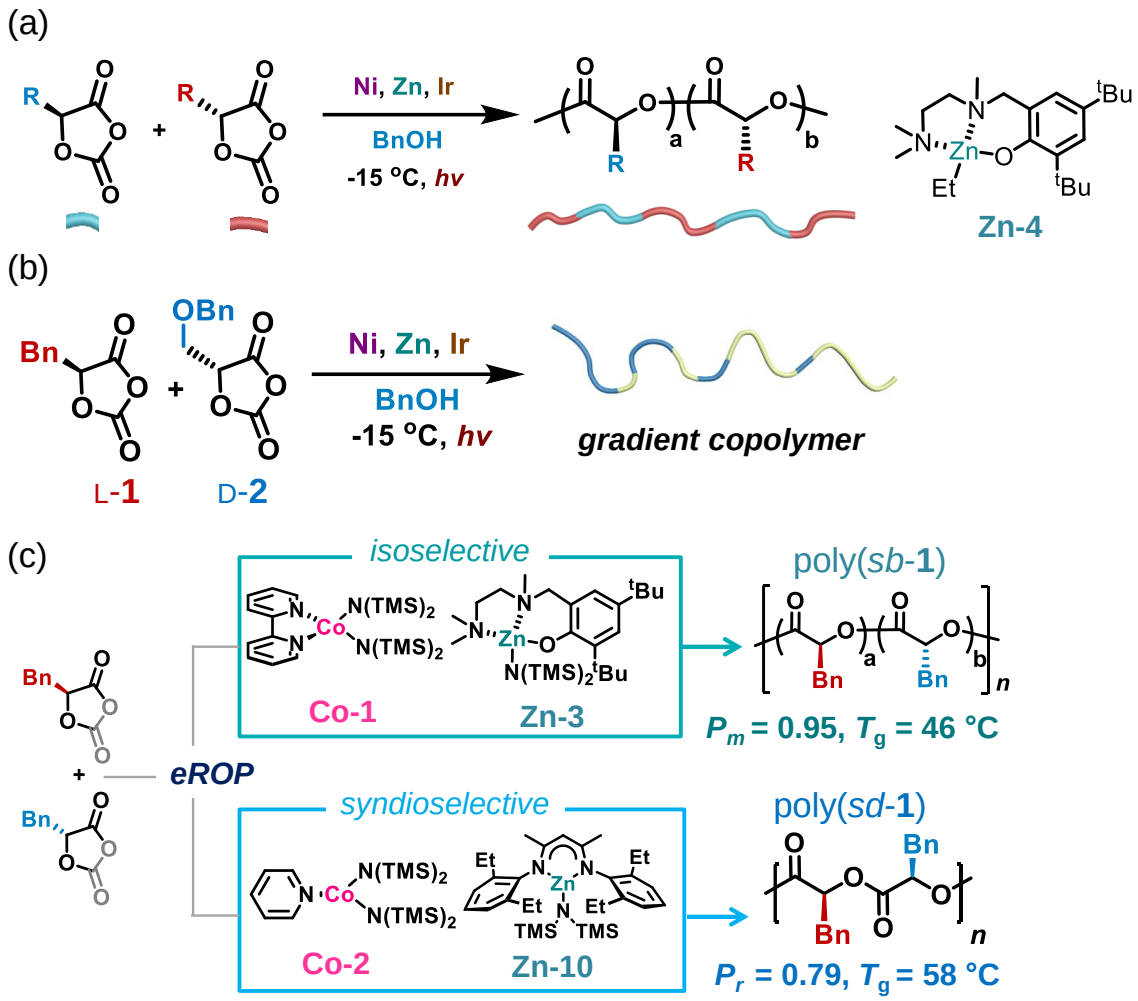

Figure 4.4 (a) Scheme of photoredox isoselective ROP of OCAs to synthesize stereoblock copolymers, mediated by Zn/Ni/Ir catalysts. (b) The same catalytic system allows for the one-pot synthesis of gradient copolymers. (c) Co/Zn complex-mediated stereoselective eROP of racemic 1. The selection of different catalysts could enable the synthesis of poly(**1**) with different microstructures and T_gs.

Nevertheless, extensive utilization of these metal-catalyzed stereoselective ROP of OCAs for high MW stereoregular polyesters is still limited because of reliance on an

external energy source (light or electricity). Following our results in Chapter 2, we then investigated whether the Mn/Zn catalytic system without external energy could be adapted for stereoselective ROP of racemic OCAs.

4.2 Results and discussions

4.2.1 The discovery of Mn-1/Zn-2 for stereoselective ring-opening polymerization of racemic 1 (*rac*-1)

After screening a series of Zn and Hf complex (**Figure 4.5** and **Table 4.1**), we found that the combination of **Zn-2** and **Mn-1** ([L-**1**]/[D-**1**]/[**Zn-2**]/[**Mn-1**] = 200/200/1/1) at −15 °C produced stereoblock copolymer poly(*sb*-**1**) with a M_n of 56.2 kDa (close to the calculated MW of 59.3 kDa), a narrow $Đ$ (1.03), and a high probability of *meso* dyad formation (P_m, 0.95; **Table 4.1**, entry 5; **Figure 4.6**). In contrast, $Zn(HMDS)_2$-mediated stereoselective polymerization of *rac*-**1** afforded an atactic polymer (**Table 4.1**, entry 1), confirming that the tridentate ligand of **Zn-2** complex influenced the stereoselectivity of OCA polymerization. However, the use of **Mn-1** likely improved the polymerization kinetics but did not affect the stereochemistry preference, since ROP of *rac*-**1** at the same [**1**]/[Zn] ratio without **Mn-1** ([L-**1**]/[D-**1**]/[**Zn-2**] = 200/200/1) showed incomplete monomer conversion (81.3% at 48 hours) with a P_m value of 0.96 (**Table 4.1**, entry 7).

The kinetic studies in **Figure 4.7** suggested the polymerization of either enantiomer at the same [**1**]/[Zn] ratio was identical and more rapid than the ROP of *rac*-**1** (at a [**1**]/[Zn] ratio of 400, the polymerization rate constant of L-**1** was 74.1-times higher than that of *rac*-**1**. Therefore, it was likely that chain-end-controlled mechanism dominated in this isoselective polymerization, not enantiomorphic-site-control mechanism, which was also confirmed by using similar Zn catalyst (same ligand,

different leaving groups) in the photoredox ROP.[2] Additionally, the ^{13}C NMR analysis of the α-methine peaks suggested that the ratio of tetrad *mmr* / *rmm* / *mrm* is about 1/1/1 (**Figure 4.6b**). The proposed stereoblock via the chain-end-controlled mechanism (isoselective ROP) should have a stereo-sequence as -*RRRSSS*- (-*mmrmm*-) and the ratio of *mmr* / *rmm* / *mrm* should be 1/1/1. On the other hand, the enantiomorphic-site mechanism should have a stereosequence as -*RRRSRRR*- or -*SSSRSSS*- (-*mmrrmm*-) and the ratio of *mmr* / *rmm* / *mrr* / *rrm* should be 1/1/1/1, which was not seen in our case. Taken together, both kinetics and NMR analysis revealed that the polymerization proceeded via chain-end-controlled isoselective ROP.

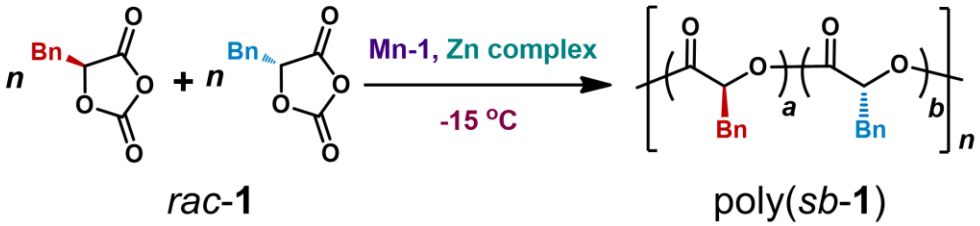

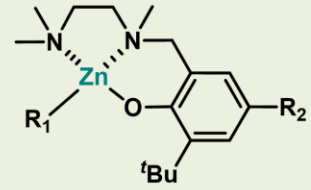

	R_1	R_2	P_m
Zn-2	$OCH(Me)CO_2Me$	^{t}Bu	0.95
Zn-3	$N(SiMe_3)_2$	^{t}Bu	0.90
Zn-4	Et	^{t}Bu	conversion < 5%
Zn-5	$OCH(Me)CO_2Me$	OMe	0.86
Zn-6	$OCH(Me)CO_2Me$	NO_2	conversion: 56 %
Zn-7	$OCH(Me)CO_2Me$	F	0.93

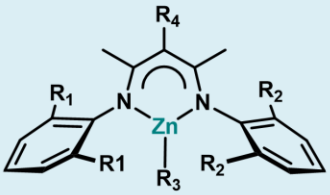

	R_1	R_2	R_3	R_4	P_m
Zn-8	^{i}Pr	^{i}Pr	$N(SiMe_3)_2$	H	0.73
Zn-9	^{i}Pr	^{i}Pr	$OCH(Me)CO_2Me$	H	conversion: 31 %
Zn-10	Et	Et	$N(SiMe_3)_2$	H	0.68
Zn-11	Et	Et	$OCH(Me)CO_2Me$	H	0.83
Zn-12	Et	^{i}Pr	$N(SiMe_3)_2$	H	0.75
Zn-13	Et	^{i}Pr	$OCH(Me)CO_2Me$	H	0.84
Zn-14	Et	Et	$OCH(Me)CO_2Me$	CN	0.77

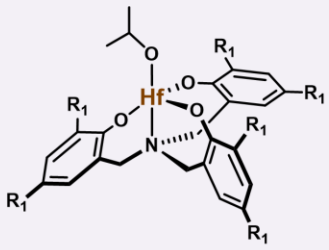

	R_1	P_m
Hf-1	^{t}Bu	conversion: 23 %
Hf-2	Me	conversion: 24 %

Figure 4.5 Screen of various Zn and Hf complexes for isoselective ROP of *rac*-**1** in the presence of **Mn-1**.

Table 4.1. The discovery of **Mn-1**/**Zn-2** for isoselective ring-opening polymerization of racemic **1** (*rac*-**1**)

Entry	Zn complex	[L-**1**]/[D-**1**]	Time (h)	Conv. (%)	M_n (kDa)	MW_{cal} (kDa)	$Đ$	P_m
1	**Zn-1** [a]	100/100	1	100	26.9	29.7	1.04	0.75
2	**Zn-2**	100/100	1	100	29.1	29.7	1.03	0.95
3	**Zn-3** [a]	100/100	1	100	22.4	29.7	1.06	0.90
4	**Zn-4** [a]	100/100	2	< 5	N.D.	< 1.6	N.D.	N.D.
5	**Zn-2**	200/200	1	100	56.2	59.3	1.03	0.95
6	**Zn-2**	300/300	60	83.3	73.3	74.1	1.03	0.95
7	**Zn-2** [b]	200/200	48	81.3	48.7	48.2	1.03	0.96
8	**Zn-5**	100/100	1	100	30.3	29.7	1.09	0.86
9	**Zn-6**	100/100	21	56.5	N.D.	16.8	N.D.	N.D.
10	**Zn-7**	100/100	1	100	28.9	29.7	1.04	0.93
11	**Zn-7**	300/300	120	31.5	N.D.	28.1	N.D.	N.D.
12	**Zn-8** [a]	100/100	2	100	17.9	29.7	1.08	0.73
13	**Zn-9**	100/100	2	24.2	N.D.	7.27	N.D.	N.D.
14	**Zn-10** [a]	100/100	1	100	19.0	29.7	1.07	0.68
15	**Zn-11**	100/100	1	100	22.0	29.7	1.07	0.83
16	**Zn-12** [a]	100/100	2	100	22.1	29.7	1.07	0.75
17	**Zn-13**	100/100	2	93.8	35.4	27.9	1.04	0.84
18	**Zn-14**	100/100	1.5	100	23.5	29.7	1.06	0.77
19	**Hf-1**	100/100	72	23.2	N.D.	6.87	N.D.	N.D.
20	**Hf-2**	100/100	72	24.0	N.D.	7.21	N.D.	N.D.

[a] Addition of 1 equiv. BnOH ([Zn] / [BnOH] = 1/1)

[b] No **Mn-1** was added.

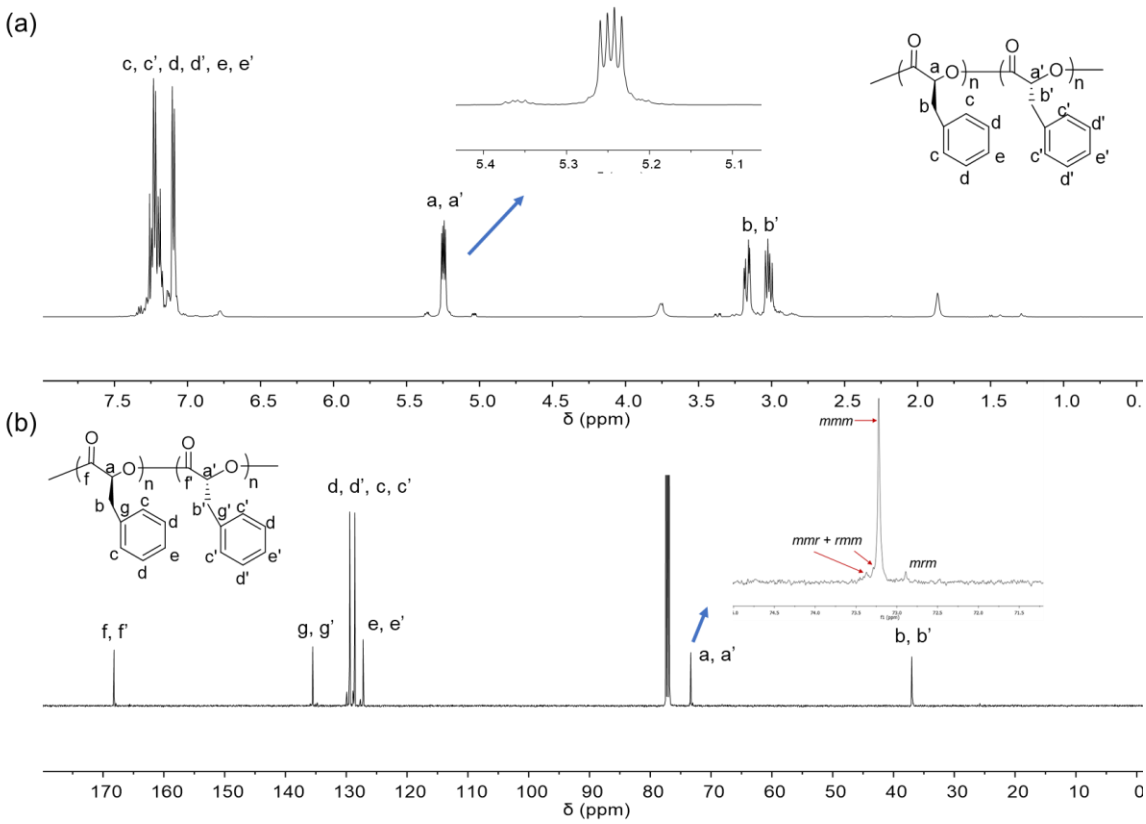

Figure 4.6 NMR spectra of poly(*sb*-**1**) in $CDCl_3$ (Table 4.1, entry 5). (a) ^{1}H NMR spectrum; (b) ^{13}C NMR spectrum.

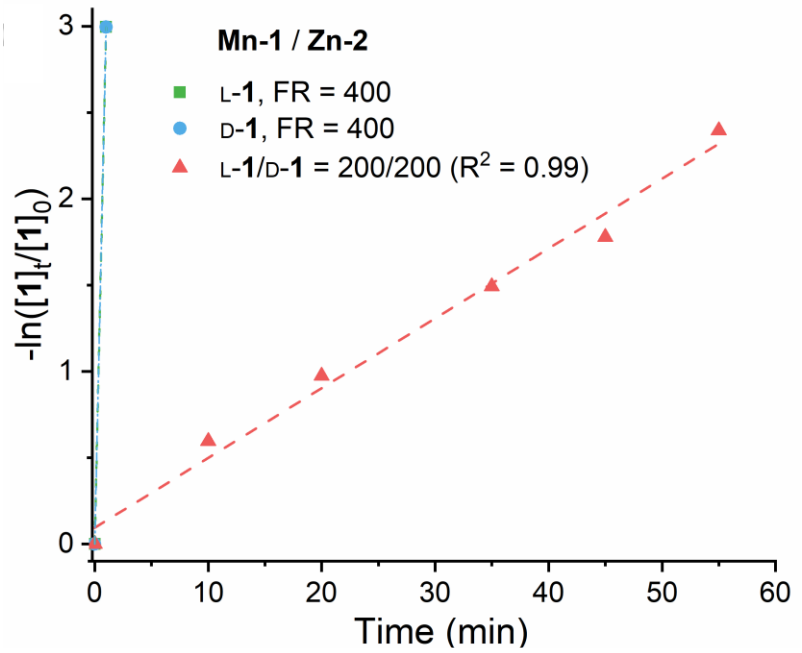

Figure 4.7 Kinetic plots of the ROP of L-**1**, D-**1** and *rac*-**1** in the presence of **Mn-1** / **Zn-2** at -15 °C. For *rac*-**1**, [L-**1**] = [D-**1**] = 1/1. [**1**] / [**Mn-1**] / [**Zn-2**] = 400/1/1. [**1**] = 310.0 mM.

4.2.2 Stereoselective ring-opening polymerization of other racemic-OCAs

Furthermore, these two metal complexes (**Mn-1**/**Zn-2**) facilitated the isoselective reactions of other racemic OCAs (*rac*-**2**–**5**). In all cases, polymerization controls were good, the M_n values were close to the calculated MWs, and all the $Đ$ vales were less than 1.1 (**Table 4.2**). This **Mn-1**/**Zn-2** catalytic system produced stereoblock copolymers with P_m values ranging from 0.79 to 0.91, as determined by microstructural analysis (**Figures 4.8-4.11**).

Table 4.2 Stereoselective ring-opening polymerization of other racemic-OCAs by **Mn-1**/**Zn-2**

Entry	OCA (FR)	Time (h)	Conv. (%)	M_n (kDa)	MW_{cal} (kDa)	$Đ$	P_m
1	*rac*-**2** (200)	1.5	100	32.9	35.7	1.09	0.83
2	*rac*-**3** (200)	1.5	100	44.7	44.1	1.03	0.90
3	*rac*-**4** (200)	1.5	100	15.9	14.5	1.09	0.91
4	*rac*-**5** (100) [a]	24	100	13.0	13.5	1.02	0.79

[a] The polymerization was mediated by **Zn-3**/**Mn-1**/BnOH (1/1/1); P_m = 0.75 for **Zn-2**/**Mn-1**.

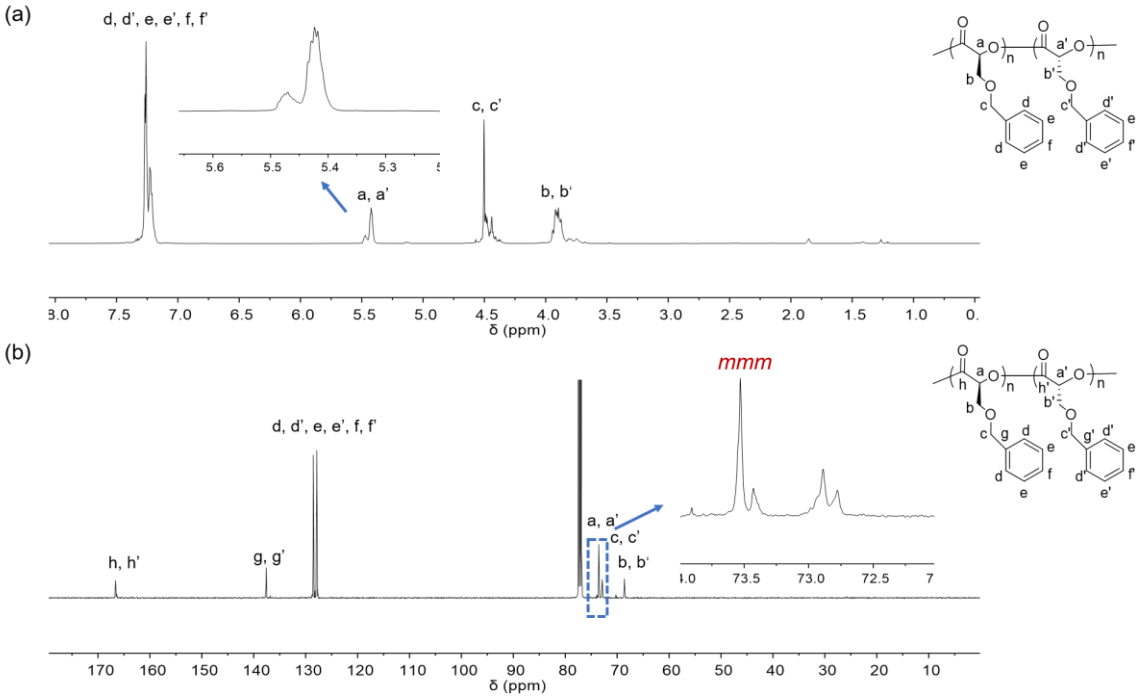

Figure 4.8 NMR spectra of poly(*sb*-**2**) in $CDCl_3$ (Table 4.2, entry 1). (a) ^1H NMR spectrum; (b) ^{13}C NMR spectrum.

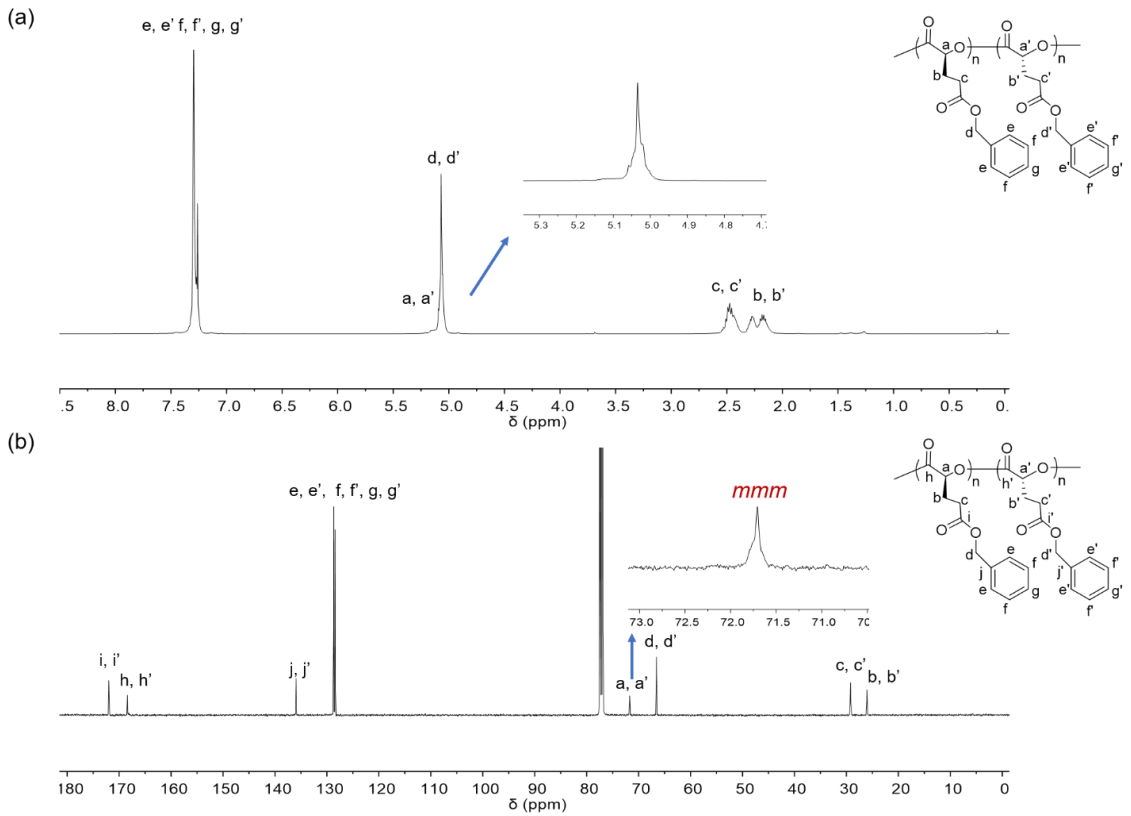

Figure 4.9 NMR spectra of poly(*sb*-**3**) in $CDCl_3$ (Table 4.2, entry 2). (a) ^{1}H NMR spectrum; (b) ^{13}C NMR spectrum.

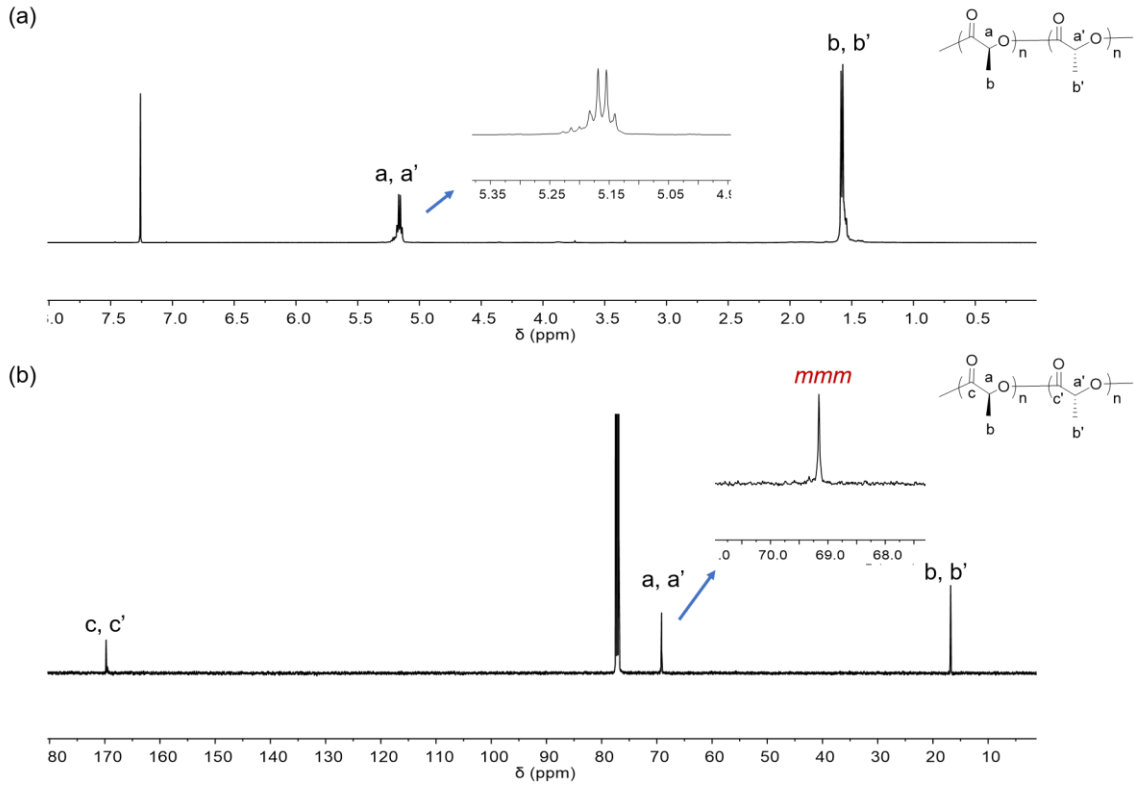

Figure 4.10 NMR spectra of poly(*sb*-**4**) in $CDCl_3$ (Table 4.2, entry 3). (a) ^{1}H NMR spectrum; (b) ^{13}C NMR spectrum.

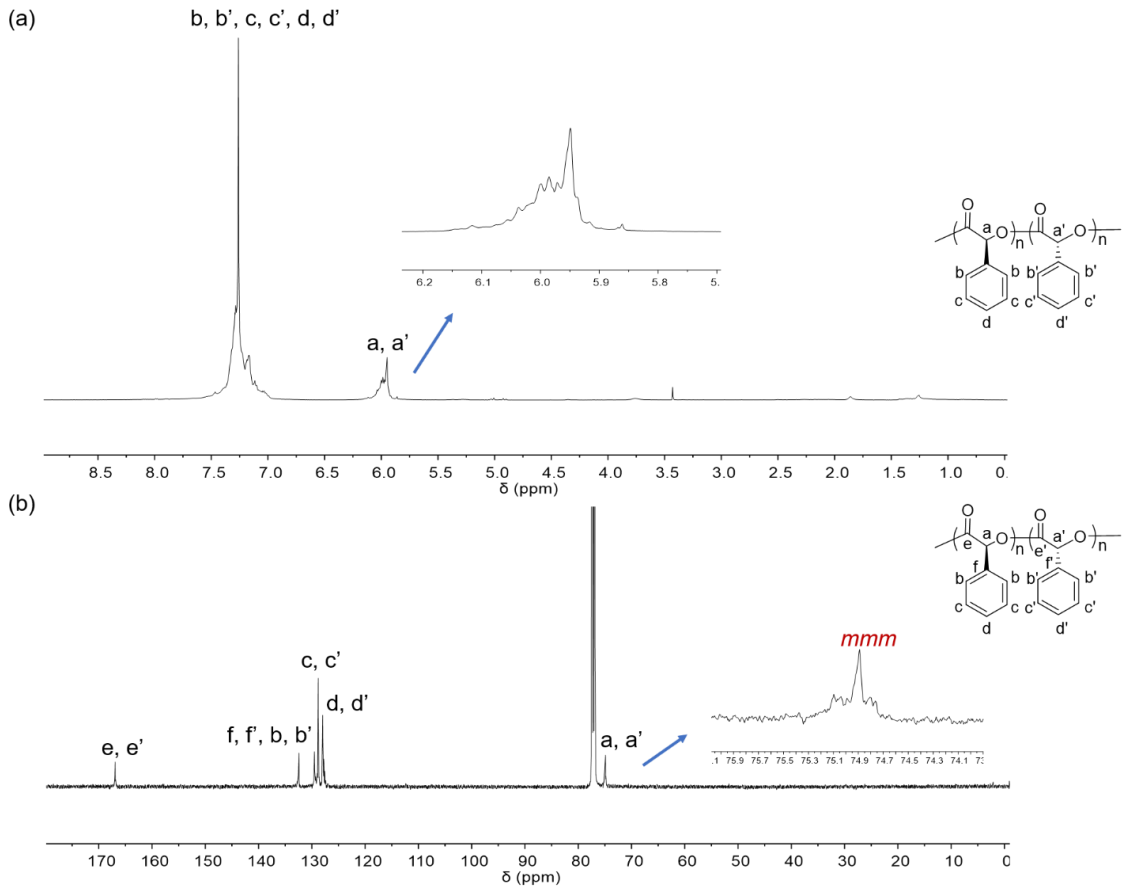

Figure 4.11 NMR spectra of poly(*sb*-**5**) in $CDCl_3$ (Table 4.2, entry 4). (a) ^{1}H NMR spectrum; (b) ^{13}C NMR spectrum.

4.2.3 Thermal properties of stereoblock copolymers

Understanding the effect of polymer structure on the glass transition temperature (T_g) is a critical parameter, particularly as it subsequently influences the resulting mechanical properties. The glass transition temperatures of polyesters with various microstructures utilizing a Mn/Zn catalyst system were determined by differential scanning calorimetry (DSC) analysis in **Table 4.3** and **Figure 4.12**. As anticipated, the addition of long side chains on the backbone could disrupt the crystallinity (smaller T_m peaks of poly(L-**3**) compared with poly(L-**4**)), and the rigidity of the polymer chain contributed to the increased T_g. (e.g. poly(L-**5**) > poly(L-**1**), poly(L-**2**) and poly(L-**3**)).

Moreover, the stereochemistry of polymers can alter their physicochemical properties. For example, poly(*sb*-**1**) (**Table 4.3**, entry 6) had a melting temperature (T_m) of 146 °C and a glass transition temperature (T_g) of 37 °C; whereas the homopolymer poly(L-**1**) (**Table 4.3**, entry 1) only had T_g around 49 °C and no observable T_m. Stereoblock poly(*sb*-**4**) (**Table 4.3**, entry 9) also had significant changes in T_g and T_m compared with poly(L-**4**) (**Table 4.3**, entry 4). However, for poly(**3**) with less crystallinity (small T_m peaks), changes of T_m and T_g in stereoblock poly(*sb*-**3**) compared with poly(L-**3**) were not substantial (**Table 4.3**, entry 3 and 8).

Table 4.3 Thermal properties of various homopolymers and stereoblock copolymers

Entry	polymer	P_m [b]	M_n (kDa) [c]	$Đ$ [c]	T_g / T_m (°C) [d]
1	poly(L-**1**)	1	170.9	1.09	49 / –
2	poly(L-**2**)	1	66.1	1.04	10 / –
3	poly(L-**3**)	1	133.8	1.02	5 / 136
4	poly(L-**4**)	1	26.2	1.07	– / 169
5	poly(L-**5**)	1	54.7	1.06	107 / -
6	poly(*sb*-**1**)	0.96	73.6	1.02	37 / 146
7	poly(*sb*-**2**)	0.83	32.9	1.09	11 / –
8	poly(*sb*-**3**)	0.90	44.7	1.03	9 / 130
9	poly(*sb*-**4**)	0.91	15.9	1.09	53 / 144
10	poly(*sb*-**5**) [e]	0.79	13.0	1.02	89 / 216

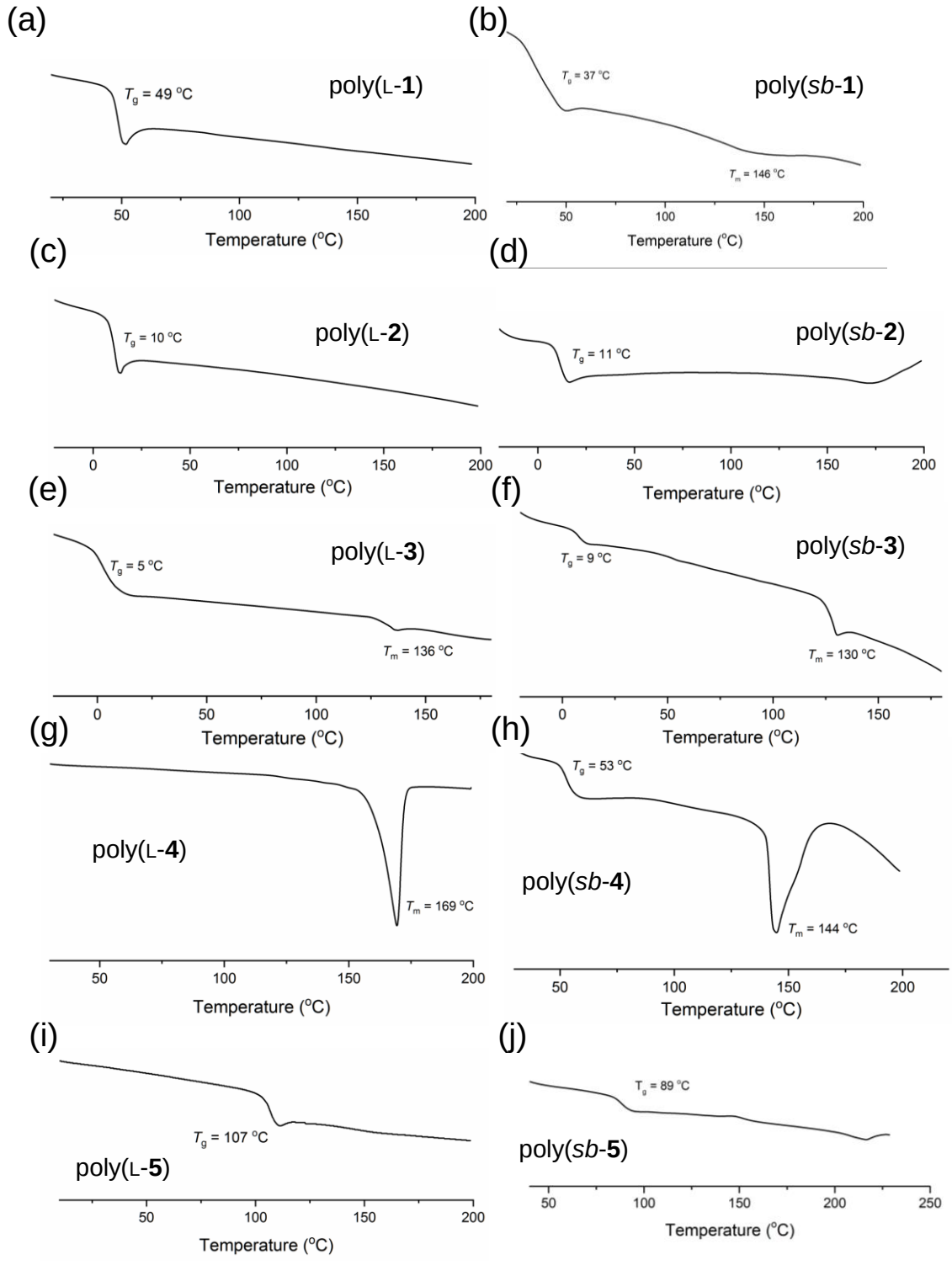

Figure 4.12 Differential scanning calorimetry measurements of T_gs and T_ms of various homopolymers and their corresponding stereoblock copolymers.

4.2.4 Synthesis of gradient copolymers

Our previously reported strategy for the synthesis of gradient (*grad*) copolymers from two OCA co-monomers via photoredox ROP featured the use of an isoselective Zn complex and co-monomers having opposite chiralities and different polymerization rates.[2] Using a similar strategy for this Mn/Zn-mediated one-pot redox ROP, we found that **Zn-2**/**Mn-1** at −15 °C mediated gradient copolymerization to form poly(L-**1**-*grad*-D-**3**) (**Figure 4.13**), with a high M_n of 65.9 kDa (which is close to the calculated MW of 73.7 kDa) and a narrow $Đ$ of 1.02. ^{1}H NMR spectroscopy demonstrated that the structure poly(L-**1**-*grad*-D-**3**) was highly stereoregular, as evidenced by the well-defined methine quartet at 5.2 ppm (**Figure 4.14a** and **4.16**), similar with block (*b*) copolymer poly(L-**1**-*b*-L-**3**) (**Figure 4.14a** and **4.18**). In comparison, the random (*r*) copolymer poly(L-**1**-*r*-L-**3**) exhibited a broad peak in this region (**Figure 4.14a** and **4.19**).

We note that at a [**OCA**]/[**Zn-2**] ratio of 200, the polymerization rate constant of L-**1** was 21.7-times higher than that of D-**3** in the homopolymerization (k(**1**/**1**) > k(**3**/**3**)). (**Figure 4.14b**). ^{1}H NMR spectroscopic analysis of the copolymerization kinetics also showed that L-**1** was converted more rapidly than D-**3**: for instance, at 25 min, conversion of L-**1** was 43%, whereas that of D-**3** was only 19% ([L-**1**]/[D-**3**]/[Zn]/[Mn] = 200/200/1/1; **Figure 4.15a**). The L-**1**/D-**3** ratio in the copolymer also decreased markedly with time, from 2.1 at 25 min to 1.2 at 4 h, indicating the formation of a gradient copolymer (**Figure 4.15a**). Using the D-**1**/L-**3** pair instead of the L-**1**/D-**3** pair did not affect either the polymerization results or the microstructure of the obtained polymer (**Figure 4.16** and **4.17**). Notably, replacing D-**3** with L-**3** resulted in the formation of a random copolymer poly(L-**1**-*r*-L-**3**) (**Figure 4.19**). This was confirmed by analysis of the polymerization

kinetics: the conversions of L-**1** and L-**3** were similar throughout the copolymerization, and the reaction was almost completed within 1 hour (**Figure 4.15b**). These results suggest that the use of co-monomers with the same chirality is more likely to result in stereoerrors—and thereby the formation of random copolymers—than the use of co-monomers with different chirality. Using this one-pot copolymerization strategy for monomers with opposite chiralities and different reaction rates, other gradient copolymers can be produced from various OCA enantiomers, including poly(L-**1**-*grad*-D-**2**) (**Figure 4.20**) and poly(D-**2**-*grad*-L-**3**) (**Figure 4.21**).

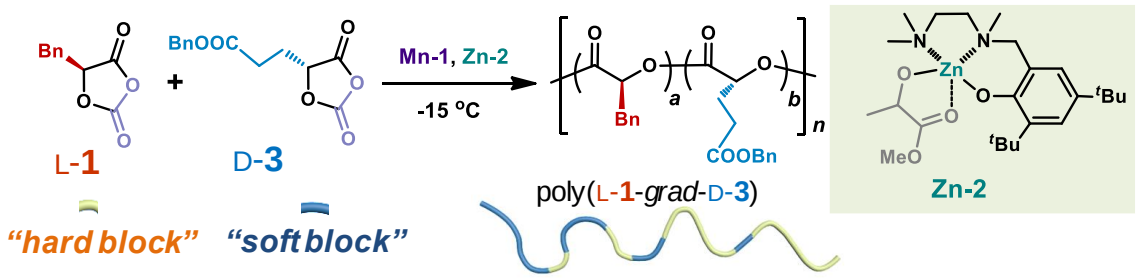

Figure 4.13 One-pot **Mn-1**/**Zn-2**-catalyzed ring-opening polymerization of L-**1** and D-**3** to synthesize poly(L-**1**-*grad*-D-**3**).

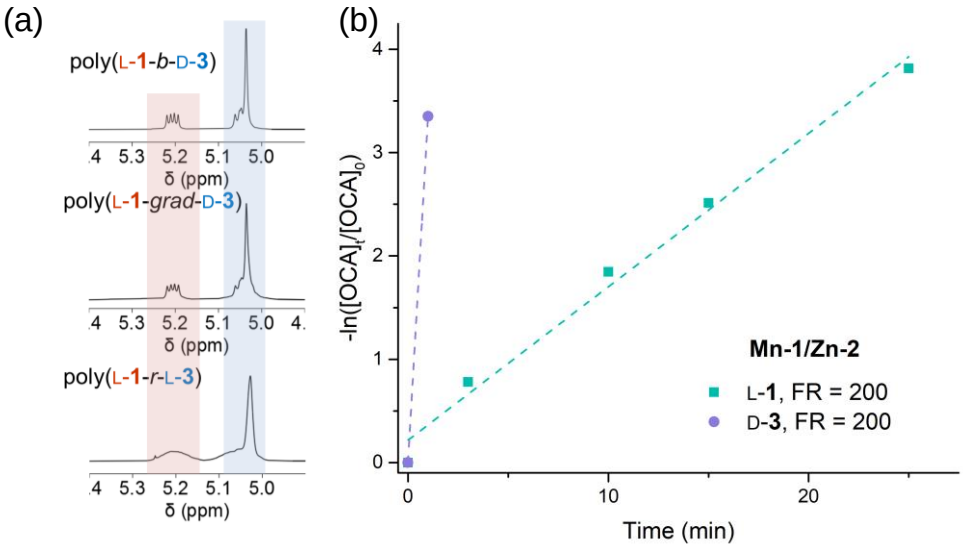

Figure 4.14 (a) ^{1}H NMR spectra of highly isotactic poly(L-**1**-*grad*-D-**3**), block copolymer poly(L-**1**-*b*-D-**3**), and random copolymer poly(L-**1**-*r*-L-**3**). Peaks corresponding to the α-methine protons of **1** (~5.2 ppm) and **3** (~5.0 ppm) are highlighted in red and blue, respectively. (b) Kinetic plots of the ROP of L-**1** and D-**3** in the presence of **Mn-1** / **Zn-2** at -15 °C. [OCA]/[**Mn-1**]/[**Zn-2**] = 200/1/1. [OCA] = 25.0 mM.

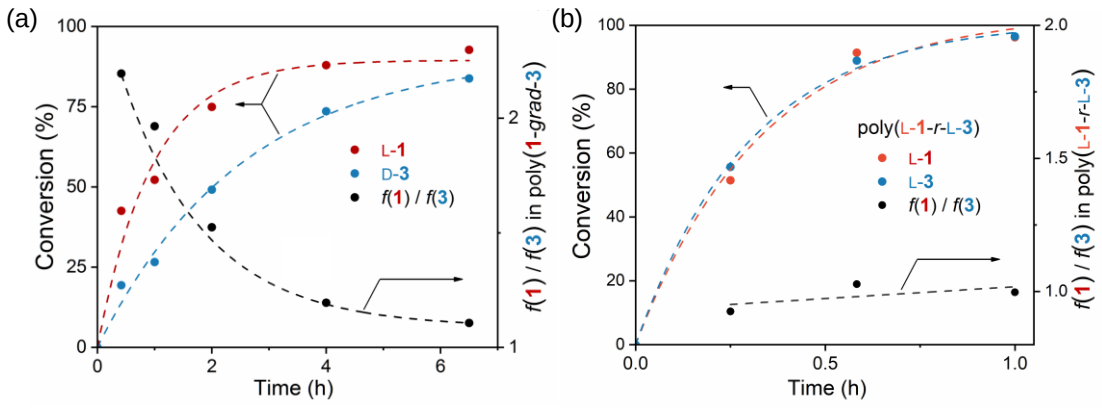

Figure 4.15 (a) Kinetics of L-**1** and D-**3** copolymerization to form the gradient copolymer ([L-**1**]/[D-**3**]/[**Mn-1**]/[**Zn-2**] = 200/200/1/1, [L-**1**] = 0.350 M). (b) Kinetics of L-**1** and L-**3** copolymerization to form the random copolymer poly(L-**1**-*r*-L-**3**) ([L-**1**]/[L-**3**]/[**Mn-1**]/[**Zn-2]** = 200/200/1/1, [L-1] = 0.115 M). We note that we used lower concentrations of OCAs compared to those in (a), because the copolymerization occurred very rapidly (reaction finished within 10 min) for NMR kinetic studies when using concentrations in (a).

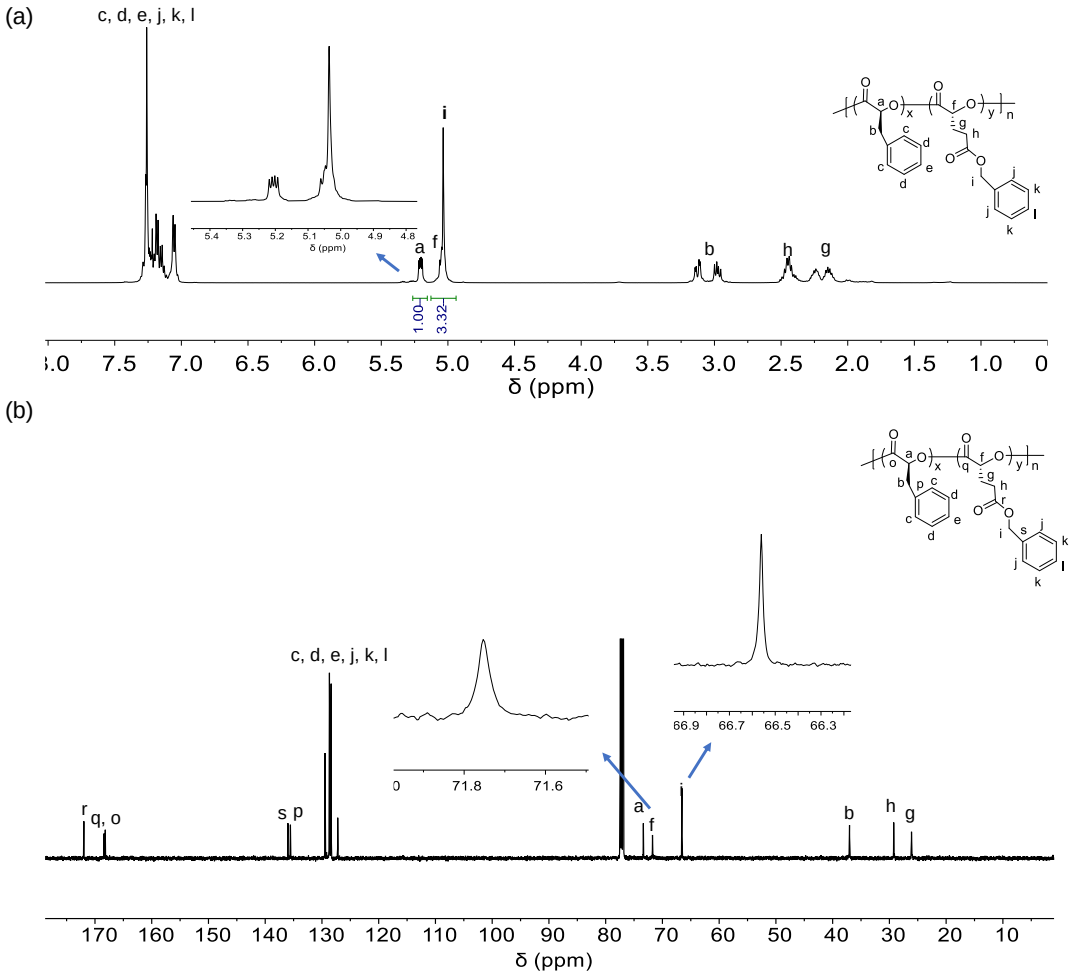

Figure 4.16 NMR spectra of poly(L-**1**$_{200}$-*grad*-D-**3**$_{200}$) in $CDCl_3$. (a) ^{1}H NMR spectrum; (b) ^{13}C NMR spectrum.

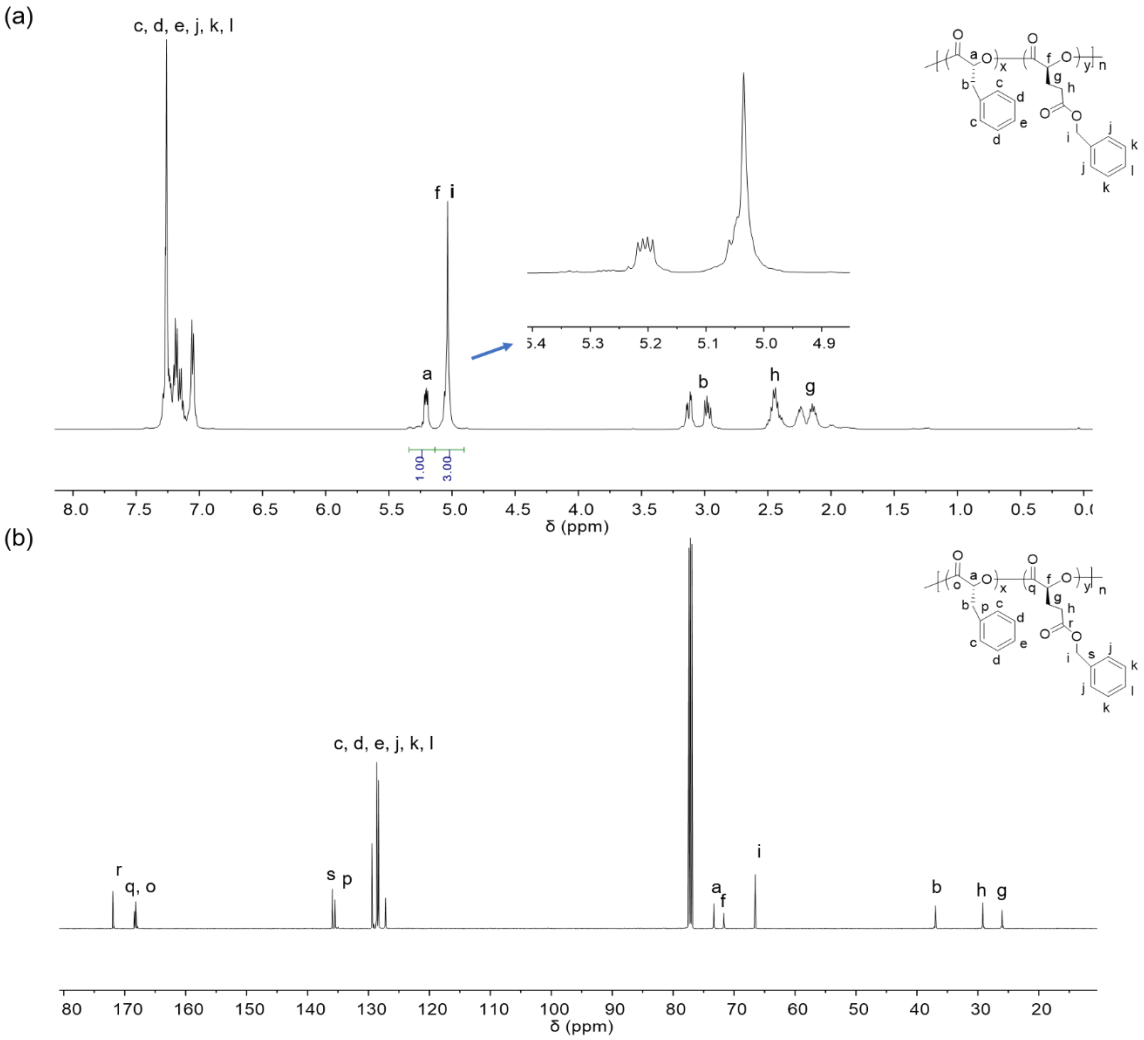

Figure 4.17 NMR spectra of poly(D-**1**$_{200}$-*grad*-L-**3**$_{200}$) in $CDCl_3$. (a) ^{1}H NMR spectrum; (b) ^{13}C NMR spectrum.

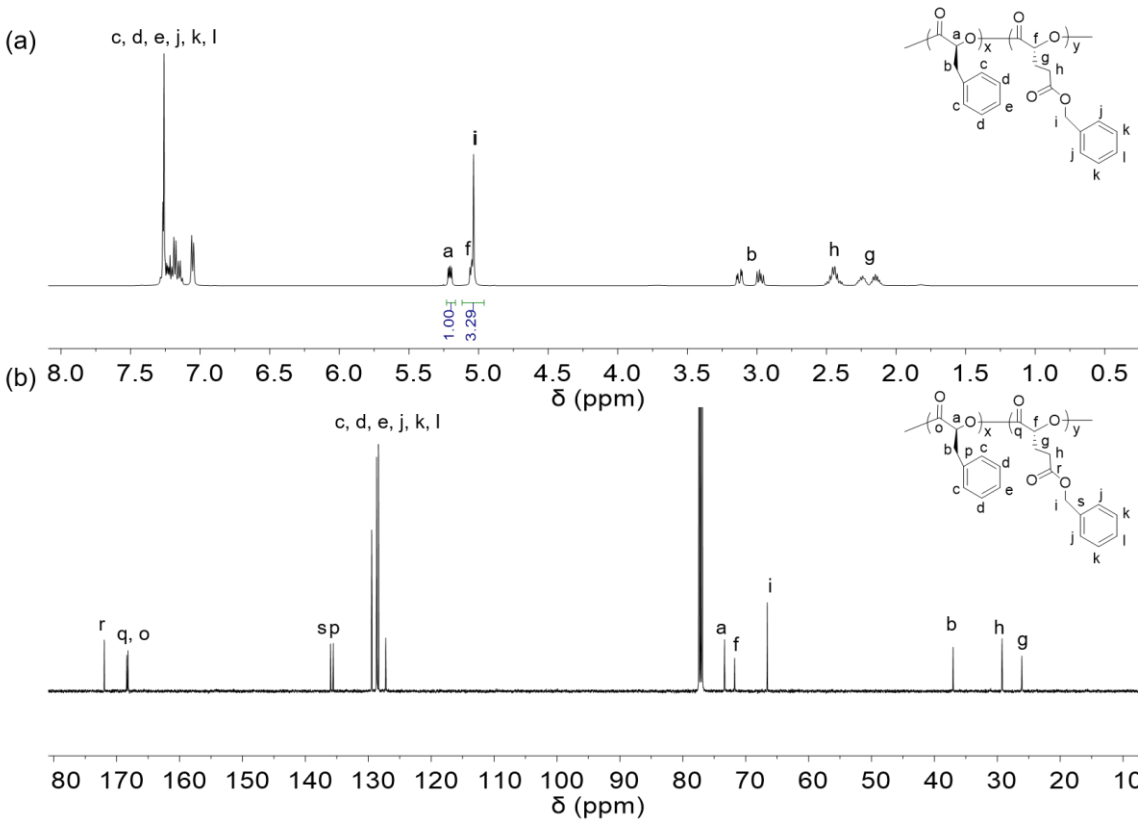

Figure 4.18 NMR spectra of poly(L-**1**-*b*-D-**3**) in $CDCl_3$. (a) ^{1}H NMR spectrum; (b) ^{13}C NMR spectrum.

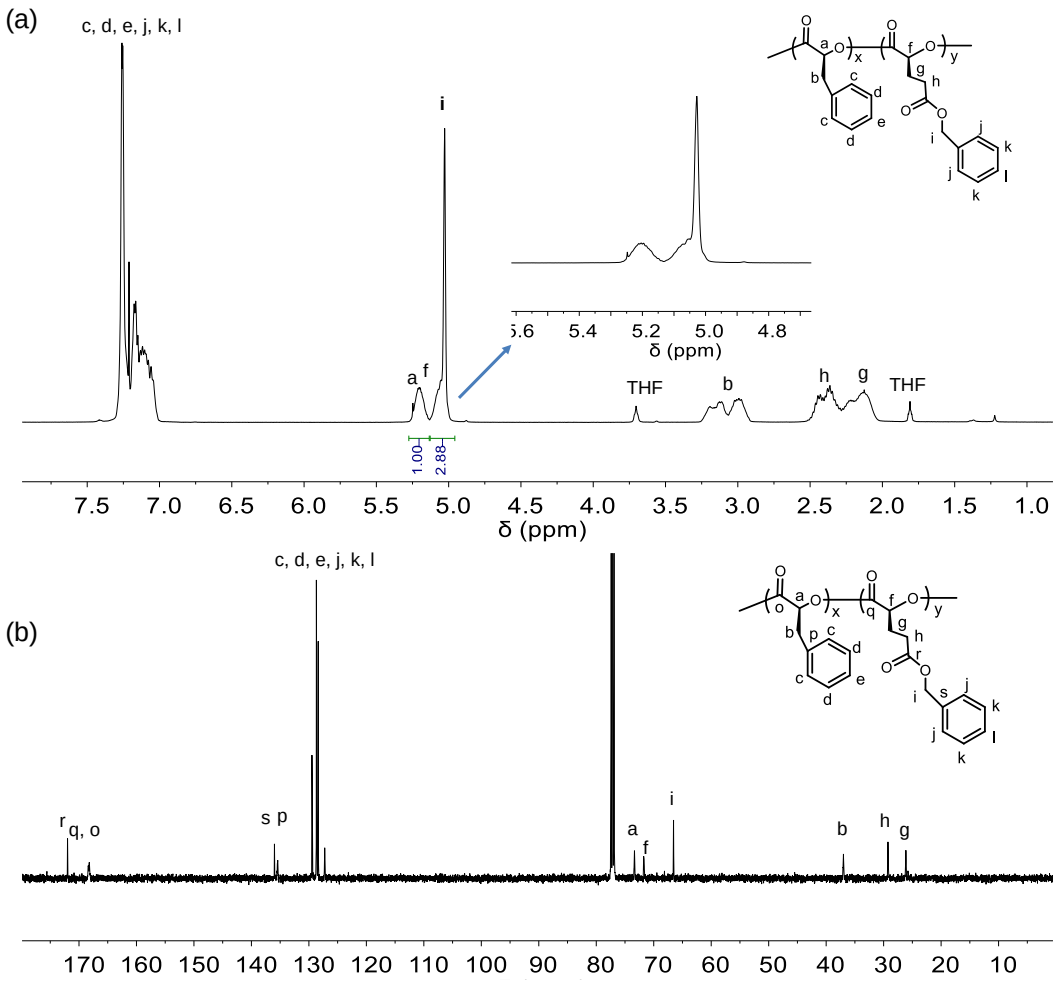

Figure 4.19 (a) ^{1}H, and (b) ^{13}C NMR spectra of poly(L-**1**-*r*-L-**3**) in $CDCl_3$ (Figure 5b).

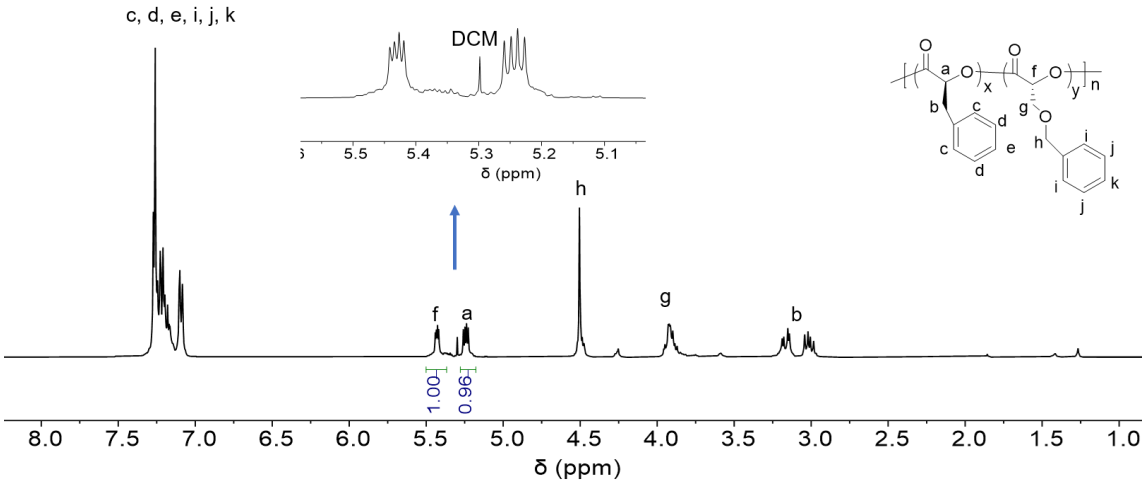

Figure 4.20 ^{1}H NMR spectra of poly(L-**1**-*grad*-D-**2**) in $CDCl_3$ ([L-**1**]/[D-**2**]/[**Mn-1**]/[**Zn-2**] = 100/100/1/1).

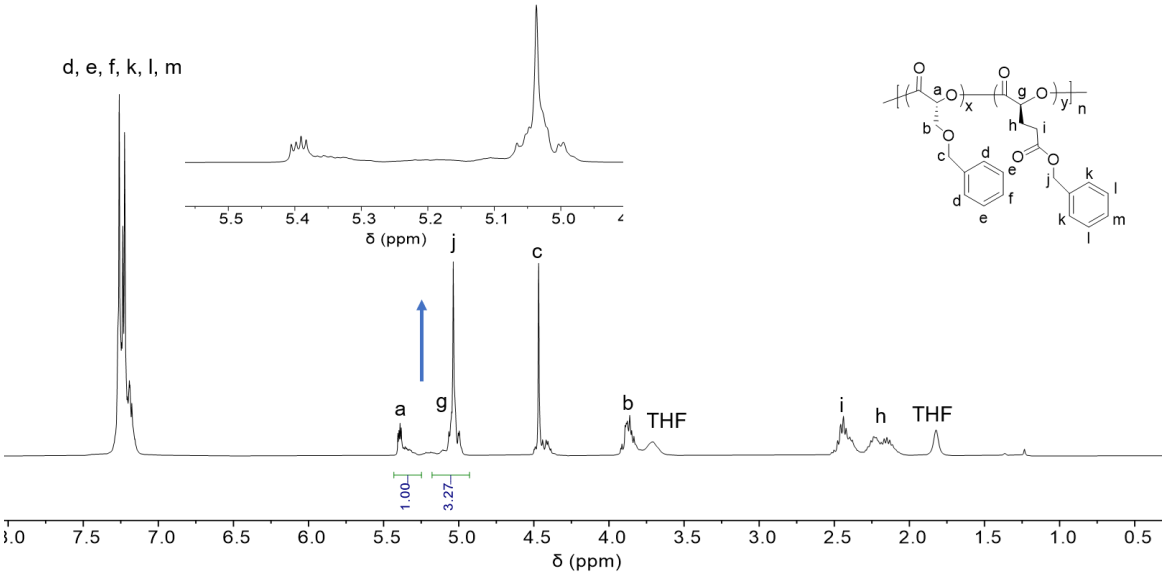

Figure 4.21 ^{1}H NMR spectra of poly(D-**2**-*grad*-L-**3**) in $CDCl_3$ ([D-**2**]/[L-**3**]/[**Mn-1**]/[**Zn-2**] = 100/100/1/1).

4.3 Materials and methods

4.3.1 General

O-benzyl-L-serine, *O*-benzyl-D-serine, L-glutamic acid-γ-benzyl ester, D-glutamic acid-γ-benzyl ester, *S*-(+)-mandelic acid and *R*-(-)-mandelic acid were purchased from Chem-Impex (Wood Dale, IL). L-phenylalanine and D-phenylalanine were purchased from Alfa Aesar (Haverhill, MA). Anhydrous tetrahydrofuran (THF) was dried by alumina columns and stored with 4Å molecular sieve in the dark bottle in the glove box (MBraun, Labstar Pro, < 1 ppm oxygen and moisture). Benzyl alcohol, hexane, toluene, diethyl ether, dichloromethane were dried and stored by 4Å molecular sieves in the glove box. All other chemicals were purchased from Sigma-Aldrich (St. Louis, MO) unless otherwise noted. All metal catalysts were synthesized in the glove box, characterized by NMR, and stored in the glove box freezer (−30 °C).

4.3.2 OCA monomers

L-PheOCA (L-**1**) and D-PheOCA (D-**1**),[19] L-Ser(Bn)OCA (L-**2**) and D-Ser(Bn)OCA (D-**2**),[20] L-Glu(Cbz)OCA (L-**3**) and D-Glu(Cbz)OCA (D-**3**),[21] L-LacOCA (L-**4**) and D-LacOCA (D-**4**),[22] and L-ManOCA (L-**5**) and D-ManOCA (D-**5**),[23] were synthesized and recrystallized according to the literature. All OCA monomers were recrystallized three times and stored in -30 °C freezer in the glove box.

4.3.3 Zn and Hf complexes

(**NNO**)Zn complexes (**Zn-2** to **Zn-7** in Table 4.1) was prepared according to the literature.[24, 25] β-diiminate Zn complexes (**Zn-8** to **Zn-14** in Table 4.1) were synthesized

according to the literature.[26] All Zn complexes were stored in the glove box freezer (−30 ^{o}C). **Hf-1** and **Hf-2** complexes was synthesized according to the literature.[16]

4.3.4 Instrument and characterization

4.3.4.1 NMR spectroscopy

All room temperature NMR and homodecoupling ^{1}H NMR spectra were recorded on Agilent U4-DD2 (400 MHz) or Bruker Avance II (500 MHz). All ^{13}C NMR spectra are proton decoupled.

4.3.4.2 FTIR spectroscopy

Fourier-transform infrared spectra were recorded on an Agilent Cary 630 FTIR spectrometer (Agilent Technologies Inc., Santa Clara, CA, USA) equipped with Diamond ATR and transmission sampling accessory.

Monomer conversion measurement:

A small aliquot of polymer solution (20 μL) was removed out of the glove box and quenched with 5% acetic acid / THF solution (20 μL). The mixture (~10 μL) was immediately dropped onto the FTIR-ATR diamond sampler and formed a film within 10-20 seconds for the spectra measurement. The peak at 1800 cm^{-1} is assigned as the anhydride bond stretch in OCA; the peak at 1760 cm^{-1} corresponds to the formation of the ester bond in the polymer. The monomer conversion was determined by the intensity ratio between 1760 cm^{-1} and 1800 cm^{-1}: conversion% = I_{1760} / (I_{1760}+ I_{1800}).

4.3.4.3 Gel permeation chromatography (GPC)

GPC experiments were performed on a system equipped with an isocratic pump with degasser (Agilent 1260 series, Agilent Technologies, Santa Clara, CA, USA), Wyatt

DAWN HELEOS multiangle laser light scattering (MALS) detector (GaAs 30 mW laser at λ=690nm), and a Wyatt Optilab rEX differential refractive index (DRI) detector with a 690 nm light source (Wyatt Technology, Santa Barbara, CA, USA). Separations were performed using serially connected size exclusion columns (100 Å, 500 Å, 10^3 Å, and 10^4 Å Phenogel columns, 5 μm, 300 × 4.6 mm, Phenomenex, Torrance, CA, USA) at 35 °C using THF as the mobile phase with a flow rate of 0.35 mL/min. The polymer molecular weight (MW) and molecular weight distribution (*Đ*) were determined using Zimm model fit of MALS-DRI data by ASTRA software (Version 6.1, Wyatt Technology). Data collection interval: 0.5 sec.

The refractive index increment dn/dc value was determined by the Wyatt Optilab rEX refractive index detector using ASTRA software dn/dc template (Version 6.1, Wyatt Technology). Five polymer / THF solutions with different concentrations were sequentially injected into the refractive index detector and the refractive index values were plotted versus concentration in ASTRA software. The slope of the linear fitting data is the dn/dc value.

4.3.4.4 Differential scanning calorimetry (DSC)

DSC measurements were performed on TA Instruments DSC Q2000 instrument equipped with photocalorimeter accessory and RCS90 cooling system. Polymer samples in crimped aluminum pans were analyzed under nitrogen at a heating rate of 10 °C/min from 0 to 230 °C. Glass transition temperature (T_g, defined as the inflection point based on ASTM method) and melting temperature (T_m, defined as the peak point) were obtained and reported from the second heating run.

4.3.5 Polymerization procedure

4.3.5.1 Isoselective polymerization of racemic OCA (*rac*-1) mediated by Mn-1 / Zn-2

In a glove box, prior to the polymerization, all reagents were cooled in the cold trap equipped with a thermometer at -15 to -20 ^{o}C, which was cooled by the liquid nitrogen and ethanol in a dewar. L-**1** (15 mg, 150 μL of 100 mg/mL, 0.078 mmol, 200 equiv.) and D-**1** (15 mg, 150 μL of 100 mg/mL, 0.078 mmol, 200 equiv.) were mixed **Mn-1** (50.6 μL of 2.9 mg/mL in THF, 0.391 μmol, 1 equiv.) and **Zn-2** (15.6 μL of 12.2 mg/mL in THF, 0.391 μmol, 1 equiv) in a 7-mL glass vial equipped with a magnetic stir bar at -15 ^{o}C. The solution was stirred around -15 ^{o}C ± 5 ^{o}C (with a cooling fan to keep the reaction temperature) over 1 hour. The OCA monomer conversion was monitored by FTIR. The resulted polymer's MW and *Đ* were directly measured by GPC after the polymerization. The P_m values of poly(*rac*-**1**) were determined by ^{13}C NMR spectra, based on the reported assignments of the tetrad peaks of poly(**1**).[18, 27]

4.3.5.2 Gradient copolymer synthesis of L-1 and D-3 mediated by Mn-1/Zn-2

In a glove box, prior to the polymerization, all reagents were cooled in the cold trap equipped with a thermometer at −20-30 ^{o}C, which was cooled by the liquid nitrogen and ethanol in the dewar. L-**1** (10 mg, 100 μL of 100 mg/mL, 0.052 mmol, 200 equiv.) and D-**3** (13.76 mg, 137.6 μL of 100 mg/mL, 0.052 mmol, 200 equiv.) was mixed with **Mn-1** (23.3 μL of 4.2 mg/mL in THF, 0.260 μmol, 1 equiv.), **Zn-2** (34.3 μL of 3.7 mg/mL in THF, 0.260 μmol, 1 equiv.) in a 7-mL glass vial equipped with a magnetic stir bar at -20 ^{o}C. The solution was stirred at −15 ^{o}C ± 5 ^{o}C over 4-8 hours. The OCA monomer conversion was monitored by FTIR. The resulted polymer's MW and *Đ* were directly measured by GPC after the polymerization.

4.4 Conclusions

Stereoselective synthesis of functional polyesters with high molecular weight remains challenging from *O*-carboxyanhydrides. Herein we present a strategy for stereoselective ring-opening polymerization of racemic *O*-carboxyanhydrides—without the need for an external energy source—using Mn catalysts and a selected Zn complex with an achiral ligand. The obtained stereoblock copolymers are highly isotactic with high molecular weights (> 70 kDa) and narrow molecular weight distributions ($Đ$ < 1.1). Furthermore, in one-pot copolymerization of two different *O*-carboxyanhydrides, the use of such Zn complex mediates kinetic resolution of the co-monomers during enchainment, which shows a chirality preference that allows for the synthesis of gradient copolymers.

References

1. Zhu, Y.; Romain, C.; Williams, C. K., Sustainable polymers from renewable resources. *Nature* **2016,** *540* (7633), 354-362.
2. Feng, Q.; Yang, L.; Zhong, Y.; Guo, D.; Liu, G.; Xie, L.; Huang, W.; Tong, R., Stereoselective photoredox ring-opening polymerization of O-carboxyanhydrides. *Nature Communications* **2018,** *9* (1), 1559.
3. Malanga, M., Syndiotactic polystyrene materials. *Advanced Materials* **2000,** *12* (23), 1869-1872.
4. Ovitt, T. M.; Coates, G. W., Stereoselective ring-opening polymerization of meso-lactide: Synthesis of syndiotactic poly(lactic acid). *J. Am. Chem. Soc.* **1999,** *121* (16), 4072-4073.
5. Chamberlain, B. M.; Cheng, M.; Moore, D. R.; Ovitt, T. M.; Lobkovsky, E. B.; Coates, G. W., Polymerization of lactide with zinc and magnesium beta-diiminate complexes: Stereocontrol and mechanism. *J. Am. Chem. Soc.* **2001,** *123* (14), 3229-3238.
6. Ovitt, T. M.; Coates, G. W., Stereochemistry of lactide polymerization with chiral catalysts: New opportunities for stereocontrol using polymer exchange mechanisms. *J. Am. Chem. Soc.* **2002,** *124* (7), 1316-1326.
7. Hador, R.; Botta, A.; Venditto, V.; Lipstman, S.; Goldberg, I.; Kol, M., The dual-stereocontrol mechanism: heteroselective polymerization of rac-Lactide and syndioselective polymerization of meso-Lactide by chiral aluminum salan catalysts. *Angewandte Chemie-International Edition* **2019,** *58* (41), 14679-14685.
8. Press, K.; Goldberg, I.; Kol, M., Mechanistic Insight into the Stereochemical Control of Lactide Polymerization by Salan-Aluminum Catalysts. *Angewandte Chemie-International Edition* **2015,** *54* (49), 14858-14861.
9. Lee, J.; Yoon, M.; Lee, H.; Nayab, S., Stereoselective polymerization of methyl methacrylate and rac-lactide mediated by iminomethylpyridine based Cu(ii) complexes. *Rsc Advances* **2020,** *10* (27), 16209-16220.
10. Stosser, T.; Williams, C. K., Selective polymerization catalysis from monomer mixtures: using a commercial Cr-Salen catalyst to access ABA block polyesters. *Angewandte Chemie-International Edition* **2018,** *57* (21), 6337-6341.
11. Myers, D.; White, A. J. P.; Forsyth, C. M.; Bown, M.; Williams, C. K., Phosphasalen Indium Complexes Showing High Rates and Isoselectivities in rac-Lactide Polymerizations. *Angewandte Chemie-International Edition* **2017,** *56* (19), 5277-5282.
12. Marin, P.; Tschan, M. J. L.; Isnard, F.; Robert, C.; Haquette, P.; Trivelli, X.; Chamoreau, L. M.; Guerineau, V.; del Rosal, I.; Maron, L.; Venditto, V.; Thomas, C. M., Polymerization of rac-Lactide Using Achiral Iron Complexes: Access to Thermally Stable Stereocomplexes. *Angewandte Chemie-International Edition* **2019,** *58* (36), 12585-12589.
13. Fortun, S.; Daneshmand, P.; Schaper, F., Isotactic rac-Lactide Polymerization with Copper Complexes: The Influence of Complex Nuclearity. *Angewandte Chemie-International Edition* **2015,** *54* (46), 13669-13672.
14. Cui, Y.; Jiang, J.; Pan, X.; Wu, J., Highly isoselective ring-opening polymerization of rac-O-carboxyanhydrides using a zinc alkoxide initiator. *Chemical Communications* **2019,** *55* (86), 12948-12951.

15. Jiang, J.; Cui, Y.; Lu, Y.; Zhang, B.; Pan, X.; Wu, J., Weak Lewis pairs as catalysts for highly isoselective ring-opening polymerization of epimerically labile rac-O-carboxyanhydride of mandelic acid. *Macromolecules* **2020,** *53* (3), 946-955.
16. Sun, Y.; Jia, Z.; Chen, C.; Cong, Y.; Mao, X.; Wu, J., Alternating sequence controlled copolymer synthesis of α-hydroxy acids via syndioselective ring-opening polymerization of O-carboxyanhydrides using zirconium/hafnium alkoxide initiators. *J. Am. Chem. Soc.* **2017,** *139* (31), 10723-10732.
17. Jia, Z. W.; Chen, S. C.; Jiang, J. X.; Mao, X. Y.; Pan, X. B.; Wu, J. C., Ring-Opening Alternating Copolymerization of O-Carboxyanhydrides of Lactic Acid and Malic Acid Using Hafnium Alkoxide Initiators with Different Stereo Selectivities and Activities. *Inorganic Chemistry* **2020,** *59* (14), 10353-10360.
18. Zhong, Y. L.; Feng, Q. Y.; Wang, X. Q.; Chen, J.; Cai, W. J.; Tong, R., Functionalized polyesters via stereoselective electrochemical ring-opening polymerization of *O*-carboxyanhydrides. *Acs Macro Letters* **2020,** *9* (8), 1114-1118.
19. Yin, Q.; Tong, R.; Xu, Y.; Baek, K.; Dobrucki, L. W.; Fan, T. M.; Cheng, J., Drug-Initiated Ring-Opening Polymerization of O-Carboxyanhydrides for the Preparation of Anticancer Drug–Poly (O-carboxyanhydride) Nanoconjugates. *Biomacromolecules* **2013,** *14* (3), 920-929.
20. Lu, Y.; Yin, L.; Zhang, Y.; Zhang, Z.; Xu, Y.; Tong, R.; Cheng, J., Synthesis of Water-Soluble Poly(α-hydroxy acids) from Living Ring-Opening Polymerization of O-Benzyl-l-serine Carboxyanhydrides. *ACS Macro Lett.* **2012,** *1* (4), 441-444.
21. Thillaye du Boullay, O.; Bonduelle, C.; Martin-Vaca, B.; Bourissou, D., Functionalized polyesters from organocatalyzed ROP of gluOCA, the O-carboxyanhydride derived from glutamic acid. *Chem. Commun.* **2008,** (15), 1786-1788.
22. Thillaye du Boullay, O.; Marchal, E.; Martin-Vaca, B.; Cossío, F. P.; Bourissou, D., An activated equivalent of lactide toward organocatalytic ring-opening polymerization. *J. Am. Chem. Soc.* **2006,** *128* (51), 16442-16443.
23. Buchard, A.; Carbery, D. R.; Davidson, M. G.; Ivanova, P. K.; Jeffery, B. J.; Kociok-Koehn, G. I.; Lowe, J. P., Preparation of Stereoregular Isotactic Poly(mandelic acid) through Organocatalytic Ring-Opening Polymerization of a Cyclic O-Carboxyanhydride. *Angew. Chem. Int. Ed.* **2014,** *53* (50), 13858-13861.
24. Williams, C. K.; Breyfogle, L. E.; Choi, S. K.; Nam, W.; Young, V. G.; Hillmyer, M. A.; Tolman, W. B., A Highly Active Zinc Catalyst for the Controlled Polymerization of Lactide. *J. Am. Chem. Soc.* **2003,** *125* (37), 11350-11359.
25. Brown, N. J.; Harris, J. E.; Yin, X.; Silverwood, I.; White, A. J. P.; Kazarian, S. G.; Hellgardt, K.; Shaffer, M. S. P.; Williams, C. K., Mononuclear Phenolate Diamine Zinc Hydride Complexes and Their Reactions With CO2. *Organometallics* **2014,** *33* (5), 1112-1119.
26. Chamberlain, B. M.; Cheng, M.; Moore, D. R.; Ovitt, T. M.; Lobkovsky, E. B.; Coates, G. W., Polymerization of lactide with zinc and magnesium β-diiminate complexes: stereocontrol and mechanism. *J. Am. Chem. Soc.* **2001,** *123* (14), 3229-3238.
27. Zhong, Y.; Feng, Q.; Wang, X.; Yang, L.; Korovich, A. G.; Madsen, L. A.; Tong, R., Photocatalyst-independent photoredox ring-opening polymerization of O-carboxyanhydrides: stereocontrol and mechanism. *Chemical Science* **2021,** *12*, 3702-3712.

CHAPTER 5

Mechanical and thermal properties of functionalized poly(α-hydroxy acids)

5.1 Introduction

Although the recent focus and development on ring-opening polymerization of *O*-carboxyanhydrides to prepare poly(α-hydroxy acids) (PAHAs) with different tacticities is of great significance, systematic studies on their material properties are still lacking, especially on their mechanical properties. This can be attributed to difficulties in the large-scale production of high-molecular-weight PAHAs using currently available methods. As aforementioned, many PAHAs with molecular weights (MWs) less than 5 kDa cannot be formed into film and used for mechanical property characterization.[1,2]

However, our synthesis is operationally simple and does not require external energy triggers compared to previously reported methods. In addition, it can be utilized to prepare homopolymers, block copolymers, stereoblock copolymers, and even gradient copolymers with high molecular weights, which allowed us to explore their mechanical and thermal properties, and to establish the sequence-structure-property relationship of functionalized PAHAs.

5.2 Results and discussions

5.2.1 Mechanical and thermal properties of poly(1) with various microstructures

We initiated the mechanical property study by synthesizing a series of poly(**1**) with various composition, including high-MW poly(L-**1**) (FR = 1300; M_n = 170.9 kDa), low-MW poly(L-**1**) (FR = 400; M_n = 48.2 kDa), high-MW poly(D-**1**) (FR = 1300; M_n = 166.0 kDa), poly(*sc*-**1**), poly(L-**1**-*b*-D-**1**) and poly(*sb*-**1**) (FR, feeding ratio; *sc*, stereocomplex*; b*, block; *sb*, stereoblock). All the polyesters were processed into films (~200 μm) via solvent casting and then subjected to dynamic mechanical analysis (DMA) and differential scanning calorimetry (DSC) characterization.

5.2.1.1 The effect of MW on mechanical properties

As illustrated in **Figure 5.1**, high-MW poly(L-**1**) (M_n = 170.9 kDa) exhibited a fracture strength (σ) of 12.5 MPa and a fracture strain (ε) of 73.6% (**Table 5.1**, entry 1); whereas low-MW poly(L-**1**) (M_n = 48.2 kDa) had a lower σ (4.9 MPa) and a moderate ε (53.7%, entry 2), indicating the importance of high MW for imparting toughness (a 4.46-fold difference in toughness was observed).[3] This can be attributed to that high-MW poly(L-**1**) had a higher glass transition temperature (T_g) than low-MW poly(L-**1**) (**Figure 5.2a** vs **5.2b**), as well as the length and orientation degree of the molecular chains increased with growing MW.[4]

5.2.1.2 The effect of stereocomplex on mechanical properties

High-MW poly(D-**1**) (M_n = 166.0 kDa) (**Table 5.1**, entry 3) exhibited comparable behavior with high-MW poly(L-**1**): a tensile strength (σ) of 12.7 MPa and a fracture strain (ε) of 71.7 % (**Figure 5.1**) and same T_g of 49 °C (**Figure 5.2**), implying their similar

crystallinity. In order to further improve the properties of poly(**1**), stereocomplex (poly(*sc*-**1**)) was produced followed by the literature[5]. Briefly, dissolved solutions of high-MW poly(L-**1**) and high-MW poly(D-**1**) in dichloromethane were mixed and the solvent was allowed to slowly evaporate, the sample was then dissolved again in dichloromethane and precipitated by adding methanol dropwise with vigorous stirring. Stereocomplexation is a general cocrystallization behavior between different polymers with complementary configurations.[6] For example, the *sc*-poly(propylene succinate) exhibited significantly improved properties compared with enantiopure polymers.[5] As seen in **Figure 5.1**, poly(*sc*-**1**) showed a slightly higher strength (σ) of 13.9 MPa and fracture strain (ε) of 77.5 % (**Table 5.1**, entry 4) than enantiopure parent poly(L-**1**) and poly(D-**1**) (entry 1 and 2), confirming that stereocomplex formation endowed the polymers with improved physical properties.

5.2.1.3 The effect of copolymer compositions on mechanical properties

Copolymerization is a common route to modify polymer properties. Poly(L-**1**-*b*-D-**1**) (**Table 5.1** entry 5; **Figure 5.1** and **5.2e**) showed similar glass transition temperature (T_g) of 47 °C with homopolymer but exhibited lower strength (σ) of 7.9 MPa and a strain (ε) of 62.9 %, possibly due to its low MW. Poly(*sb*-**1**) (**Table 5.1** entry 6; **Figure 5.1** and **5.2f**) revealed a T_g of 37 °C and T_m of 146 °C that were considerably different from those of homopolymer, resulting in a different strength (σ) of 6.8 MPa and a fracture strain (ε) of 49.8 %.

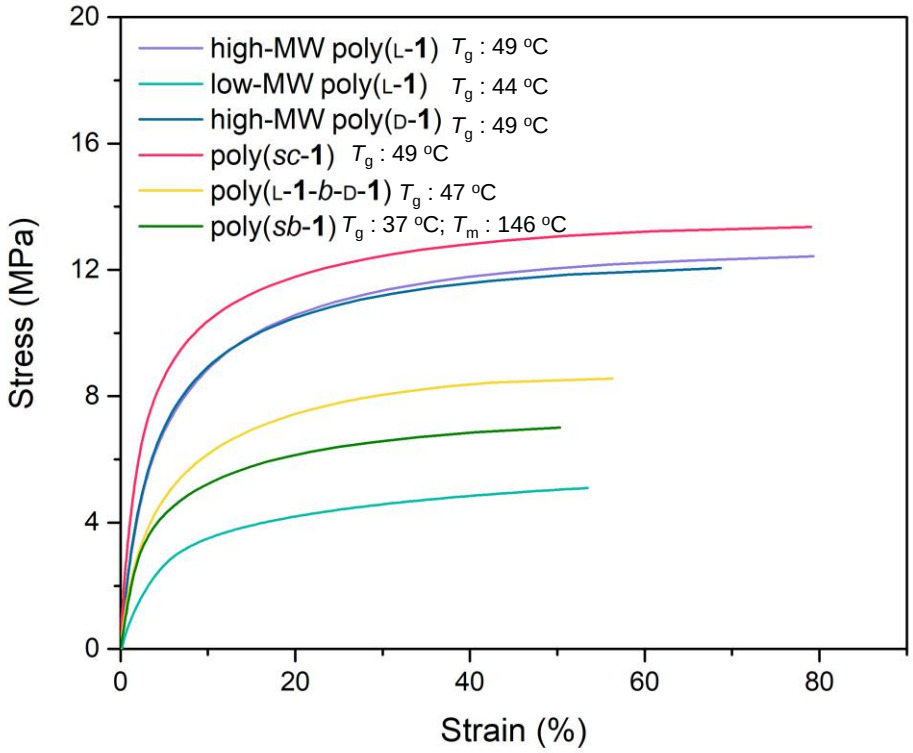

Figure 5.1 Representative stress–strain curves for uniaxial extension of poly(**1**) with various microstructures.

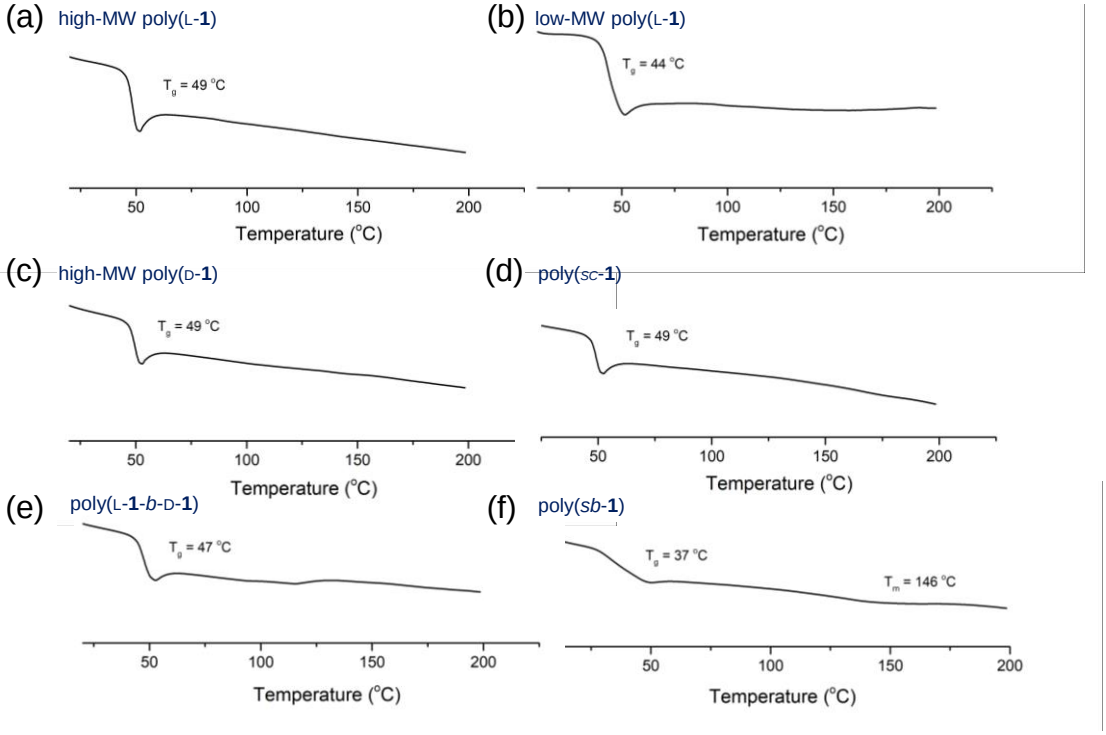

Figure 5.2 Differential scanning calorimetry measurements of T_gs and T_ms of poly(**1**) with various compositions.

Table 5.1 Thermal and mechanical properties of poly(**1**) with different compositions.

Entry	polymer	M_n (kDa)	$Đ$	T_g / T_m (°C)	E_y (MPa)	σ (MPa)	ε (%)
1	poly(L-**1**)	170.9	1.09	49 / −	391 ± 46	12.5 ± 0.8	73.6 ± 11.6
2	poly(L-**1**)	48.2	1.04	44 / −	87 ± 18	4.9 ± 0.3	53.7 ± 1.7
3	poly(D-**1**)	166.0	1.06	49 / −	280 ± 82	12.7 ± 0.9	71.7 ± 11.0
4	poly(*sc*-**1**)	166.0	1.06	49 / −	359 ± 81	13.9 ± 1.3	77.5 ± 4.7
5	poly(L-**1**-*b*-D-**1**)	98.6	1.01	47 / −	176 ± 42	7.9 ± 1.0	62.9 ± 17.6
6	poly(*sb*-**1**)	73.6	1.02	37 / 146	148 ± 51	6.8 ± 1.1	49.8 ± 6.1

5.2.2 Mechanical and thermal properties of poly(3) and poly(5)

Generally, the polymers with glass transition temperatures (T_g) below room temperature would exhibit high elasticity and flexibility. As anticipated, due to relatively low T_g (~5 °C) (**Figure 5.4**), poly(L-**3**) (M_n = 133.8 kDa) exhibited elastomeric behavior with no obvious yield point, having an extremely high fracture strain (472%) and a relatively low tensile strength (0.97 MPa; **Figure 5.3**).

Correspondingly, the polymer with high glass transition temperature would be stiffer. Poly(L-**5**) (M_n = 54.7 kDa) exhibited a brittle elongation of 2.9% and a strong tensile strength (39.7 MPa; **Figure 5.5**), due to the high glass transition temperature of 107 °C (**Figure 5.6**). Its property could compete with polystyrene, one of the most extensively used plastics on the market. Additionally, it is difficult to prepare polyesters with glass transition temperatures in excess of 100 °C using ring-opening polymerization, which further indicates the significant benefit of our synthetic method.

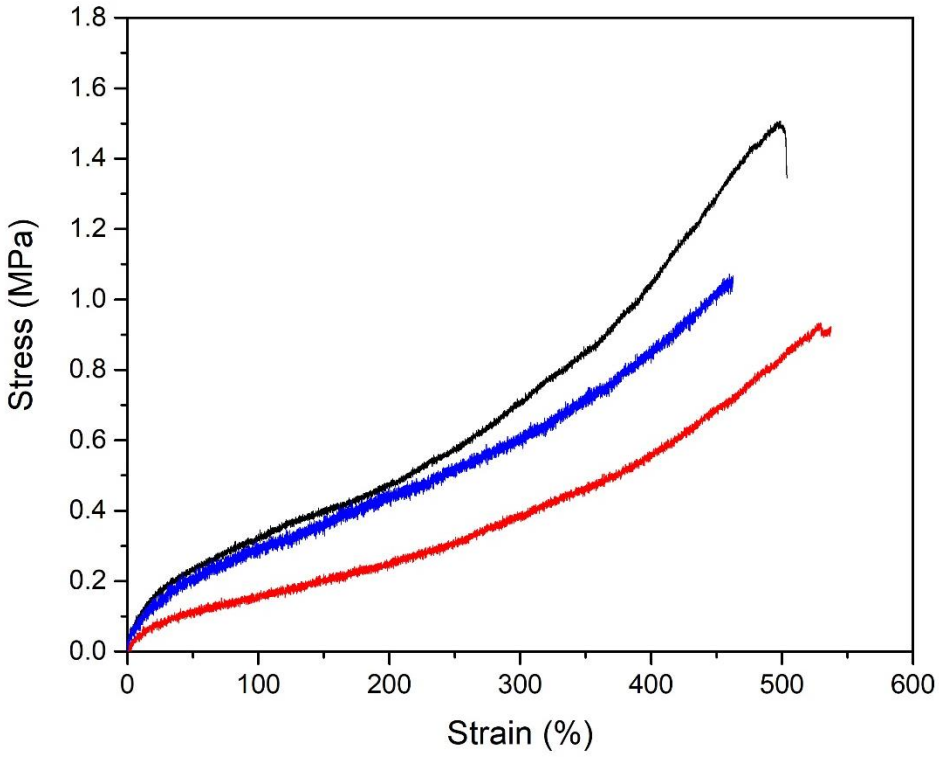

Figure 5.3 Stress–strain curves of poly(L-**3**).

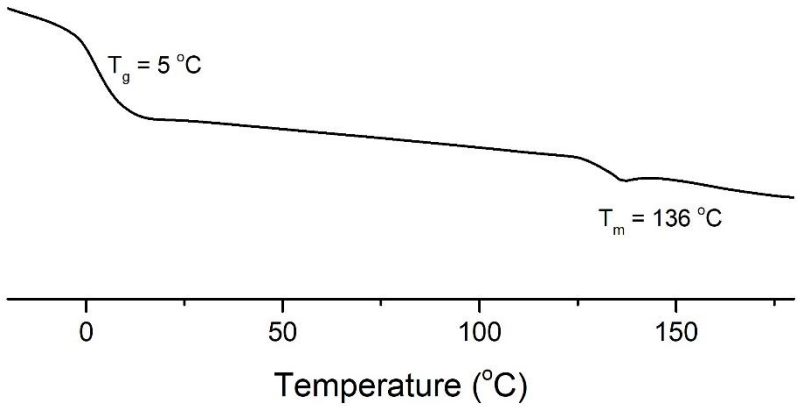

Figure 5.4 Differential scanning calorimetry measurements of T_g and T_m of poly(L-**3**).

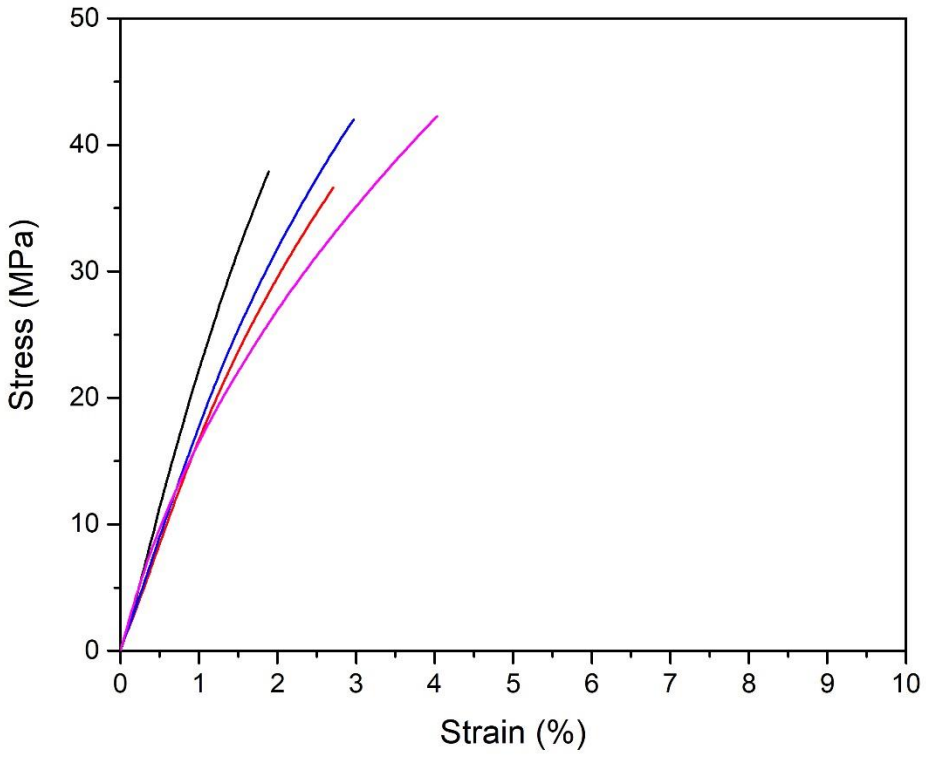

Figure 5.5 Stress–strain curves of poly(L-**5**).

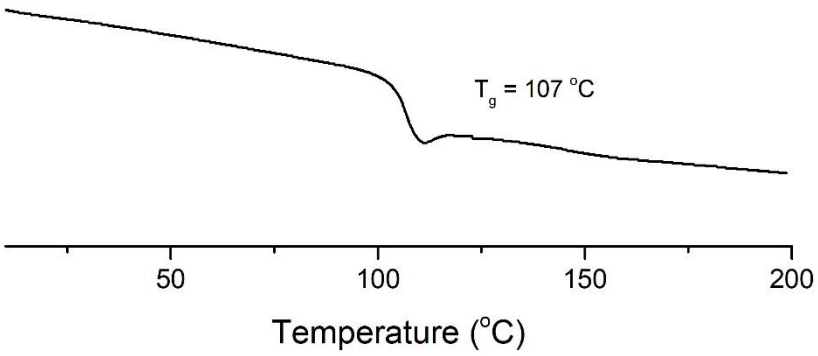

Figure 5.6 Differential scanning calorimetry measurements of T_g of poly(L-**5**).

5.2.3 Comparison of the material properties of three homopolymers

As shown in **Table 5.2** and **Figure 5.7**, among the synthesized poly(α-hydroxy acids), poly(L-**5**) was the most brittle one, with the highest strength of ~39.7 MPa, but

lowest strain of ~2.9 %; poly(L-**1**) preformed as brittle plastic with moderately high strength of ~12 MPa and a lower strain of ~70 %. However, poly(L-**3**) was flexible with an extremely high fracture strain (472%) and the lowest tensile strength (0.97 MPa).

The above-described mechanical data and differential scanning calorimetry measurements of the T_g values of the polymers (**Table 5.2**) suggested that the poly(α-hydroxy acids) with lower T_g values were more ductile (higher fracture strain) and softer (lower tensile strength) than those with high T_g values. Notably, our group[7] and others[8] have found that polyesters with long side-chains have lower T_g values than polyesters with short side-chains. This structure-property relationship would guide the design of copolymers with improved properties.

Table 5.2 Thermal and mechanical properties of various poly(α-hydroxy acids).

Entry	polymer	T_g / T_m (°C)	E_y (MPa)	σ (MPa)	ε (%)	Strain recovery ratio	Strain fixity ratio
1	poly(L-**1**)	49 / −	391 ± 46	12.5 ± 0.8	73.6 ± 11.6	0.0058	1
2	poly(L-**3**)	5 / 136	1.05 ± 0.06	0.967 ± 0.145	471.6 ± 51.3	0.940	0
3	poly(L-**5**)	107 / −	1933 ± 207	39.7 ± 2.9	2.9 ± 0.9	0	1

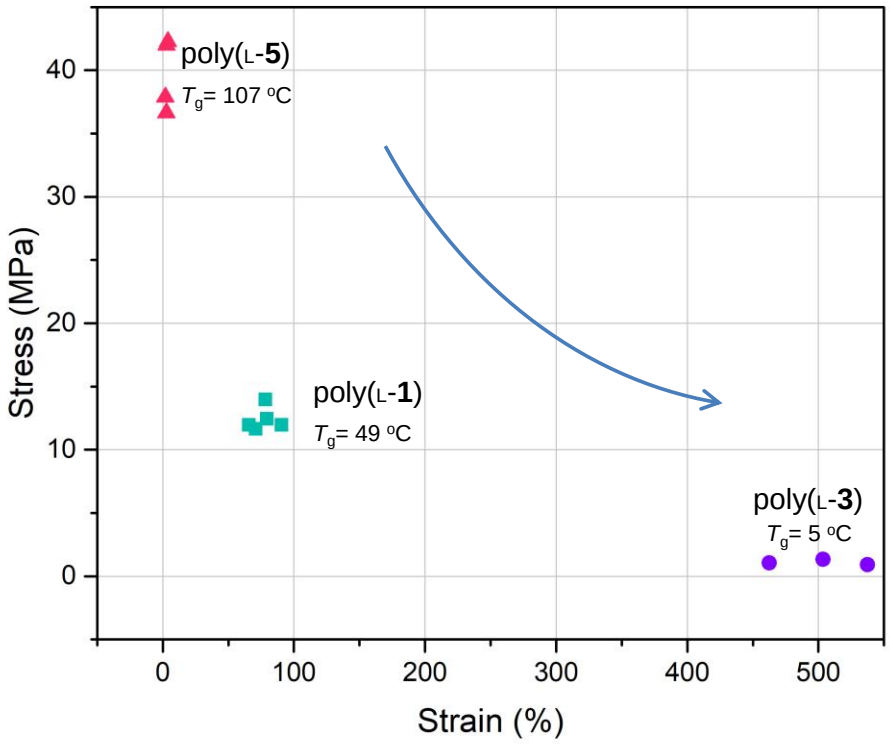

Figure 5.7 Strengths, strains, and glass-transition temperatures (T_gs) of various poly(α-hydroxy acids).

Additionally, poly(L-**3**) showed resilience (**Figure 5.8g**): a fractured sample of this polymer after the stress–strain test recovered its shape immediately at room temperature with a residual strain of 96.2 % (from 530%). The residual strain could be easily recovered when the polymer was kept at room temperature for 2 h (above its T_g [5 °C]); the strain recovery ratio was 0.940 (**Table 5.2**). Moreover, poly(L-**3**) exhibited excellent ductility as shown in the stress-strain tests exhibited immediate and complete elastic recovery when stretched to 100% at room temperature (**Figure 5.9**), whereas poly(L-**1**) and poly(L-**5**) with higher glass transition temperature did not show any pronounced shape memory properties (**Figure 5.8**).

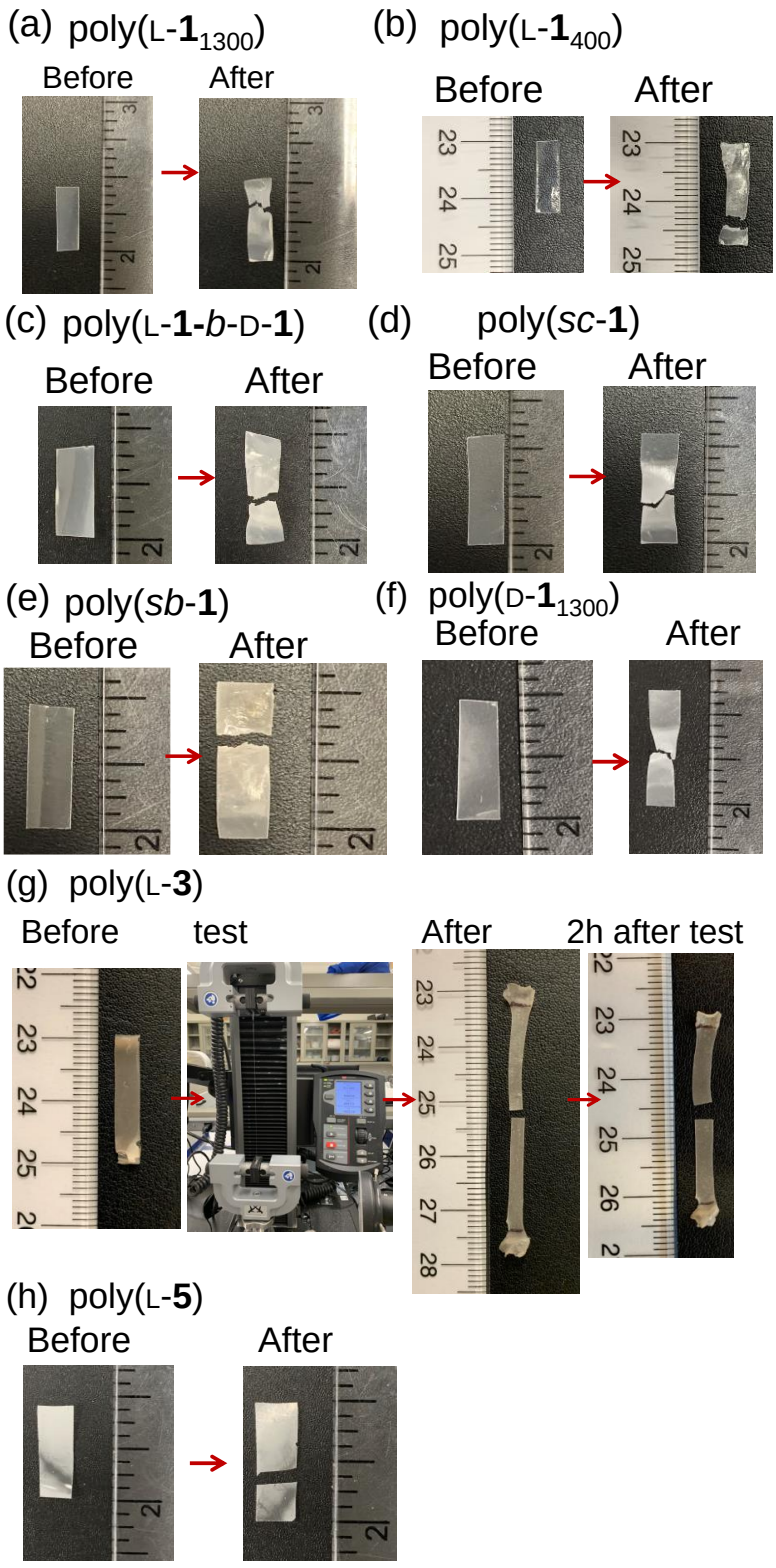

Figure 5.8 Shape recovery after polymer fracture in strain-stress tests.

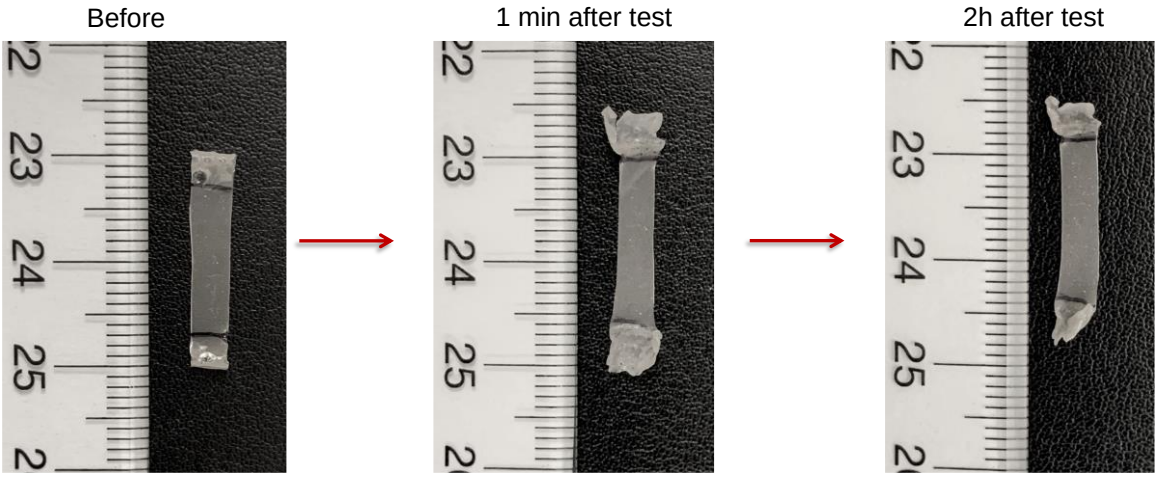

Figure 5.9 Shape recovery after poly(L-**3**) stretched in strain-stress tests with strain = 100 % (before fracture).

5.2.4 Material properties of poly(3-*b*-5) copolymers

As is well known, block polymers can undergo phase separation to form nanostructures showing improved macroscopic properties compared to homopolymer blends. Williams group[9] reported that the nanoscale phase behavior and correlated mechanical properties are highly sensitive to the block composition. Copolymers comprising elastic (soft) and glassy (hard) blocks usually exhibit characteristics of thermoplastic elastomers.[10, 11] Given that, it would be expected that the elastomeric properties of the resulting copolymers could be regulated by varying the composition of "hard" and "soft" blocks. Our investigations of the T_g values and stress–strain characteristics of the homopolymers (**Figure 5.7**) indicated that both poly(**1**) and poly(**5**) could be used as "hard" blocks and that poly(**3**) could be used as "soft" block. To determine whether multiblock copolymers would show enhanced ductility and toughness relative to their corresponding homopolymers, a diblock (*b*) copolymer poly(L-**3**-*b*-L-**5**) and two poly(L-**3**-*b*-L-**5**-*b*-L-**3**) triblock copolymers were initially synthesized.

Evaluation of these polymers (**Figure 5.10, 5.11** and **Table 5.3**) revealed that the higher soft block content, the higher elongation, but at the expense of tensile strength and glass transition temperatures. The poly(L-**3**$_{250}$-*b*-L-**5**$_{250}$-*b*-L-**3**$_{250}$) with T_g value of 7 ^oC showed the lower tensile strength (~ 3 MPa) but higher elongations (~378.6%), whereas the poly(L-**3**$_{150}$-*b*-L-**5**$_{300}$-*b*-L-**3**$_{150}$) with T_g value of 19 ^oC had a higher tensile strength of 12.4 MPa but a lower tensile strain of 73.4%. In addition, diblock and triblock copolymers with same hard and soft block content demonstrated different material properties. The fracture stress was slightly diminished, and the elongation was increased for the diblock poly(L-**3**$_{250}$-*b*-L-**5**$_{250}$) with T_g values of 13 ^oC. In summary, our results revealed that an increase in strain-to-failure of the block copolymers was counteracted by a decrease in tensile strength. Unfortunately, these block copolymers did not enhance the mechanical properties of poly(α-hydroxy acids), the tensile strength values of the copolymers were markedly lower than that of poly(L-**3**) and the strain-to-failure values of the copolymers were significantly lower than that of poly(L-**5**).

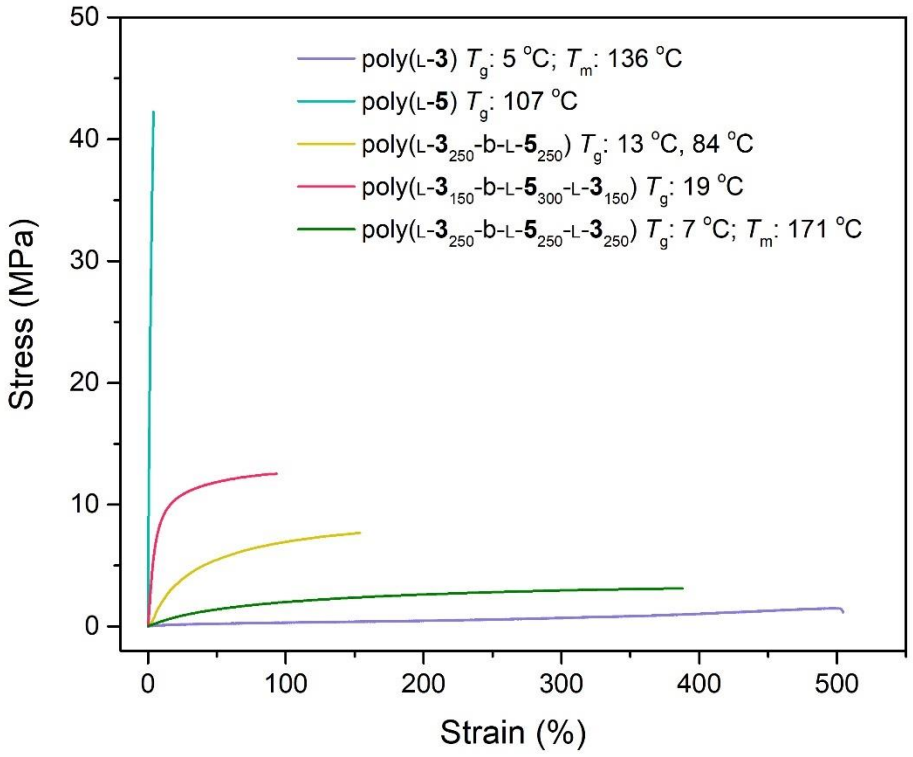

Figure 5.10 Representative stress–strain curves for uniaxial extension of poly(**3**), poly(**5**) and their copolymers.

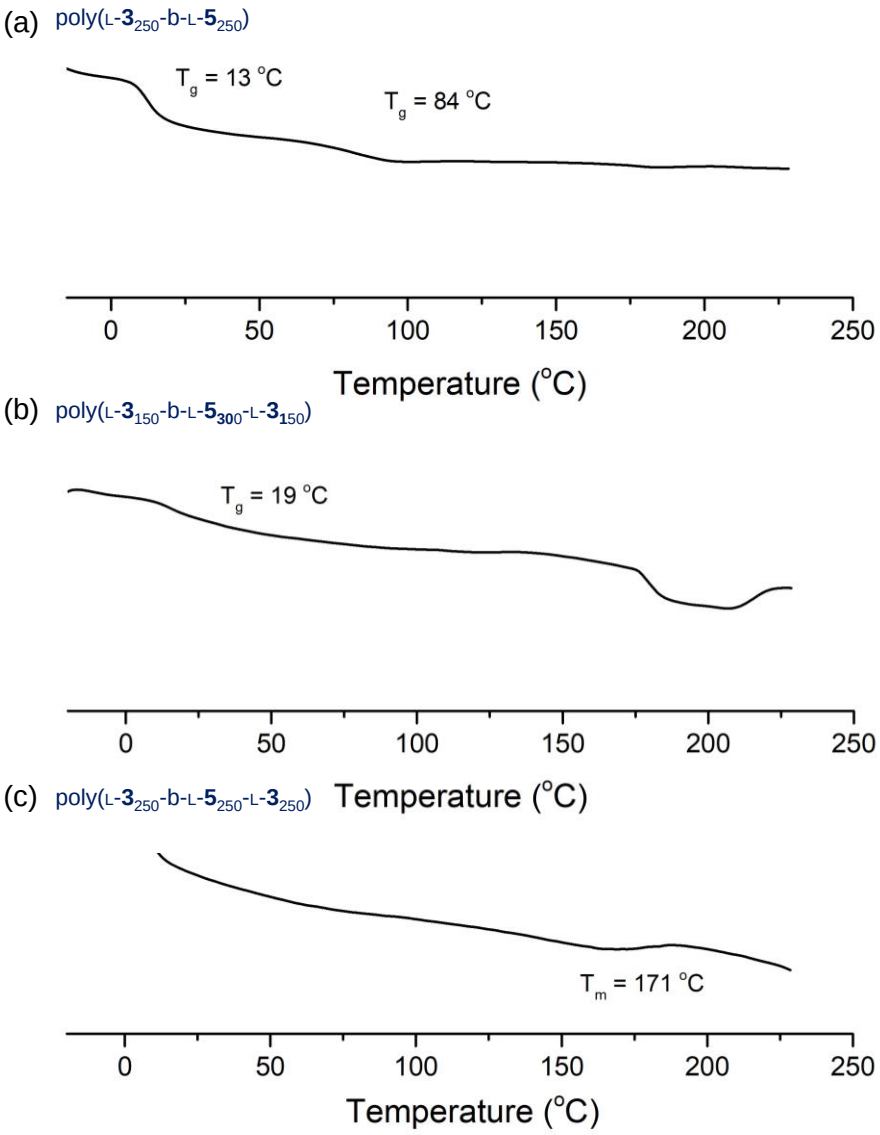

Figure 5.11 Differential scanning calorimetry measurements of T_g of poly(**3**), poly(**5**) and their copolymers.

Table 5.3 Thermal and mechanical properties of poly(**3**-*b*-**5**).

Entry	polymer	M_n (kDa)	$Đ$	T_g / T_m (°C)	E_y (MPa)	σ (MPa)	ε (%)
1	poly(L-**3**)	133.8	1.02	5 / 136	1.05 ± 0.06	0.967 ± 0.145	471.6 ± 51.3
2	poly(L-**5**)	54.7	1.06	107 / –	1933 ± 207	39.7 ± 2.9	2.9 ± 0.9
3	poly(L-**3**$_{250}$-*b*-L-**5**$_{250}$)	68.4	1.04	13, 84 / –	41 ± 17	7.8 ± 0.2	146.0 ± 27.2
4	poly(L-**3**$_{150}$-*b*-L-**5**$_{300}$-*b*-L-**3**$_{150}$)	61.6	1.02	19 / –	155 ± 27	12.4 ± 0.5	73.2 ± 17.9
5	poly(L-**3**$_{250}$-*b*-L-**5**$_{250}$-*b*-L-**3**$_{250}$)	108.2	1.01	7/171	7.5 ± 3.7	3.1 ± 0.2	378.6 ± 36.8

5.2.5 Material properties of poly(1-*grad*-3)

Although sequential addition of co-monomers is a well-established method for preparing block copolymers with tailored thermal and mechanical properties, recent studies have suggested that stereosequenced copolymers may exhibit unprecedented thermal or mechanical properties.[12] We then attempted to prepare gradient copolymers based on co-monomers **3** and **5**, but they were not successful; the obtained copolymers did not have high MWs and were brittle. Thus, co-monomers **1** (hard block) and **3** (soft block) were produced to explore whether the stereosequences of the copolymers affected their thermal and mechanical properties.

5.2.5.1 Comparison of the material properties of gradient copolymer, block copolymer and random copolymer

Indeed, we demonstrated that the stereosequences of copolymers affect their thermal and mechanical properties (**Figure 5.12a**). The gradient copolymer poly(L-**1**$_{200}$-*grad*-D-**3**$_{200}$) was stronger and more ductile than the block copolymer poly(L-**1**-*b*-D-**3**) and the random copolymer poly(L-**1**-*r*-L-**3**). Specifically, the tensile strength of poly(L-**1**$_{200}$-

grad-D-**3**$_{200}$) (14.8 MPa) was 2.46, 2.14, 1.97, and 1.18 times the respective values for poly(L-**1**-*b*-D-**3**), poly(L-**1**-*r*-L-**3**), poly(L-**1**-*b*-D-**3**-*b*-L-**1**), and poly(L-**1**); and the strain-to-failure value (317.5%) was 1.36, 1.08, 1.21, and 4.31 times the respective values for poly(L-**1**-*b*-D-**3**), poly(L-**1**-*r*-L-**3**), and poly(L-**1**), respectively (**Table 5.4**, entries 6-7, and 1). The overall toughness value for poly(L-**1**$_{200}$-*grad*-D-**3**$_{200}$) was higher than the values for the two corresponding homopolymers (by factors of 4.84 and 12.3, respectively) and the values for poly(L-**1**-*b*-D-**3**), poly(L-**1**-*b*-D-**3**-*b*-L-**1**), and poly(L-**1**-*r*-L-**3**) (by factors of 3.92, 2.55, and 2.86, respectively). Such mechanical properties of poly(L-**1**$_{200}$-*grad*-D-**3**$_{200}$) are comparable to commercially available non-degradable low-density polyethylene (LDPE) (**Figure 5.12a**; **Table 5.4**, entries 3 versus 11).

Additionally, poly(L-**1**$_{200}$-*grad*-D-**3**$_{200}$) only had one T_g (22 °C), which was similar to the T_g of the random copolymer poly(L-**1**-*r*-L-**3**) (21 °C); whereas the block copolymer poly(L-**1**-*b*-D-**3**) had two T_g values (9 and 30 °C, **Figure 5.13**). The stereocomplex (*sc*) of poly(L-**1**-*grad*-D-**3**) and poly(D-**1**-*grad*-L-**3**) had a strain-to-failure value of up to 392 %, but stereocomplex formation did not markedly affect the T_g and tensile stress values, presumably because of the low crystallinity of poly(**3**) (**Table 5.4**, entries 3-5, **Figure 5.12** and **5.13**).

5.2.5.2 The effect of gradient ratio on material properties

Notably, varying the ratio between L-**1** and D-**3** in gradient copolymers did not improve the strength and toughness of the copolymers (**Table 5.4**, entries 8-9; mechanical behavior in **Figure 5.12a**; DSC in **Figure 5.13**; NMR in **Figure 5.17** and **5.18**.). Though we could not rule out there could be a magic ratio value that would lead to improved strength and ductility compared with poly(L-**1**$_{200}$-*grad*-D-**3**$_{200}$), keeping the co-

monomer ratio at 1/1 led to better improvements compared with their corresponding block copolymers and homopolymers.

5.2.5.3 Shape memory effect

Poly(L-**1**$_{200}$-*grad*-D-**3**$_{200}$) showed resilience: a fractured sample of this polymer after the stress–strain test recovered its shape within 20 min at room temperature with a residual strain of 13.2% (**Figure 5.15**). The residual strain could be easily recovered when the polymer was kept at 40 °C for 1 h (above its T_g [22 °C]); the strain recovery ratio was 0.948 (**Table 5.5**, entry 3). poly(L-**1**$_{200}$-*grad*-D-**3**$_{200}$) also exhibited excellent ductility as shown in the stress-strain tests exhibited immediate and complete elastic recovery when stretched to 100% at room temperature (**Figure 5.14**). Introduction of a highly elastic poly(**3**) block into gradient or block copolymers provided copolymers with decent strain recovery ratios (ranging from 0.46 to 0.95); whereas poly(L-**1**) and LDPE did not show any pronounced shape memory properties (**Table 5.5**, entries 1 and 11; **Figures 5.14** and **5.15**).

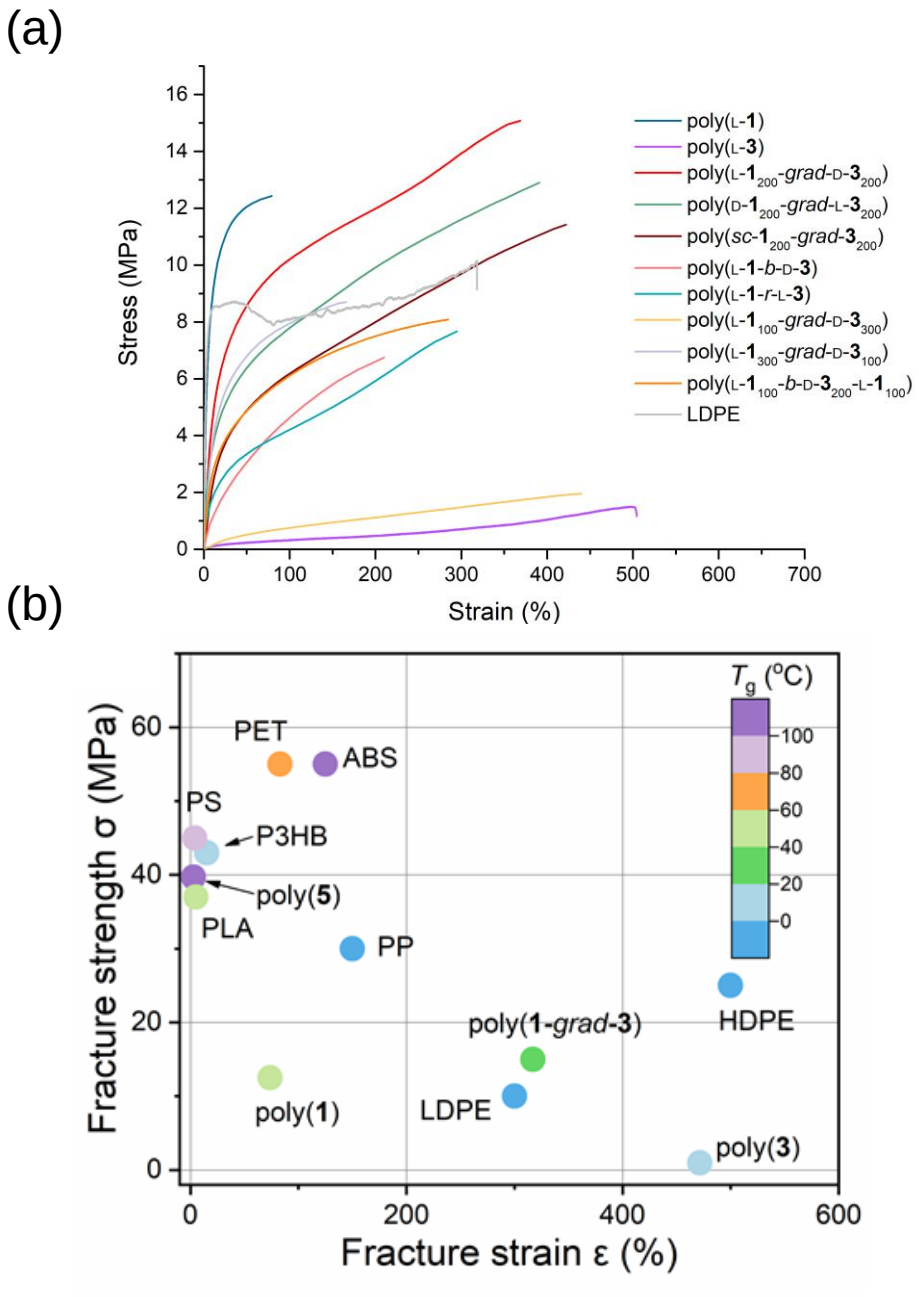

Figure 5.12 Mechanical study of a ductile and resilient gradient poly(α-hydroxy acid) copolymer. (a) Representative stress–strain curves for uniaxial extension of various poly(α-hydroxy acids) and LDPE. Polymer MWs and MW weight distributions are provided in Table 5.4. (b) Fracture strengths (σ), fracture strains (ε), and glass-transition temperatures (T_gs) of various poly(α-hydroxy acids), poly(3-hydroxybutyrate) (P3HB), polyethylene terephthalate (PET), comparing with those of commercial available polyolefins, including high-density polyethylene (HDPE), low-density polyethylene (LDPE), polypropylene (PP), polystyrene (PS), and poly(acrylonitrile-butadiene-styrene) (ABS).

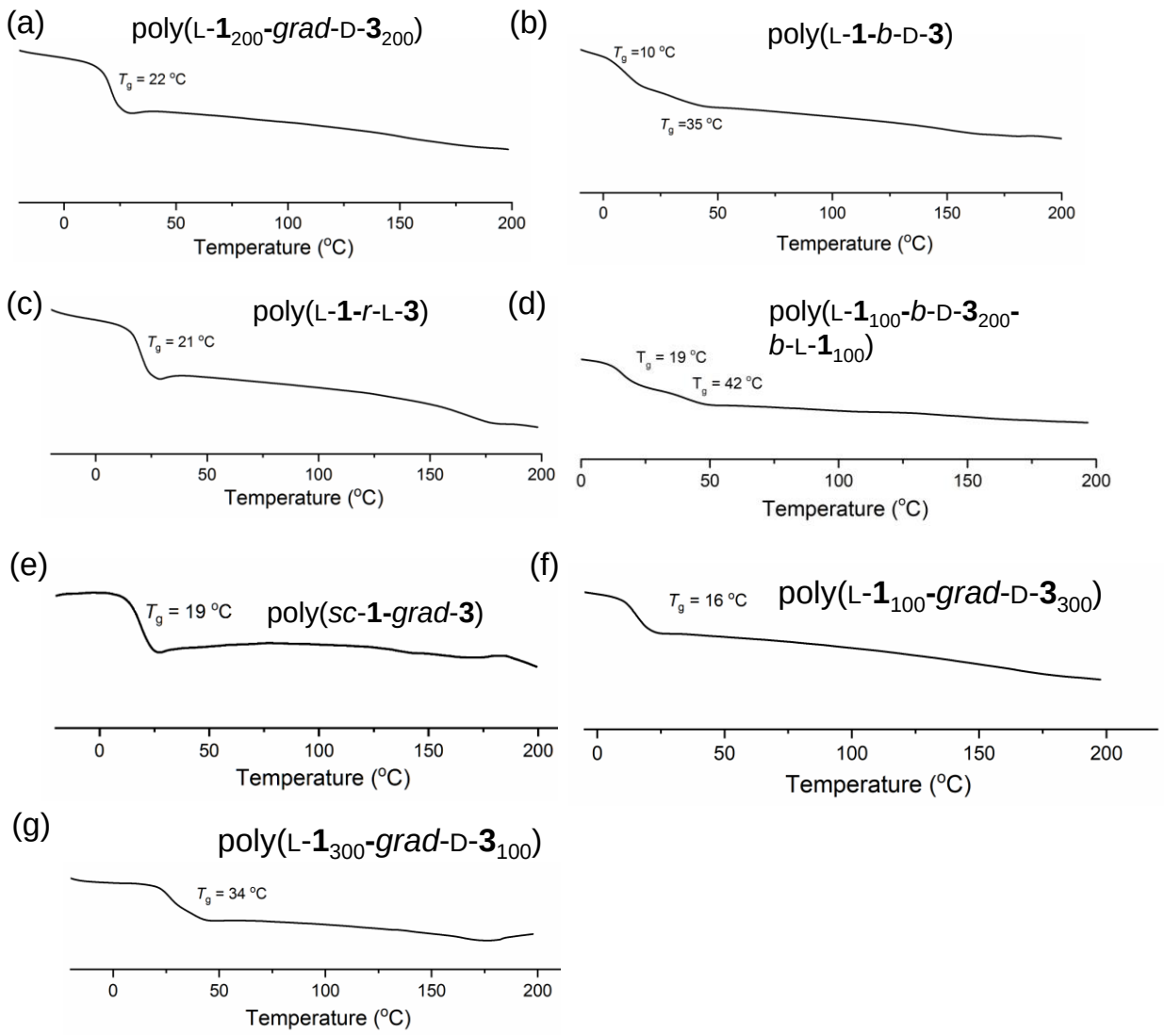

Figure 5.13 Differential scanning calorimetry measurements of T_gs and T_ms of various copolymers.

Table 5.4 Thermal and mechanical properties of various poly(α-hydroxy acids)

Entry	polymer	M_n (kDa)	$Đ$	T_g / T_m (°C)	E_y (MPa)	σ (MPa)	ε (%)
1	poly(L-**1**)	170.9	1.09	49 / –	391 ± 46	12.5 ± 0.8	73.6 ± 11.6
2	poly(L-**3**)	133.8	1.02	5 / 136	1.05 ± 0.06	0.967 ± 0.145	471.6 ± 51.3
3	poly(L-**1**$_{200}$-*grad*-D-**3**$_{200}$)	65.9	1.02	22 / –	85 ± 34	14.8 ± 0.4	317.5 ± 38.6
4	poly(D-**1**$_{200}$-*grad*- L-**3**$_{200}$)	60.3	1.06	18 / –	74 ± 13	12.0 ± 2.3	283.6 ± 32.4
5	poly(*sc*-**1**$_{200}$-*grad*-**3**$_{200}$)	65.9	1.02	19 / –	33 ± 9	11.1 ± 0.5	392.0 ± 26.9
6	poly(L-**1**-*b*-D-**3**)	54.0	1.02	10, 35 / –	8.2 ± 0.7	6.0 ± 0.6	233.5 ± 42.1
7	poly(L-**1**-*r*-L-**3**)	67.4	1.05	21 / –	40 ± 24	6.9 ± 0.8	294.9 ± 43.2
8	poly(L-**1**$_{100}$-*grad*-D-**3**$_{300}$)	57.8	1.08	16 / –	1.25 ± 0.23	2.1 ± 0.2	483.2 ± 43.4
9	poly(L-**1**$_{300}$-*grad*-D-**3**$_{100}$)	64.8	1.03	34 / –	68.5 ± 17.4	8.3 ± 0.4	128.5 ± 37.4
10	poly(L-**1**$_{100}$-*b*-D-**3**$_{200}$-L-**1**$_{100}$)	64.0	1.07	19, 41 / –	44.3 ± 25.7	7.5 ± 0.9	262.6 ± 22.3
11	LDPE	/	/	/	160.3 ± 55.1	9.95 ± 0.2	311.6 ± 10.9

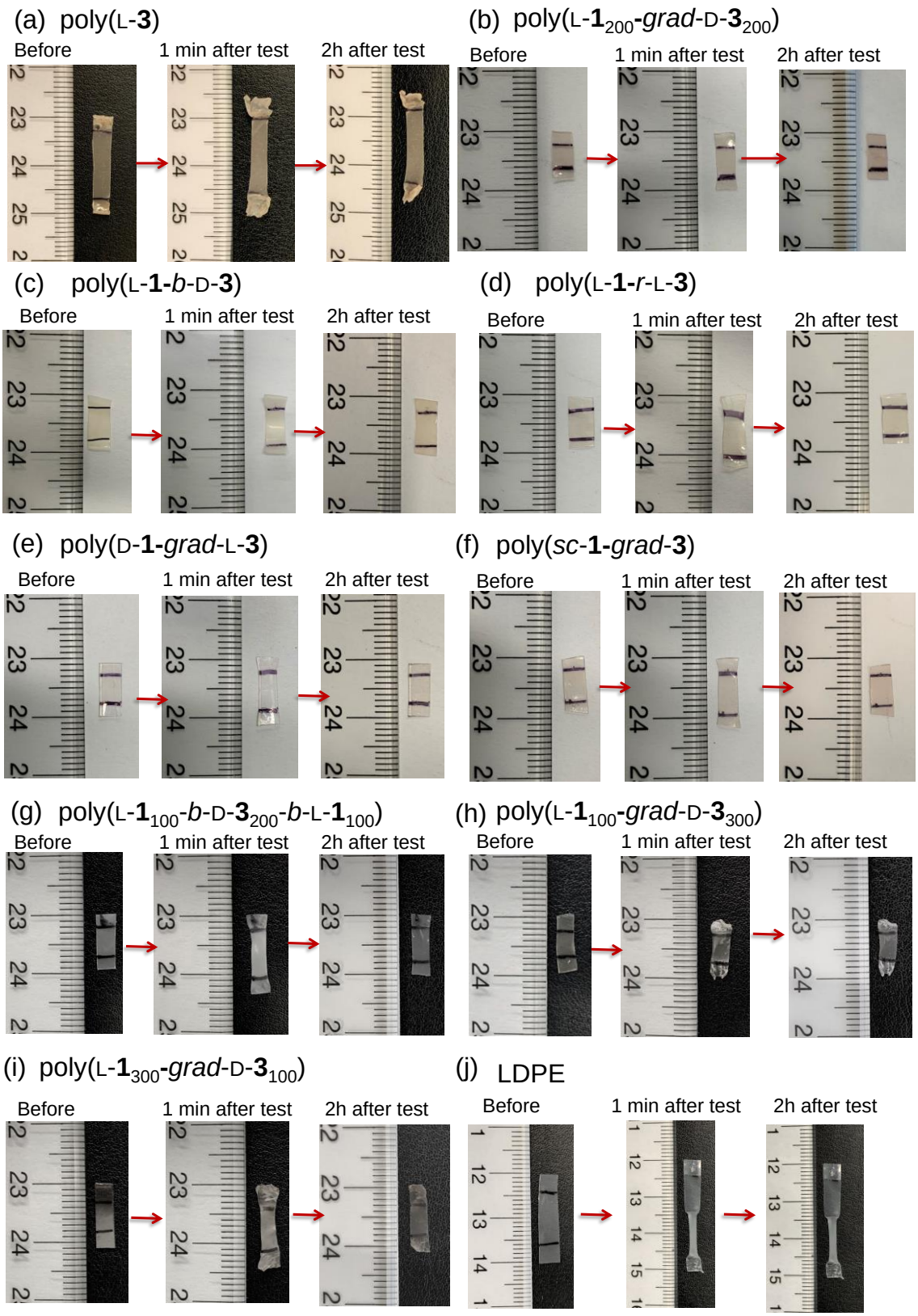

Figure 5.14 Shape recovery after polymers stretched in strain-stress tests with strain = 100 % (before fracture).

(a) poly(L-**3**)

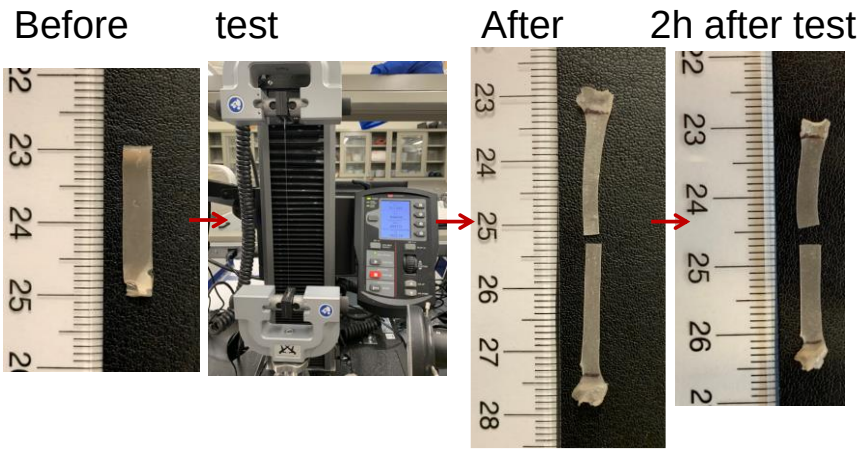

(b) poly(L-**1**-*grad*-D-**3**)

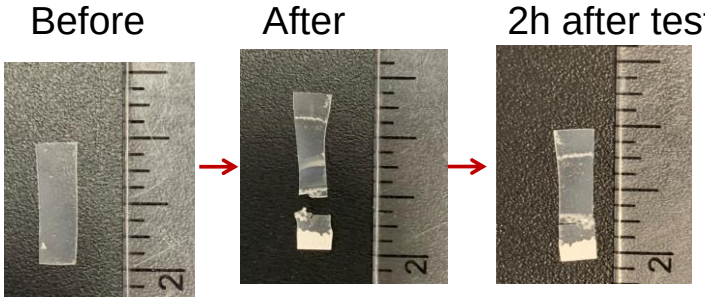

c) poly(*sc*-**1**-*grad*-**3**)

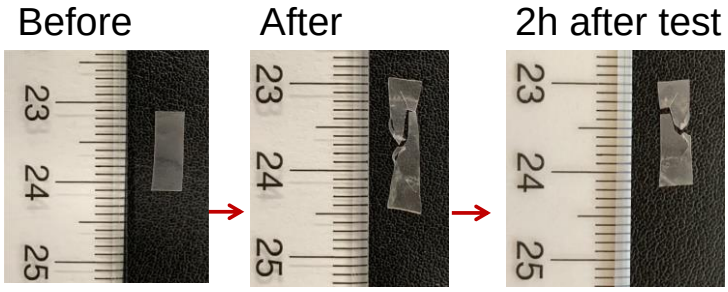

(d) poly(L-**1**-*r*-L-**3**)

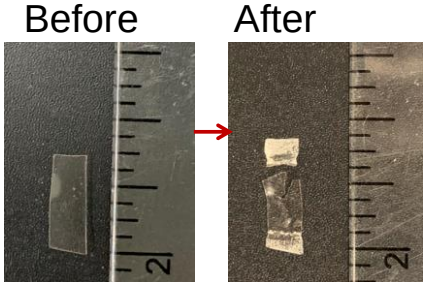

(e) poly(L-**1**-*b*-D-**3**)

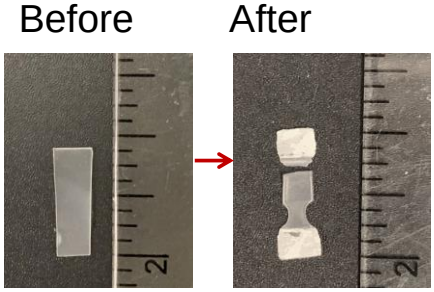

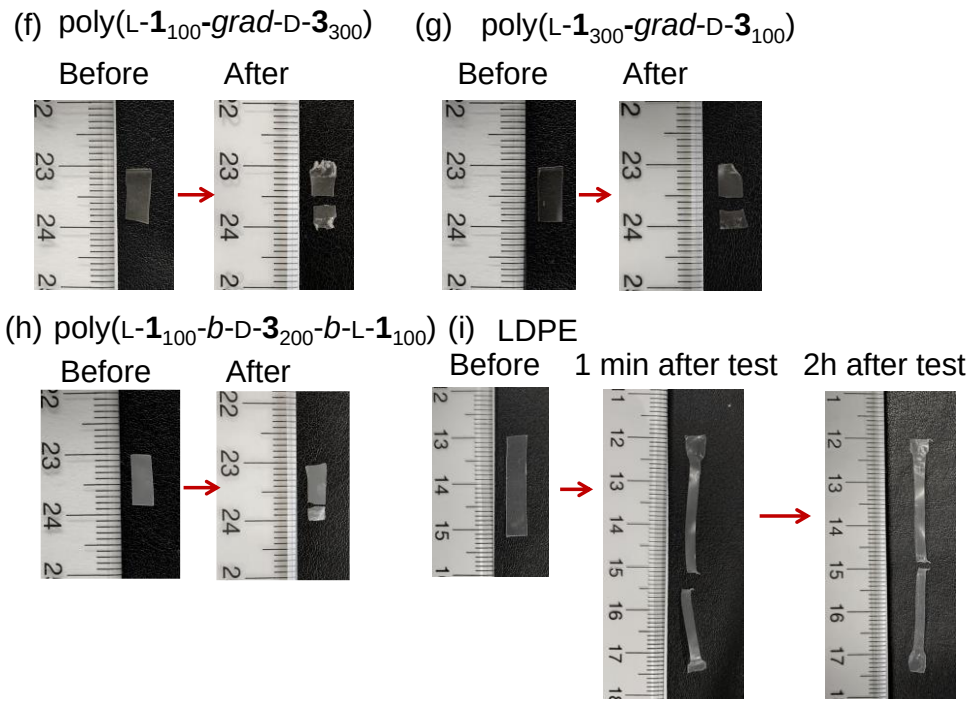

Figure 5.15 Shape recovery after polymer fracture in strain-stress tests. Note that poly(L-**3**) exhibited excellent ductility as shown in the stress-strain tests in (a).

Table 5.5 Shape-memory properties of various poly(α-hydroxy acids) and LDPE

Entry	Polymer	Strain recovery ratio	Strain fixity ratio
1	poly(L-**1**)	0.0058	/
2	poly(L-**3**)	0.940	0
3	poly(L-$\mathbf{1}_{200}$-*grad*-D-$\mathbf{3}_{200}$)	0.948	0
4	poly(D-$\mathbf{1}_{200}$-*grad*-L-$\mathbf{3}_{200}$)	0.938	0
5	poly(L-**1**-*b*-D-**3**)	0.936	0.088
6	poly(L-**1**-*r*-L-**3**)	0.946	0
7	poly(*sc*-$\mathbf{1}_{200}$-*grad*-$\mathbf{3}_{200}$)	0.941	0
8	poly(L-$\mathbf{1}_{100}$-*grad*-D-$\mathbf{3}_{300}$)	0.974	0
9	poly(L-$\mathbf{1}_{300}$-*grad*-D-$\mathbf{3}_{100}$)	0.962	0.012
10	poly(L-$\mathbf{1}_{100}$-*b*-D-$\mathbf{3}_{200}$-*b*-$\mathbf{1}_{100}$)	0.950	0.078
11	LDPE	0.012	0.985

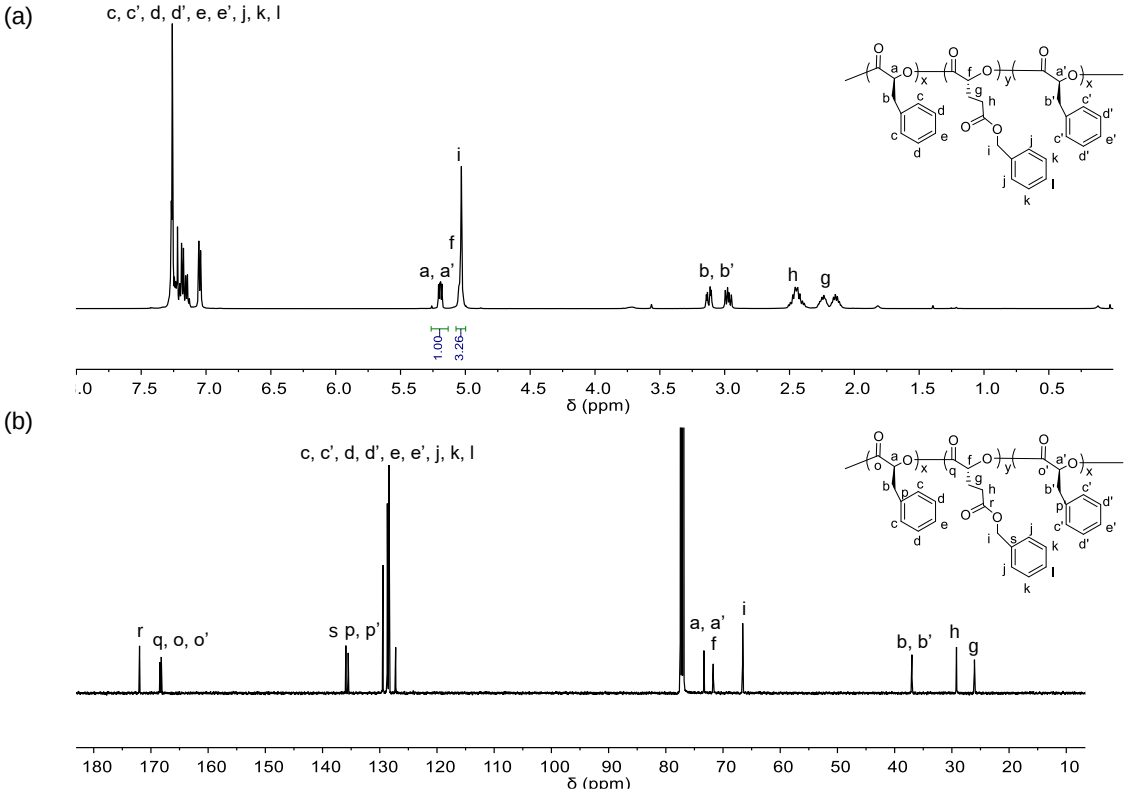

Figure 5.16 NMR spectra of poly(L-**1**$_{100}$-*b*-D-**3**$_{200}$-b-L-**1**$_{100}$) in $CDCl_3$ (Table 5.4, entry 10). (a) ^{1}H NMR spectrum; (b) ^{13}C NMR spectrum.

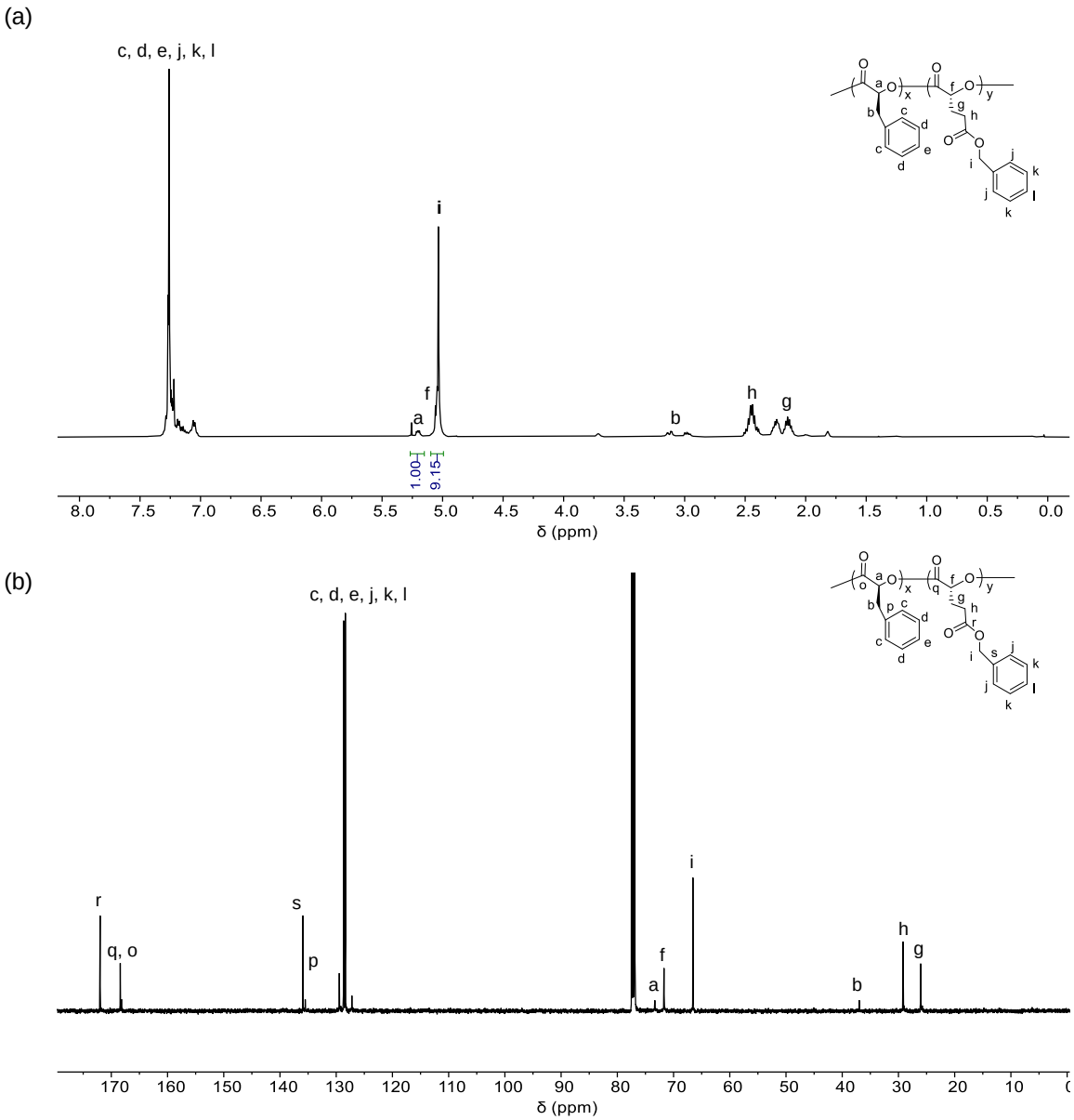

Figure 5.17 NMR spectra of poly(L-**1**$_{100}$-*grad*-D-**3**$_{300}$) in $CDCl_3$ (Table 5.4, entry 8). (a) ^{1}H NMR spectrum; (b) ^{13}C NMR spectrum.

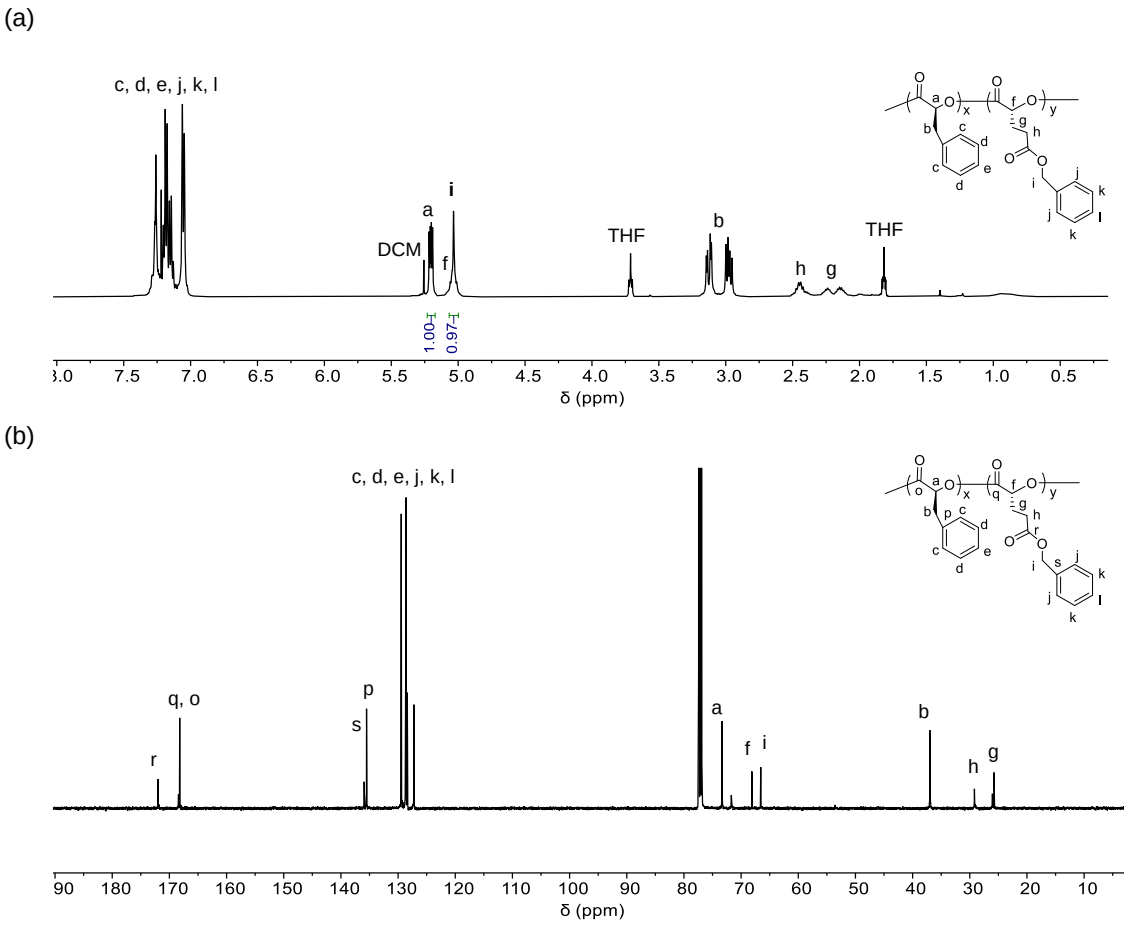

Figure 5.18 NMR spectra of poly(L-**1**$_{300}$-*grad*-D-**3**$_{100}$) in $CDCl_3$ (Table 5.4, entry 9). (a) ^{1}H NMR spectrum; (b) ^{13}C NMR spectrum.

5.3 Instrument and characterization

5.3.1 Differential scanning calorimetry (DSC)

DSC measurements were performed on TA Instruments DSC Q2000 instrument equipped with photocalorimeter accessory and RCS90 cooling system. Polymer samples in crimped aluminum pans were analyzed under nitrogen at a heating rate of 10 °C/min from 0 to 230 °C. Glass transition temperature (T_g, defined as the inflection point based on ASTM method) and melting temperature (T_m, defined as the peak point) were obtained and reported from the second heating run.

5.3.2 Mechanical testing of polymers

Solvent-cast polyester sheets were prepared by pouring DCM solutions of the polyester (~100 mg/mL) into a polydimethylsiloxane mold. The solvent was slowly evaporated in the fume hood over 1-2 weeks, and DCM peak was no longer observed in ^{1}H NMR spectroscopy, confirming that the polyester sheets were sufficiently dry for mechanical tests. Tensile stress-strain testing was performed by an Instron 5966 universal testing system (10 kN load cell) or dynamic mechanical analyzer (DMA, Q800, TA instrument) on test specimens (10 mm × 4 mm × 0.2 mm, length × width × thickness) at 10 mm/min or 5 N/min extension rate, using the ASTM D882-18 standard, at ambient temperature (22 ^{o}C) and humidity (~ 16%). All values are reported as the average of three to five samples.

5.3.3 Shape-memory effect

The shape-memory properties (fixed strain ε_f, residual strain ε_r, strain recovery capability, etc.) are defined or quantified using the following equations:

ε_f: the fixed strain after being stretched to ε_{max} (100 %) and left to relax freely at ambient temperature (20 °C).

Strain fixity ratio = $\varepsilon_f/\varepsilon_{max} \times 100\%$ (eq. 1)

ε_r: the remaining strain after being heated to 40 °C and left to cool to ambient temperature (20 °C).

Strain recovery ratio = $(\varepsilon_{max}-\varepsilon_r) / \varepsilon_{max} \times 100\%$ (eq. 2)

5.4 Conclusions

A series of homopolymers, block copolymers, stereoblock copolymers, and gradient copolymers were synthesized using our simple and scalable synthetic method catalyzed by Mn/Zn complex. After evaluating their mechanical and thermodynamic properties, a general structure-property relationship was established. Most importantly, it allowed us to prepare a gradient copolymer that is tougher, more ductile, and more resilient than the corresponding block copolymers and homopolymers, and that outperforms commodity polyolefins such as LDPE in terms of shape recovery resilience. Studies aimed at elucidating how the stereosequence influences mechanical properties and at expanding the scope of stereosequences to include syndiotactic blocks are underway. We anticipate that the findings described herein will accelerate the discovery of new degradable polyester materials by allowing for the control of polymer stereosequences. The use of the resulting degradable polyester elastomers for packaging, fiber, and biomedical applications can be foreseen.

Reference

1. Liu, T.; Simmons, T. L.; Bohnsack, D. A.; Mackay, M. E.; Smith, M. R.; Baker, G. L., Synthesis of polymandelide: A degradable polylactide derivative with polystyrene-like properties. *Macromolecules* **2007,** *40* (17), 6040-6047.
2. Wang, X.; Chin, A. L.; Tong, R., Controlled Ring-Opening Polymerization of O-Carboxyanhydrides to Synthesize Functionalized Poly (α-Hydroxy Acids). *Organic Materials* **2021,** *3* (01), 041-050.
3. Li, M.; Zhang, S.; Zhang, X.; Wang, Y.; Chen, J.; Tao, Y.; Wang, X., Unimolecular Anion‐Binding Catalysts for Selective Ring‐Opening Polymerization of O‐carboxyanhydrides. *Angewandte Chemie International Edition* **2021,** *60* (11), 6003-6012.
4. Zaarour, B.; Zhu, L.; Jin, X., Controlling the surface structure, mechanical properties, crystallinity, and piezoelectric properties of electrospun PVDF nanofibers by maneuvering molecular weight. *Soft Materials* **2019,** *17* (2), 181-189.
5. Longo, J. M.; DiCiccio, A. M.; Coates, G. W., Poly (propylene succinate): a new polymer stereocomplex. *Journal of the American Chemical Society* **2014,** *136* (45), 15897-15900.
6. Xie, Q.; Yu, C.; Pan, P., Stereocomplex crystallization of polymers with complementary configurations. In *Crystallization in Multiphase Polymer Systems*, Elsevier: 2018; pp 535-573.
7. Zhong, Y.; Feng, Q.; Wang, X.; Yang, L.; Korovich, A. G.; Madsen, L. A.; Tong, R., Photocatalyst-independent photoredox ring-opening polymerization of O-carboxyanhydrides: stereocontrol and mechanism. *Chemical Science* **2021**.
8. Baker, G. L.; Vogel, E. B.; Smith, M. R., Glass Transitions in Polylactides. *Polymer Reviews* **2008,** *48* (1), 64-84.
9. Zhu, Y.; Radlauer, M. R.; Schneiderman, D. K.; Shaffer, M. S.; Hillmyer, M. A.; Williams, C. K., Multiblock polyesters demonstrating high elasticity and shape memory effects. *Macromolecules* **2018,** *51* (7), 2466-2475.
10. Gregory, G. L.; Sulley, G. S.; Carrodeguas, L. P.; Chen, T. T.; Santmarti, A.; Terrill, N. J.; Lee, K.-Y.; Williams, C. K., Triblock polyester thermoplastic elastomers with semi-aromatic polymer end blocks by ring-opening copolymerization. *Chemical science* **2020,** *11* (25), 6567-6581.
11. Paul, H.; Small Jr, R.; Scaiano, J., Hydrogen abstraction by tert-butoxy radicals. A laser photolysis and electron spin resonance study. *Journal of the American Chemical Society* **1978,** *100* (14), 4520-4527.
12. Tang, X.; Westlie, A. H.; Watson, E. M.; Chen, E. Y.-X., Stereosequenced crystalline polyhydroxyalkanoates from diastereomeric monomer mixtures. *Science* **2019,** *366* (6466), 754-758.

CHAPTER 6

Single Lewis acidic zinc complex for copolymerization of *O*-carboxyanhydrides and epoxides to synthesize functionalized poly(ester-*b*-carbonates)

6.1 Introduction

The high molecular-weight polyesters derived from ring-opening polymerization (ROP) of *O*-carboxyanhydrides (OCAs) have shown great promise in replacing non-degradable polyolefins. However, an equivalent of CO_2 is lost with the incorporation of every repeat unit in the polymer, which is not atom economical. On the other hand, CO_2 is a naturally abundant and nontoxic one-carbon building block that can be used to synthesize organic molecules and polymers. Therefore, the chemical fixation of CO_2 into usable materials is an essential topic in both chemistry and environmental science. Nevertheless, it remains challenging to activate CO_2 for polymerization, as its chemistry is thermodynamically stable and kinetically inert. In the past few decades, the copolymerization of CO_2 with epoxides to produce polycarbonates has been a tremendous achievement in polymer chemistry. Polycarbonate, with its renewable resources and excellent biodegradability, is another potentially sustainable alternative (like aliphatic polyester) for petroleum-based plastics. Another valuable approach to recycle CO_2 is the terpolymerization of epoxide, CO_2, and anhydride or cyclic ester to produce poly(ester-*b*-carbonate) (*b*: block). Therefore, we reasoned that it is feasible to recycle CO_2 by using controlled OCA(CO_2)/epoxide ring opening copolymerization to produce poly(ester-*b*-carbonate). From the sustainability standpoint, the synthesis of sequence-defined copolymers, such as poly(ester-*b*-carbonate), is more attractive to

researchers, since it enables the material properties of the constituent homopolymers to be combined in single copolymers with new sets of features.[1, 2]

However, synthesizing sequence-defined copolymers from monomer mixtures is widely regarded as one of the paramount challenges in polymer chemistry.[3] Traditional strategies for polymerizing two mechanistically incompatible monomers into a single block copolymer involve using bifunctional initiators[4] or catalysts[5] or changing the active species upon formation of the first block[6, 7] (**Figure 6.1a**). Recently, the emergence of switchable / tandem polymerization strategies in which a single catalyst is used to access and switch between catalytic cycles of ring-opening polymerization (ROP) and ring-opening copolymerization (ROCOP) has opened a realm of auto-tandem catalysis processes for preparing sequence-controlled block copolymers (**Figure 6.1b**).[8-13] The copolymer sequences generated in this way can be precisely controlled by external stimuli, such as changes in gas pressure,[14] changes in redox state,[15] and electricity.[16, 17] Such strategies have been used for switchable polymerization chemistry focusing on the preparation of poly(ester-*co*-carbonates) from various combinations of renewable monomers including lactones, anhydrides, epoxides, and CO_2.[18] By combining the properties of their respective homopolymers, the obtained aliphatic poly(ester-*co*-carbonates) show improved thermal and mechanical properties relative to those of the homopolymers.[19] Nevertheless, the currently available methods for switchable polymerization reactions involving organometallic catalysts are energy-intensive: the reactions often require elevated temperature (50–120 °C) and high CO_2 pressure (5–20 bar).[14, 18, 19] Switchable / tandem polymerization reactions involving organocatalysts, such as bifunctional organoborons[20, 21] and Lewis pairs,[22-24] also require high temperature (50–

100 °C) and pressurized CO_2 (~10 bar) and provide copolymers that have molecular weights (MWs) of less than 100 kDa and broad MW distributions ($Đ$ > 1.2). Finally, the monomers that have been used for switchable / tandem polymerization have a restricted functionality window—most of the monomers have no functionality other than simple pendant alkyl side chains. Therefore, the search for milder, more energy-efficient methods for controlled tandem polymerization to afford high-MW functionalized poly(ester-*co*-carbonates) is ongoing.

The incorporation of functional-group-bearing OCAs into switchable polymerization reactions has been explored. For example, the Williams group recently reported ground-breaking work showing that OCAs and epoxides can be copolymerized by a dinuclear Zn complex (**Figure 6.1c**).[25] In these reactions, the CO_2 molecule released from the ROP of the OCA is recycled into a ROCOP reaction between the epoxide and CO_2 to produce poly(ester-*b*-carbonates) (*b*, block) with high atom economy. Similarly, switchable polymerization has also been achieved with organocatalysts.[26] Notably, the dinuclear-Zn-complex-catalyzed copolymerizations reported by Williams et al. require a high temperature (80 °C), whereas the same reactions involving organocatalysts can be carried out at room temperature. However, both of these one-pot methods for the tandem copolymerization give polymers with low MWs (< 20 kDa) and relatively broad MW distributions ($Đ$ ~ 1.2), and excess epoxide is required. Thus far, a facile method for preparing high-MW functionalized poly(ester-*b*-carbonates) has not been achieved, and the lack of such a method limits access to these degradable block copolymers, which show promising thermal and mechanical properties.

In this study, we identified a Zn complex that mediates strikingly selective one-pot tandem polymerizations of OCAs and epoxides at room temperature to afford high-MW (>200 kDa) functionalized poly(ester-b-carbonates) with narrow MW distributions (Đ < 1.1), using a remarkably simple and scalable experimental setup (**Figure 6.1d**). The copolymers can be sequentially and efficiently degraded to the corresponding monomers and monomer derivatives for recycling.

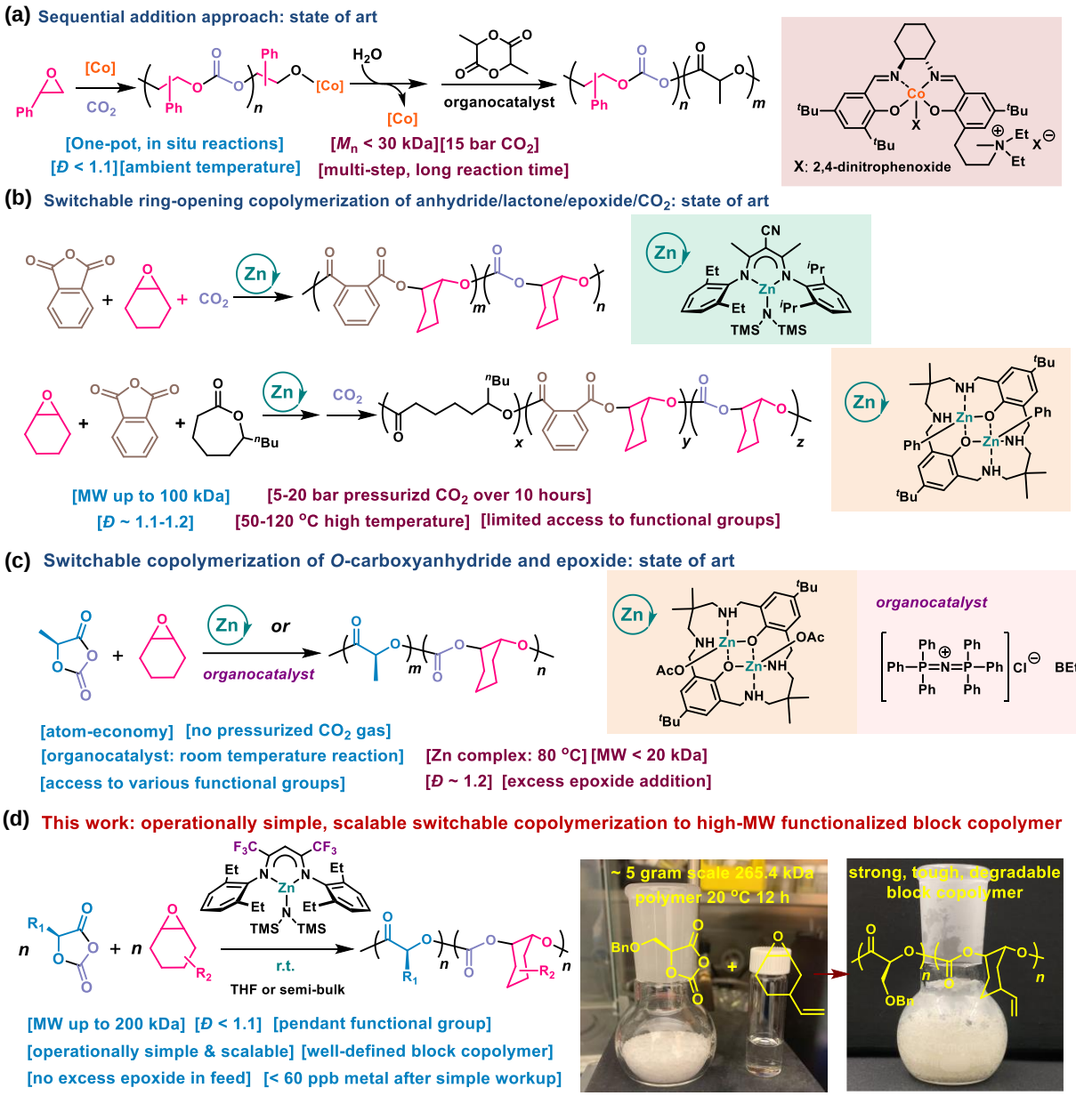

Figure 6.1 Strategies for synthesis of high-molecular-weight (MW) functionalized poly(ester-b-carbonates). (a) Synthesis of block copolymers by sequential addition of epoxides/CO_2 and lactides. (b) Mechanism-switchable anhydride/epoxide/lactone/CO_2 ring-opening copolymerization with catalysis by a single metal complex. (c) Mechanism-switchable *O*-carboxyanhydride (OCA)/epoxide polymerization to afford low-MW copolymers with broad MW distributions. (d) Scalable tandem OCA/epoxide copolymerization at room temperature to afford high-MW functionalized block copolymers, as reported in this paper. The pros and cons of the various strategies are indicated in blue and red type, respectively.

6.2 Results and discussions

6.2.1 The discovery of single Lewis acidic zinc complex for OCA/epoxide copolymerization

We began by studying (BDI)Zn complexes (BDI = β-diiminate) as catalysts for OCA/epoxide copolymerization. These versatile complexes have been used for stereoselective ROP of lactones[27] and OCAs[28] and can also mediate epoxide/CO_2 ROCOP[29] and epoxide/anhydride ROCOP.[30] We initially focused on the copolymerization of cyclohexene oxide (CHO) and OCA L-**2** mediated by various (BDI)Zn complexes at room temperature in THF ([L-**2**]/[CHO]/[Zn] = 100/100/1; **Figure 6.2**). Much to our dismay, catalysts **BDIZn-4** and **BDIZn-5**, which have an electron-withdrawing cyano group and are active for CHO/CO_2 and CHO/anhydride copolymerization,[30, 31] did not initiate CHO/CO_2 copolymerization after the L-**2** was consumed. Previous studies of ROCOP catalysts demonstrated that increasing the Lewis acidity of a catalyst by changing the ligand structure improves epoxide activation.[32, 33] Indeed, we found that **BDIZn-7**, which has two electron-withdrawing CF_3 groups in the BDI ligand backbone,[34] mediated L-**2**/CHO copolymerization at room temperature, resulting in 100% OCA conversion and 90% CHO conversion after 12 h. The obtained copolymer had a M_n of 29.9 kDa and a $Đ$ of 1.01 (expected MW = 32.0 kDa). We reasoned that **BDIZn-7** outperformed **BDIZn-4** and **BDIZn-5** because the electron-withdrawing CF_3 group has a higher value of electronegativity of 3.49 (Pauling scale) compared with the CN group(2.77).[35] The substituent on the *N*-aryl group of the (BDI)Zn complex also affected the polymerization outcome (compare the results for **BDIZn-7** with those for **BDIZn-6** and **BDIZn-8** in **Figure 6.2**). Screening of other metal

complexes that have been used to catalyze polyester and polycarbonate synthesis did not yield results comparable to those obtained with **BDIZn-7** (**Table 6.1**), and neither did Zn complexes with tridentate ligands (**Table 6.2**).

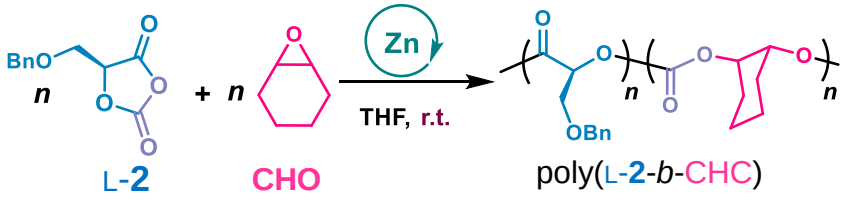

[L-**2**]/[CHO]/[Zn] = 100/100/1, 12h

Expected MW: 32.0 kDa

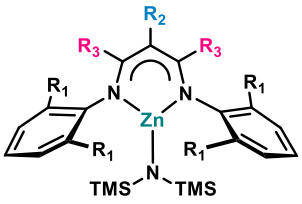

(BDI)Zn complex

	R_1	R_2	R_3	Conv. [OCA] %	Conv. [CHO] %
BDIZn-1	Me	H	Me	100	0
BDIZn-2	Et	H	Me	100	0
BDIZn-3	^{i}Pr	H	Me	100	0
BDIZn-4	Me	CN	Me	100	0
BDIZn-5	Et	CN	Me	100	0
BDIZn-6	Me	H	CF3	100	69
BDIZn-7	Et	H	CF3	100	90
BDIZn-8*	^{i}Pr	H	CF3	100	0

Figure 6.2 Identification of the reactive **BDIZn-7** complex that enabled efficient L-**2**/CHO copolymerization at room temperature with high monomer conversion. Detailed polymerization data are provided in **Table 6.2**. *, **BDIZn-8** had the initiating group of -Et instead of -N(TMS)$_2$.

Table 6.1 The screen of metal complexes for the copolymerization of L-**2**/CHO at room temperature [a]

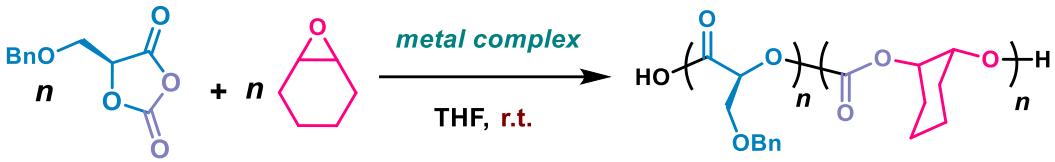

entry	catalyst	OCA Conv. (%) [b]	CHO Conv. (%)	Copolymer yield (%)	M_n (kDa)	MW_{cal} (kDa)	$Đ$
1	$Mn[N(TMS)_2]_2$	100	0	0	/	17.8	/
2	$Co[N(TMS)_2]_2$	100	0	0	/	17.8	/
3	$Mg[N(TMS)_2]_2$	100	0	0	/	17.8	/
4	$Fe[N(TMS)_2]_2$	100	0	0	/	17.8	/
5	$Y[N(TMS)_2]_3$	100	0	0	/	17.8	/
6	$Y[N(SiHMe_2)_2]_3$	100	0	0	/	17.8	/
7	$Ce[N(TMS)_2]_3$	87.9	0	0	/	15.6	/
8	$Zn[N(TMS)_2]_2$	100	0	0	/	17.8	/
9	$Sn[N(TMS)_2]_2$	91.1	0	0	/	16.2	/
10	(Salcy)MnCl	36.3	0	0	/	6.46	/
11	(Salcy)Co	43.7	0	0	/	7.78	/
12	(Salcy)CrCl	38.3	0	0	/	6.82	/
13	(Salcy)AlCl	43.9	0	0	/	7.81	/
14	$Hf(O^iPr)_4$	37.9	0	0	/	6.75	/
15	$Zr(O^iPr)_4$	53.6	0	0	/	9.54	/

[a] Abbreviation: salcy, 1,2-cyclohexanediamino-*N*,*N*'-bis(3,5-di-tert-butyl-salicylidene); Conv., monomer conversion; M_n, number-average molecular weight; MW_{cal}, molecular weight calculated from the FR and monomer conversion; $Đ$, molecular weight distribution. Polymerization conditions: [L-**2**]/[CHO]/[metal complex] = 100/100/1 in THF for 17 hours at room temperature in a glove box.

[b] Determined from the intensity of the Fourier transform infrared peak at 1805 cm^{-1}, which corresponds to the anhydride group of the OCA.

Table 6.2 The screen of Zn complexes for copolymerization of L-2/CHO at room temperature [a]

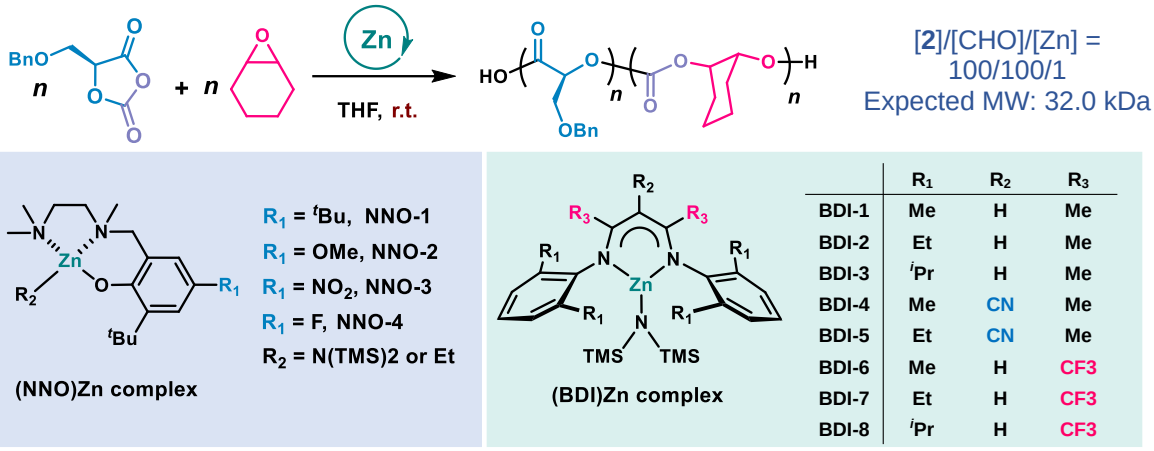

	R1	R2	R3
BDI-1	Me	H	Me
BDI-2	Et	H	Me
BDI-3	iPr	H	Me
BDI-4	Me	CN	Me
BDI-5	Et	CN	Me
BDI-6	Me	H	CF3
BDI-7	Et	H	CF3
BDI-8	iPr	H	CF3

entry	Zn catalyst	OCA Conv. (%) [b]	CHO Conv. (%) [c]	Copolymer yield (%)	M_n (kDa) [d]	MW_{cal} (kDa)	$Đ$ [d]
1	(**NNO-1**)ZnN(TMS)$_2$	100	0	0	/	17.8	/
2	(**NNO-1**)ZnEt	100	0	0	/	17.8	/
3	(**NNO-2**)ZnEt	100	0	0	/	17.8	/
4	(**NNO-3**)ZnEt	69.7	0	0	/	12.4	/
5	(**NNO-4**)ZnN(TMS)$_2$	100	0	0	/	17.8	/
6	(**NNO-4**)ZnEt	100	0	0	/	17.8	/
7	(**BDI-1**)ZnN(TMS)$_2$	100	0	0	/	17.8	/
8	(**BDI-2**)ZnN(TMS)$_2$	100	0	0	/	17.8	/
9	(**BDI-3**)ZnN(TMS)$_2$	100	0	0	/	17.8	/
10	(**BDI-4**)ZnN(TMS)$_2$	100	0	0	/	17.8	/
11	(**BDI-5**)ZnN(TMS)$_2$	100	0	0	/	17.8	/
12	(**BDI-6**)ZnN(TMS)$_2$	100	68.5	86.0	51.3	27.5	1.01
13	(**BDI-7**)ZnN(TMS)$_2$	100	89.5	95.3	29.9	30.5	1.01
14	(**BDI-8**)ZnEt	100	0	0	/	17.8	/

[a] Abbreviation: Conv., monomer conversion; M_n, number-average molecular weight; MW_{cal}, molecular weight calculated from the FR and monomer conversion; $Đ$, molecular

weight distribution. Polymerization conditions: [L-**2**]/[CHO]/[Zn] = 100/100/1 in THF for 12 h at room temperature in a glove box.

b Determined from the intensity of the Fourier transform infrared peak at 1805 cm^{-1}, which corresponds to the anhydride group of the OCA.

c Determined by ^{1}H NMR spectra.

d Determined by GPC.

6.2.2 The identification of obtained copolymer composition

We then determined whether the copolymerization of OCA and epoxide afforded a random copolymer, a mixture of two homopolymers, or a block copolymer. A DOSY NMR study (DOSY = diffusion-ordered spectroscopy) of the obtained polymer showed a single diffusion coefficient for all resonances, as would be expected for a copolymer (**Figure 6.3a**); whereas the DOSY NMR spectrum of a physical mixture of poly(L-**2**) and poly(CHC) homopolymers showed two diffusion coefficients (**Figure 6.3b**). To determine whether the two monomers were incorporated randomly or into a well-defined block copolymer, we monitored the **BDIZn-7**-mediated copolymerization in deuterated toluene by means of real-time ^{1}H NMR spectroscopy (**Figure 6.4**). The typical NMR spectra shown in **Figure 6.4** clearly demonstrate that the polymerization occurred in two stages: in the first stage, ROP of L-**2** proceeded with release of CO_2 to form poly(L-**2**) block; and, in the second stage, ROCOP of CHO and the CO_2 released by the ring-opening of L-**2** afforded a poly(CHC) block (poly(CHC) block formation started at ~182 min), confirming the formation of a sequence-defined block copolymer. Notably, these NMR studies also suggested that no polyether side products (~3.46 ppm) formed during the polymerization (**Figure 6.5a**). Carbonate bond formation was confirmed from the ^{13}C NMR spectrum of the obtained block copolymer (153.9 ppm), and such NMR spectrum also suggested isoselective enchainment of the poly(CHC) block with a high probability

of meso dyad formation (P_m = 0.85, **Figure 6.5b**).[36] Furthermore, the narrow unimodal MW distribution of the block copolymer, as determined by gel permeation chromatography (GPC, **Figure 6.5c-d**), was supported by the matrix-assisted laser desorption/ionization mass spectrum (MALDI-MS) of the oligomer ([L-**2**]/[CHO]/[**BDIZn-7**] = 5/5/1; **Figure 6.6**).

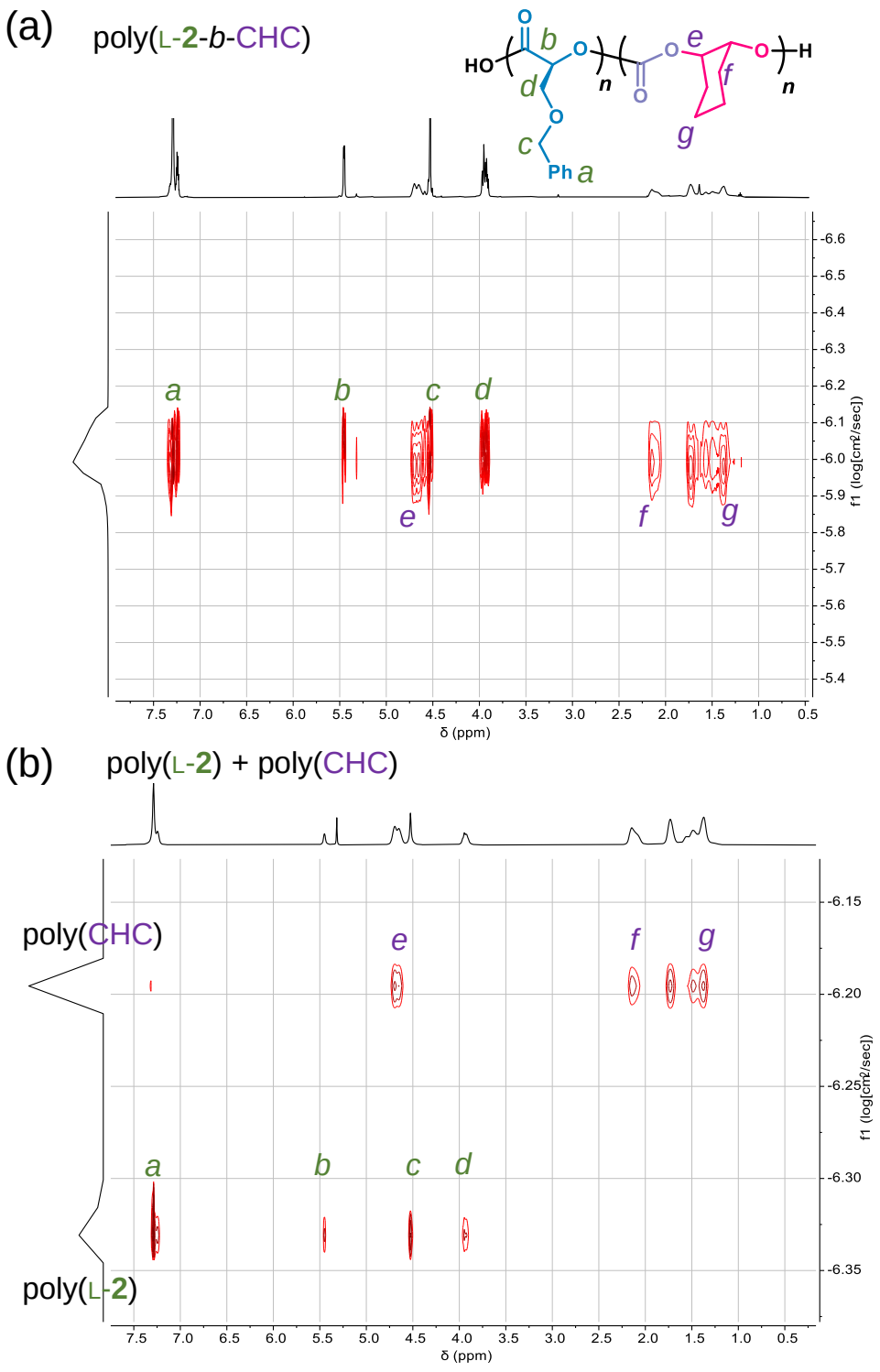

Figure 6.3 DOSY NMR spectra of (a) block copolymer poly(L-**2**-*b*-CHC), and (b) the physical blend of two homopolymers poly(L-**2**) (M_n = 45.8 kDa) and poly(CHC) (M_n = 42.9 kDa) that had similar molecular weights but different diffusivities.

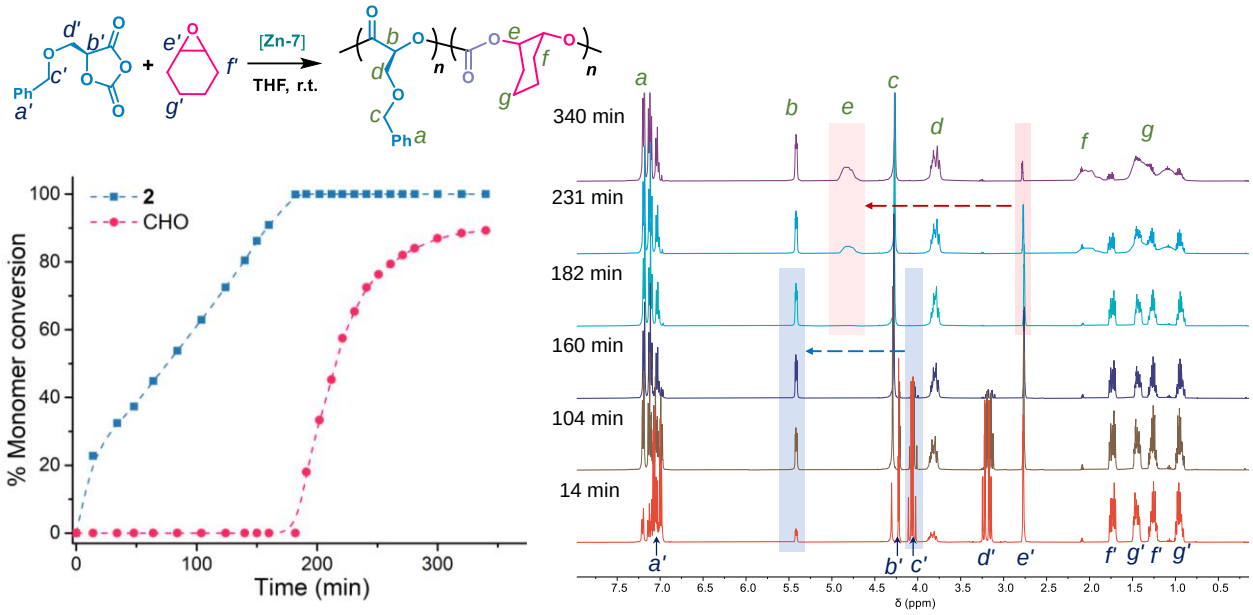

Figure 6.4 Representative kinetics data for monomer conversion as determined by real-time ^{1}H NMR spectroscopy for Zn-mediated block copolymerization of *O*-carboxyanhydride L-2 and cyclohexene oxide (CHO). The peak shifts due to conversion of L-**2** to the poly(L-**2**) block and conversion of CHO to the poly(CHC) block are highlighted in blue and red, respectively.

(a)

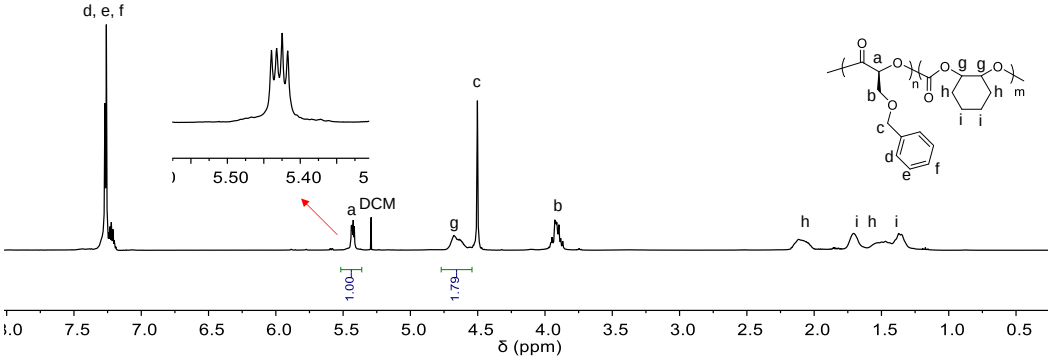

(b)

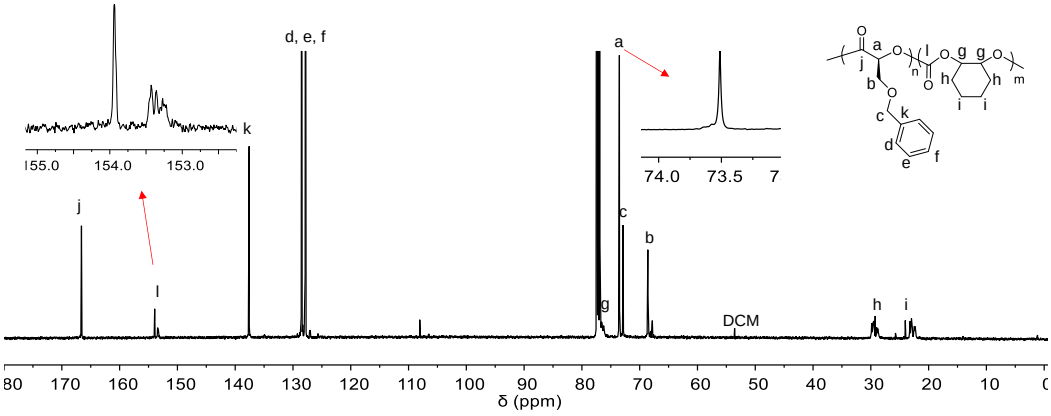

(c)

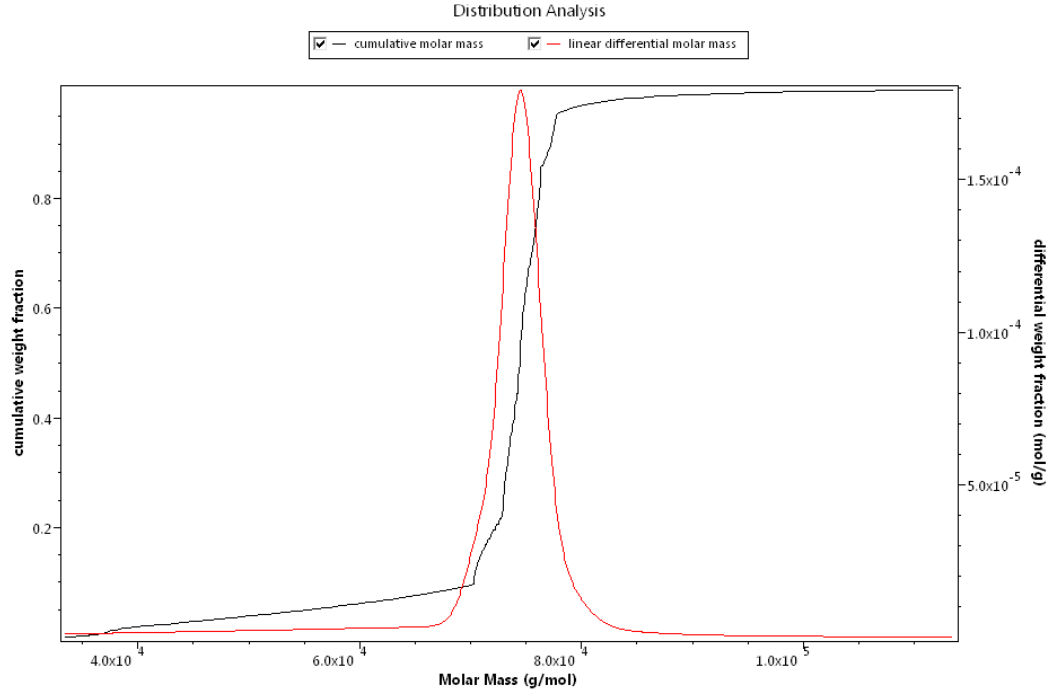

(Data continue on the next page)

(d)

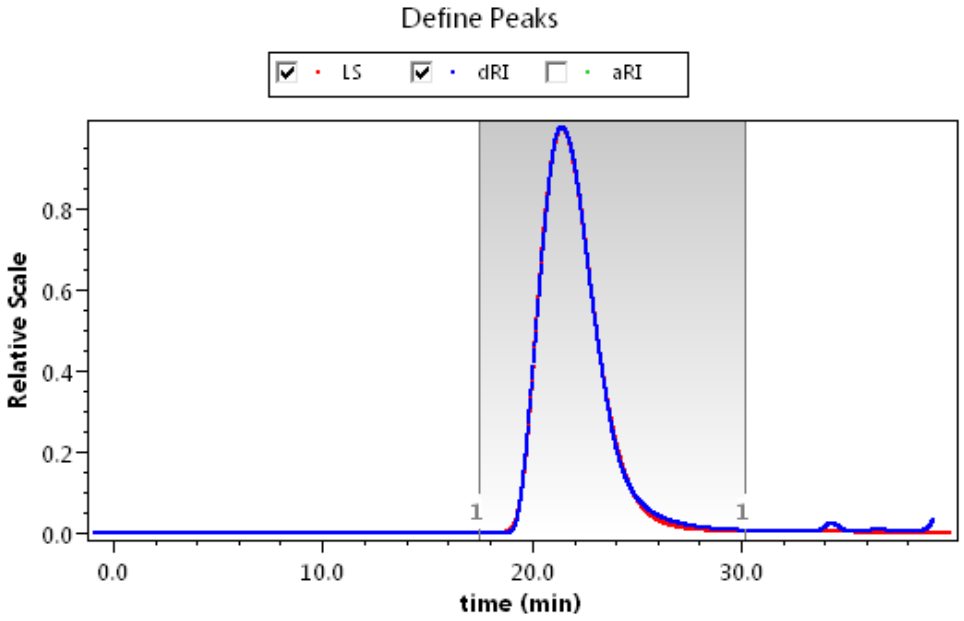

Results

Peak Results

	Peak 1
Masses	
Injected Mass (µg)	0.00
Calculated Mass (µg)	3349.33
Mass Recovery (%)	n/a
Mass Fraction (%)	100.0
Molar mass moments (g/mol)	
Mn	7.762×10^4 (±0.053%)
Mw	7.819×10^4 (±0.045%)
Mz	7.944×10^4 (±0.207%)
Polydispersity	
Mw/Mn	1.007 (±0.070%)
Mz/Mn	1.023 (±0.213%)

Figure 6.5 (a) ^{1}H and (b) ^{13}C NMR spectra of poly(L-**2**-*b*-CHC). The insets in both (a) and (b) showed that there was no epimerization on α-methine in the poly(L-**2**) block. The carbonate peak (peak l) in (b) showed the isoselective polycarbonate enchainment (*mmm* peak at 153.9 ppm), assigned according to the references.[36, 37] (c, d) The GPC raw data of poly(L-**2**-*b*-CHC) ([L-**2**]/[CHO]/[**BDIZn-7**] = 300/300/1), including dw/dlogMW versus MWs plots (c), which is used for the MW distribution calculation in GPC, and signals in the light scattering (LS) and refractive index (dRI) detectors versus time (d). The peak results in (d) clearly indicate the unimodal narrow MW distribution of the obtained polymers.

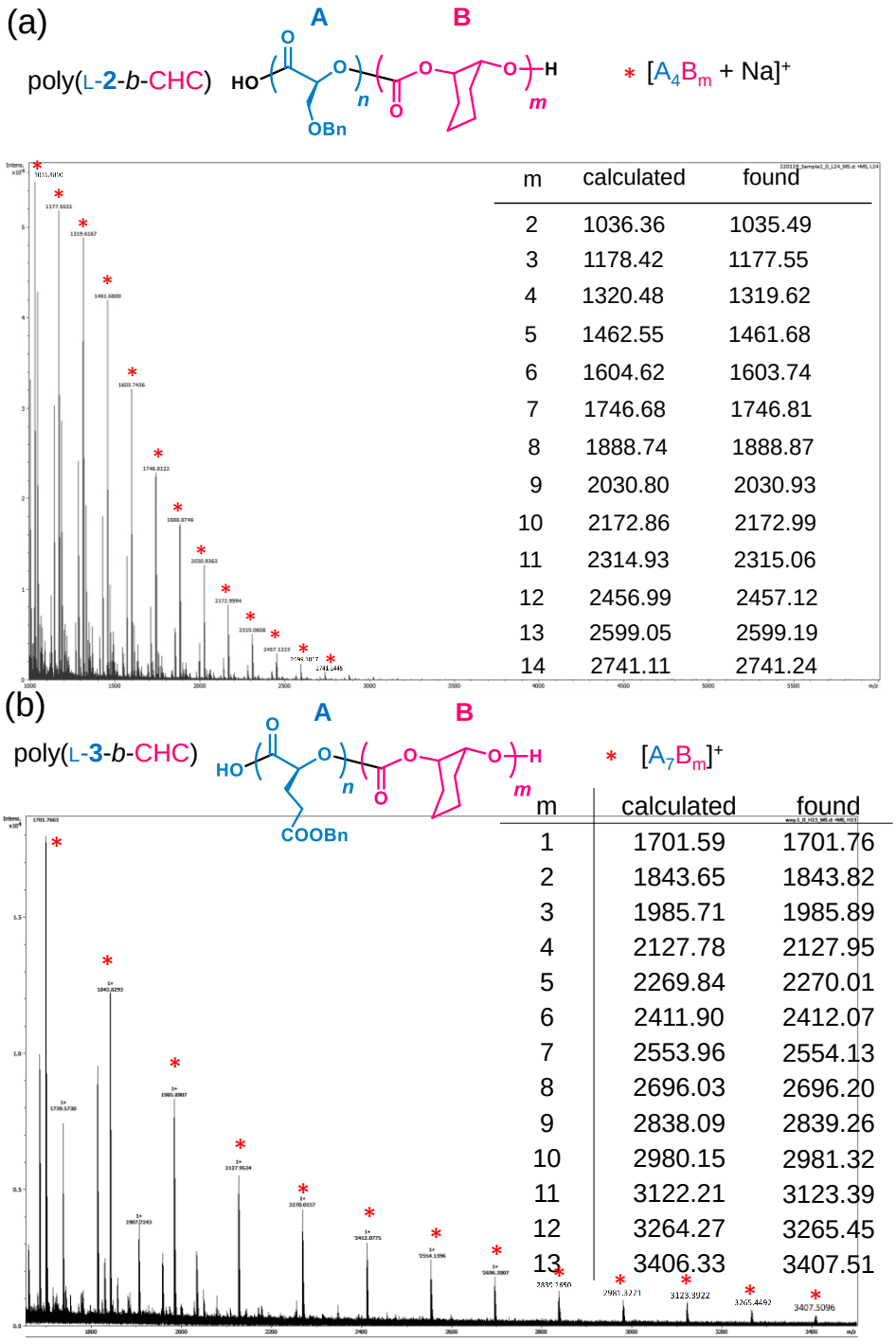

m	calculated	found
2	1036.36	1035.49
3	1178.42	1177.55
4	1320.48	1319.62
5	1462.55	1461.68
6	1604.62	1603.74
7	1746.68	1746.81
8	1888.74	1888.87
9	2030.80	2030.93
10	2172.86	2172.99
11	2314.93	2315.06
12	2456.99	2457.12
13	2599.05	2599.19
14	2741.11	2741.24

m	calculated	found
1	1701.59	1701.76
2	1843.65	1843.82
3	1985.71	1985.89
4	2127.78	2127.95
5	2269.84	2270.01
6	2411.90	2412.07
7	2553.96	2554.13
8	2696.03	2696.20
9	2838.09	2839.26
10	2980.15	2981.32
11	3122.21	3123.39
12	3264.27	3265.45
13	3406.33	3407.51

Figure 6.6 MALDI-MS of (a) oligo(L-**2**-*b*-CHC), and (b) (L-**3**-*b*-CHC). For all reactions, [OCA]/[CHO]/[**BDIZn-7**] = 5/5/1.

6.2.3 The condition optimization of copolymerization of OCA and CHO

The discovery of **BDIZn-7**-mediated auto-tandem block copolymerization of L-**2** and CHO prompted us to optimize the reaction conditions. Examination of the initiating group on **BDIZn-7** revealed that a complex with a bis(trimethylsilyl)amido group gave the best results (**Table 6.3**, entry 1); Zn complexes bearing an ethyl, methyl lactate, or acetate group did not adequately incorporate CHO into the copolymer (entries 2–4). Surprisingly, the addition of BnOH into the reaction mixture did not efficiently enchain the CHO/CO_2 ROCOP in the copolymerization (entry 5), suggesting that the Zn-alkoxide might not be efficiently converted to a Zn-carbonate to initiate CHO/CO_2 copolymerization (see next chapter on mechanistic studies). The presence of CHO was essential to the ROP of OCA in the copolymerization (**Table 6.4**, entry 3). Although lowering the reaction temperature slowed the first stage (ROP of OCA, entry 5), increasing the temperature reduced the amount of CO_2 dissolved in the reaction mixture (entry 6). Externally applying CO_2 with a gauge pressure of 1 bar during the second stage (CHO/CO_2 ROCOP) had a negligible effect on the MW (entry 7), indicating that the soluble CO_2 liberated from L-**2** was sufficient.

Table 6.3 Effects of initiating groups on Zn complexes for copolymerization of 2/CHO at room temperature [a]

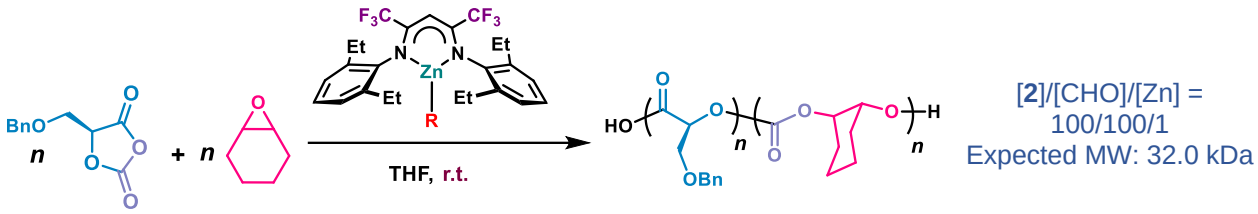

Entry	Catalyst	OCA Conv. (%) [b]	CHO Conv. (%) [c]	Copolymer yield (%)	M_n (kDa) [d]	MW_{cal} (kDa)	$Đ$ [d]
1	(**BDI-7**)ZnN(TMS)$_2$	100	89.5	95.3	29.9	30.5	1.01
2	(**BDI-7**)Zn(MeLac)	100	0	0	19.7	17.8	1.17
3	(**BDI-7**)ZnEt	100	41.0	73.8	24.1	23.6	1.03
4	(**BDI-7**)ZnOAc	100	33.0	70.2	16.0	22.5	1.02
5	(**BDI-7**)ZnN(TMS)$_2$ + BnOH [e]	100	29.5	68.7	23.2	22.0	1.12

[a] Abbreviation: Conv., monomer conversion; M_n, number-average molecular weight; MW_{cal}, molecular weight calculated from the FR and monomer conversion; $Đ$, molecular weight distribution; MeLac, methyl lactate, i.e., -OCH(Me)COOMe. Polymerization conditions: [L-**2**]/[CHO]/[Zn] = 100/100/1 in THF for 17 hours at room temperature in a glove box. [L-**2**]=[CHO]= 0.414 M.

[b] Determined from the intensity of the Fourier transform infrared peak at 1805 cm^{-1}, which corresponds to the anhydride group of the OCA.

[c] Determined by ^{1}H NMR spectra.

[d] Determined by GPC.

[e] Polymerization conditions: [L-**2**]/[CHO]/[Zn]/[BnOH] = 100/100/1/1 in THF for 17 hours at room temperature in a glove box. [L-**2**] = [CHO] = 0.414 M.

Table 6.4 Optimization of the copolymerization conditions [a]

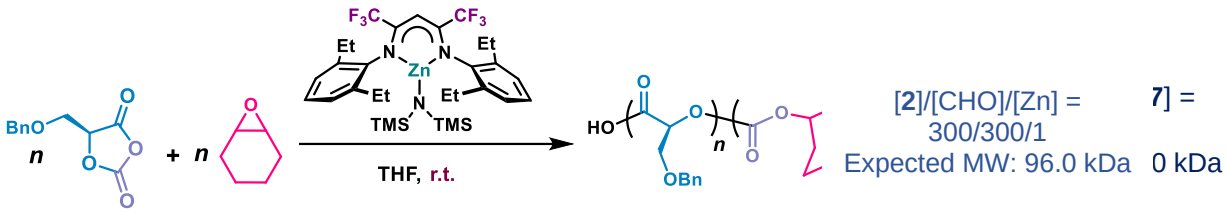

entry	conditions	OCA Conv. (%) [b]	CHO Conv. (%) [c]	Copolymer yield (%)	M_n (kDa) [d]	MW_{cal} (kDa)	$Đ$ [d]
1	as shown	100	89.5	95.3	77.6	91.6	1.01
2	no L-**2**, CHO/Zn = 300/1 + CO_2 (1 bar) for 3h	/	75.8	0	42.9	32.3	1.06
3	no CHO, OCA/Zn=300/1	7.7	/	0	/	/	/
4	in toluene	100	90.5	95.8	74.6	92.0	1.01
5	-15 ˚C	52.3	0	0	23.5	27.9	1.13
6	50 ˚C	100	0	0	47.3	53.4	1.01
7	in the glove box (4.5 h) + CO_2 (1 bar, 12 h) [e]	100	83.0	92.4	66.0	88.8	1.01
8	only 10 μL THF solvent (semi-bulk)	100	72.5	87.8	88.1	84.3	1.03
9	no solvent	19.7	/	0	/	/	/

[a] Abbreviation: Conv., monomer conversion; M_n, number-average molecular weight; MW_{cal}, molecular weight calculated from the FR and monomer conversion; $Đ$, molecular weight distribution. Polymerization conditions: [L-**2**]/[CHO]/[**BDIZn-7**] = 300/300/1 in THF for 12 hours at room temperature in a glove box.

[b] Determined from the intensity of the Fourier transform infrared peak at 1805 cm^{-1}, which corresponds to the anhydride group of the OCA.

[c] Determined by ^1H NMR spectra.

[d] Determined by GPC.

[e] The ROP of OCA finished, which was monitored by FTIR, and then external CO_2 (gauged pressure at 1 bar) was applied to the reaction solution.

6.2.4 Copolymerization scope and multiblock copolymerization

With an optimized set of conditions in hand, we examined the copolymerization of OCAs L-**1**-L-**4** with various epoxides at room temperature (**Table 6.5**). Firstly, we investigated whether our method could afford copolymers with MWs predictable from the initial monomer/catalyst feed ratio. We found that the M_n values of the copolymers increased linearly as the [L-**2**]/[CHO]/[**BDIZn-7**] feed ratio was increased from 50/50/1 to 300/300/1, and all the obtained copolymers had $Đ$ values of <1.1 (**Figure 6.7a**; GPC traces of the copolymers are shown in **Figure 6.7b**). At the highest [L-**2**]/[CHO]/[**BDIZn-7**] ratio (300/300/1), the conversion of L-**2** was quantitative, and CHO conversion reached 89.5% in 4 hours (**Table 6.5**, entry 1). Note that no epimerization of the α-methine hydrogen was observed in the ^{1}H or ^{13}C NMR spectrum of the poly(L-**2**) block of high-MW poly(L-**2**-*b*-CHC) (**Figure 6.5a, b**). Importantly, the copolymerization could be conducted on a multigram scale under semibulk conditions in neat CHO (liquid, [CHO]/[L-**2**]/[**BDIZn-7**] = 300/300/1) containing a trace of THF (10 μL) to dissolve the **Zn-7**; under these conditions, we obtained a copolymer with M_n and $Đ$ values comparable to those of the copolymer obtained from a solution-phase reaction (compare entries 1 and 2 in **Table 6.5**). Inductively coupled plasma mass spectrometry (ICP-MS) revealed that a negligible amount of Zn ([Zn] < 60 ppb) remained in the copolymer after the dichloromethane solution of the copolymer was added to cold methanol to precipitate the copolymer (**Table 6.6**).

Table 6.5 Copolymerization of epoxides and *O*-carboxyanhydrides at room temperature.[a]

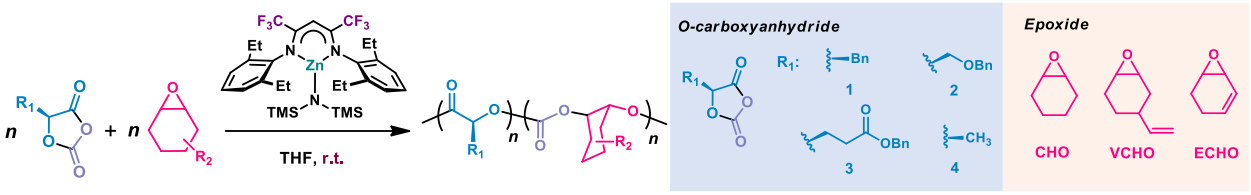

Entry	OCA/epoxide	FR	Time (h)	OCA conv. (%) [b]	Epoxide conv. (%) [c]	M_n (kDa) [d]	MW_{cal} (kDa)	$Đ$ [d]
1	L-**2**/CHO	300/300	4	100	89.5	77.6	91.6	1.01
2	L-**2**/CHO [e]	300/300	4	100	72.5	88.1	84.3	1.03
3 [f]	L-**1**/CHO	300/300	2	100	63.0	60.4	71.3	1.01
4	L-**3**/CHO	300/300	12	100	89.5	92.5	104.2	1.01
5	L-**4**/CHO	300/300	1	100	100	71.3	64.2	1.05
6	L-**1**/VCHO	300/300	12	100	87.0	101.7	88.3	1.01
7	L-**2**/VCHO	300/300	12	100	100	177.6	103.8	1.01
8	L-**2**/VCHO	600/600	12	100	100	265.4	207.7	1.01
9	L-**3**/VCHO	300/300	24	100	100	141.3	116.5	1.02
10	L-**4**/VCHO	300/300	12	100	100	79.2	72.3	1.03
11	L-**2**/ECHO	100/100	12	100	100	20.0	31.8	1.04
12	L-**2**/CHO /VCHO [g]	300/150/150	12	100	100/ 100	90.2	99.9	1.01
13	L-**4**/VCHO + L-**2**/CHO [h]	300/300 + 300/300	12 + 12	100/ 100	100/ 73.5	155.1 (79.2)	157.0 (72.3)	1.09 (1.03)

[a] Abbreviations: OCA, *O*-carboxyanhydride; FR, [OCA]/[**BDIZn-7**] feed ratio; Conv., conversion; M_n, number-average molecular weight; MW_{cal}, molecular weight calculated from FR and monomer conversion; $Đ$, molecular weight distribution; CHO, cyclohexene oxide; VCHO, vinyl cyclohexene oxide; ECHO, 3,4-epoxy-1-cyclohexene; CHC, cyclohexene carbonate. Polymerization conditions: [OCA] = [epoxide] = 2.0 M in THF at room temperature in a glove box. [b] Determined from the intensity of the Fourier transform IR peak at 1805 cm^{-1}, which corresponds to the anhydride group of the OCA. [c] Determined by ^1H NMR spectroscopy. [d] Determined by GPC. [e] THF (10 μL) was used to dissolve **BDIZn-7** (0.53 μmol) for this semibulk polymerization. n(L-**2**) = n(CHO) = 0.159 mmol. [f] The poly(CHC)/cyclic CHC ratio was 0.926/0.074 at the end of copolymerization, as measured by ^1H NMR spectroscopy (see Figure 6.11). [g] CHO and VCHO were mixed together ([CHO] = [VCHO]) with L-**2** for the copolymerization. [h] An L-**2**/CHO mixture was added to the reaction mixture after formation of the first diblock

copolymer was complete, as confirmed by ^{1}H NMR spectroscopy (see section 6.3.7.3). The numbers in parenthesis in the M_n and $Đ$ columns are GPC results for the first diblock, i.e., poly(L-**4**-*b*-VCHC).

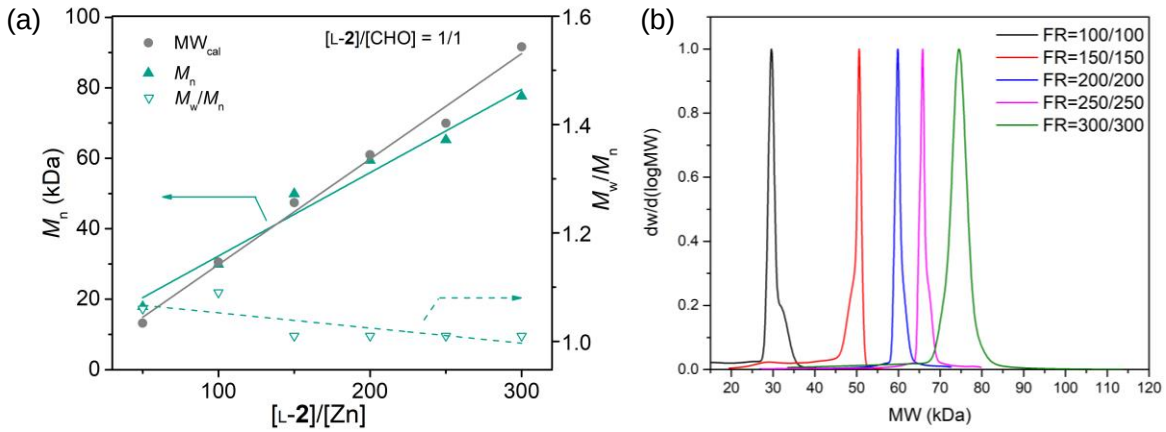

Figure 6.7 Controlled living copolymerization of *O*-carboxyanhydride L-**2** and cyclohexene oxide (CHO). (a) Plots of M_n and MW distribution (M_w/M_n) versus [L-**2**]/[**BDIZn-7**] feed ratio at room temperature. (b) SEC overlay of poly(L-**2**-*b*-CHC) (data in Figure 6.7a). Note that the y axis is the raw data of dw/dlogM, which is the normalized distribution of molecular weights (MWs) at each time slice, and is used for the MW distribution calculation in GPC.

Table 6.6 Measurement of residue metal concentrations in purified polymers by inductively coupled plasma mass spectrometry (ICP-MS) [a]

	[Zn] (ppb)
10% HNO_3 (v/v)	42.8
Poly(L-**2**-*b*-CHC) (**BDIZn-7** mediated copolymerization)	55.0

[a] Abbreviations: ppb: parts per billion, that equals to μg/L. The **BDIZn-7**-mediated copolymerization was performed at an [L-**2**]/[CHO]/[**BDIZn-7**] ratio of 300/300/1 at room temperature, and the obtained polymer was dissolved in DCM and precipitated by MeOH. For ICP-MS studies, the polymer was dissolved in 10% HNO_3 (v/v) at 70-80 ^oC at a concentration of 1 mg/mL for three days in order to completely degrade the polymer. The obtained polymer solution was then analyzed by ICP-MS.

The reactions of L-**3** and L-**4** with CHO gave M_n that were all close to our expected values (**Table 6.5**, entries 4-5). The $Đ$ values of all the obtained polymers were less than 1.1 (GPC traces are shown in **Figures 6.9-6.10**), suggesting that side reactions did not occur.[38] Notably, a cyclic carbonate of CHO formed in an overnight reaction of L-**1** with CHO (see the ^{1}H NMR kinetic studies in **Figure 6.11**), but this compound was not detected in reactions involving other OCA/CHO combinations (see the NMR spectra in **Figures 6.9–6.10**). In addition, we explored the copolymerization of OCAs L-**1**-L-**4** with two other epoxides: vinyl cyclohexene oxide (VCHO) and 3,4-epoxy-1-cyclohexene (ECHO, **Table 6.5**, entries 6–11). Both copolymerizations were achieved with high monomer conversions and gave products with low $Đ$ values (<1.1), and ^{1}H NMR spectroscopy showed no evidence of ether linkages or cyclic carbonates (**Figures 6.12–6.16**). Notably, copolymerization with VCHO allowed for the preparation of a functionalized high-MW copolymer with a M_n of 265.4 kDa and a $Đ$ of 1.01 ([L-**2**]/[VCHO]/[**BDIZn-7**] = 600/600/1; **Table 6.5**, entry 8). The versatility of **BDIZn-7** was also apparent in the L-**2**/CHO/VCHO terpolymerization, which proceeded with high conversion of all the monomers (entry 12) without undesired polyether formation (**Figure 6.17**). Nevertheless, we note that **BDIZn-7** displayed lower reactivity toward alkylene oxides (e.g. propylene oxide; epoxide conversion < 10%) compared to CHO derivatives in both ROCOP of epoxide/CO_2 and the copolymerization of OCA/epoxide, behavior that is similar to that of many Zn complexes in the epoxide/CO_2 ROCOP.[39] Finally, we determined whether multiblock copolymers could be prepared in one pot by sequential addition of the OCA/epoxide monomer combinations, e.g., L-**4**/VCHO followed by L-**2**/CHO (entry 13). In this way, tetrablock copolymer poly(L-**4**-*b*-VCHC-*b*-L-**2**-*b*-CHC;

VCHC = vinyl cyclohexene carbonate) could be readily synthesized with quantitative monomer conversion and remarkable control of M_n and $Đ$ (GPC traces are shown in **Figure 6.18**), indicating the living nature of our copolymerization with an active chain-end.

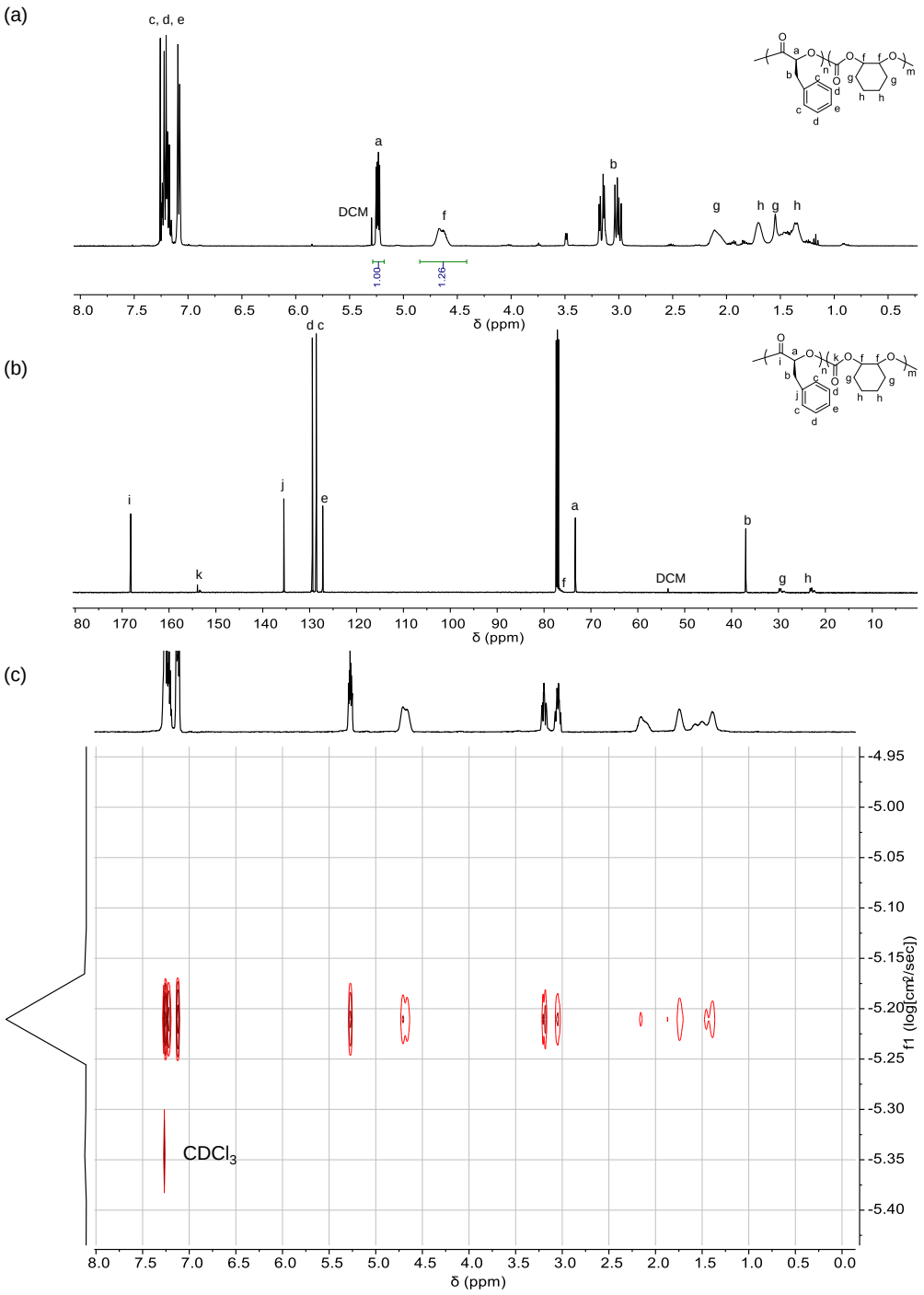

(Data continue on the next page)

(d)

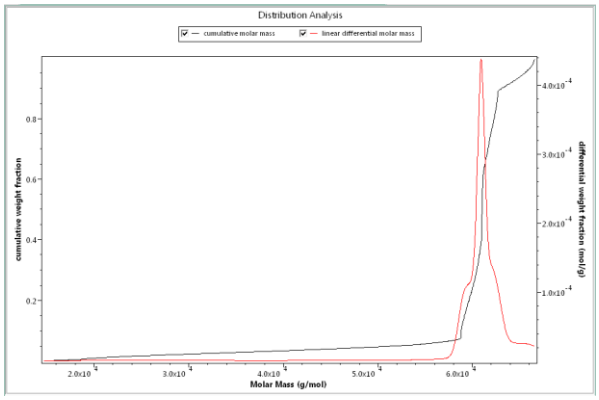

(e)

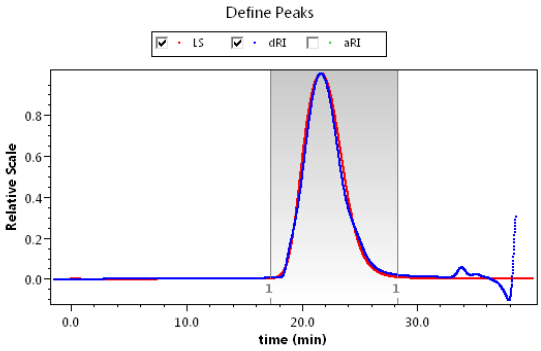

Results

Peak Results

	Peak 1
Masses	
Injected Mass (µg)	0.00
Calculated Mass (µg)	2817.08
Mass Recovery (%)	n/a
Mass Fraction (%)	100.0
Molar mass moments (g/mol)	
Mn	6.038×10^4 (±0.204%)
Mw	6.111×10^4 (±0.163%)
Mz	6.183×10^4 (±0.355%)
Polydispersity	
Mw/Mn	1.012 (±0.261%)
Mz/Mn	1.024 (±0.410%)

Figure 6.8 (a) ^{1}H, (b) ^{13}C, and (c) DOSY NMR spectra of poly(L-**1**-*b*-CHC). (d, e) The GPC raw data of poly(L-**1**-*b*-CHC) ([L-**1**]/[CHO]/[**BDIZn-7**] = 300/300/1; Table 6.5, entry 3), including dw/dlogMW versus MWs plots (d), which is used for the MW distribution calculation in GPC, and signals in the light scattering (LS) and refractive index (dRI) detectors versus time (e). The peak results in (e) clearly indicate the unimodal narrow MW distribution of the obtained polymers.

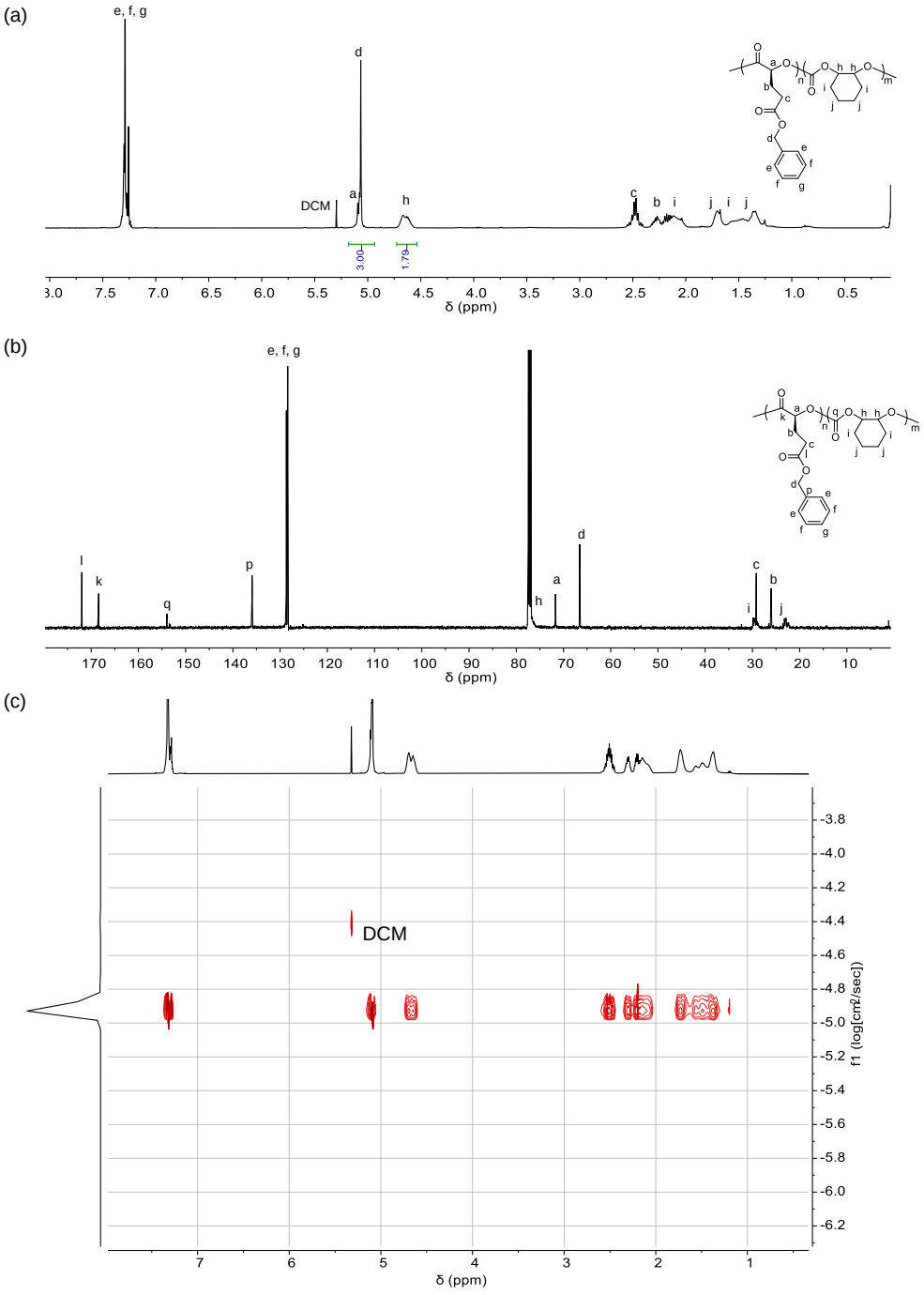

(Data continue on the next page)

(d)

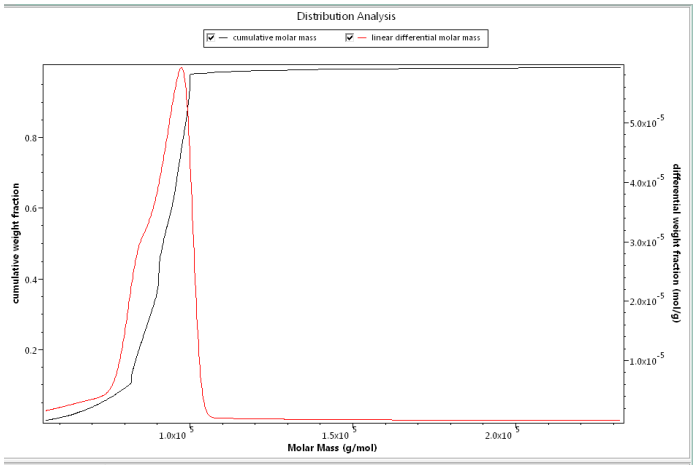

(e)

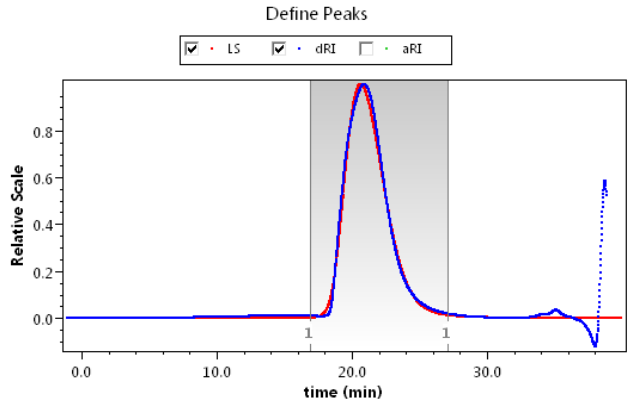

Results

Peak Results

	Peak 1
Masses	
Injected Mass (µg)	0.00
Calculated Mass (µg)	2256.84
Mass Recovery (%)	n/a
Mass Fraction (%)	100.0
Molar mass moments (g/mol)	
Mn	9.247×10^4 (±0.309%)
Mw	9.366×10^4 (±0.079%)
Mz	9.591×10^4 (±0.187%)
Polydispersity	
Mw/Mn	1.013 (±0.318%)
Mz/Mn	1.037 (±0.361%)

Figure 6.9 (a) ^{1}H, (b) ^{13}C, and (c) DOSY NMR spectra of poly(L-**3**-*b*-CHC). (d, e) The GPC raw data of poly(L-**3**-*b*-CHC) ([L-**3**]/[CHO]/[**BD1Zn-7**] = 300/300/1; Table 6.5, entry 4), including dw/dlogMW versus MWs plots (d), which is used for the MW distribution calculation in SEC, and signals in the light scattering (LS) and refractive index (dRI) detectors versus time (e). The peak results in (e) clearly indicate the unimodal narrow MW distribution of the obtained polymers.

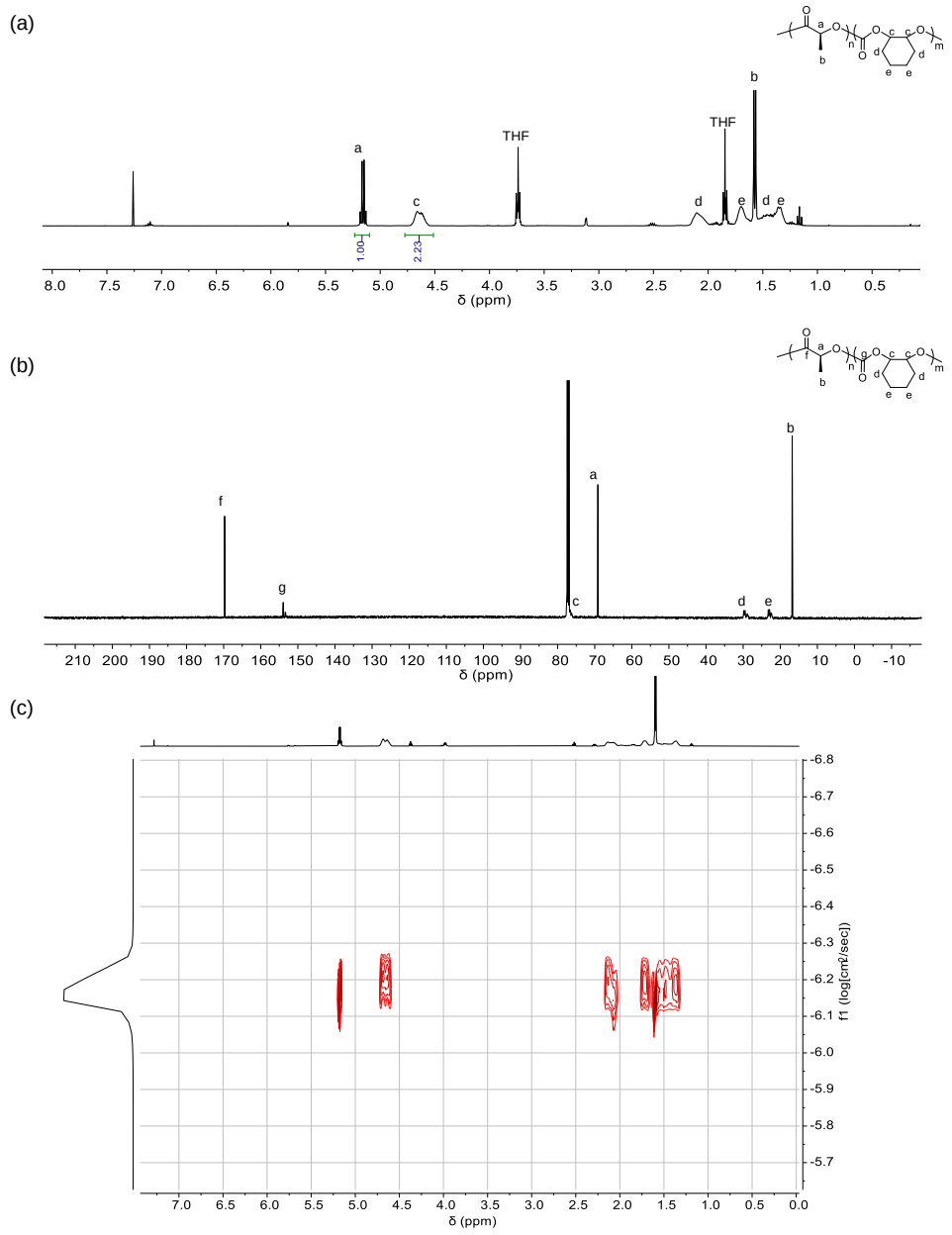

(Data continue on the next page)

(d)

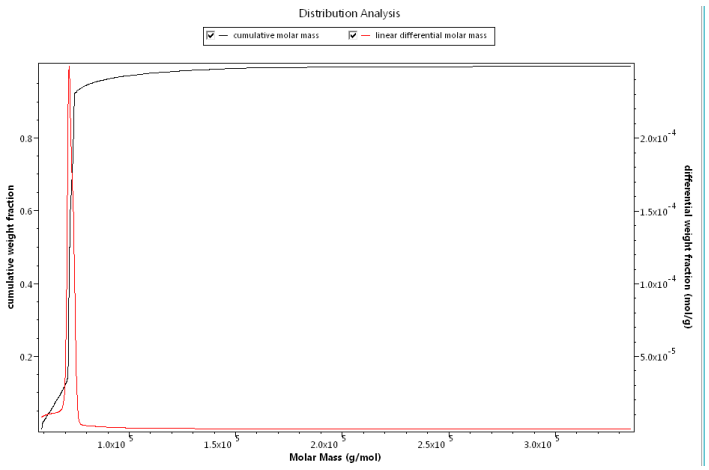

(e)

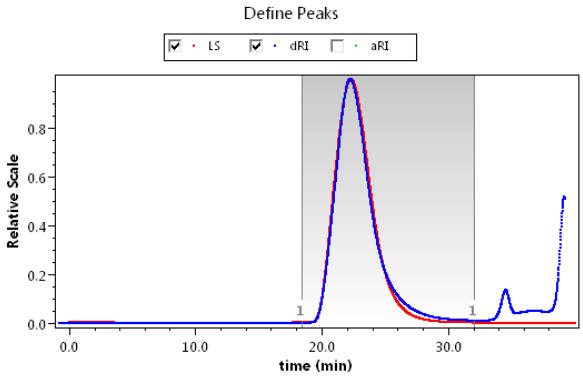

Results

Peak Results

	Peak 1
Masses	
Injected Mass (µg)	0.00
Calculated Mass (µg)	5378.18
Mass Recovery (%)	n/a
Mass Fraction (%)	100.0
Molar mass moments (g/mol)	
Mn	7.134×10^4 (±0.799%)
Mw	7.509×10^4 (±0.138%)
Mz	7.676×10^4 (±0.350%)
Polydispersity	
Mw/Mn	1.053 (±0.811%)
Mz/Mn	1.076 (±0.873%)

Figure 6.10 (a) ^{1}H, (b) ^{13}C, and (c) DOSY NMR spectra of poly(L-**4**-*b*-CHC). (d, e) The GPC raw data of poly(L-**4**-*b*-CHC) ([L-**4**]/[CHO]/[**BDIZn-7**] = 300/300/1; Table 6.5, entry 5), including dw/dlogMW versus MWs plots (d), which is used for the MW distribution calculation in SEC, and signals in the light scattering (LS) and refractive index (dRI) detectors versus time (e). The peak results in (e) clearly indicate the unimodal narrow MW distribution of the obtained polymers.

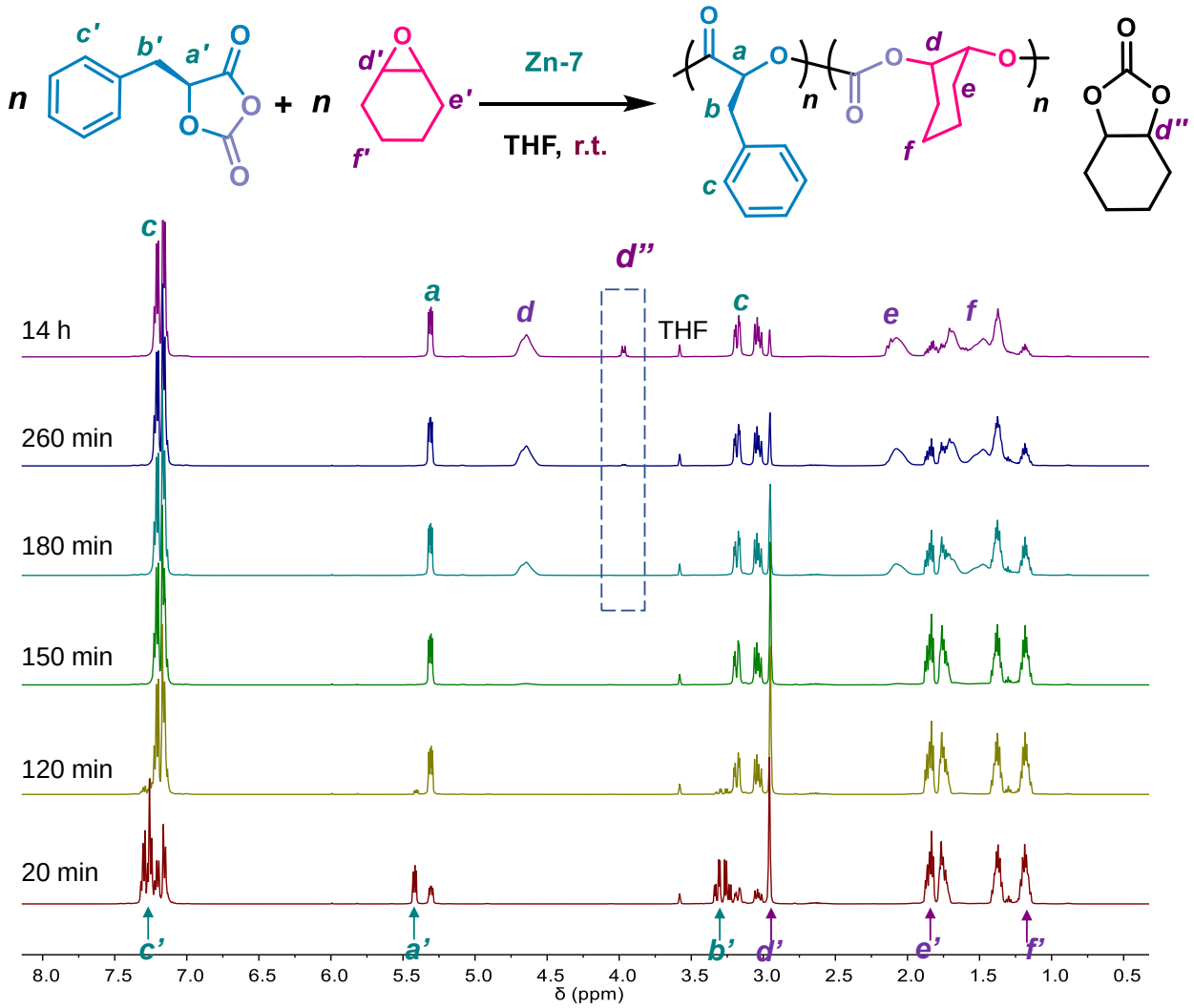

Figure 6.11 ^{1}H NMR spectra overlay of in-situ monitored poly(L-**1**-*b*-CHC) copolymerization process (Table 6.5, entry 3). The formation of the second PCHC block started around 150 min. Note that at 240 min, the cyclohexene carbonate as the side product was found in the NMR spectra, and the peaks corresponding to such cyclic carbonate (d') increased overnight, which was not seen in other copolymerization processes.

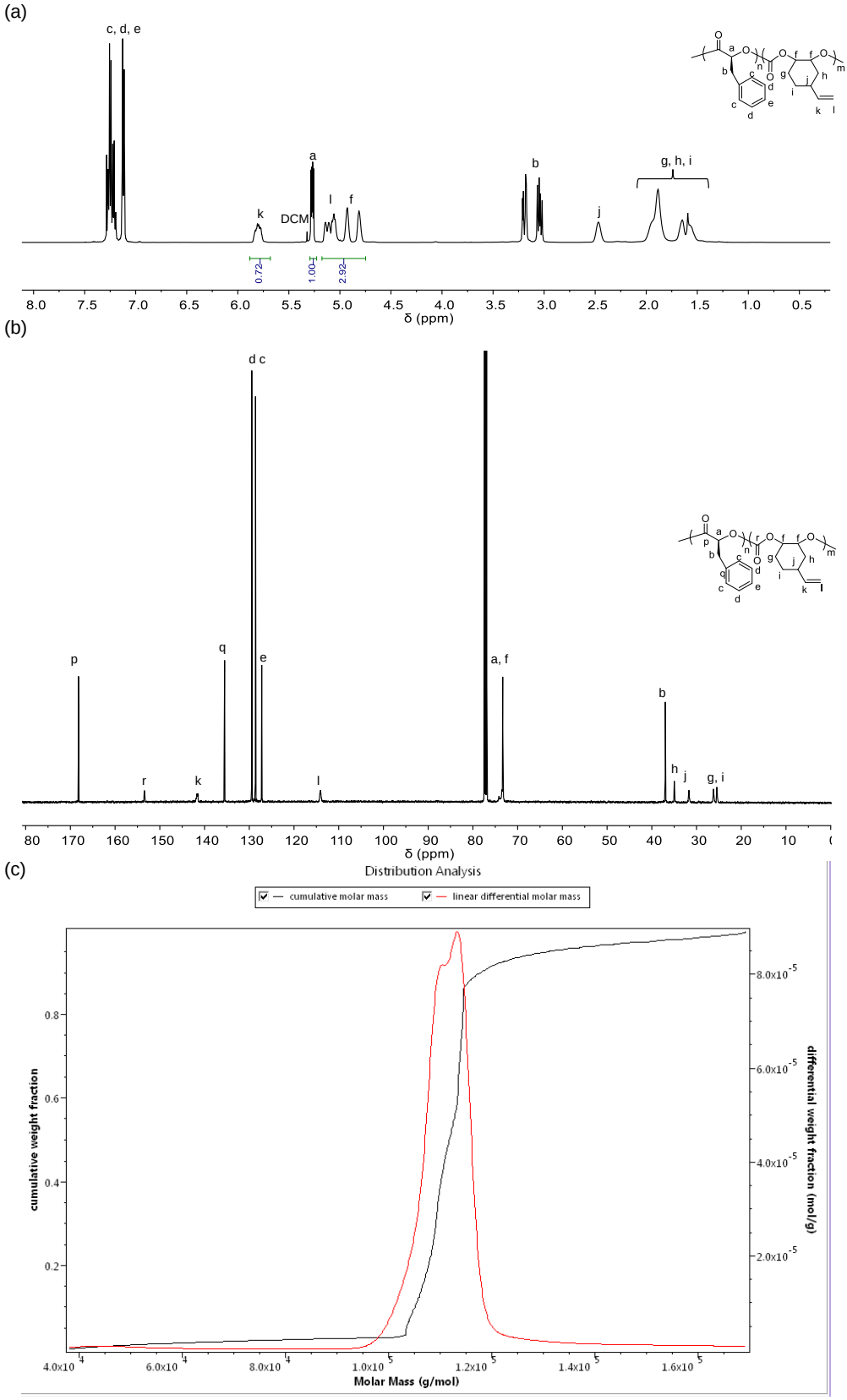

(Data continue on the next page)

(d)

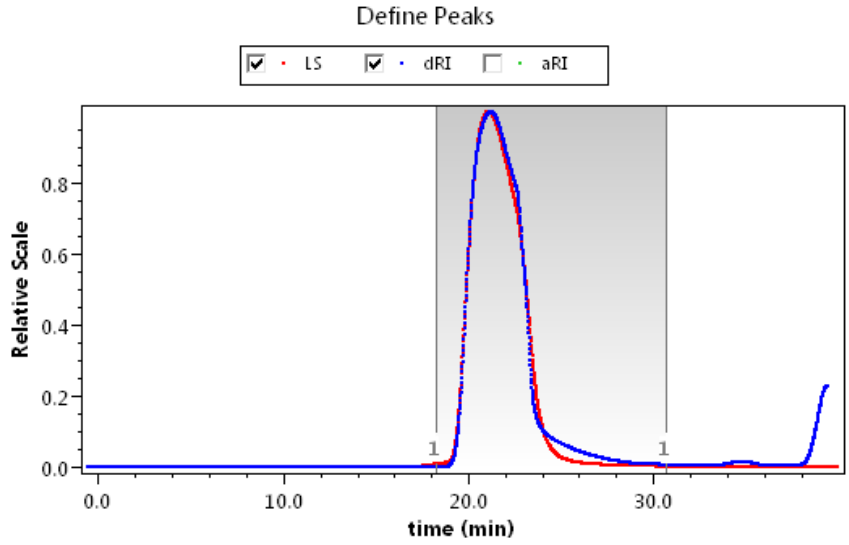

Results

Peak Results

	Peak 1
Masses	
Injected Mass (µg)	0.00
Calculated Mass (µg)	2279.09
Mass Recovery (%)	n/a
Mass Fraction (%)	100.0
Molar mass moments (g/mol)	
Mn	1.017×10^5 (±0.058%)
Mw	1.099×10^5 (±0.029%)
Mz	1.242×10^5 (±0.171%)
Polydispersity	
Mw/Mn	1.081 (±0.065%)
Mz/Mn	1.221 (±0.181%)

Figure 6.12 (a) ^{1}H and (b) ^{13}C NMR spectra of poly(L-**1**-*b*-VCHC). (c, d) The GPC raw data of poly(L-**1**-*b*-VCHC) ([L-**1**]/[VCHO]/[**BDIZn-7**] = 300/300/1; Table 6.5, entry 6), including dw/dlogMW versus MWs plots (c), which is used for the MW distribution calculation in GPC, and signals in the light scattering (LS) and refractive index (dRI) detectors versus time (d). The peak results in (d) clearly indicate the unimodal narrow MW distribution of the obtained polymers.

(a)

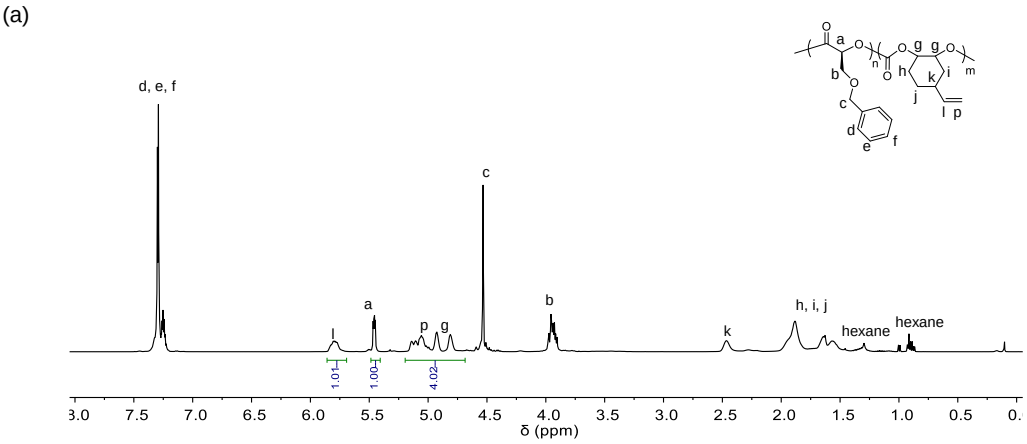

(b)

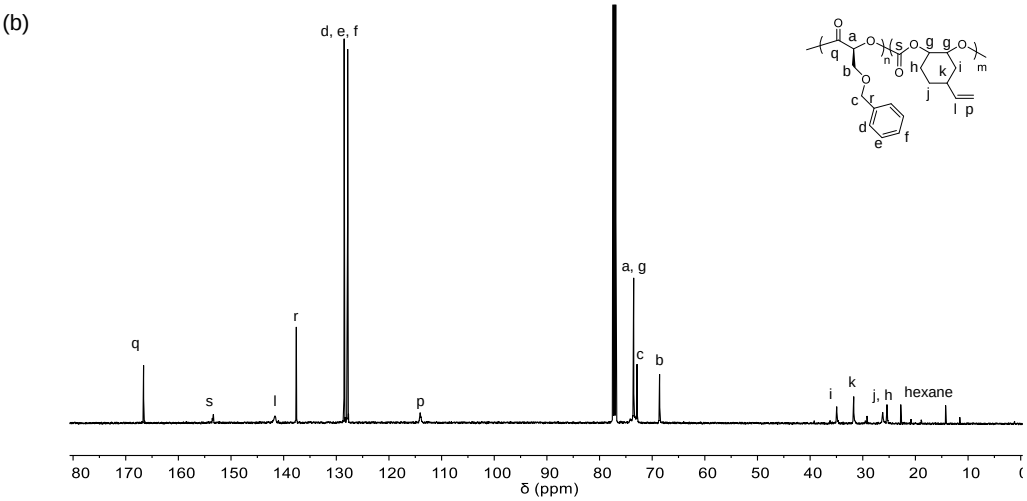

(c)

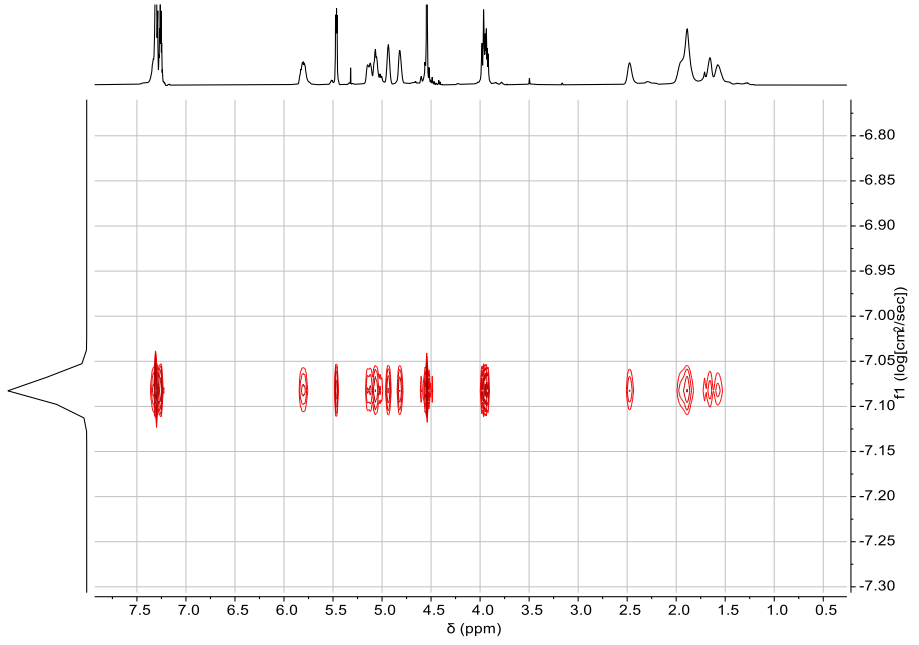

(Data continue on the next page)

(d)

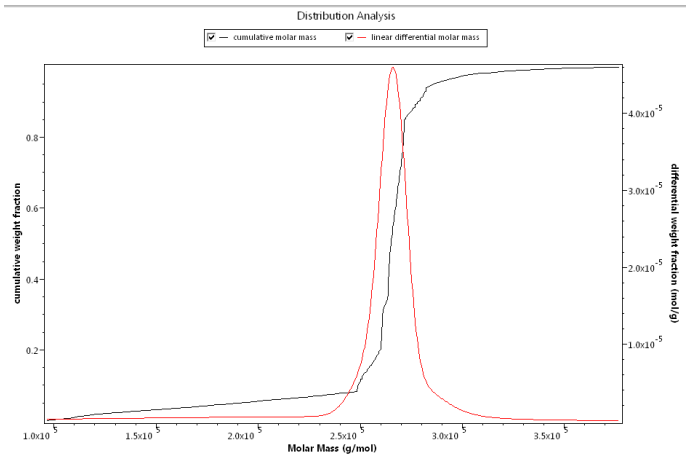

(e)

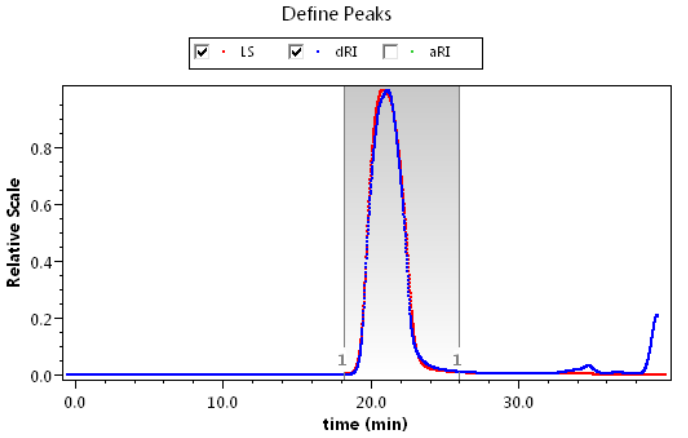

Results

Peak Results

	Peak 1
Masses	
Injected Mass (µg)	0.00
Calculated Mass (µg)	3287.67
Mass Recovery (%)	n/a
Mass Fraction (%)	100.0
Molar mass moments (g/mol)	
Mn	2.654×10^5 (±0.020%)
Mw	2.681×10^5 (±0.020%)
Mz	2.779×10^5 (±0.084%)
Polydispersity	
Mw/Mn	1.010 (±0.028%)
Mz/Mn	1.047 (±0.087%)

Figure 6.13 (a) ^{1}H, (b) ^{13}C, and (c) DOSY NMR spectra of poly(L-**2**-*b*-VCHC). (d, e) The GPC raw data of poly(L-**2**-*b*-VCHC) ([L-**2**]/[VCHO]/[**BDIZn-7**] = 600/600/1; Table 6.5, entry 8), including dw/dlogMW versus MWs plots (d), which is used for the MW distribution calculation in GPC, and signals in the light scattering (LS) and refractive index (dRI) detectors versus time (e). The peak results in (e) clearly indicate the unimodal narrow MW distribution of the obtained polymers.

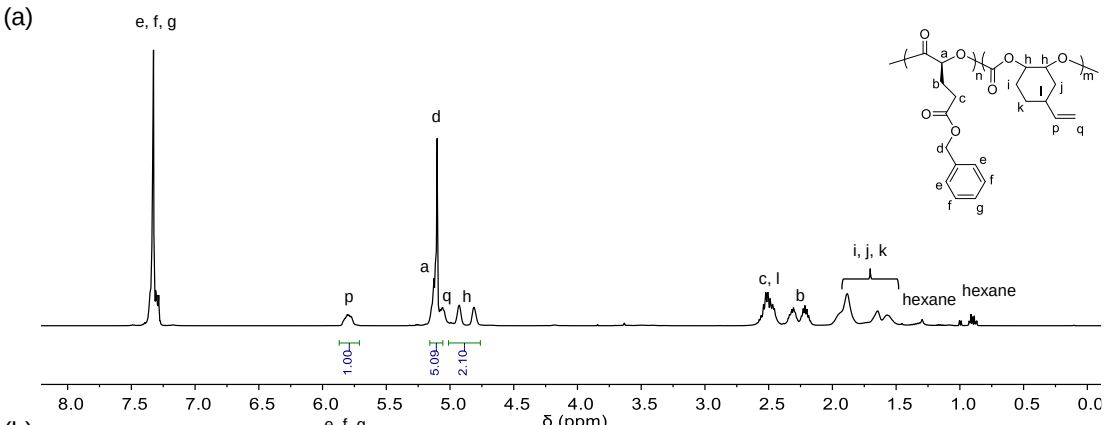

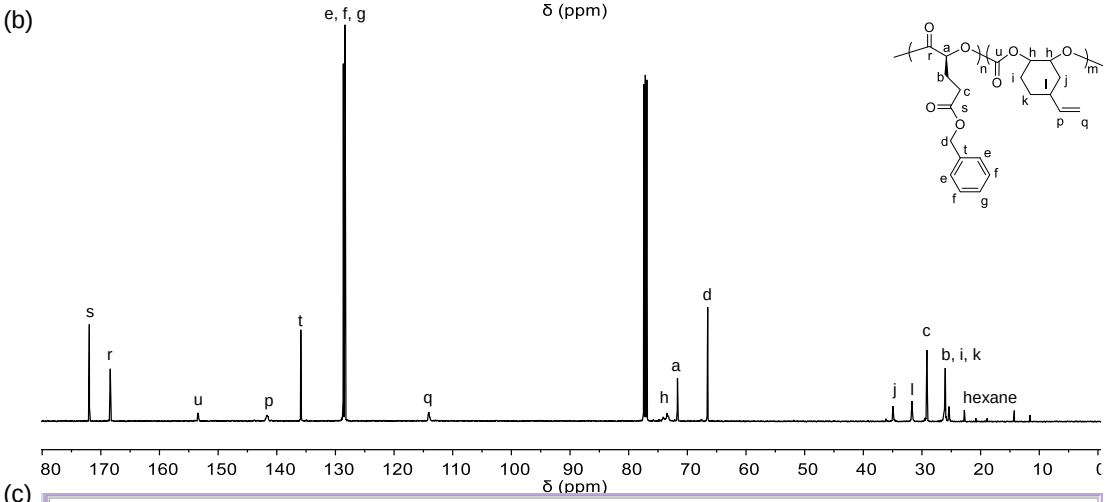

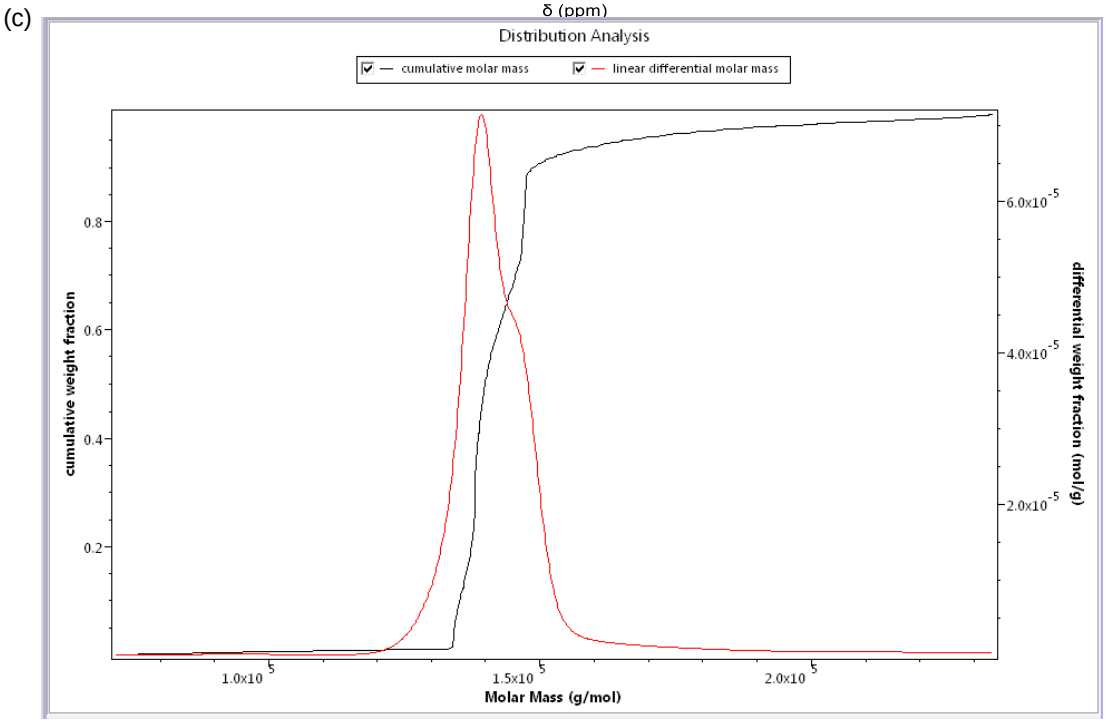

(Data continue on the next page)

(d)

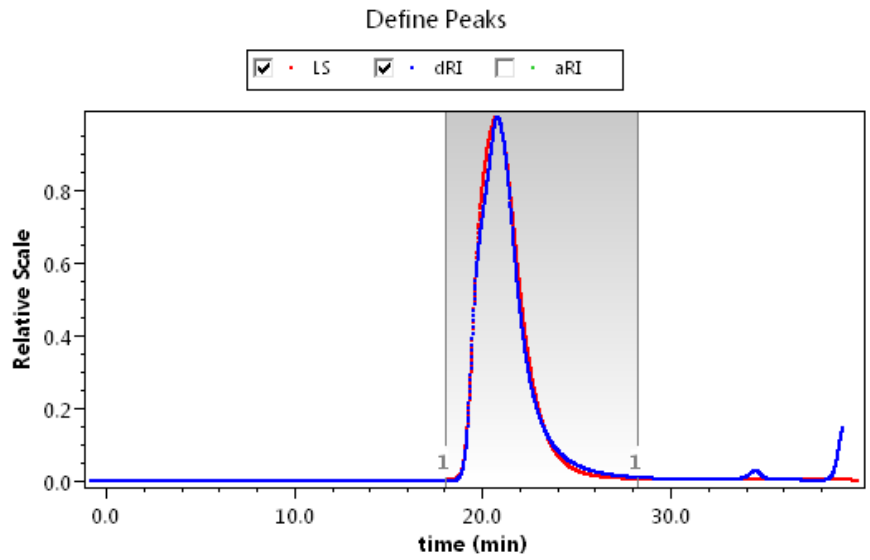

Results

Peak Results

	Peak 1
Masses	
Injected Mass (µg)	0.00
Calculated Mass (µg)	2500.50
Mass Recovery (%)	n/a
Mass Fraction (%)	100.0
Molar mass moments (g/mol)	
Mn	1.413×10^5 (±0.083%)
Mw	1.439×10^5 (±0.038%)
Mz	1.472×10^5 (±0.088%)
Polydispersity	
Mw/Mn	1.018 (±0.091%)
Mz/Mn	1.041 (±0.121%)

Figure 6.14 (a) ^{1}H and (b) ^{13}C NMR spectra of poly(L-**3**-*b*-VCHC). (c, d) The GPC raw data of poly(L-**3**-*b*-VCHC) ([L-**3**]/[VCHO]/[**BDIZn-7**] = 300/300/1; Table 6.5, entry 9), including dw/dlogMW versus MWs plots (c), which is used for the MW distribution calculation in GPC, and signals in the light scattering (LS) and refractive index (dRI) detectors versus time (d). The peak results in (d) clearly indicate the unimodal narrow MW distribution of the obtained polymers.

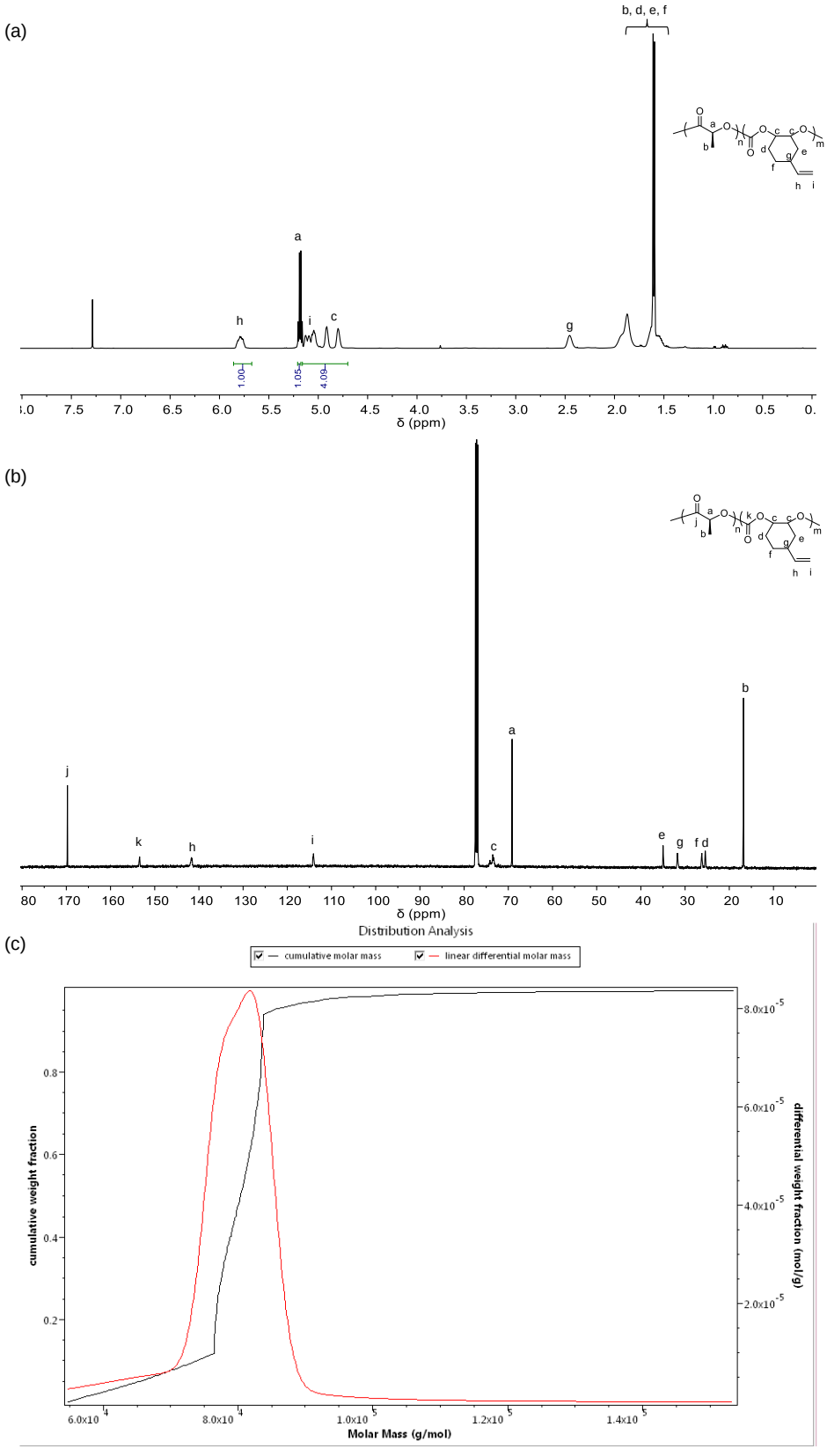

(Data continue on the next page)

(d)

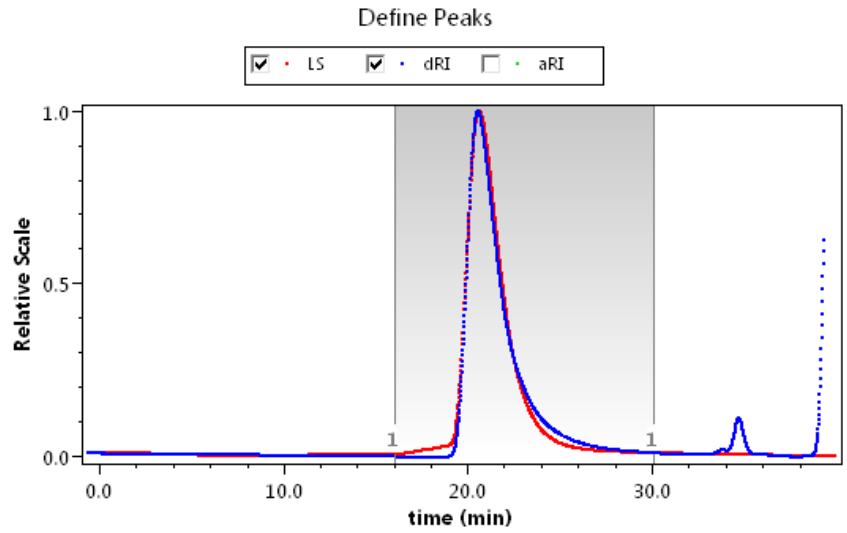

Results

Peak Results

	Peak 1
Masses	
Injected Mass (µg)	0.00
Calculated Mass (µg)	241.77
Mass Recovery (%)	n/a
Mass Fraction (%)	100.0
Molar mass moments (g/mol)	
Mn	7.915×10^4 (±0.595%)
Mw	8.185×10^4 (±0.419%)
Mz	8.900×10^4 (±1.510%)
Polydispersity	
Mw/Mn	1.034 (±0.728%)
Mz/Mn	1.124 (±1.623%)

Figure 6.15 (a) ^{1}H and (b) ^{13}C NMR spectra of poly(L-**4**-*b*-VCHC). (c, d) The GPC raw data of poly(L-**4**-*b*-VCHC) ([L-**4**]/[VCHO]/[**BDIZn-7**] = 300/300/1; Table 6.5, entry 10), including dw/dlogMW versus MWs plots (c), which is used for the MW distribution calculation in GPC, and signals in the light scattering (LS) and refractive index (dRI) detectors versus time (d). The peak results in (d) clearly indicate the unimodal narrow MW distribution of the obtained polymers.

(a)

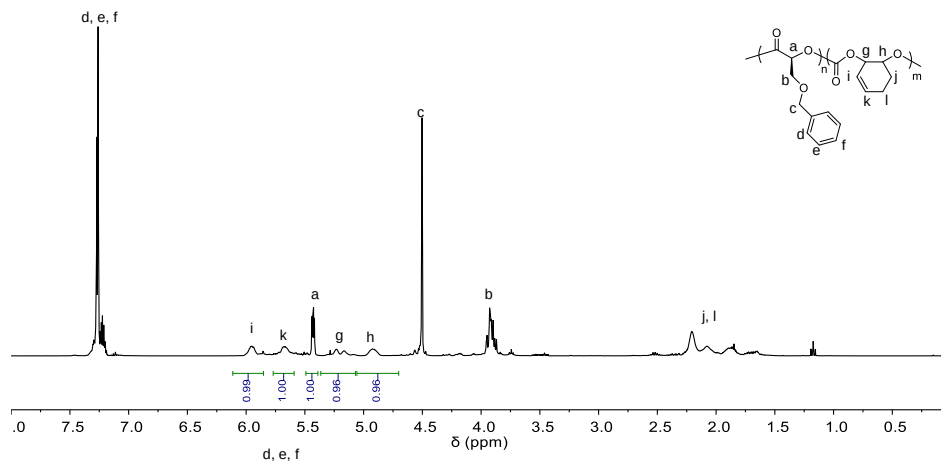

(b)

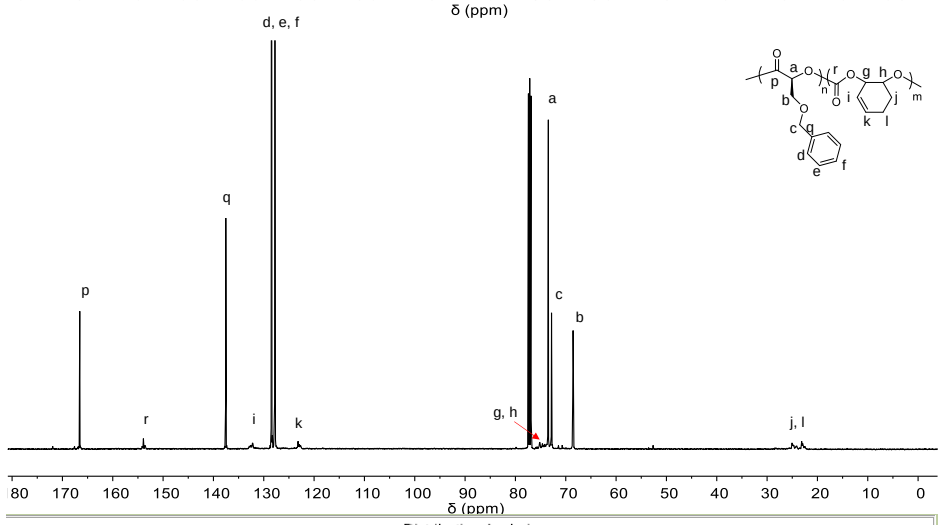

(c)

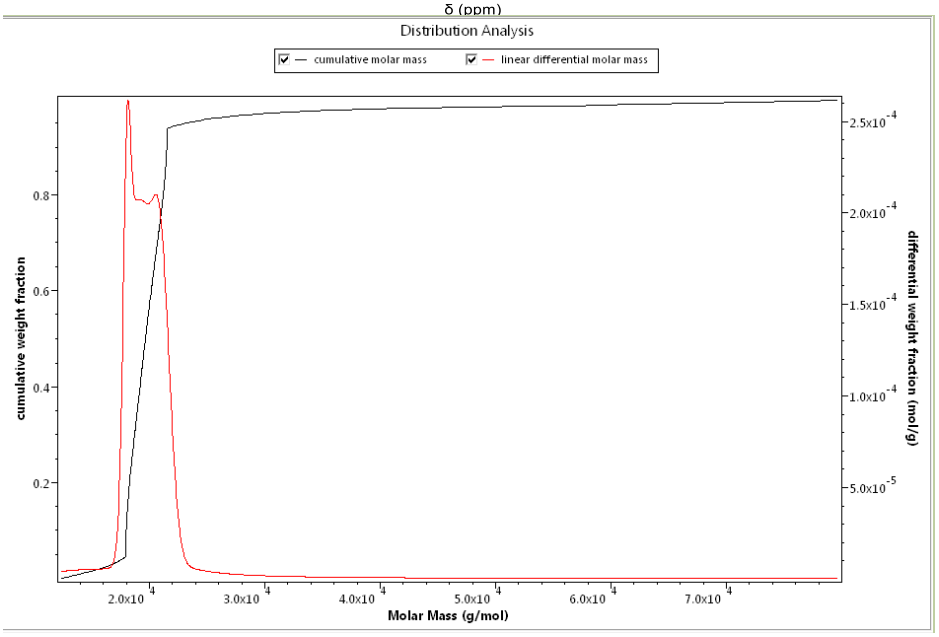

(Data continue on the next page)

(d)

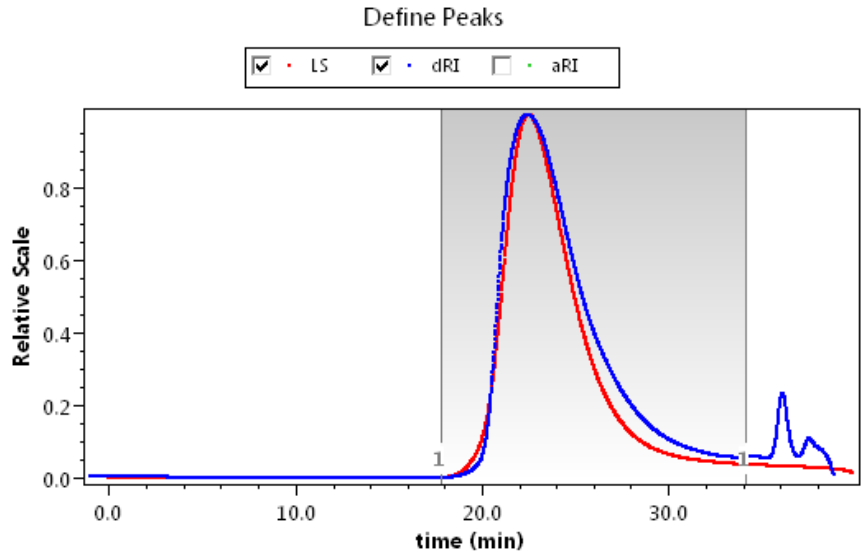

Results

Peak Results

	Peak 1
Masses	
Injected Mass (µg)	0.00
Calculated Mass (µg)	328.70
Mass Recovery (%)	n/a
Mass Fraction (%)	100.0
Molar mass moments (g/mol)	
Mn	2.012×10^4 (±0.678%)
Mw	2.076×10^4 (±0.484%)
Mz	2.153×10^4 (±1.030%)
Polydispersity	
Mw/Mn	1.032 (±0.833%)
Mz/Mn	1.070 (±1.233%)

Figure 6.16 (a) ^{1}H and (b) ^{13}C NMR spectra of poly(L-**2**-*b*-ECHC). (c, d) The GPC raw data of poly(L-**2**-*b*-ECHC) ([L-**2**]/[ECHO]/[**BDIZn-7**] = 100/100/1; Table 6.5, entry 11), including dw/dlogMW versus MWs plots (c), which is used for the MW distribution calculation in GPC, and signals in the light scattering (LS) and refractive index (dRI) detectors versus time (d). The peak results in (d) clearly indicate the unimodal narrow MW distribution of the obtained polymers.

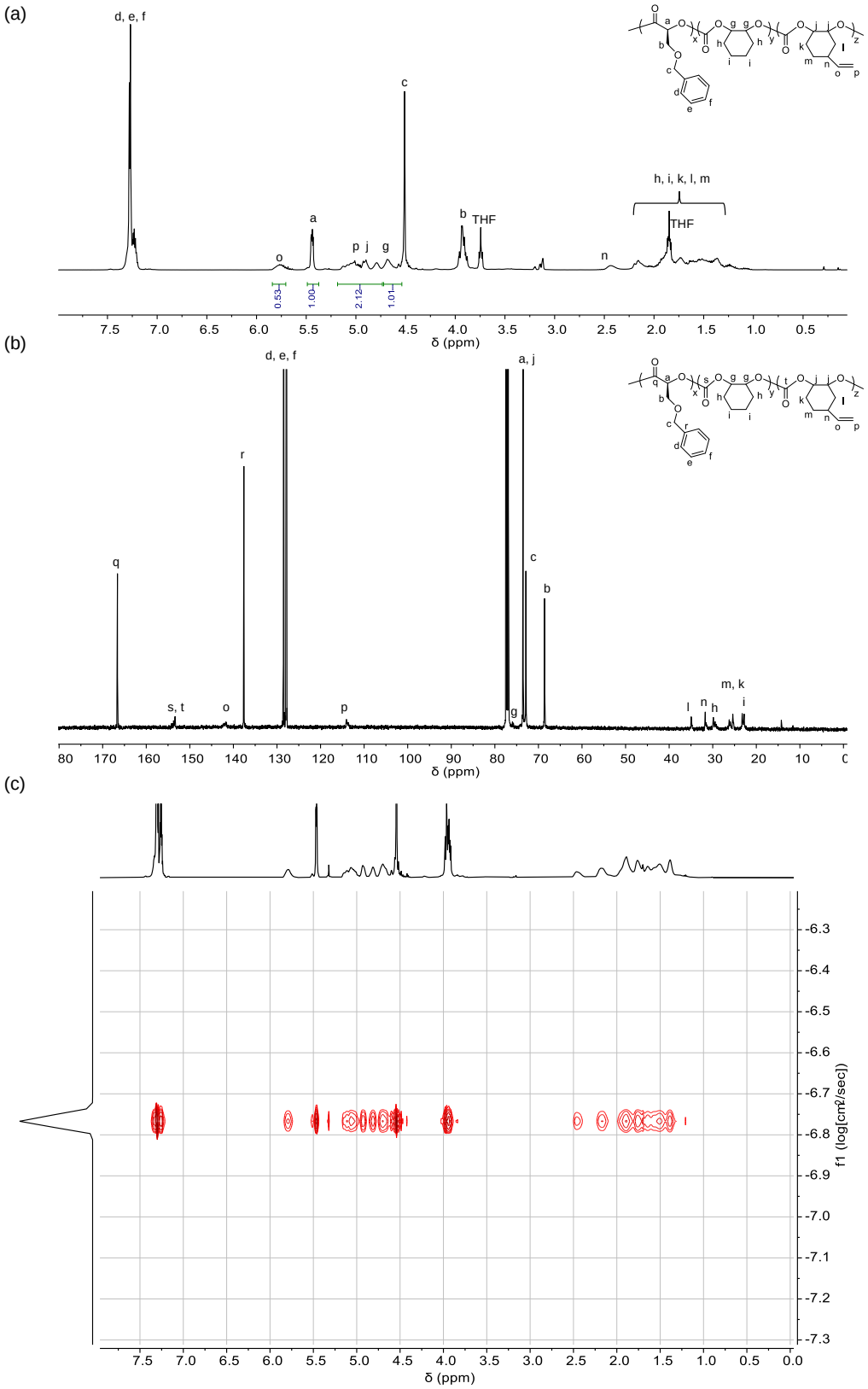
(a)
d, e, f
c
a
o
p j g
b
THF
h, i, k, l, m
THF
n
0.53
1.00
2.12
1.01
δ (ppm)
(b)
d, e, f
a, j
r
q
c
b
s, t
o
p
g
l
n
h
m, k
i
δ (ppm)
(c)
f1 (log[cm²/sec])
δ (ppm)

(Data continue on the next page)

(d)

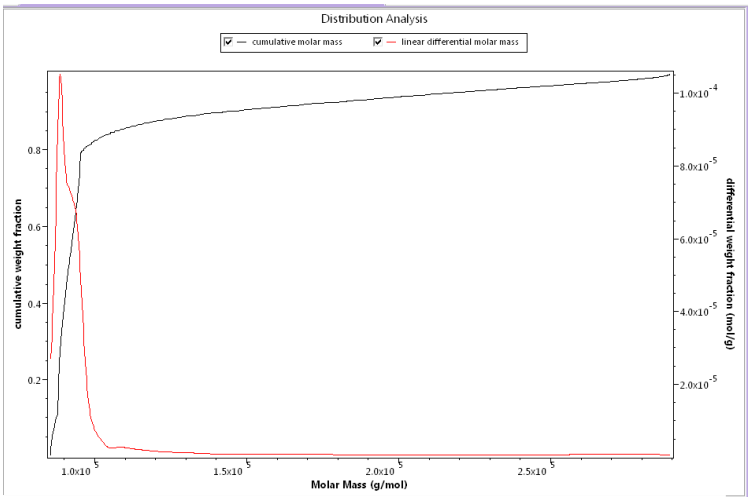

(e)

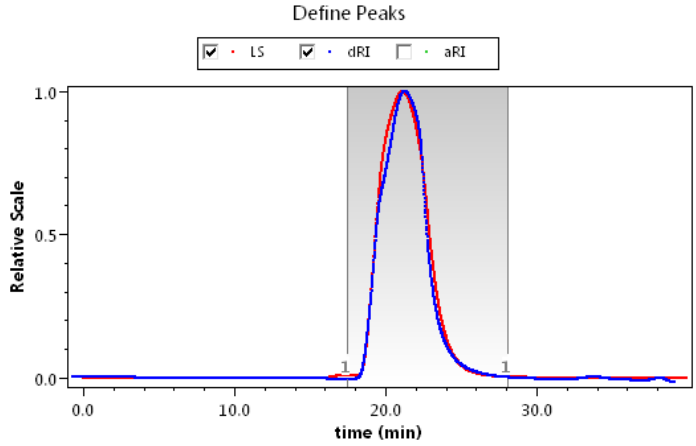

Results

Peak Results

	Peak 1
Masses	
Injected Mass (µg)	0.00
Calculated Mass (µg)	4789.96
Mass Recovery (%)	n/a
Mass Fraction (%)	100.0
Molar mass moments (g/mol)	
Mn	9.022×10^4 (±0.089%)
Mw	9.105×10^4 (±0.092%)
Mz	9.863×10^4 (±0.940%)
Polydispersity	
Mw/Mn	1.009 (±0.128%)
Mz/Mn	1.093 (±0.944%)

Figure 6.17 (a) ^{1}H, (b) ^{13}C, and (c) DOSY NMR spectra of poly(L-**2**-*b*-CHC-*co*-VCHC). (d, e) The GPC raw data of poly(L-**2**-*b*-CHC-*co*-VCHC) ([L-**2**]/[VCHO]/[CHO]/[**BDIZn-7**] = 300/150/150/1; Table 6.5, entry 12), including dw/dlogMW versus MWs plots (d), which is used for the MW distribution calculation in GPC, and signals in the light scattering (LS) and refractive index (dRI) detectors versus time (e). The peak results in (e) clearly indicate the unimodal narrow MW distribution of the obtained polymers.

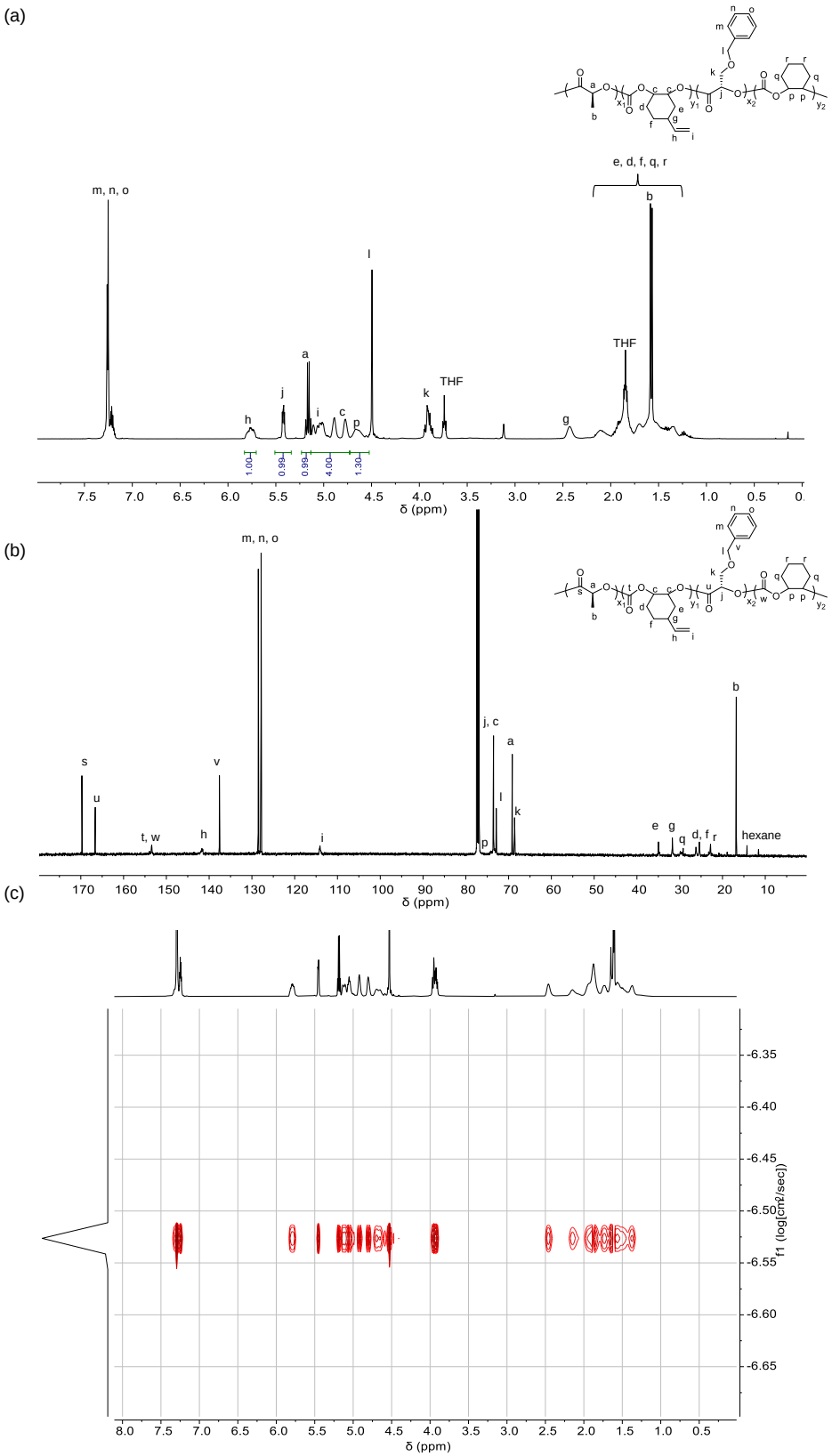

(Data continue on the next page)

(d)

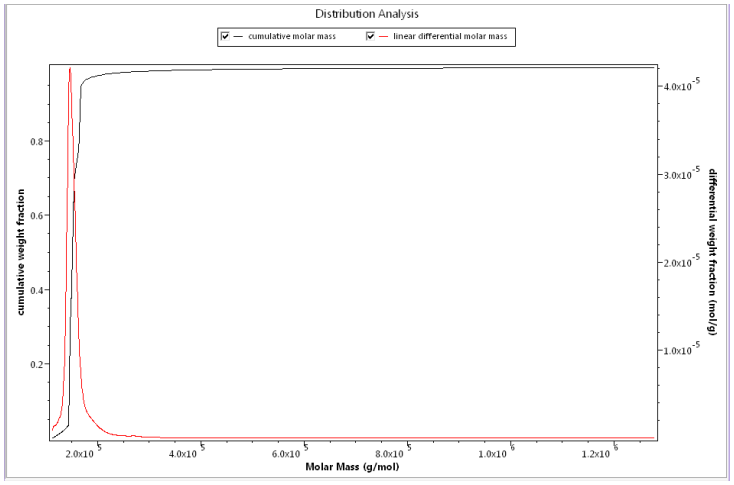

(e)

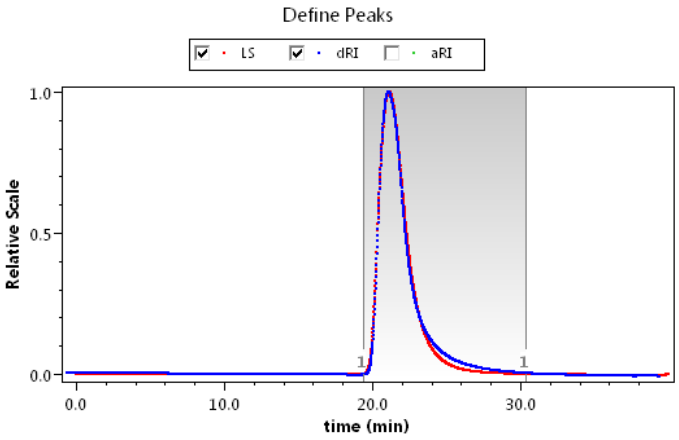

Results

Peak Results

	Peak 1
Masses	
Injected Mass (µg)	0.00
Calculated Mass (µg)	962.04
Mass Recovery (%)	n/a
Mass Fraction (%)	100.0
Molar mass moments (g/mol)	
Mn	1.551×10^5 (±0.623%)
Mw	1.690×10^5 (±0.024%)
Mz	1.747×10^5 (±0.046%)
Polydispersity	
Mw/Mn	1.089 (±0.623%)
Mz/Mn	1.126 (±0.624%)

Figure 6.18 (a) ^{1}H, (b) ^{13}C, and (c) DOSY NMR spectra of poly(L-**4**-*b*-VCHC-*b*-L-**2**-*b*-CHC). (d, e) The GPC raw data of poly(L-**4**-*b*-VCHC-*b*-L-**2**-*b*-CHC) ([L-**4**]/[VCHO]/[**BDIZn-7**] = 300/300/1 were added first; after the reaction finished, [L-**4**]/[CHC] = 300/300 were added; Table 6.5, entry 13), including dw/dlogMW versus MWs plots (d), which is used for the MW distribution calculation in GPC, and signals in the light scattering (LS) and refractive index (dRI) detectors versus time (e). The peak results in (e) clearly indicate the unimodal narrow MW distribution of the obtained polymers.

6.2.5 Sequential degradation of functionalized poly(ester-*b*-carbonates)

In addition to polymerization, we also explored the degradation method to close their life cycles. It's well known that polyesters and polycarbonates can be fully degraded to their respective monomers or monomer derivatives.[40-45] To avoid the difficulty in separating the monomers from each other after poly(ester-*b*-carbonate) degradation, we investigated a sequential degradation strategy for quantitatively recycling the monomers (**Figure 6.19**). First, poly(L-**2**-*b*-CHC) was treated with $Zn[N(TMS)_2]_2$ (10 wt%) in MeOH at 50 °C for 12 h[40] to completely degrade the poly(L-**2**) block into the corresponding methyl esters, as indicated by ^{1}H NMR spectroscopy (**Figure 6.20**). Under these conditions, the poly(CHC) block was insoluble in the reaction mixture and retained its original MW and narrow *Đ* (**Figure 6.19 and 6.20g**). After the insoluble Zn-alkoxides and polycarbonates were removed from the reaction mixture by centrifugation, dichloromethane was added, the insoluble material was filtered off, and the polycarbonates in the filtrate was treated with 1,5,7-triazabicyclo[4.4.0]dec-5-ene (TBD, 4 mol%) at 110 °C in toluene for 12 h; this procedure quantitatively yielded the cyclic carbonate monomer, as determined by ^{1}H NMR spectroscopy (**Figure 6.20**). Note that the degradation of the poly(VCHC) block of poly(L-**2**-*b*-VCHC) required a larger amount of 1,5,7-triazabicyclo[4.4.0]dec-5-ene (20 wt%) to fully degrade the polymers into the epoxide monomer (VCHO, **Figure 6.21**).

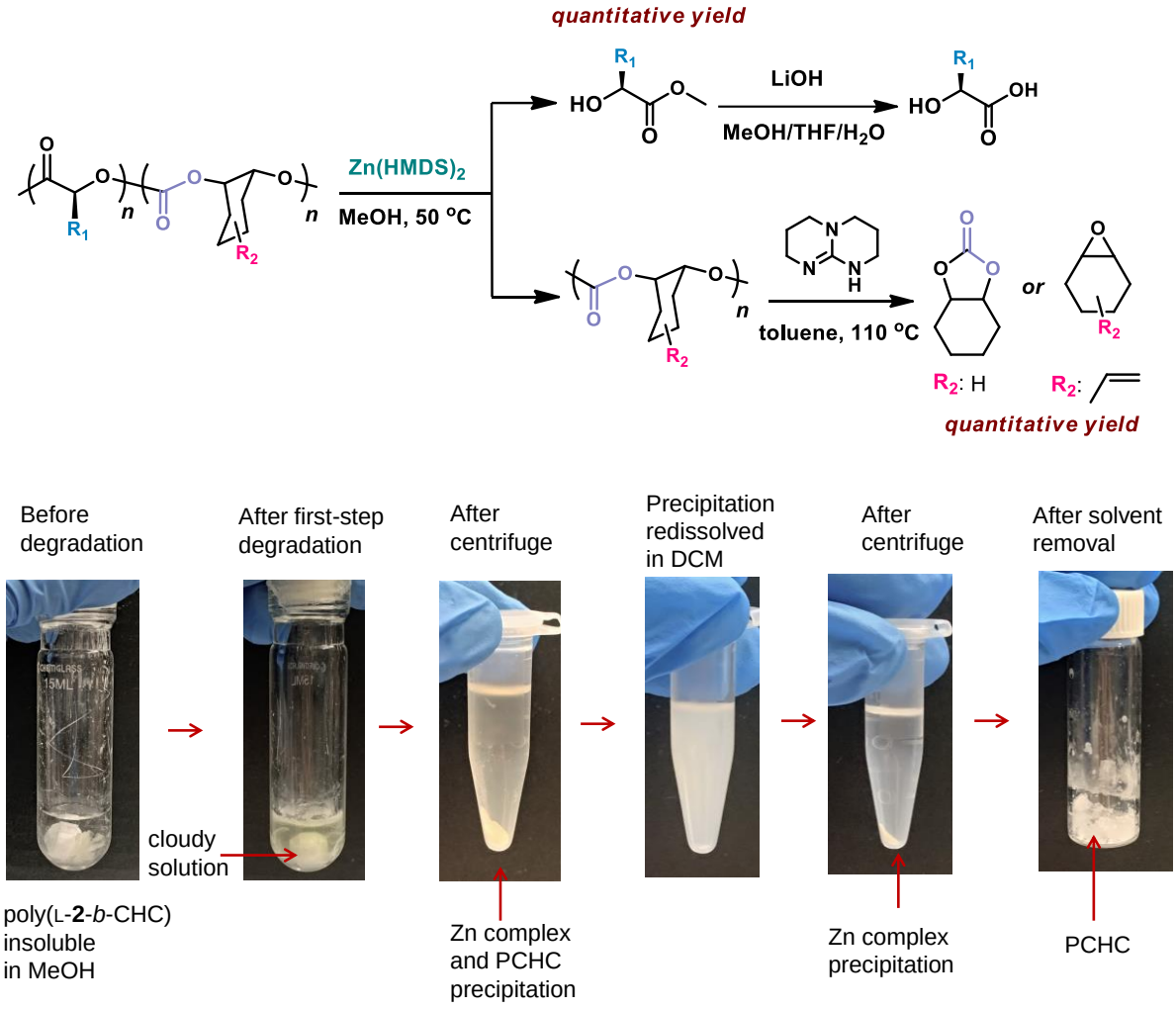

Figure 6.19 Efficient sequential degradation of poly(ester-*b*-carbonates) to α-hydroxy acids (the precursors of *O*-carboxyanhydrides) and cyclic carbonate or epoxide monomers. The degradation process of poly(ester-*b*-carbonates) by convenient centrifugation / dissolving steps as shown in the figure that separates the degraded polyester from the complete polycarbonate (GPC traces of the copolymer and PCHC after first step degradation were shown in Figure 6.20g).

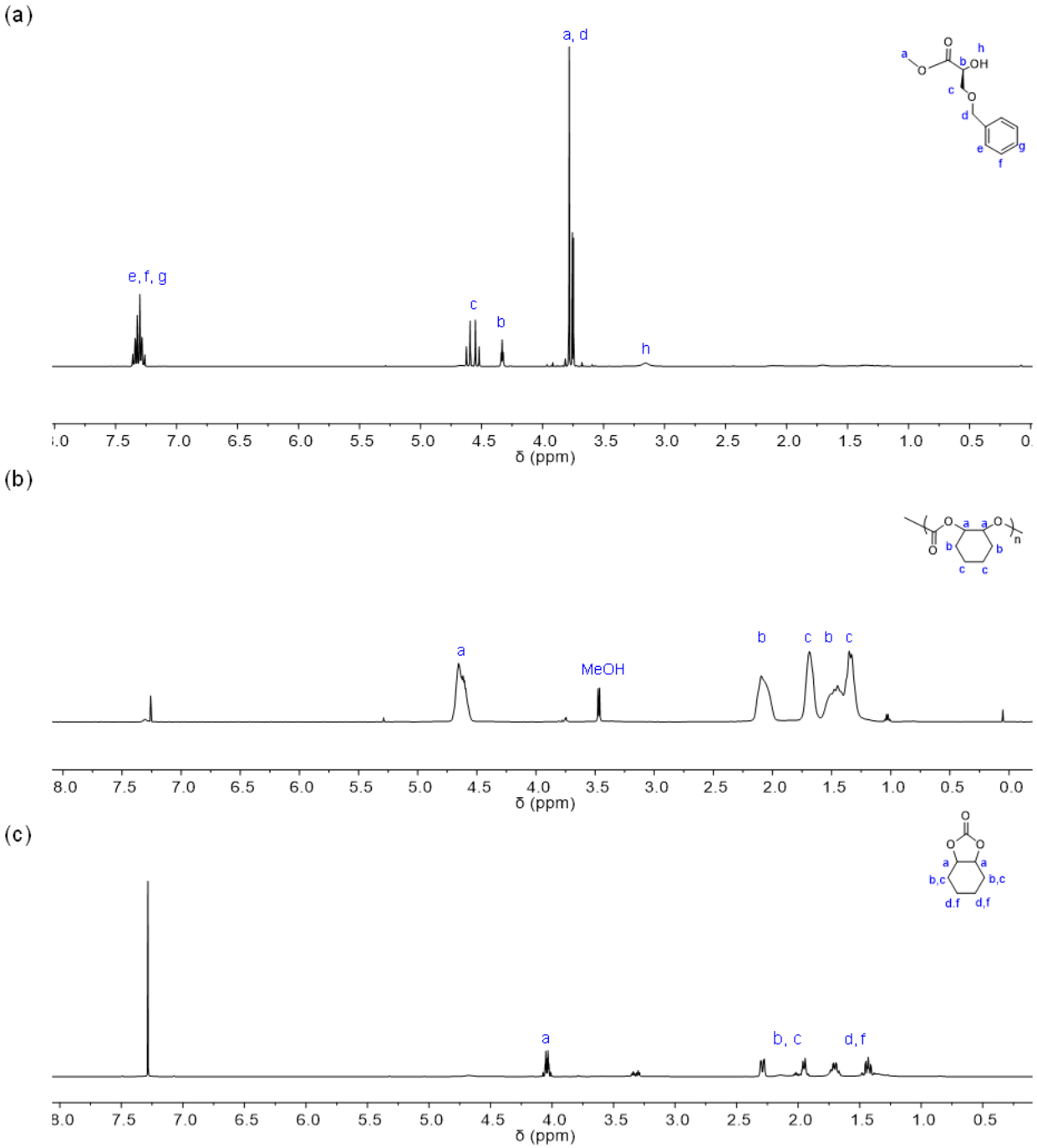

(Data continue on the next page)

(d)

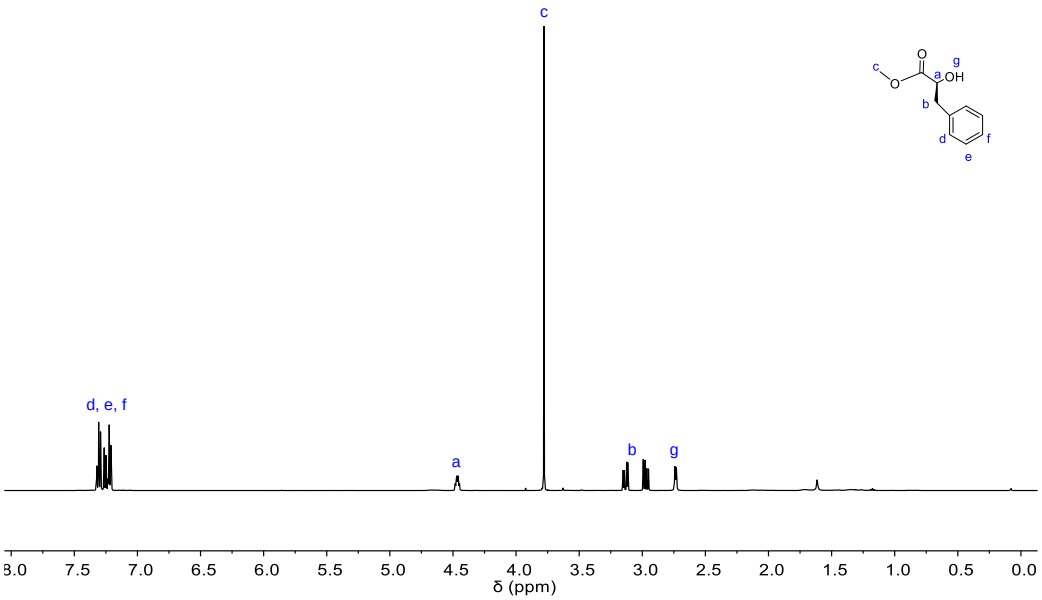

(e)

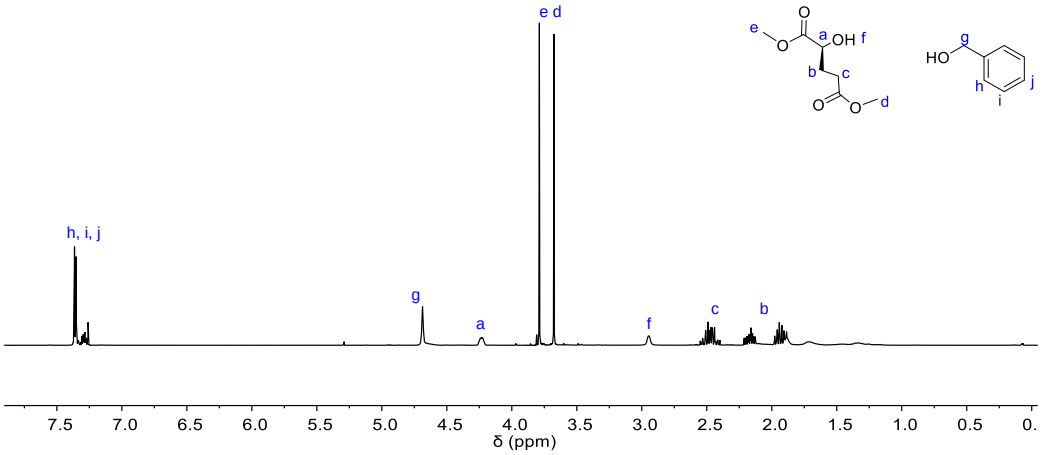

(f)

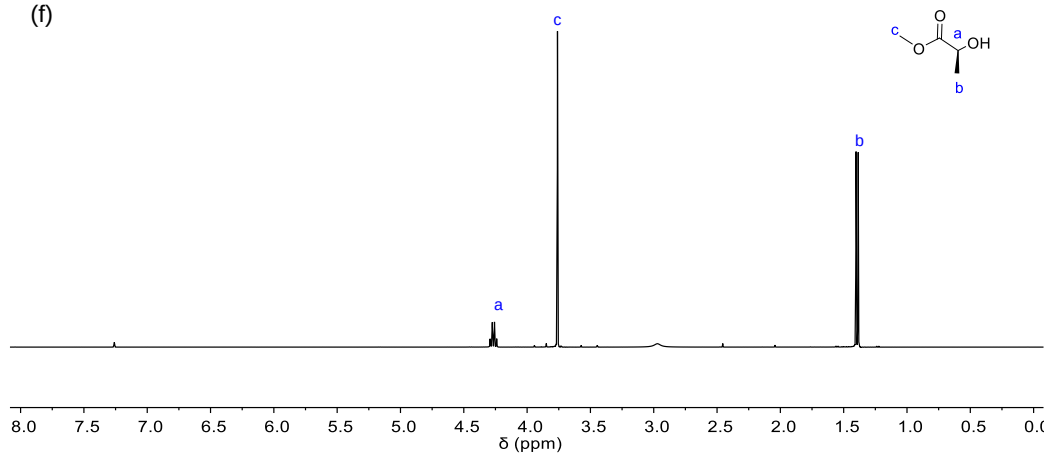

(Data continue on the next page)

(g)

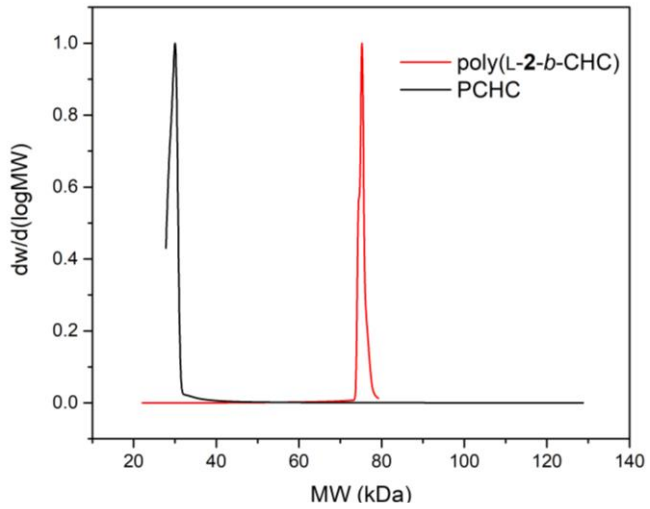

Figure 6.20 The degradation of poly(L-**2**-*b*-CHC) following procedures as shown in Figure 6.19. (a) ^{1}H NMR spectrum of the degradation solution after the first step (treating the copolymer with $Zn(N(TMS)_2)_2$ in MeOH). (b) ^{1}H NMR spectrum of the PCHC block after first step degradation, which is not soluble in methanol and can be soluble in toluene. (c) ^{1}H NMR spectrum of the second step degradation when treating PCHC with TBD, which provided cyclic cyclohexene carbonate. ^{1}H NMR spectra of the degradation solution of (d) poly(L-**1**-*b*-CHC), (e) poly(L-**3**-*b*-CHC) and (f) poly(L-**4**-*b*-CHC) after the first step. (g) GPC traces comparison of the original poly(L-**2**-*b*-CHC) (M_n = 74.6 kDa, $Đ$ = 1.01, red color), and PCHC after the first step $Zn(N(TMS)_2)_2$-mediated degradation of polyester block (M_n = 29.9 kDa, $Đ$ = 1.03, black color, ^{1}H NMR in (b)).

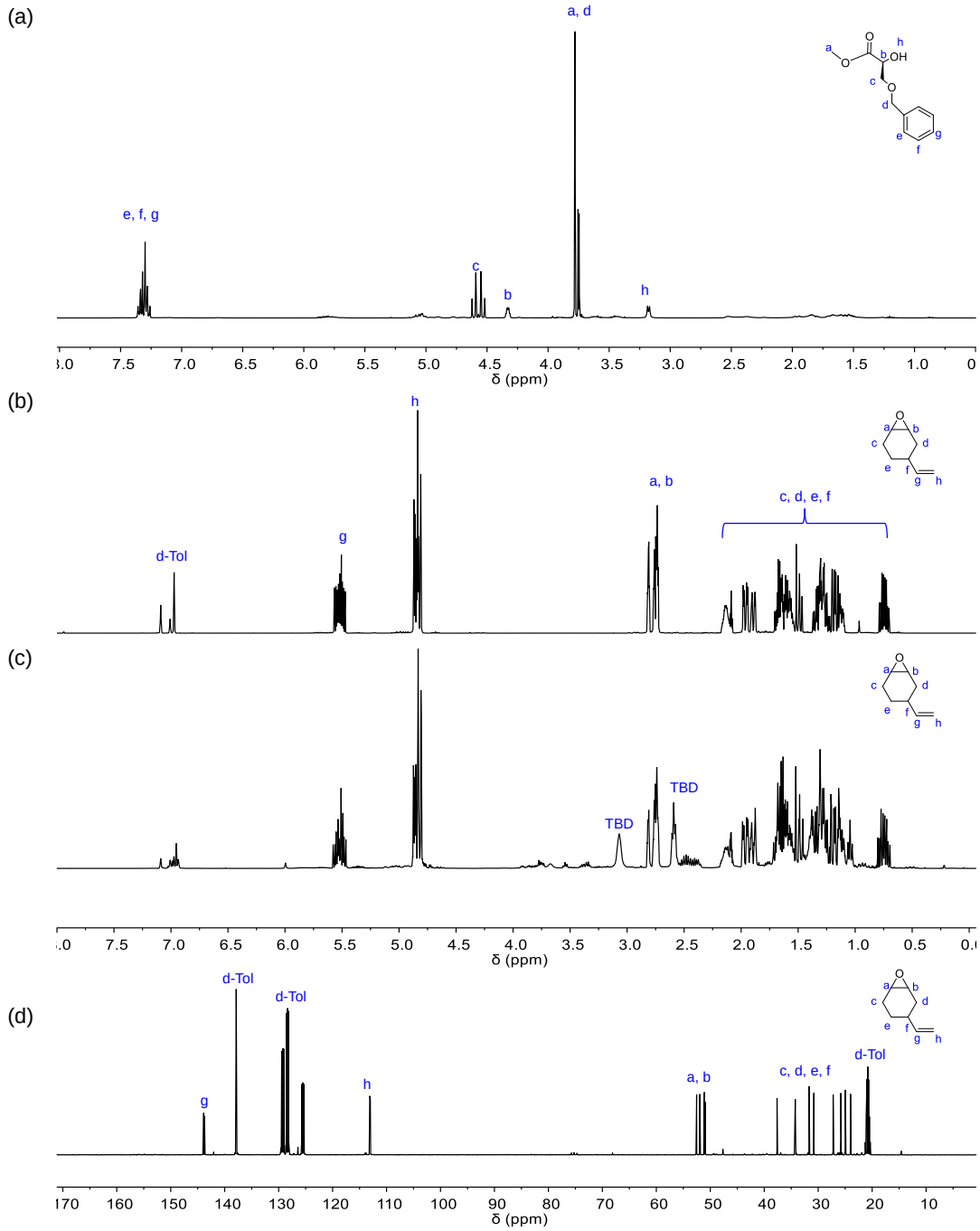

Figure 6.21 The degradation of poly(L-**2**-*b*-VCHC) following procedures as shown in Figure 6.19. (a) ^{1}H NMR spectrum of the degradation solution after the first step (treating the copolymer with $Zn(N(TMS)_2)_2$ in MeOH). (b) ^{1}H NMR spectrum of pure VCHO, compared to the ^{1}H NMR spectrum of the degradation solution after the second step (treating PVCHC with TBD). (d) ^{13}C NMR spectrum of the degradation solution in (c). The results showed that the treatment of the PVCHC with TBD led to the formation of the original VCHO epoxide monomer.

6.3 Materials and methods

6.3.1 General

O-benzyl-L-serine, L-glutamic acid-γ-benzyl ester were purchased from Chem-Impex (Wood Dale, IL). L-phenylalanine was purchased from Alfa Aesar (Haverhill, MA). Anhydrous tetrahydrofuran (THF) was dried by alumina columns and stored with 4Å molecular sieve in the dark bottle in the glove box (MBraun, Labstar Pro, < 1 ppm oxygen and moisture). Anhydrous THF-d_8, benzyl alcohol, hexane, toluene, diethyl ether, diisopropyl ether were dried and stored by 4Å molecular sieves in the glove box. LDPE (low-density polyethylene) was purchased from McMaster-Carr (Elmhurst, IL). PP (polypropylene, F1000HC) was purchased from Braskem. All other chemicals were purchased from Sigma-Aldrich (St. Louis, MO) unless otherwise noted. All metal catalysts were synthesized in the glove box, characterized by NMR, and stored in the glove box freezer (−30 °C). Research-grade bone-dry CO_2 (Airgas, Radnor Township, PA) was dried through a Drierite column before use.

6.3.2 OCA monomers

L-PheOCA (L-**1**)[46], L-Ser(Bn)OCA (L-**2**)[47], L-Glu(Cbz)OCA (L-**3**)[48], L-LacOCA (L-**4**)[49], were synthesized and recrystallized according to the literature. Warning: the synthesis of OCA involves the use of chemical hazards such as phosgene (15 wt% in toluene, Sigma-Aldrich) and triphosgene (TCI-America). All OCA monomers were recrystallized three times and stored in -30 °C freezer in the glove box.

6.3.3 Epoxide monomers

Cyclohexene oxide (CHO), (±)-propylene oxide (PO), vinyl cyclohexene oxide (VCHO) and 3,4-epoxy-1-cyclohexene (ECHO) were purchased from Sigma-Aldrich.

The epoxides were dried over calcium hydride for three days, degassed via three freeze-pump-thaw cycles, then vacuum transferred under nitrogen, and stored in the glove box.

6.3.4 Zn complexes

$Zn(HMDS)_2$ was prepared and distilled according to the literature[50]. (**NNO**)Zn complexes (Table 6.2) was prepared according to the literature[51, 52]. β-diiminate Zn complexes (Tables 6.2 and 6.3) were synthesized according to the literature.[27, 29, 33, 34, 53] All Zn complexes were stored in the glove box freezer (−30 °C).

6.3.5 Other metal complexes (in Table 6.1)

$Y(N(SiMe_3)_2)_3$, $Sn(N(SiMe_3)_2)_2$, $Mg(N(SiMe_3)_2)_2$ were purchased from Sigma-Aldrich. (1R,2R)-salcy-Co^{II} (salcy = 1,2-cyclohexanediamino-*N*,*N*'-bis(3,5-di-*tert*-butyl-salicylidene)), (1R,2R)-salcy-Mn^{III} chloride, (1R,2R)-salcy-Cr^{III} chloride, (1R,2R)-salcy-Al^{III} chloride, $Zr(O^iPr)_4$, and $Hf(O^iPr)_4$ were purchased from Strem (Newburyport, MA). $Mn(N(SiMe_3)_2)_2$, $Fe(N(SiMe_3)_2)_2$, $Ce(N(SiMe_3)_2)_3$, and $Y(N(SiHMe_2)_2)_3$, were prepared and recrystallized according to the literature, and were stored in the glove box freezer.

6.3.6 Instrument and characterization

6.3.6.1 NMR spectroscopy

All room temperature NMR and homodecoupling ^1H NMR spectra were recorded on Agilent U4-DD2 (400 MHz) or Bruker Avance II (500 MHz). All ^{13}C NMR spectra are proton decoupled.

Diffusion Ordered NMR Spectroscopy (DOSY-NMR)

DOSY-NMR experiments were performed on a Bruker 400 MHz Avance III spectrometer with a Micro5 XYZ gradient probe, using a convection-compensated double stimulated echo sequence (Bruker dstegp3s), with a diffusion gradient pulse time (δ) of 4

ms, a diffusion encoding time (Δ) of 50 ms, and a linear gradient list of 16 points from 11.3 G*cm^{-1} to 141 G*cm^{-1}. The DOSY processing for each spectrum was performed using the Bayesian fit function in Mestrelab MestreNova, with a resolution factor of 0.10, 0 repetitions, and 64 points in the diffusion dimension. The identical diffusion peaks observed for the protons of each of the two polymer block species confirmed the successful synthesis of the block copolymers.

6.3.6.2 FTIR spectroscopy

Fourier-transform infrared spectra were recorded on an Agilent Cary 630 FTIR spectrometer (Agilent Technologies Inc., Santa Clara, CA, USA) equipped with Diamond ATR and transmission sampling accessory.

OCA Monomer conversion measurement using FTIR:

A small aliquot of polymer solution (20 μL) was removed out of the glove box and quenched with 5% acetic acid / THF solution (20 μL). The mixture (~10 μL) was immediately dropped onto the FTIR-ATR diamond sampler and formed a film within 10-20 seconds for the spectra measurement. The peak at 1800 cm^{-1} is assigned as the anhydride bond stretch in OCA; the peak at 1760 cm^{-1} corresponds to the formation of the ester bond in the polymer. The OCA monomer conversion was determined by the intensity ratio between 1760 cm^{-1} and 1800 cm^{-1}: conversion% = I_{1760} / (I_{1760}+ I_{1800}).

6.3.6.3 Gel permeation chromatography (GPC)

GPC experiments were performed on a system equipped with an isocratic pump with degasser (Agilent 1260 series, Agilent Technologies, Santa Clara, CA, USA), Wyatt DAWN HELEOS multiangle laser light scattering (MALS) detector (GaAs 30 mW laser at λ=690nm), and an Wyatt Optilab rEX differential refractive index (DRI) detector with

a 690 nm light source (Wyatt Technology, Santa Barbara, CA, USA). Separations were performed using serially connected size exclusion columns (100 Å, 500 Å, 10^3 Å, and 10^4 Å Phenogel columns, 5 μm, 300 × 4.6 mm, Phenomenex, Torrance, CA, USA) at 35 °C using THF as the mobile phase with a flow rate of 0.35 mL/min. The polymer molecular weight (MW) and molecular weight distribution (*Đ*) were determined using Zimm model fit of MALS-DRI data by ASTRA software (Version 6.1, Wyatt Technology). Data collection interval: 0.5 sec.

The refractive index increment dn/dc value was determined by the Wyatt Optilab rEX refractive index detector using ASTRA software dn/dc template (Version 6.1, Wyatt Technology). Five polymer / THF solutions with different concentrations were sequentially injected into the refractive index detector and the refractive index values were plotted versus concentration in ASTRA software. The slope of the linear fitting data is the dn/dc value.

The dn/dc values: poly(L-**1**-*b*-CHC), 0.118; poly(L-**2**-*b*-CHC), 0.1096; poly(L-**3**-*b*-CHC), 0.1057; poly(L-**4**-*b*-CHC), 0.099; poly(L-**1**-*b*-VCHC), 0.125; poly(L-**2**-*b*-VCHC), 0.1113; poly(L-**3**-*b*-VCHC), 0.1181; poly(L-**4**-*b*-VCHC), 0.0925; poly(L-**2**-*b*-ECHC), 0.134; poly(L-**2**-*b*-CHC-*co*-VCHC). 0.102; poly(L-**4**-*b*-VCHC-*b*-L-**2**-*b*-CHC), 0.122.

6.3.6.4 Matrix assisted laser desorption ionization mass spectrometry (MALDI-MS)

MALDI-MS was carried out on a Bruker Daltonics UltrafleXtreme MALDI set to positive ion reflectron mode. Samples were dissolved in THF at 10 mg/mL. α-Cyano-4-hydroxycinnamic acid (10 mg/mL in THF) or *trans*-2-[3-(4-*tert*-butylphenyl)-2-methyl-2-propenylidene] malononitrile (DCTB, 10 mg/mL in THF) were used as matrix. The

components were mixed in the ratio of 1:1 (polymer: matrix), spotted onto a plate and allowed to dry completely before MALDI analysis.

6.3.7 Polymerization procedures

6.3.7.1 The copolymerization of OCA L-2 and CHO mediated by BDIZn-7 (solution)

In a glove box, OCA L-**2** (35.3 mg, 0.159 mmol, 300 equiv.) was mixed with CHO (15.60 mg, 0.159 mmol, 300 equiv.), (BDI-7)ZnN(TMS)$_2$ (**BDIZn-7**, 10.6 μL of 35 mg/mL in THF, 0.53 μmol, 1 equiv.) and THF (63.8 μL) in a 7-mL glass vial. The glass vial was sealed and left at room temperature in the glove box for 12 hours. After the reaction, an aliquot of the reaction solution was taken out of the box to determine the OCA conversion by FTIR (see 6.3.6.2). After solvent evaporation, a sample of the crude polymer was removed to determine the epoxide monomer conversion by ^{1}H NMR and to characterize the resulted polymer's MW and *Đ* by GPC. The remaining polymer was purified by dissolving in a minimum amount of DCM and precipitating it into methanol twice and dried under vacuum. To scale up the polymerization, e.g., using 500 mg OCA L-**2** and 221.0 mg CHO in a 20 mL flask, we mixed 400 μL THF and 149.1 μL **BDIZn-7** (35 mg/mL in THF) in a sealed flask in a glove box at room temperature for 12-hours reaction, followed by the same workup procedures to remove the solvent and purify the polymer.

The figure below shows at the beginning (left) and the end of the polymerization (right). The obtained polymer solution became viscous (no stir bar for better presentation).

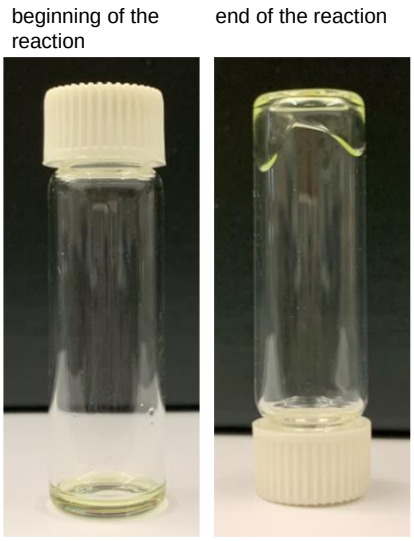

6.3.7.2 The copolymerization of OCA L-2 and CHO mediated by BDIZn-7 (semi-bulk)

In a glove box, the OCA L-**2** (35.3 mg, 0.159 mmol, 300 equiv.) was mixed with CHO (15.60 mg, 0.159 mmol, 300 equiv.) in a 7-mL glass vial. The OCA monomer could not be completely dissolved in CHO. (BDI-7)ZnN(TMS)$_2$ (**BDIZn-7**, 10 μL THF, 0.53 μmol, 1 equiv.) was added into the mixture and initiated the polymerization. All OCA monomers became completely dissolved into the solution in 30 min. The glass vial was sealed and left at room temperature in the glove box for 12 hours. After the reaction, the reaction solution was dissolved in 500 μL DCM, and an aliquot was taken out of the box to determine the OCA monomer conversion by FTIR (see 6.3.6.2). After solvent evaporation, a sample of the crude polymer was removed to determine the epoxide monomer conversion by ^{1}H NMR and to characterize the resulted polymer's MW and *Đ* by GPC. The remaining polymer was purified by dissolving in a minimum amount of DCM and precipitating it into methanol twice and dried under vacuum.

The figure below shows at the beginning (left, in the liquid state due to CHO is a liquid) and the end of the polymerization (right). The obtained polymer became extremely viscous (no stir bar for better presentation).

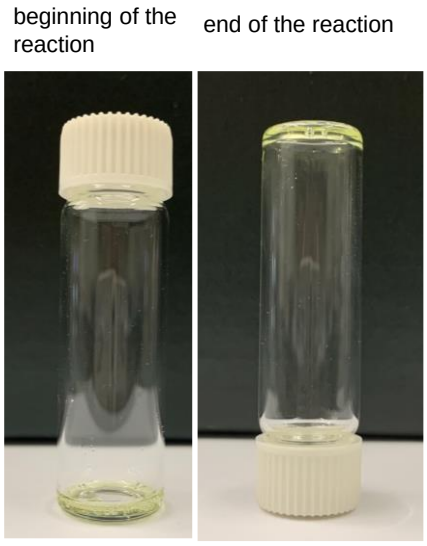

6.3.7.3 Block copolymerization of L-4, VCHO, and L-2, CHO mediated by BDIZn-7

In a glove box, the OCA L-**4** (18.5 mg, 0.159 mmol, 300 equiv.) was mixed with VCHO (19.80 mg, 0.159 mmol, 300 equiv.), **BDIZn-7** (10.6 μL of 35 mg/mL in THF, 0.53 μmol, 1 equiv.) and THF (100 μL) in a 7-mL glass vial. The glass vial was sealed and left at room temperature in the glove box for 12 hours. Upon the quantitative conversion of VCHO was achieved, measured by ^{1}H NMR of an aliquote of the reaction solution taken out of the box. The OCA L-**2** (35.3 mg, 0.159 mmol, 300 equiv.), CHO (15.60 mg, 0.159 mmol, 300 equiv.) and THF (63.8 μL) was added into the remaining mixture and left at room temperature in the glove box for 12 hours. After the reaction, an aliquot of the reaction solution was taken out of the box to determine the OCA monomer conversion by FTIR (6.3.6.2). After solvent evaporation, a sample of the crude polymer

was removed to determine the epoxide monomer conversion by ^{1}H NMR and to characterize the resulted polymer's MW and *Đ* by GPC. The remaining copolymer was purified by dissolving in a minimum amount of DCM and precipitating it into methanol twice and dried under vacuum.

6.3.8 Degradation of poly(ester-*b*-carbonate)

The degradation of polyester blocks was performed according to our reported protocols. In brief, in a glove box, poly(L-**2**-*b*-CHC) (80 mg) and Zn(HMDS)$_2$ (10 wt%, 8 mg) were sequentially added in anhydrous methanol (2 mL) in a flask with a stir bar. The polymer was insoluble in MeOH. The flask was sealed and was moved out of the glove box and was stirred at 50 degree for 12 hours. During the degradation, the polyester block was gradually dissolved in the methanol solution, forming a cloudy solution. After the reaction, yellow precipitates (Zn-alkoxide and polycarbonates) were observed upon a quick centrifugation (see Figure 6.19). The solution (containing methyl esters) was carefully transferred into another clean vials to separate from the precipitations. The obtained solution was evaporated for NMR analysis that confirmed the complete degradation of the polyester block to methyl esters with a quantities yield (Figure S24a). After separation, the final yield for the methyl ester of L-**2** was 95.6 %.

The precipitation was re-dissolved in DCM (1 mL), and the insoluble part (likely Zn-oxides) was removed via filtration (see Figure 6.19). After solvent removal, the filtrate (polycarbonate block) had a yield of 88.2% based on the theoretical molecular mass of the polycarbonate block. The polycarbonate and TBD (4 mol% for poly(CHC), 20 wt% for poly(VCHC)) were dissolved in toluene-d8 (1 mL), and the resulted solution was heated at 110 ^{o}C for overnight to degrade polycarbonates. The resulted solution was

cooled down for NMR analysis that confirmed the complete degradation of the polycarbonate block to 5-member-ring carbonates (for CHO) or epoxides for (VCHO) with quantitively yields (see Figures 6.19-6.21).

6.4 Conclusions

Constructing sequence-controlled block copolymers from a mixture of co-monomers has been a long-standing challenge in polymer chemistry. For instance, currently available one-pot synthesis of poly(ester-*b*-carbonate) are energy- and material-intensive, requiring high-pressure CO_2 gas and high temperature. A scalable and atom-economical synthetic solution to this challenge via a single Lewis acidic zinc complex has been presented herein for the copolymerization of *O*-carboxyanhydrides (OCAs) and epoxides without additional pressurized CO_2. The CO_2 released in the ROP of OCA was efficiently recycled into the second polycarbonate block. Additionally, the obtained functionalized poly(ester-*b*-carbonate) could be degraded into corresponding hydroxy acid and cyclic carbonate or epoxide, thereby closing its life cycle. To our knowledge, the scalable synthesis of such high-MW functionalized poly(ester-*b*-carbonates) copolymers from equimolar mixtures of OCAs and epoxides using a single metal complex has never been achieved before.

References

1. Bates, F. S.; Hillmyer, M. A.; Lodge, T. P.; Bates, C. M.; Delaney, K. T.; Fredrickson, G. H., Multiblock Polymers: Panacea or Pandora's Box? *Science* **2012,** *336* (6080), 434-440.
2. Bates, C. M.; Bates, F. S., 50th Anniversary Perspective: Block Polymers—Pure Potential. *Macromolecules* **2017,** *50* (1), 3-22.
3. Lutz, J.-F.; Ouchi, M.; Liu, D. R.; Sawamoto, M., Sequence-Controlled Polymers. *Science* **2013,** *341* (6146), 1238149.
4. Mecerreyes, D.; Moineau, G.; Dubois, P.; Jérôme, R.; Hedrick, J. L.; Hawker, C. J.; Malmström, E. E.; Trollsas, M., Simultaneous Dual Living Polymerizations: A Novel One-Step Approach to Block and Graft Copolymers. *Angewandte Chemie International Edition* **1998,** *37* (9), 1274-1276.
5. Bielawski, C. W.; Louie, J.; Grubbs, R. H., Tandem Catalysis: Three Mechanistically Distinct Reactions from a Single Ruthenium Complex. *Journal of the American Chemical Society* **2000,** *122* (51), 12872-12873.
6. Schmidt, S. C.; Hillmyer, M. A., Synthesis and Characterization of Model Polyisoprene−Polylactide Diblock Copolymers. *Macromolecules* **1999,** *32* (15), 4794-4801.
7. Wu, G.-P.; Darensbourg, D. J.; Lu, X.-B., Tandem Metal-Coordination Copolymerization and Organocatalytic Ring-Opening Polymerization via Water To Synthesize Diblock Copolymers of Styrene Oxide/CO2 and Lactide. *Journal of the American Chemical Society* **2012,** *134* (42), 17739-17745.
8. Jeske, R. C.; Rowley, J. M.; Coates, G. W., Pre-Rate-Determining Selectivity in the Terpolymerization of Epoxides, Cyclic Anhydrides, and CO2: A One-Step Route to Diblock Copolymers. *Angewandte Chemie International Edition* **2008,** *47* (32), 6041-6044.
9. Romain, C.; Williams, C. K., Chemoselective Polymerization Control: From Mixed-Monomer Feedstock to Copolymers. *Angewandte Chemie International Edition* **2014,** *53* (6), 1607-1610.
10. Romain, C.; Zhu, Y.; Dingwall, P.; Paul, S.; Rzepa, H. S.; Buchard, A.; Williams, C. K., Chemoselective Polymerizations from Mixtures of Epoxide, Lactone, Anhydride, and Carbon Dioxide. *Journal of the American Chemical Society* **2016,** *138* (12), 4120-4131.
11. Ji, H.-Y.; Wang, B.; Pan, L.; Li, Y.-S., One-Step Access to Sequence-Controlled Block Copolymers by Self-Switchable Organocatalytic Multicomponent Polymerization. *Angewandte Chemie International Edition* **2018,** *57* (51), 16888-16892.
12. Xu, J.; Wang, X.; Hadjichristidis, N., Diblock dialternating terpolymers by one-step/one-pot highly selective organocatalytic multimonomer polymerization. *Nature Communications* **2021,** *12* (1), 7124.
13. Zhang, Z.; Zeng, T.-Y.; Xia, L.; Hong, C.-Y.; Wu, D.-C.; You, Y.-Z., Synthesis of polymers with on-demand sequence structures via dually switchable and interconvertible polymerizations. *Nature Communications* **2018,** *9* (1), 2577.
14. Kernbichl, S.; Reiter, M.; Adams, F.; Vagin, S.; Rieger, B., CO2-Controlled One-Pot Synthesis of AB, ABA Block, and Statistical Terpolymers from β-

Butyrolactone, Epoxides, and CO2. *Journal of the American Chemical Society* **2017,** *139* (20), 6787-6790.
15. Wang, X.; Thevenon, A.; Brosmer, J. L.; Yu, I.; Khan, S. I.; Mehrkhodavandi, P.; Diaconescu, P. L., Redox Control of Group 4 Metal Ring-Opening Polymerization Activity toward l-Lactide and ε-Caprolactone. *Journal of the American Chemical Society* **2014,** *136* (32), 11264-11267.
16. Qi, M.; Dong, Q.; Wang, D.; Byers, J. A., Electrochemically Switchable Ring-Opening Polymerization of Lactide and Cyclohexene Oxide. *Journal of the American Chemical Society* **2018,** *140* (17), 5686-5690.
17. Hern, Z. C.; Quan, S. M.; Dai, R.; Lai, A.; Wang, Y.; Liu, C.; Diaconescu, P. L., ABC and ABAB Block Copolymers by Electrochemically Controlled Ring-Opening Polymerization. *Journal of the American Chemical Society* **2021,** *143* (47), 19802-19808.
18. Deacy, A. C.; Gregory, G. L.; Sulley, G. S.; Chen, T. T. D.; Williams, C. K., Sequence Control from Mixtures: Switchable Polymerization Catalysis and Future Materials Applications. *Journal of the American Chemical Society* **2021,** *143* (27), 10021-10040.
19. Sulley, G. S.; Gregory, G. L.; Chen, T. T. D.; Peña Carrodeguas, L.; Trott, G.; Santmarti, A.; Lee, K.-Y.; Terrill, N. J.; Williams, C. K., Switchable Catalysis Improves the Properties of CO2-Derived Polymers: Poly(cyclohexene carbonate-b-ε-decalactone-b-cyclohexene carbonate) Adhesives, Elastomers, and Toughened Plastics. *Journal of the American Chemical Society* **2020,** *142* (9), 4367-4378.
20. Xie, R.; Zhang, Y.-Y.; Yang, G.-W.; Zhu, X.-F.; Li, B.; Wu, G.-P., Record Productivity and Unprecedented Molecular Weight for Ring-Opening Copolymerization of Epoxides and Cyclic Anhydrides Enabled by Organoboron Catalysts. *Angewandte Chemie International Edition* **2021,** *60* (35), 19253-19261.
21. Yang, G.-W.; Zhang, Y.-Y.; Xie, R.; Wu, G.-P., Scalable Bifunctional Organoboron Catalysts for Copolymerization of CO2 and Epoxides with Unprecedented Efficiency. *Journal of the American Chemical Society* **2020,** *142* (28), 12245-12255.
22. Zhang, D.; Boopathi, S. K.; Hadjichristidis, N.; Gnanou, Y.; Feng, X., Metal-Free Alternating Copolymerization of CO2 with Epoxides: Fulfilling "Green" Synthesis and Activity. *Journal of the American Chemical Society* **2016,** *138* (35), 11117-11120.
23. Pappuru, S.; Chakraborty, D., Progress in metal-free cooperative catalysis for the ring-opening copolymerization of cyclic anhydrides and epoxides. *European Polymer Journal* **2019,** *121*, 109276.
24. Zhang, J.; Wang, L.; Liu, S.; Kang, X.; Li, Z., A Lewis Pair as Organocatalyst for One-Pot Synthesis of Block Copolymers from a Mixture of Epoxide, Anhydride, and CO2. *Macromolecules* **2021,** *54* (2), 763-772.
25. Raman, S. K.; Raja, R.; Arnold, P. L.; Davidson, M. G.; Williams, C. K., Waste not, want not: CO2 (re)cycling into block polymers. *Chemical Communications* **2019,** *55* (51), 7315-7318.
26. Tang, J.; Li, M.; Wang, X.; Tao, Y., Switchable Polymerization Organocatalysis: From Monomer Mixtures to Block Copolymers. *Angewandte Chemie International Edition* **2022,** *n/a* (n/a), e202115465.
27. Chamberlain, B. M.; Cheng, M.; Moore, D. R.; Ovitt, T. M.; Lobkovsky, E. B.; Coates, G. W., Polymerization of lactide with zinc and magnesium β-diiminate

complexes: stereocontrol and mechanism. *Journal of the American Chemical Society* **2001,** *123* (14), 3229-3238.
28. Wang, R.; Zhang, J.; Yin, Q.; Xu, Y.; Cheng, J.; Tong, R., Controlled Ring-Opening Polymerization of O-Carboxyanhydrides Using a β-Diiminate Zinc Catalyst. *Angewandte Chemie International Edition* **2016,** *55* (42), 13010-13014.
29. Cheng, M.; Moore, D. R.; Reczek, J. J.; Chamberlain, B. M.; Lobkovsky, E. B.; Coates, G. W., Single-Site β-Diiminate Zinc Catalysts for the Alternating Copolymerization of CO2 and Epoxides: Catalyst Synthesis and Unprecedented Polymerization Activity. *Journal of the American Chemical Society* **2001,** *123* (36), 8738-8749.
30. Jeske, R. C.; DiCiccio, A. M.; Coates, G. W., Alternating Copolymerization of Epoxides and Cyclic Anhydrides: An Improved Route to Aliphatic Polyesters. *Journal of the American Chemical Society* **2007,** *129* (37), 11330-11331.
31. Coates, G. W.; Moore, D. R., Discrete Metal-Based Catalysts for the Copolymerization of CO2 and Epoxides: Discovery, Reactivity, Optimization, and Mechanism. *Angewandte Chemie International Edition* **2004,** *43* (48), 6618-6639.
32. DiCiccio, A. M.; Longo, J. M.; Rodríguez-Calero, G. G.; Coates, G. W., Development of Highly Active and Regioselective Catalysts for the Copolymerization of Epoxides with Cyclic Anhydrides: An Unanticipated Effect of Electronic Variation. *Journal of the American Chemical Society* **2016,** *138* (22), 7107-7113.
33. Reiter, M.; Vagin, S.; Kronast, A.; Jandl, C.; Rieger, B., A Lewis acid β-diiminato-zinc-complex as all-rounder for co- and terpolymerisation of various epoxides with carbon dioxide. *Chemical Science* **2017,** *8* (3), 1876-1882.
34. Kronast, A.; Reiter, M.; Altenbuchner, P. T.; Jandl, C.; Pöthig, A.; Rieger, B., Electron-Deficient β-Diiminato-Zinc-Ethyl Complexes: Synthesis, Structure, and Reactivity in Ring-Opening Polymerization of Lactones. *Organometallics* **2016,** *35* (5), 681-685.
35. Bratsch, S. G., A group electronegativity method with Pauling units. *Journal of Chemical Education* **1985,** *62* (2), 101.
36. Nakano, K.; Nozaki, K.; Hiyama, T., Spectral Assignment of Poly[cyclohexene oxide-alt-carbon dioxide]. *Macromolecules* **2001,** *34* (18), 6325-6332.
37. Guerin, W.; Diallo, A. K.; Kirilov, E.; Helou, M.; Slawinski, M.; Brusson, J.-M.; Carpentier, J.-F.; Guillaume, S. M., Enantiopure Isotactic PCHC Synthesized by Ring-Opening Polymerization of Cyclohexene Carbonate. *Macromolecules* **2014,** *47* (13), 4230-4235.
38. Webster, O. W., Living Polymerization Methods. *Science* **1991,** *251* (4996), 887-893.
39. Paul, S.; Zhu, Y.; Romain, C.; Brooks, R.; Saini, P. K.; Williams, C. K., Ring-opening copolymerization (ROCOP): synthesis and properties of polyesters and polycarbonates. *Chemical Communications* **2015,** *51* (30), 6459-6479.
40. Wang, X.; Chin, A. L.; Zhou, J.; Wang, H.; Tong, R., Resilient Poly(α-hydroxy acids) with Improved Strength and Ductility via Scalable Stereosequence-Controlled Polymerization. *Journal of the American Chemical Society* **2021,** *143* (40), 16813-16823.
41. Darensbourg, D. J.; Wei, S.-H., Depolymerization of Polycarbonates Derived from Carbon Dioxide and Epoxides to Provide Cyclic Carbonates. A Kinetic Study. *Macromolecules* **2012,** *45* (15), 5916-5922.

42. Li, C.; Sablong, R. J.; van Benthem, R. A. T. M.; Koning, C. E., Unique Base-Initiated Depolymerization of Limonene-Derived Polycarbonates. *ACS Macro Letters* **2017,** *6* (7), 684-688.
43. Carrodeguas, L. P.; Chen, T. T. D.; Gregory, G. L.; Sulley, G. S.; Williams, C. K., High elasticity, chemically recyclable, thermoplastics from bio-based monomers: carbon dioxide, limonene oxide and ε-decalactone. *Green Chemistry* **2020,** *22* (23), 8298-8307.
44. Singer, F. N.; Deacy, A. C.; McGuire, T. M.; Williams, C. K.; Buchard, A., Chemical Recycling of Poly(Cyclohexene Carbonate) Using a Di-MgII Catalyst. *Angewandte Chemie International Edition* **2022,** *61* (26), e202201785.
45. Yu, Y.; Fang, L.-M.; Liu, Y.; Lu, X.-B., Chemical Synthesis of CO2-Based Polymers with Enhanced Thermal Stability and Unexpected Recyclability from Biosourced Monomers. *ACS Catalysis* **2021,** *11* (13), 8349-8357.
46. Yin, Q.; Tong, R.; Xu, Y.; Baek, K.; Dobrucki, L. W.; Fan, T. M.; Cheng, J., Drug-initiated ring-opening polymerization of O-carboxyanhydrides for the preparation of anticancer drug–poly (O-carboxyanhydride) nanoconjugates. *Biomacromolecules* **2013,** *14* (3), 920-929.
47. Lu, Y.; Yin, L.; Zhang, Y.; Zhang, Z.; Xu, Y.; Tong, R.; Cheng, J., Synthesis of water-soluble poly (α-hydroxy acids) from living ring-opening polymerization of O-benzyl-l-serine carboxyanhydrides. *ACS macro letters* **2012,** *1* (4), 441-444.
48. du Boullay, O. T.; Bonduelle, C.; Martin-Vaca, B.; Bourissou, D., Functionalized polyesters from organocatalyzed ROP of gluOCA, the O-carboxyanhydride derived from glutamic acid. *Chemical communications* **2008,** (15), 1786-1788.
49. Thillaye du Boullay, O.; Marchal, E.; Martin-Vaca, B.; Cossío, F. P.; Bourissou, D., An activated equivalent of lactide toward organocatalytic ring-opening polymerization. *Journal of the American Chemical Society* **2006,** *128* (51), 16442-16443.
50. Lee, D.-Y.; Hartwig, J. F., Zinc trimethylsilylamide as a mild ammonia equivalent and base for the amination of aryl halides and triflates. *Organic letters* **2005,** *7* (6), 1169-1172.
51. Williams, C. K.; Breyfogle, L. E.; Choi, S. K.; Nam, W.; Young, V. G.; Hillmyer, M. A.; Tolman, W. B., A highly active zinc catalyst for the controlled polymerization of lactide. *Journal of the American Chemical Society* **2003,** *125* (37), 11350-11359.
52. Brown, N. J.; Harris, J. E.; Yin, X.; Silverwood, I.; White, A. J.; Kazarian, S. G.; Hellgardt, K.; Shaffer, M. S.; Williams, C. K., Mononuclear phenolate diamine zinc hydride complexes and their reactions with CO2. *Organometallics* **2014,** *33* (5), 1112-1119.
53. Moore, D. R.; Cheng, M.; Lobkovsky, E. B.; Coates, G. W., Mechanism of the alternating copolymerization of epoxides and CO2 using β-diiminate zinc catalysts: evidence for a bimetallic epoxide enchainment. *Journal of the American Chemical Society* **2003,** *125* (39), 11911-11924.

CHAPTER 7

Polymerization kinetics and mechanistic studies on the copolymerization of OCA and epoxide

7.1 Introduction

The switchable/tandem copolymerization from monomer mixtures is considered to be one of the greatest problems in polymer science. One of the research challenges in this process is to understand the intrinsic copolymerization kinetics in the system of interest by experimental or computational methods.[1] It will provide information on the monomer distribution and composition of the resulting copolymers, allowing us to propose the switchable/tandem copolymerization mechanism. Although there are numerous reports of mechanism-switching copolymerization[2], to the best of our knowledge, no detailed kinetic studies have been investigated to elucidate the polymerization reaction rates and thus support the proposed mechanism of copolymerization of epoxides and OCAs. Herein, we discovered a new mechanism in tandem copolymerization of OCA and epoxide for the first time based on detailed kinetic studies and DFT calculation.

7.2 Results and discussions

7.2.1 Polymerization kinetics of copolymerization of OCA and epoxide

We used ^{1}H NMR spectroscopy to profile the kinetics of [L-**2**]/[CHO] copolymerization at various **BDIZn-7** concentrations ([L-**2**] = [CHO] = 787.8 mM in deuterated toluene). Surprisingly, the rate of L-**2** consumption during ROP of OCA clearly showed a strict zero-order dependence on **BDIZn-7** concentration, with no

induction period at any of the tested **BDIZn-7** concentrations (**Figure 7.1a**). When the individual monomer concentrations were varied, double logarithm plots of apparent first-stage polymerization rate constant (k_{app}) versus monomer concentration gave reaction orders of 2.05 ± 0.18 and −1.99 ± 0.12 for CHO and L-**2**, respectively (**Figure 7.1d-g**). Thus, the first stage, ROP of L-**2**, exhibited the following rate law:

$$-d[\text{L-}\mathbf{2}]/dt = k_{p1}[\text{CHO}]^{2.05}/[\text{L-}\mathbf{2}]^{1.99} \quad (1)$$

where k_{p1} is the propagation rate constant of the first stage ROP of OCA. When equal amounts of CHO and L-**2** were used and experimental errors are considered, the rate law becomes

$$-d[\text{L-}\mathbf{2}]/dt = k_{p1} \quad (2)$$

as presented in **Figure 7.1a**.

Additionally, investigation of the rate of ROCOP of CHO and CO_2 liberated from L-**2** revealed a reaction order of 0.52 ± 0.05 with respect to **BDIZn-7** concentration, a first-order dependence on [CHO], and no dependence on the concentration of L-**2**, which was the CO_2 source (**Figures 7.1b-c, h**). Since **BDIZn-7** is monomeric in crystal form,[3] the reaction order of **BDIZn-7** suggested that the Zn complex at the poly(CHC) chain-end likely participated in a monomeric transition state (cycle II in **Figure 7.3a, c**).[4] The independence of poly(CHC) enchainment with respect to the concentration of L-**2** (the CO_2 source, **Figure 7.1h**) agrees well with previously reported rate laws for BDI-Zn-mediated CHO/CO_2 copolymerization.[4] Therefore, the second stage, **BDIZn-7**-mediated copolymerization of CHO and CO_2, showed the following rate law:

$$-d[\text{CHO}]/dt = k_{p2}[\text{CHO}]^{1}[\mathbf{BDIZn\text{-}7}]^{0.52} \quad (3)$$

where k_{p2} is the propagation rate constant of the second stage ROCOP of CHO/CO_2.

The zero-order dependence of the rate on catalyst concentration, the inverse order dependence on monomer concentration, and the dispensability of an alcohol initiator (**Figure 7.1**) in the ROP of L-**2** seem counterintuitive because the rates of most controlled ROPs of OCAs mediated by metal-alkoxide initiators exhibit first-order dependence on monomer concentration and positive reaction orders with respect to catalyst concentration.[5, 6] However, zero-order polymerization rates have been observed sporadically for other tandem anhydride/epoxide/CO_2[7] or anhydride/epoxide/lactone[8, 9] polymerizations. Interestingly, in one switchable anhydride/CHO/lactone polymerization,[8] even lactone homopolymerization was significantly faster than the zero-order anhydride/CHO ROCOP; anhydride/CHO copolymerization occurred first, without lactone ROP. In addition to the computationally predicted differences in activation energy for the different polymerization mechanisms,[10] zero-order kinetics may be critical for a clean switch in the polymerization mechanism because chain propagation rate is independent of monomer concentration, allowing for circumvention of chain transfer or undesired mechanism switching due to the tapered reaction rate that is observed for polymerizations with first-order kinetics.[11, 12]

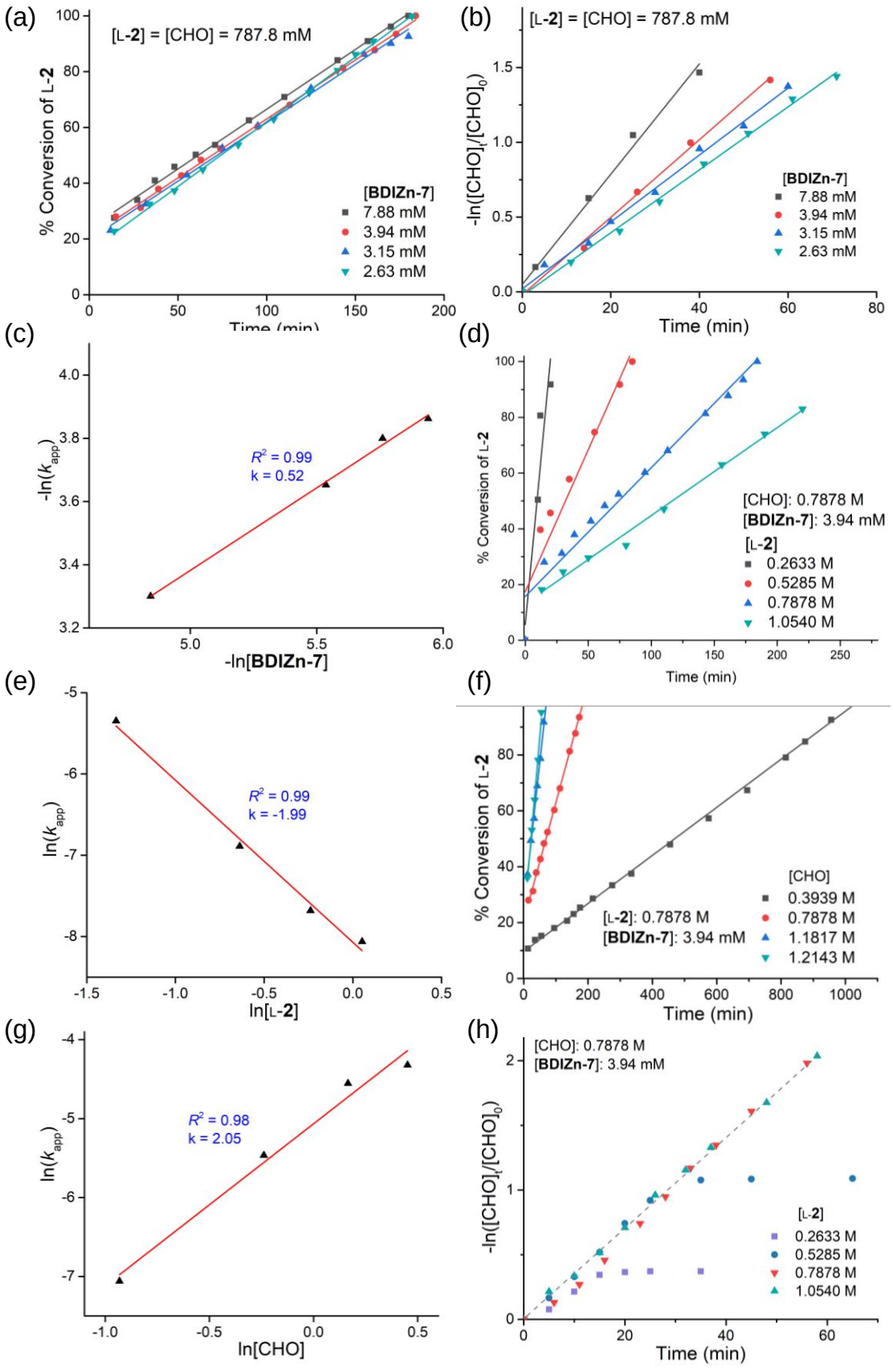
(a)
[L-2] = [CHO] = 787.8 mM
% Conversion of L-2
Time (min)
[BDIZn-7]
7.88 mM
3.94 mM
3.15 mM
2.63 mM
(b)
[L-2] = [CHO] = 787.8 mM
-ln([CHO]t/[CHO]0)
Time (min)
[BDIZn-7]
7.88 mM
3.94 mM
3.15 mM
2.63 mM
(c)
R2 = 0.99
k = 0.52
-ln(kapp)
-ln[BDIZn-7]
(d)
% Conversion of L-2
Time (min)
[CHO]: 0.7878 M
[BDIZn-7]: 3.94 mM
[L-2]
0.2633 M
0.5285 M
0.7878 M
1.0540 M
(e)
R2 = 0.99
k = -1.99
ln(kapp)
ln[L-2]
(f)
% Conversion of L-2
Time (min)
[L-2]: 0.7878 M
[BDIZn-7]: 3.94 mM
[CHO]
0.3939 M
0.7878 M
1.1817 M
1.2143 M
(g)
R2 = 0.98
k = 2.05
ln(kapp)
ln[CHO]
(h)
[CHO]: 0.7878 M
[BDIZn-7]: 3.94 mM
-ln([CHO]t/[CHO]0)
Time (min)
[L-2]
0.2633 M
0.5285 M
0.7878 M
1.0540 M

Figure 7.1 (a) Plots of L-**2** conversion versus time at various **BDIZn-7** concentrations in the polymerization of the poly(L-**2**) block of poly(L-**2**-*b*-CHC). (b) Plots of CHO conversion versus time at various **BDIZn-7** concentrations in the polymerization of the poly(CHC) block of poly(L-**2**-*b*-CHC). (c) The plot of ln(k_{app}) versus ln[**BDIZn-7**] for the second stage ROCOP in (b). (d) The plot of the first stage L-**2** conversion versus time at various L-**2** concentrations. [CHO]/[**BDIZn-7**] = 200/1. [CHO] = 0.787 M in deuterated toluene. (e) The plot of ln(k_{app}) versus ln[L-**2**] for the first stage ROP in (a). (f) The plot of the first stage L-**2** conversion versus time at various CHO concentrations. [L-**2**]/[**BDIZn-7**] = 200/1. [L-**2**] = 0.787 M in deuterated toluene. (g) The plot of ln(k_{app}) versus ln[CHO] for the first stage ROP in (a). (f) The plot of the second stage CHO conversion versus time at various L-**2** concentrations. [CHO]/[**BDIZn-7**] = 200/1. [CHO] = 0.787 M in deuterated toluene. All kinetic studies were in-situ monitored by ^{1}H NMR.

7.2.2 Mechanistic studies on the copolymerization of OCA and epoxide

The unusual zero-order dependence of the L-**2** ROP rate on **BDIZn-7** concentration motivated us to explore the polymerization mechanism. Notably, we found that the ROP did not occur in the absence of CHO (**Chapter 6, Table 6.4**, entry 3), and even the ring-opening reaction failed to occur when an equimolar mixture of L-**2** and **BDIZn-7** was used (**Figure 7.2c**); these results suggest that CHO was indispensable for the copolymerization. Nevertheless, no reactions between L-**2** and CHO or between **BDIZn-7** and CHO were observed (**Figure 7.2b, d**); the ^{1}H NMR peaks of CHO seemed to remain unchanged during the ROP of OCA (**Chapter 6, Figure 6.4**), even in the NMR spectrum of an equimolar L-**2**/CHO/**BDIZn-7** mixture (**Figure 7.2a**). The MALDI-MS of oligo(L-**2**-*b*-CHC) suggested that CHO was unlikely to have initiated the ROP (**Chapter 6, Figure 6.6**). The electrospray ionization mass spectrum (ESI-MS) of the L-**2**/CHO/**BDIZn-7** mixture ([L-**2**]/[CHO]/[**BDIZn-7**] = 3/3/1) indicated that the Zn-carbonate remained at the chain-end during enchainment (**Figure 7.4**), ruling out the possibility that CHO initiated the ROP of L-**2**; this behavior was different from that previously proposed for OCA/epoxide copolymerization.[2, 13] Given that addition of

BnOH resulted in inefficient enchainment in the ROCOP (**Chapter 6, Table 6.3**, entry 5), and that the Zn-alkoxide-mediated ROP of OCA followed first-order kinetic rates[5, 6] that differed from our observed kinetics (**Figure 7.1a**), ROP of L-**2** (the first stage in the copolymerization) disfavored the Zn-alkoxide-mediated pathway. Instead, the Zn-carbonate was likely involved in enchainment during the first-stage (ROP) enchainment. The absence of Zn concentration from the observed rate law (eq. 1) and the inverse reaction order with respect to L-**2** concentration imply that the mechanism involves a Zn-complex-activated monomer that regulates the chain-end reactivities;[14] and the need for CHO led us to postulate that this Zn-activated monomer might require CHO for the enchainment. Indeed, in the ESI-MS of a L-**2**/CHO/**BDIZn-7** mixture and a L-**3**/CHO/**BDIZn-7** mixture, we detected silylamide-capped OCA-Zn-carbonate complexes (**M1** in **Figures 7.4 and 7.5**), supporting the plausibility of the proposed activated-monomer species. Thus, we hypothesize that the first stage (ROP of OCA) proceeds via the monomer-activated mechanism shown in **Figure 7.3a**. First, CHO/**BDIZn-7**-mediated ring-opening of L-**2** generates Zn-carbonate complex **IM3** as the activated monomer. In the presence of abundant CHO, propagation by means of a bimetallic intermolecular reaction between the activated monomer and the Zn-alkoxide chain (via **TS2**) induces decarboxylation, giving rise to a new Zn-carbonate (**IM4**) upon release of CHO, CO_2, and **BDIZn-7** (**Figure 7.6**).

To evaluate the validity of this mechanistic hypothesis and to gain further insight into reaction pathways, we performed extensive density functional theory (DFT) calculations on a slightly simplified system (i.e., we used L-**4** instead of L-**2**) at the SMD_{THF}/wB97M-V/def2-TZVP // SMD_{THF}/B3LYP-D3/6-31G(d)[LANL2DZ(Zn)] level

of theory (**Figure 7.3b, c**). Note that the direct ring-opening of L-**4** or CHO by **BDIZn-7** was predicted to be highly endergonic, with the activation energy barrier of 63.13 kcal/mol (**IM5**) or 77.80 kcal/mol (**IM6**), respectively; whereas the CHO/**BDIZn-7**-mediated reaction via our proposed activated-monomer mechanism was favored, with a free energy barrier of 4.15 kcal/mol (**IM1** to **TS1**) and a total free energy decrease of 7.77 kcal/mol from IM1 to the activated monomer (**IM3**, **Figure 7.3b**). Additionally, we performed DFT calculations on the second stage (the ROCOP cycle) involving a monomeric Zn-mediated CHO ring-opening followed by CO_2 insertion (**Figure 7.3c**; **Figure 7.7**). The overall driving force for one second-stage cycle is predicted to be a free energy decrease of 7.85 kcal/mol (**Figure 7.3c**). Our calculated energy profiles showed that the dinuclear-Zn-complex-mediated decarboxylation (via **TS2**) and the ring-opening of CHO (via **TS3**) were likely the rate-limiting steps. Additionally, the DFT computation also rationalized the mechanism switching: the calculated energy barrier for OCA ring-opening (**BDIZn-7** to **TS1**, 12.62 kcal/mol) was much lower than that calculated for CHO-ring-opening (**IM7** to **TS3**, 18.41 kcal/mol). Taken together, these results indicate that the absence of CO_2 enabled rapid initiation of OCA ROP via the activated-monomer mechanism; the zero-order ROP kinetics ensured that the rate of the first-stage polymerization did not taper before the OCA monomer was consumed; and the computed activation energy barriers for the two polymerizations supported the thermodynamic chain-end preference during the copolymerization, which assured the precise block structure in the obtained copolymer.

(a)

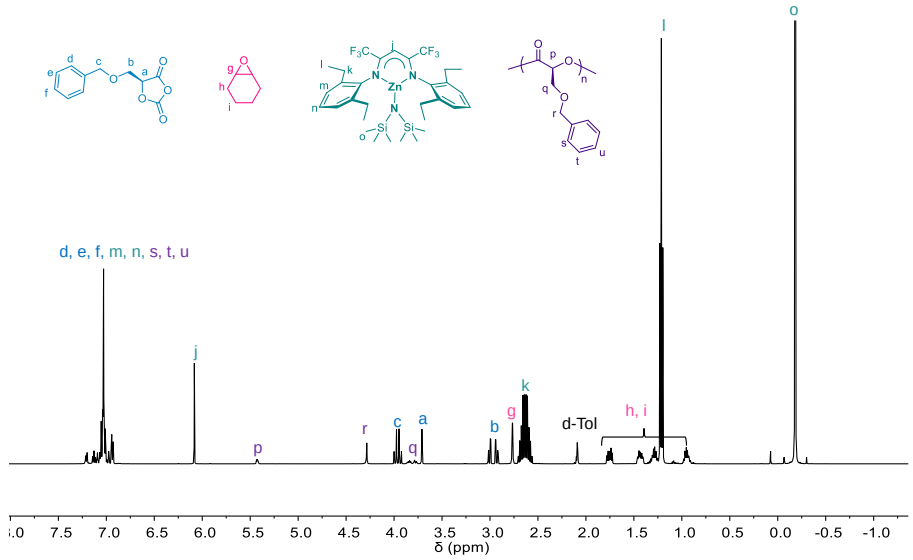

(b)

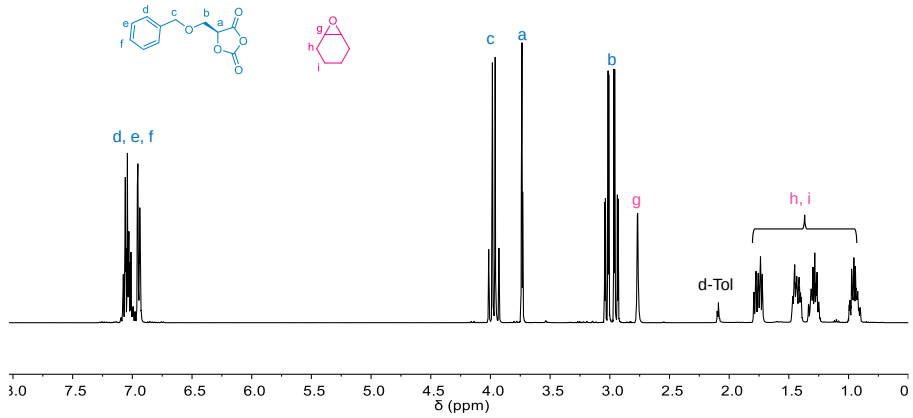

(c)

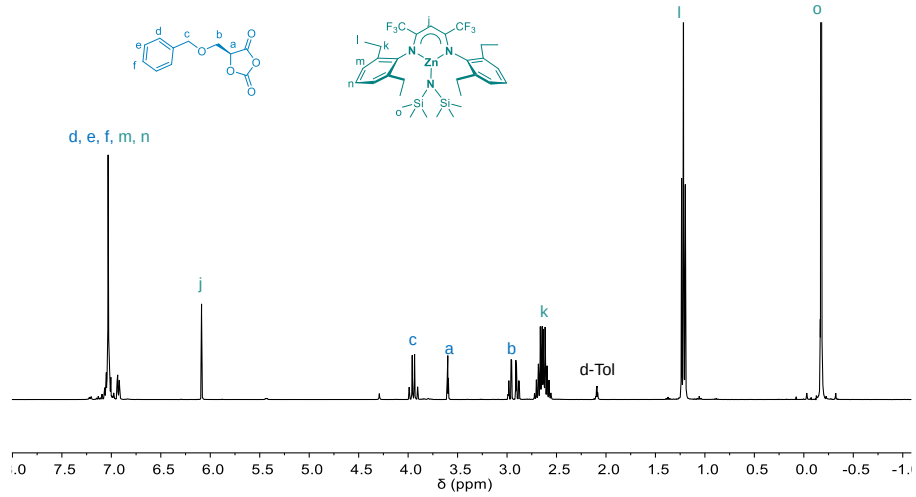

(Data continue on the next page)

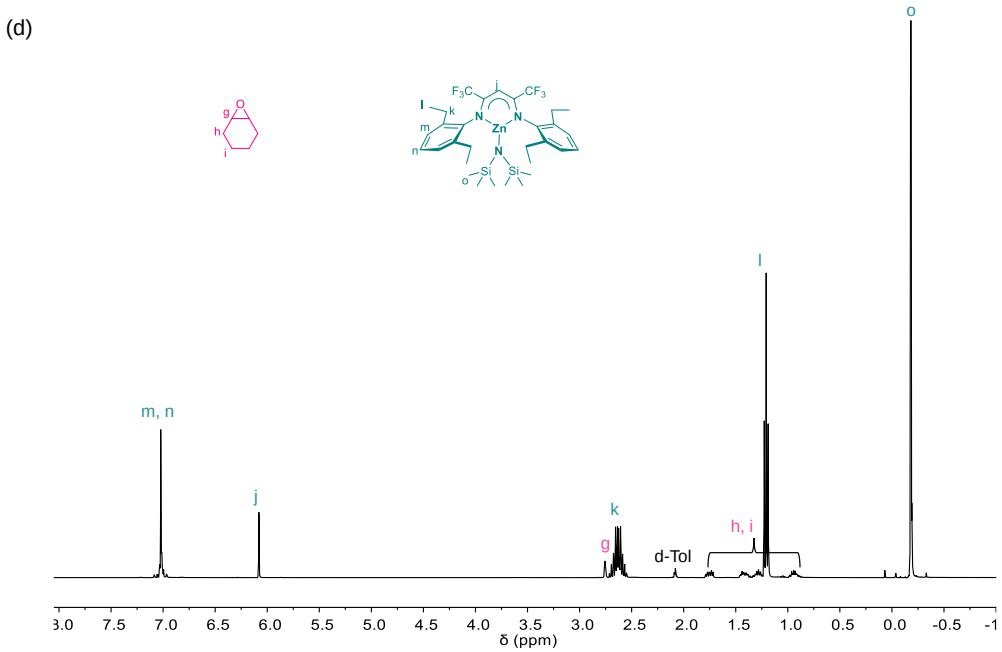

Figure 7.2 ^{1}H NMR spectra of (a) the mixture of L-**2**/CHO/**BDIZn-7** at the ratio of 1/1/1, (b) the mixture of L-**2**/CHO at the ratio of 1/1, (c) the mixture of L-**2**/**BDIZn-7** at the ratio of 1/1, and (d) the mixture of CHO/**Zn-7** at the ratio of 1/1.

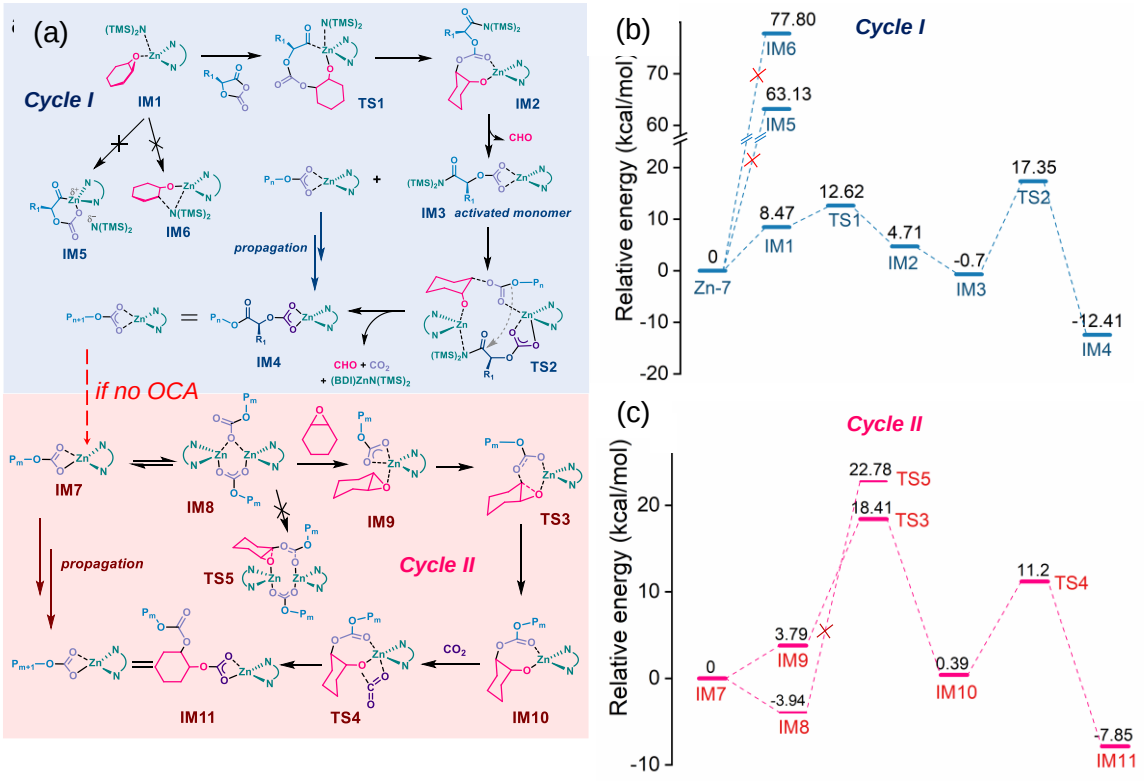

Figure 7.3 Proposed mechanism for auto-tandem block copolymerization of *O*-carboxyanhydride / epoxide with supporting evidence. (a) Proposed copolymerization mechanism that switches from *O*-carboxyanhydride ring-opening polymerization (ROP, cycle I) to epoxide/CO_2 ring-opening copolymerization (ROCOP, cycle II). The proposed mechanism was supported by the free energies of (b) ROP in cycle I and (c) ROCOP in cycle II calculated by means of density functional theory. Detailed three-dimensional structures of optimized intermediate states are shown in Figures 7.6-7.7, and section 7.3.3.

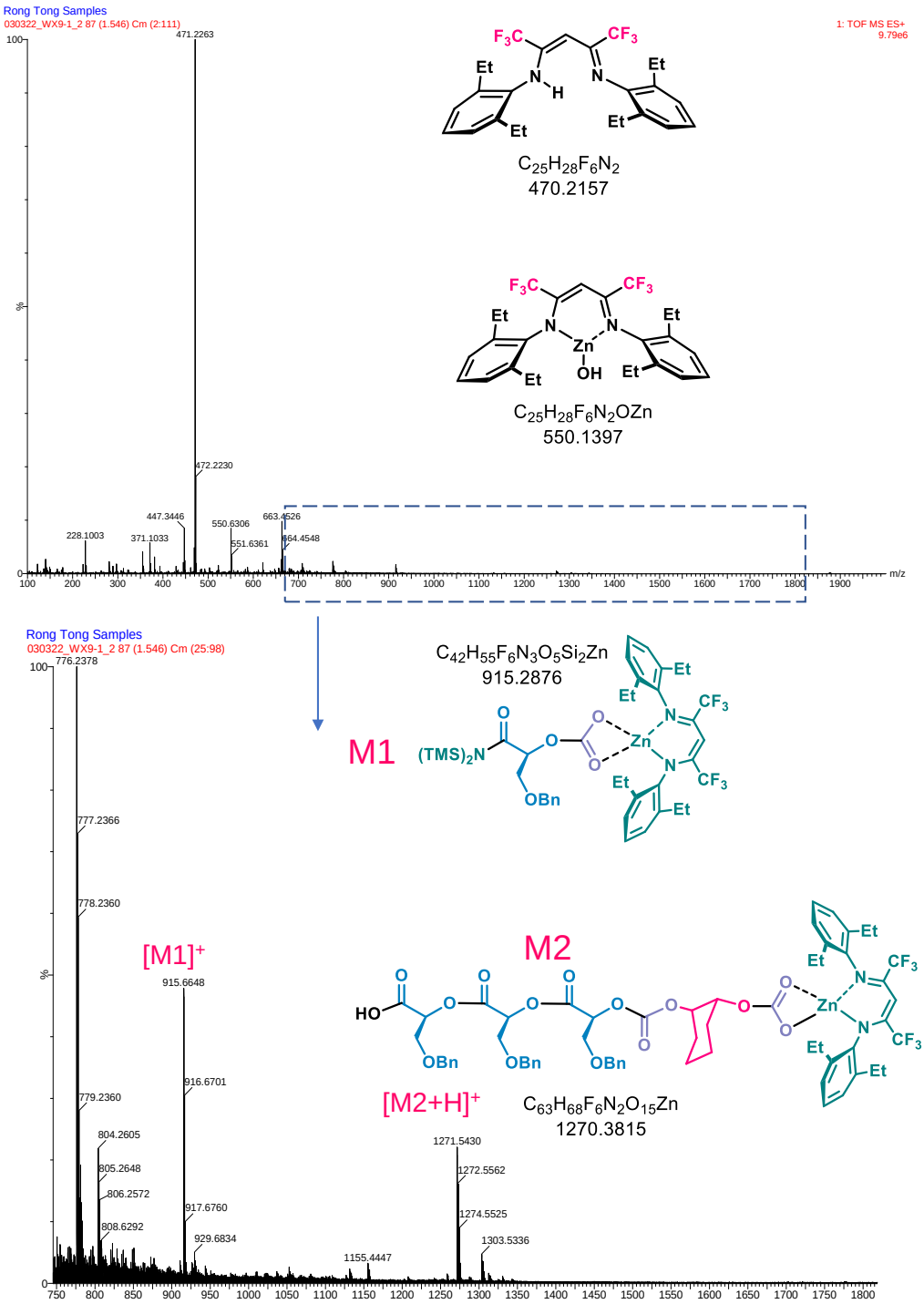

Figure 7.4 The ESI-MS spectra of the reaction mixture of L-**2**/CHO/**BDIZn-7** ([L-**2**]/[CHO]/[**BDIZn-7**] = 3/3/1). The data showed the plausible existence of the Zn-activated OCA monomer (**M1**, corresponding to **IM3** in Figure 7.3a) as we proposed in Figure 7.3, and the BDI-Zn complex stayed at the chain-end for polycarbonate enchainment (**M2**, corresponding to **IM11** in Figure 7.3a).

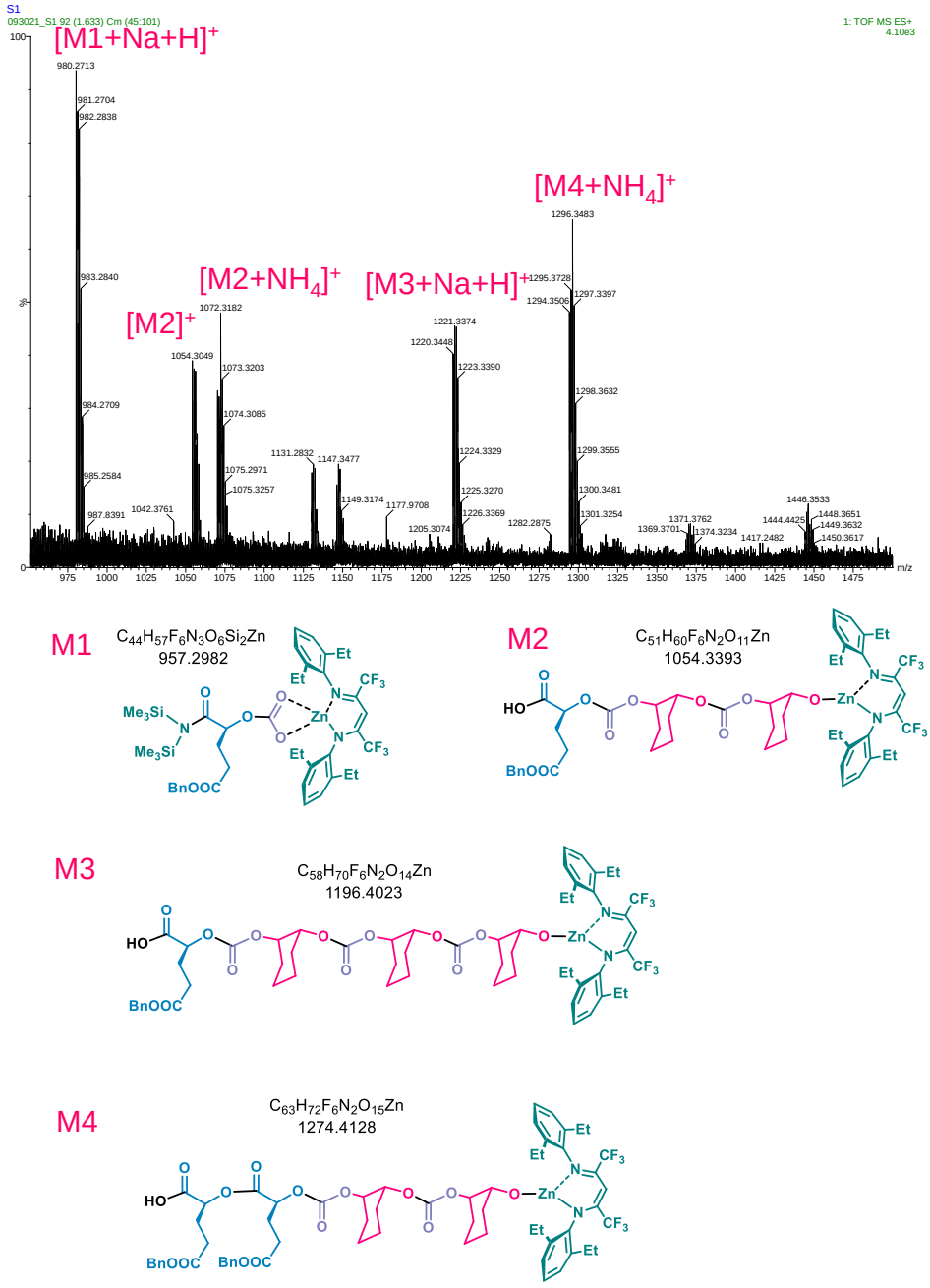

Figure 7.5 The ESI-MS spectra of the reaction mixture of L-**3**/CHO/**BDIZn-7** ([L-**3**]/[CHO]/[**BDIZn-7**] = 3/3/1). [The results confirmed the plausible existence of activated OCA monomer as shown in Figure 7.3a. Notably, the polymerization of L-**3** did not proceed perfectly compared with that of L-**2**. Indeed, the ROP of L-**3** in the first stage was slower than that of L-**2**, which could give rise to various oligomers as seen in this ESI-MS spectrum. The Zn-alkoxides (**M2**, **M3**, **M4**) correspond to **IM10** in Figure 7.3a.]

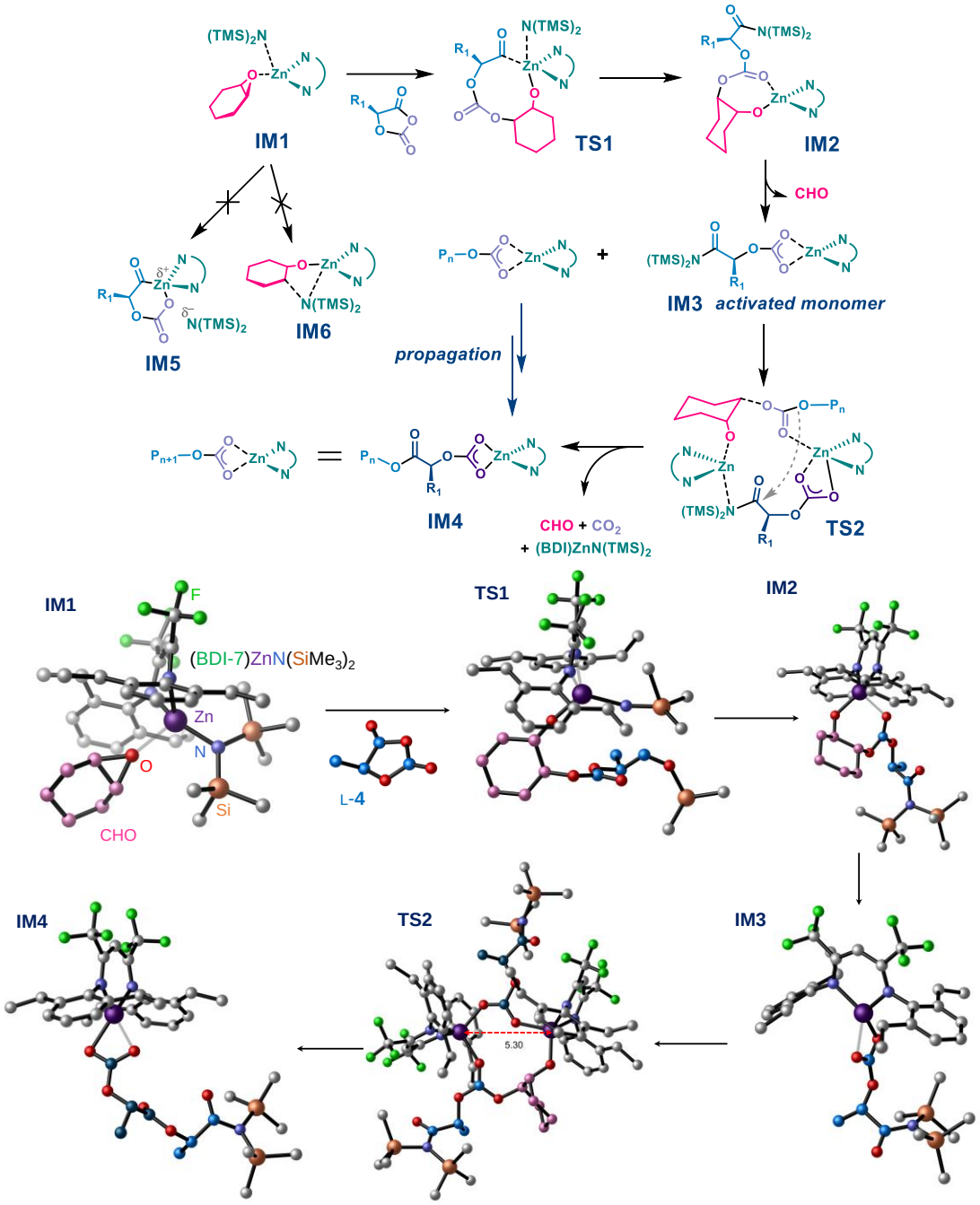

Figure 7.6 DFT computed intermediate states in Cycle I (ROP of OCA) via the activated monomer mechanism. We note that TMS group migration occurred in **TS1** based on computation, which has been previous observed.[15] In our NMR studies (Figure 7.2, we did not find such intermediate compounds, presumably due to the rapid reaction through such intermediate state.

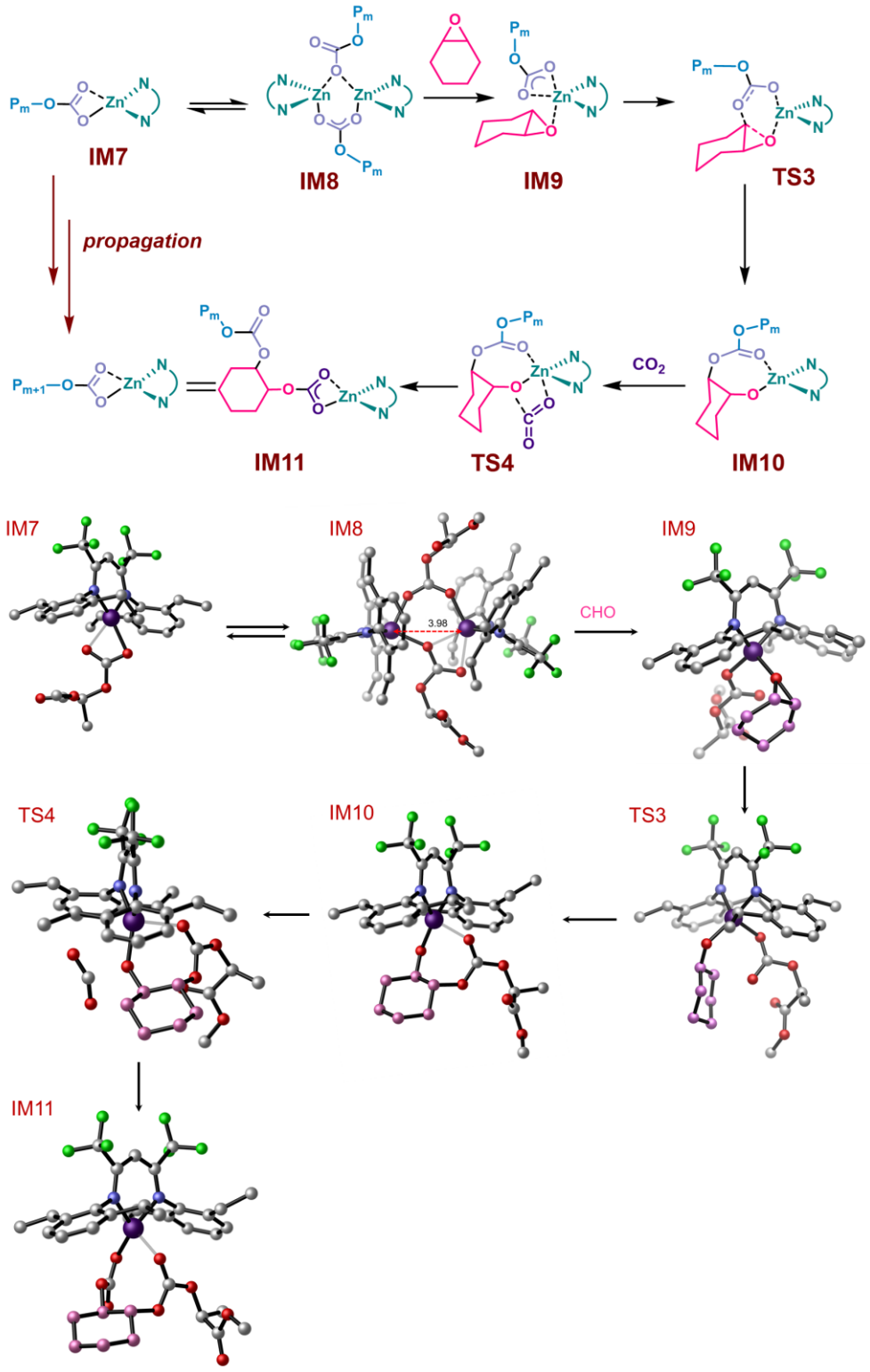

Figure 7.7 DFT computed intermediate states in Cycle II (ROCOP of CHO/CO_2) after the OCA is consumed up.

7.3 Instruments and methods

7.3.1 Electrospray ionization mass spectrometry (ESI-MS)

The ESI-MS analysis of air-sensitive samples followed the literature.[16] In brief, in a glove box, a 100 μL aliquote of the sample containing air-sensitive Zn complex were taken up into the 250 μL Hamilton gastight syringe. The syringe was punched into a 1 mL LC sampler vial capped with rubber septum to avoid the contact between needle and air, and was sealed in a zip bag. The zip bag was removed from the glove box and immediately analyzed by ESI-MS (Agilent 6220 Accurate-Mass Time-of-Flight LC/MS).

7.3.2 The NMR measurement of polymerization kinetics and monomer conversions in the copolymerization of OCA L-2 and CHO

In a glove box, the OCA L-**2** (120.3 mg, 0.542 mmol, 300 equiv.) was mixed with CHO (53.18 mg, 0.542 mmol, 300 equiv.), **BDIZn-7** (53.8 μL of 35 mg/mL in toluene-d8, 1.80 μmol, 1 equiv.) and toluene-d8 (579.2 μL) in the NMR tube. The NMR tube was further sealed by parafilm and was taken out of the glove box for ^{1}H NMR measurement. The peak at 4.21 ppm is assigned as the α-proton in L-**2**; the peak at 5.41 ppm corresponds to the α-proton in poly(L-**2**) (see Figure S3); The peak at 2.76 ppm is assigned as the α-proton in CHO; the peak at 4.79 ppm corresponds to the α-proton in poly(CHC) (see Figure 6.5). The polyether peak of homopolymerization of CHO was reportedly around 3.46 ppm, which was not found in our studies.[17, 18] The CH peaks in five-membrane cyclohexene carbonate was reportedly around 4.02 pm,[19] which was not found in our studies except in the overnight reaction of L-**1**/CHO (See Figure 6.11). The individual monomer conversion was determined by the integrated area ratios of corresponding protons between the monomer and the polymer.

All the catalysts' concentrations were varied. For zero-ordered reactions, reaction rate is

$$\text{rate} = -\mathrm{d}[\mathbf{OCA}]/\mathrm{d}t = k_{app}\,[\mathbf{OCA}]^0 = k_{app} \qquad (4)$$

where k_{app} is the apparent zero-order rate constant. Thus [**OCA**] versus t showed a linear relationship (examples see Figure 7.1).

The semi-logarithmic plots were drawn for first-ordered reactions to calculate the kinetic constants and reaction orders according to the kinetic laws:

$$\text{rate} = -\mathrm{d}[\mathbf{CHO}]/\mathrm{d}t = k_{app}\cdot[\mathbf{CHO}] \qquad (5)$$

where k_{app} is the apparent rate constant. Eq. 5 equals to

$$\ln[\mathbf{CHO}]_0/\ln[\mathbf{CHO}]_t = k_{app}\cdot t + C \qquad (6)$$

thus $\ln[\mathbf{CHO}]_0/\ln[\mathbf{CHO}]_t$ versus t was plotted (examples see Figure 7.1).

7.3.3 Computation method

All geometry optimizations were performed using the B3LYP functional[20, 21] with a mixed basis of LANL2DZ for Zn[22] and 6-31G(d) for other atoms with Grimme's general dispersion correction D3[23] using the Gaussian 16 program.[24] The harmonic vibrational frequency analyses were performed on all structures, including intermediate (all real frequencies) and transition states (one imaginary frequency) at the same level of theory. Single-point energies were calculated using ωB97M-V functional[25] with the def2-TZVP basis set[26] using ORCA 5.0.[27, 28] Solvation effects were all considered in the geometry optimization and energy calculation using the SMD model in THF.[29] The reported Gibbs free energies were gained by adding the single-point energies and the Gibbs free energy corrections at 298.15 K and a standard-state concentration in solution of 1 M. We note that ωB97M-V has been formulated by "training" with an extensive set

of main-group and transition-metal molecular properties with remarkable accuracy compared with many other DFT functionals.[30, 31] The geometry of the structures were rendered by CYLView.[32]

7.4 Conclusions

Mechanistically, four distinctive features in our newly discovered auto-tandem polymerization contribute to this highly efficient chemistry. First, the unique monomer-activation mechanism of OCA with low activation energy barrier ensures the rapid initiation of OCA polymerization. Second, the zero-order kinetics in OCA polymerization significantly suppresses the tapering effect and enables a clean mechanism switch. Third, the distinctive ROP mechanism of OCA that involves but does not consume bystander co-monomer allows for a smooth transition to the second polymerization cycle; whereas conventional metal-alkoxide-mediated polymerization could lead to undesired chain termination during the transition. Fourth, the highly active electron-deficient Zn complex allows for the entire polymerization undergoing at room temperature without pressured gas. As previous attempts that rationalize the distinct mechanism selection behavior by a single catalyst focused on the free energy difference between different polymerization cycles, our findings are important because we reveal such selectivity results both from the low activation barriers and from the beneficial zero-order kinetics at the first stage of the polymerization. The principles described herein provide a new perspective on other polymerization systems concerning sequence control and block resolution.[12]

7.5 Computational results

Cartesian coordinates of structures

CO_2

C	0.00000000	0.00000000	0.00005200
O	0.00000000	0.00000000	1.16892100
O	0.00000000	0.00000000	-1.16896000

BDIZn-7

Zn	-0.04058300	0.45470200	-0.08888800
Si	0.26053100	3.29811000	-1.53460600
Si	-0.69853800	3.27309600	1.36294000
N	-1.47358600	-1.13758700	-0.22428800
N	1.59263900	-0.89219800	-0.10415500
N	-0.22680600	2.44484100	-0.09555400
C	-1.10300200	-2.36537800	-0.53828200
C	0.21805500	-2.83524000	-0.67322800
C	1.42871300	-2.17343600	-0.39974700
C	-2.18207100	-3.45052600	-0.76484000
C	2.66974800	-3.09208800	-0.46685400
C	-2.83492400	-0.74255500	0.02064100
C	-3.58411000	-0.15372200	-1.02554900
C	-4.87005300	0.31790100	-0.73344400
C	-5.39719000	0.22486600	0.55287300
C	-4.63657300	-0.33434100	1.57786500
C	-3.34410300	-0.81946000	1.33978700
C	-3.00076700	-0.04921500	-2.42475200
C	-3.74414600	0.86593400	-3.40169800
C	-2.49775300	-1.40297500	2.46103400
C	-3.04605100	-1.23250200	3.88043800
C	2.84392400	-0.33184300	0.34130200
C	3.09138400	-0.29278100	1.73865900
C	4.24213500	0.35850600	2.19258700
C	5.12517900	0.96714100	1.29965000
C	4.86697700	0.92273900	-0.06561200
C	3.73003000	0.27489700	-0.57489500
C	2.12224300	-0.95847100	2.70394800
C	2.43780000	-0.81101100	4.19435900
C	3.48670200	0.27225600	-2.07589300
C	4.69850600	-0.15140500	-2.92174500
C	-0.89638700	4.73996400	-1.98568500
C	0.23862200	2.14021200	-3.04275900
C	2.01555200	4.02871400	-1.41374400
C	-2.52923600	3.78803300	1.35068600
C	-0.44997900	2.15800000	2.88070500
C	0.31859300	4.84223800	1.71877100
H	0.31216200	-3.86893000	-0.95631600
H	-5.46598200	0.76884500	-1.52006300
H	-6.39744100	0.59708500	0.75892400
H	-5.05277500	-0.38738200	2.57838100
H	-2.93673000	-1.05371500	-2.86062500
H	-1.96170300	0.29151700	-2.34337000
H	-3.82493300	1.89055300	-3.01968400
H	-4.75656000	0.50478100	-3.61567800
H	-3.20505000	0.90518100	-4.35519500
H	-2.33867100	-2.47109600	2.27199200
H	-1.49620400	-0.95504400	2.41421300
H	-3.20464200	-0.17789800	4.13464100
H	-2.33394300	-1.64666800	4.60325300

H	-3.99698600	-1.75944600	4.01895800
H	4.45371100	0.39509600	3.25609200
H	6.01151200	1.47436400	1.67182900
H	5.55682100	1.39981600	-0.75627000
H	2.06136100	-2.02671400	2.46331200
H	1.11265600	-0.56691800	2.51882500
H	2.46533300	0.23904900	4.50794600
H	3.40007700	-1.26667500	4.45492200
H	1.66429800	-1.31380800	4.78593300
H	3.18509300	1.28218100	-2.38579900
H	2.64440300	-0.38228700	-2.31165700
H	5.53785600	0.54402700	-2.81411800
H	4.42543500	-0.17222300	-3.98358800
H	5.05145700	-1.14925700	-2.64241800
H	-0.91585300	5.52688300	-1.22157300
H	-1.92833400	4.39710300	-2.13627100
H	-0.56734000	5.20977500	-2.92351200
H	0.72976400	1.17464400	-2.86555100
H	0.75883300	2.60797400	-3.88992300
H	-0.78810500	1.93655300	-3.37136600
H	2.05867100	4.86286100	-0.70236200
H	2.35386500	4.41327000	-2.38626400
H	2.74780000	3.28259300	-1.07941300
H	-2.81260000	4.28141600	2.29107100
H	-3.18951900	2.92009200	1.22175400
H	-2.74908300	4.48766800	0.53408400
H	-0.78051900	2.67586000	3.79155400
H	0.60761500	1.90027100	3.02415800
H	-1.02398900	1.22362800	2.82507100
H	-0.00745300	5.28978800	2.66832000
H	0.20923100	5.61307500	0.94620100
H	1.38850000	4.61660800	1.81469000
F	-3.07900400	-3.08088800	-1.70300900
F	-1.66730300	-4.62719900	-1.17570700
F	-2.87532900	-3.70888700	0.36551500
F	2.37163700	-4.36487300	-0.79832100
F	3.55487900	-2.65658000	-1.38847000
F	3.31677700	-3.14874500	0.71725600

CHO

O	1.52652400	0.03355100	0.78306800
C	0.99118100	0.83165000	-0.29842000
C	1.09177300	-0.63531600	-0.41563700
H	1.90964800	-1.05171300	-1.00844800
H	1.75148000	1.43805700	-0.79426200
C	-0.13507500	-1.51169300	-0.28768700
C	-0.33769900	1.51962200	-0.02965500
C	-1.54964000	0.58043400	-0.17207700
C	-1.28841300	-0.80246100	0.43879200
H	0.13588400	-2.44335400	0.22739700
H	-0.45115300	-1.79446200	-1.30235900
H	-2.19180900	-1.42137100	0.37858700
H	-1.04304700	-0.69782000	1.50337600
H	-1.78434000	0.45385400	-1.23883900
H	-2.42999000	1.04492400	0.28878300
H	-0.44186800	2.36980400	-0.71512400
H	-0.29975800	1.94025400	0.98445200

L-**4** OCA

C	0.68283900	0.85842900	0.09207900

C	0.80052200	-0.60661600	0.46403700
O	-0.56911800	-1.07186100	0.35608300
O	1.52622300	1.70322900	0.01777800
C	1.72624800	-1.39346400	-0.44920900
O	-0.64990500	1.09934400	-0.18178000
C	-1.37647200	-0.06919100	-0.01922200
O	-2.55509700	-0.14113600	-0.19676100
H	1.10177400	-0.69481500	1.51291200
H	1.41300000	-1.30643800	-1.49429300
H	1.72612800	-2.44749700	-0.15846900
H	2.74345800	-1.00280300	-0.34881800

IM1

O	0.68366900	-0.08365000	2.00010000
C	1.53554800	0.28041900	3.14696600
C	1.49305200	-1.09623200	2.69833900
C	2.95804400	0.70255900	3.41890800
H	0.86648500	0.52470500	3.97122700
C	1.34321500	-2.02977100	3.87312000
H	2.30477100	-1.38464500	2.03289000
C	3.20178800	-0.24544700	4.66332400
H	3.63564000	0.47183600	2.59264200
H	3.09237000	1.74960600	3.70926500
C	2.76020900	-1.74987000	4.52101000
H	1.24047500	-3.09256600	3.63019400
H	0.52692800	-1.73996500	4.54173000
H	4.26608400	-0.22816300	4.92412300
H	2.67150600	0.19215700	5.51901100
H	2.79999600	-2.21235800	5.51384300
H	3.50665100	-2.27345500	3.91005700
Zn	-0.23818800	0.57271300	0.07925200
N	1.30837800	-0.16530300	-1.15934500
N	-1.52655500	-1.03326400	-0.51466200
C	0.90847800	-0.62787000	-2.34263200
C	-1.41500700	-1.44616600	-1.76440700
C	-2.52843100	-1.53803600	0.39575300
C	-0.36107000	-1.13002200	-2.65450900
C	1.89214200	-0.57950600	-3.53229000
C	-2.47939400	-2.39486000	-2.36814500
C	-2.24525800	-2.70187100	1.14802500
C	-3.72234400	-0.80741500	0.59693700
H	-0.51632900	-1.40870900	-3.68243600
F	2.93015100	-1.43326300	-3.40392400
F	2.40906000	0.66407700	-3.64828200
F	1.30111900	-0.86586200	-4.70864000
C	-3.19219500	-3.13562900	2.08339500
C	-0.93280400	-3.44394200	0.95763100
C	-4.63439300	-1.28405300	1.54599300
C	-4.00176900	0.45332900	-0.20237100
C	-4.37873400	-2.43707400	2.28209500
H	-3.00024300	-4.03169600	2.66369100
H	-0.79682600	-3.67186100	-0.10397800
H	-0.11226400	-2.76152200	1.21443100
H	-5.56177300	-0.74640200	1.70945300
H	-3.18825400	1.16764000	-0.02381500
H	-3.94839500	0.21203300	-1.27011600
H	-5.10300000	-2.78939200	3.01182500
F	-2.40606000	-3.62291300	-1.80944700
F	-3.73407300	-1.94262300	-2.18502000
F	-2.32446800	-2.56320600	-3.69700600

C	2.69425600	-0.15481400	-0.77263200
C	3.31159100	-1.39600800	-0.44531200
C	3.39686200	1.05686700	-0.60086300
C	4.62442000	-1.38711300	0.03478300
C	4.70891200	1.01112300	-0.10484700
C	5.32565800	-0.19317400	0.20846800
H	5.10956500	-2.32607200	0.28026000
H	5.25040700	1.94421400	0.02936700
H	6.34559400	-0.20795300	0.58374900
C	-0.76527700	-4.74224800	1.75376600
H	-1.53922100	-5.47505200	1.49937200
H	0.20623200	-5.19564200	1.52719500
H	-0.80768700	-4.57254400	2.83589200
C	-5.34213100	1.14067700	0.07696500
H	-5.44204200	2.02989200	-0.55372300
H	-6.19280000	0.48378500	-0.13927000
H	-5.42541500	1.46860200	1.11984200
C	2.79843600	2.40877200	-0.93727600
H	2.72396500	3.00692000	-0.01848600
H	1.77739100	2.28024000	-1.29519800
C	3.60197500	3.20046300	-1.98459600
H	3.11065300	4.15671700	-2.19636900
H	4.61803400	3.41941800	-1.63812400
H	3.68040500	2.64117100	-2.92104900
C	2.54930000	-2.70261300	-0.60545200
H	1.53771700	-2.56292700	-0.20994500
H	2.41061400	-2.90853500	-1.67289000
C	3.17770700	-3.94115000	0.04276300
H	3.34508500	-3.80435800	1.11835300
H	2.51349600	-4.80300200	-0.08399100
H	4.13919300	-4.20254200	-0.41282500
N	-0.93928700	2.42514500	0.29412200
Si	-1.16487900	3.05164900	1.90499900
Si	-1.16667200	3.42498900	-1.11968600
C	-1.90695300	1.73445700	3.06112800
H	-1.95618000	2.10918700	4.09233200
H	-2.93078000	1.48875000	2.75366200
H	-1.34245400	0.79661700	3.07096100
C	-2.36556200	4.52424500	2.03252300
H	-3.38525800	4.24847800	1.74054200
H	-2.40376300	4.85648100	3.07872200
H	-2.06659200	5.38909400	1.42993100
C	-2.95910600	4.00825700	-1.39329600
H	-3.63327100	3.15800800	-1.54929100
H	-3.35678800	4.60001100	-0.56340700
H	-3.00781200	4.63277500	-2.29551700
C	-0.09029400	4.99718200	-1.09192300
H	0.97507500	4.75803400	-0.99593100
H	-0.22064700	5.57411400	-2.01698200
H	-0.35221700	5.65918000	-0.25748800
C	-0.75584400	2.48969500	-2.72475000
H	-1.01854400	3.13198900	-3.57566400
H	0.29794300	2.21913800	-2.84423400
H	-1.34826300	1.57196800	-2.82732000
C	0.47511400	3.67565400	2.65109200
H	1.27426500	2.93004100	2.57054300
H	0.81723500	4.56935700	2.11405300
H	0.37087400	3.94727200	3.71012900

TS1

C	-2.68399500	-1.42250900	1.42990900	F	2.64100700	0.02380600	-3.91788700
O	-1.50689700	-2.20154500	1.63636600	F	4.31951100	0.95717700	-2.89753300
O	0.04475500	-3.60522900	0.89760700	F	2.90383000	2.17284000	-3.99650000
C	0.86051100	-3.22653500	2.06812100	F	1.31381200	4.77994500	0.86299800
C	1.62539300	-1.91334200	1.80849500	F	1.44719700	5.13698400	-1.26860000
Zn	0.21556500	0.02173800	0.06158600	F	-0.49299800	4.86708900	-0.34953000
C	-2.78079200	-0.84365000	0.01701900	N	1.85175100	0.12138500	-1.24114500
O	-4.01210700	-0.84829400	-0.49261700	N	0.24035600	2.10816600	0.29047300
C	-2.64038100	-0.31852000	2.47903800	C	2.11130100	1.21963700	-1.93255700
C	1.79747400	-4.41496500	2.27329000	C	1.62484900	2.50653300	-1.66925900
C	2.75957300	-4.16391900	3.44243300	C	0.86434700	2.90670700	-0.55117100
C	3.54741000	-2.86529200	3.22478400	C	3.00579400	1.09970900	-3.18238100
C	2.59567000	-1.68669100	2.98768500	C	0.78570100	4.42822200	-0.32994200
O	0.80749700	-0.79868500	1.66414500	C	2.75194800	-0.98904500	-1.23758800
H	-3.54668400	-2.07441100	1.58583800	C	2.33274400	-2.23930700	-1.73926600
H	0.19052000	-3.10252900	2.92333800	C	3.20463100	-3.32813600	-1.62103500
H	2.23393500	-2.10712100	0.91462400	C	4.44842700	-3.18962300	-1.00614000
H	-3.49076900	0.35828400	2.36305900	C	4.82693300	-1.95968200	-0.46821800
H	-2.67582600	-0.76133500	3.47892400	C	3.98470400	-0.84591000	-0.55393500
H	-1.71033800	0.24405900	2.37712500	C	0.95075200	-2.37887000	-2.34463700
H	1.20371400	-5.32230200	2.43779500	C	0.50070300	-3.80117200	-2.67762200
H	2.37106600	-4.56448200	1.34859400	C	4.30591000	0.45966400	0.15416200
H	3.43798100	-5.01920000	3.55262300	C	5.47503200	0.41887500	1.14044900
H	2.18612400	-4.09024800	4.37812800	C	-0.38281700	2.56923100	1.50195700
H	4.20084200	-2.66430200	4.08398400	C	0.38974100	2.53937900	2.68934700
H	4.19989900	-2.98299500	2.34786400	C	-0.23543600	2.86647400	3.89516500
H	3.15587200	-0.76866600	2.77954500	C	-1.59002200	3.20555400	3.93484100
H	1.99578900	-1.49309400	3.88925800	C	-2.33407300	3.22197900	2.76029000
C	-1.16033500	-3.09566900	0.69694800	C	-1.75046400	2.90257800	1.52471900
O	-1.86361600	-3.43053000	-0.23966000	C	1.84419000	2.12323400	2.61014900

C	2.61255500	2.08663300	3.93106400
C	-2.60661000	2.86623000	0.27460600
C	-3.49586900	4.09985200	0.06711000
H	1.92274600	3.28411500	-2.35294300
H	2.90795500	-4.29901100	-2.00333400
H	5.11377000	-4.04560300	-0.92667400
H	5.77867400	-1.87622700	0.04622600
H	0.89810300	-1.75740700	-3.24626500
H	0.22485700	-1.94115200	-1.64498000
H	0.48258700	-4.42774700	-1.78049500
H	1.15373000	-4.27151000	-3.42246700
H	-0.51359400	-3.78226400	-3.08847800
H	4.49591800	1.24877600	-0.58215300
H	3.39907600	0.77112600	0.68380000
H	5.32944500	-0.34748700	1.91053900
H	5.56769300	1.38806400	1.64416000
H	6.42928300	0.21663600	0.63976900
H	0.33576300	2.85215300	4.81775600
H	-2.06143000	3.45115900	4.88319100
H	-3.39048400	3.47361500	2.79820400
H	2.36568600	2.78537400	1.90774500
H	1.85467400	1.12223600	2.16264300
H	2.16474900	1.37857300	4.63843800
H	2.65254200	3.07013900	4.41551300
H	3.64430400	1.76322900	3.74997100
H	-3.24410200	1.97321900	0.31277600
H	-1.96723600	2.73531800	-0.59920300
H	-4.23634900	4.21224300	0.86677800
H	-4.04469100	4.01403200	-0.87814200
H	-2.89746900	5.01581400	0.03326500
N	-1.81518900	-0.32308500	-0.66074200
Si	-2.28149900	0.03312800	-2.40091300
C	-0.82361700	0.77587300	-3.31335900
H	-1.16248300	0.98747700	-4.33748900
H	-0.51285400	1.72796200	-2.87358500
H	0.05184400	0.12992800	-3.38235900
C	-2.75443900	-1.63170800	-3.16180100
H	-2.42646200	-2.45420600	-2.51766200
H	-3.83835200	-1.72206100	-3.29523100
H	-2.28278400	-1.75481500	-4.14482900
C	-3.65750100	1.31954400	-2.57291100
H	-3.24747000	2.33539500	-2.56331700
H	-4.14508300	1.17462700	-3.54718300
H	-4.42737000	1.24790100	-1.80269700
Si	-5.54883200	-1.57358900	-0.16476100
C	-6.56507200	-0.99170600	-1.62339800
H	-7.57956600	-1.40799000	-1.57097500
H	-6.65077900	0.10096900	-1.64213300
H	-6.11857400	-1.31425600	-2.57137400
C	-5.32718400	-3.43938900	-0.11688400
H	-4.26578000	-3.70608500	-0.16983600
H	-5.74321500	-3.87026100	0.80192400
H	-5.83356900	-3.90901800	-0.96902000
C	-6.19118700	-0.85529300	1.44551800
H	-5.61653200	-1.18607500	2.31815400
H	-6.17424000	0.24138300	1.42058000
H	-7.23307800	-1.16706400	1.59920000

IM2

O	0.76007500	0.25170700	2.20279100

C	-0.27484500	-0.48785200	2.75777100
C	-1.24636200	-1.08052900	1.72024800
C	0.22831300	-1.64447300	3.65108900
H	-0.88797000	0.17837400	3.39743800
C	-2.40287300	-1.85815700	2.34459400
H	-0.70173400	-1.71316200	1.01132300
C	-0.90950400	-2.44251300	4.30395600
H	0.83869600	-2.31714800	3.03115100
H	0.89674400	-1.21629900	4.40808500
C	-1.87290800	-2.98837800	3.24053000
H	-3.04680700	-2.25555200	1.55156000
H	-3.01076900	-1.16729100	2.94446500
H	-0.50031500	-3.26582000	4.90340000
H	-1.46386000	-1.79391200	4.99789300
H	-2.71725700	-3.50811600	3.70967400
H	-1.34984000	-3.73022000	2.62020100
O	-1.86649800	0.00722700	0.94058300
C	-1.30217800	0.43135700	-0.16996400
O	-0.20428500	0.08703400	-0.61935800
Zn	1.62955400	-0.04364500	0.51055200
N	2.76340100	1.61580300	-0.11451000
N	2.80814400	-1.42878400	-0.52572200
C	3.89153000	1.45601400	-0.78198000
C	3.92904800	-1.06442700	-1.12755400
C	2.36949400	-2.79039000	-0.38243100
C	4.43392200	0.24185700	-1.24975100
C	4.74376400	2.69786200	-1.12512900
C	4.82726100	-2.14867200	-1.76579000
C	2.72366400	-3.49377700	0.79356600
C	1.47899200	-3.33806700	-1.33559900
H	5.36881400	0.32798600	-1.77516900
F	5.04651000	3.41598800	-0.02290800
F	4.09688200	3.52176900	-1.97803800
F	5.91947700	2.38888700	-1.71076800
C	2.20856100	-4.78430300	0.97101900
C	3.61703100	-2.83488300	1.83331800
C	0.99193500	-4.63234200	-1.10986200
C	1.06123900	-2.52484400	-2.55118100
C	1.35618100	-5.35337300	0.02607000
H	2.47284800	-5.35053900	1.85816000
H	4.56234600	-2.54484600	1.36166000
H	3.14745500	-1.89001000	2.14365000
H	0.31485600	-5.08177700	-1.82883700
H	0.66774500	-1.56172800	-2.20399800
H	1.95302700	-2.27933100	-3.13875400
H	0.96769400	-6.35700200	0.17960200
O	-2.00677000	1.33969600	-0.83162300
C	-3.39517900	1.58643300	-0.49104500
H	-3.44904800	1.80440100	0.57203700
C	-3.79968200	2.80094800	-1.32158300
H	-3.71012900	2.58201200	-2.39067400
H	-4.83361200	3.08559100	-1.11217000
H	-3.15144800	3.64877700	-1.07945600
C	2.24965600	2.89700200	0.29629100
C	2.49253200	3.32306800	1.62634600
C	1.40989500	3.63076400	-0.57013500
C	1.91056700	4.51973900	2.05452300
C	0.84187100	4.81963700	-0.08601500
C	1.09066300	5.26656100	1.20701200
H	2.09145000	4.87257300	3.06458300

H	0.19026000	5.39834700	-0.73494700
H	0.64257100	6.19189900	1.56059500
C	0.02782300	-3.17510300	-3.47479200
H	-0.20725200	-2.49378300	-4.30045600
H	0.39674400	-4.10993400	-3.91338800
H	-0.91009500	-3.39351800	-2.95052300
C	3.92740300	-3.66399300	3.08185500
H	4.45643100	-4.59170800	2.83375800
H	4.57011600	-3.08744800	3.75684900
H	3.02046800	-3.93087000	3.63679300
C	3.34395600	2.47030300	2.55255100
H	2.83162800	1.50675000	2.68291100
H	4.29653500	2.24634600	2.05803100
C	3.63612100	3.06054400	3.93481700
H	2.71947300	3.22087000	4.51441800
H	4.26848300	2.37026300	4.50517400
H	4.16655300	4.01820900	3.86862600
C	1.06906100	3.15234400	-1.97367600
H	0.05391900	2.73361300	-1.95961500
H	1.72479100	2.32531800	-2.25318000
C	1.14446100	4.23377600	-3.06240900
H	0.93132100	3.79237500	-4.04345600
H	0.41629600	5.03658200	-2.90250200
H	2.14025300	4.68795100	-3.10518400
C	-4.22127300	0.33187300	-0.85470700
O	-3.65586300	-0.57232200	-1.47074800
F	5.91467900	-1.63995600	-2.38011300
F	5.28520000	-3.02154200	-0.84080700
F	4.16744400	-2.86971600	-2.69700100
N	-5.57345900	0.29403200	-0.58129700
Si	-6.47481200	1.09674400	0.77548500
Si	-6.38332900	-0.98095700	-1.63353400
C	-5.38900000	2.08682000	1.96391100
H	-4.57381800	1.50282200	2.40580200
H	-4.97493800	3.00937600	1.54365800
H	-6.04910300	2.38408500	2.79122000
C	-7.77380400	2.28397500	0.09420400
H	-8.60932600	1.78091100	-0.40106300
H	-8.18851700	2.87508600	0.92188600
H	-7.33452600	2.98920100	-0.62268600
C	-7.24492200	-0.26281900	1.83735800
H	-7.81299600	0.19997400	2.65576000
H	-7.92843200	-0.93057500	1.30505700
H	-6.46046400	-0.88009000	2.29381900
C	-8.25230100	-0.67864800	-1.65674900
H	-8.75622400	-0.70428300	-0.68648100
H	-8.50532300	0.26663800	-2.15103700
H	-8.69175000	-1.48243100	-2.26456100
C	-5.85184500	-0.78027700	-3.43499700
H	-4.87456300	-1.22147200	-3.64394300
H	-6.59580900	-1.26153500	-4.08409800
H	-5.81241900	0.27920600	-3.71972000
C	-6.05967000	-2.71369500	-0.96434800
H	-4.98990600	-2.94520300	-0.96014100
H	-6.43862600	-2.82943200	0.05865800
H	-6.56648800	-3.46129900	-1.58945700

IM3

Zn	1.08657600	-0.15222200	0.08242000
N	3.05417700	-0.70546700	-0.00354800

N	1.36119500	1.89234400	0.02633500	C	3.38389700	-2.88681200	1.10775500
C	3.98941500	0.23125600	0.01015600	C	3.42379600	-4.12677000	-1.42063700
C	2.59622200	2.36916400	0.03821700	C	3.50092600	-4.27991500	0.98558900
C	0.17117200	2.70268600	0.01559200	C	3.52918700	-4.89603100	-0.26066800
C	3.79271500	1.62487900	0.03896400	H	3.43137800	-4.61990000	-2.38698000
C	5.46967900	-0.20549200	0.01784700	H	3.55907800	-4.88708700	1.88474300
C	2.80489400	3.90122300	0.05324200	H	3.62081600	-5.97674500	-0.33261800
C	-0.41604600	3.03471100	-1.22682800	C	-0.51731500	2.92976300	-3.81262400
C	-0.45724400	3.00934100	1.24405300	H	-0.62328700	4.01273600	-3.94625800
H	4.69491800	2.21128000	0.05619900	H	0.03410400	2.54309700	-4.67717600
F	5.77432900	-0.96186700	-1.05731000	H	-1.51944800	2.48598900	-3.83315000
F	5.75179900	-0.93519700	1.11815000	C	-0.67649700	2.79562200	3.81594300
F	6.32853900	0.83271700	0.01266500	H	-0.14919500	2.39834500	4.69072000
C	-1.61439600	3.75892700	-1.21201700	H	-0.84506700	3.86460500	3.99064900
C	0.23492800	2.58410400	-2.52523900	H	-1.65313200	2.30003500	3.76350500
C	-1.65565000	3.73305500	1.20370400	C	3.29634700	-2.25999900	2.49057200
C	0.15485400	2.54314900	2.55574600	H	2.31831400	-2.51417900	2.92457100
C	-2.22358000	4.11687700	-0.01009900	H	3.31553200	-1.17048500	2.40716400
H	-2.08162500	4.04213300	-2.14927300	C	4.39525300	-2.70270500	3.46947100
H	1.24610600	3.00217000	-2.58492300	H	4.27240300	-2.18771500	4.42969200
H	0.37468100	1.49462500	-2.48038200	H	4.35990500	-3.77925000	3.66870200
H	-2.15417600	3.99667600	2.13053400	H	5.39131000	-2.46510600	3.08183900
H	0.35428200	1.46500100	2.48164300	C	3.13243300	-1.88579800	-2.60465800
H	1.13894600	3.01073100	2.67891100	H	2.21822300	-1.28456300	-2.49825400
H	-3.15007500	4.68510400	-0.01980600	H	3.95159900	-1.15833200	-2.65131500
F	2.26968600	4.48696100	-1.03860500	C	3.06877300	-2.64226300	-3.93357700
F	2.23009600	4.46905400	1.13434700	H	2.23013100	-3.34765300	-3.96291100
F	4.10481300	4.25576300	0.08010500	H	2.93321800	-1.93131100	-4.75645700
C	3.30381400	-2.12409000	-0.07643300	H	3.99021400	-3.20279400	-4.12984600
C	3.29593000	-2.73608800	-1.35484900	C	-4.27975500	-1.87623800	-1.10401900

C	-2.85152200	-2.44946200	-1.04657700
O	-2.15861700	-2.09001100	0.17066000
O	-4.87861100	-2.09335300	-2.15744000
C	-2.79107800	-3.96157100	-1.23719000
C	-1.00848500	-1.40748600	0.08650500
O	-0.41310900	-1.16768700	1.18396900
H	-2.33602900	-1.95830900	-1.87517600
H	-3.25182800	-4.49293100	-0.39950200
H	-1.74829400	-4.28377600	-1.32650400
H	-3.31918900	-4.22816700	-2.15640000
O	-0.53371700	-1.01940300	-1.02576700
N	-4.78165500	-1.04665000	-0.11457200
Si	-5.82102500	0.27935100	-0.81108600
Si	-4.75939400	-1.41925500	1.65831000
C	-5.77667900	1.75217900	0.37663800
H	-6.37829800	2.55768000	-0.06774500
H	-6.17906300	1.56854200	1.37695800
H	-4.75544200	2.13727700	0.48537900
C	-5.03814200	0.91611100	-2.40740300
H	-5.52424300	1.86014700	-2.68902800
H	-3.97115600	1.13158100	-2.26457700
H	-5.13653800	0.21892800	-3.24315200
C	-7.60239300	-0.26799500	-1.10420000
H	-8.11338200	-0.53899200	-0.17309100
H	-8.17492500	0.54493300	-1.57142600
H	-7.63822400	-1.13318500	-1.77534400
C	-6.53366700	-1.24426700	2.30283300
H	-7.20071500	-1.96384200	1.81168500
H	-6.53106300	-1.48640700	3.37492600
H	-6.97753400	-0.24992400	2.20090600
C	-4.34145700	-3.23060100	1.99204000
H	-4.60111000	-3.44500300	3.03799800
H	-4.94187900	-3.90724400	1.37089300
H	-3.28577000	-3.47248100	1.85465100
C	-3.62459500	-0.25528200	2.61197700
H	-2.57888500	-0.37428700	2.30921500
H	-3.90710000	0.79371200	2.46668200
H	-3.69124200	-0.47025200	3.68738200

TS2

Zn	2.14832200	-2.22530300	-0.09745900
Zn	-1.54721600	1.57521700	-0.13089800
N	-2.46294800	2.84679400	-1.49311700
O	1.03746500	-0.46830600	0.04114500
C	1.29233200	0.75285900	0.16614100
O	0.46138200	1.70259200	-0.02005800
O	-2.60936300	-2.46924800	-1.24117300
C	-2.85837100	-1.22773900	-0.90156100
O	0.78015900	-3.56999100	-0.26596700
C	-0.58056300	-3.35590200	-0.07408600
C	-1.18748900	-2.90495100	-1.42611500
H	-0.64890300	-2.02972700	-1.78874000
H	-0.78558000	-2.55123700	0.65596600
C	-1.22443500	-4.01860400	-2.46552700
C	-1.27432300	-4.64075200	0.42493800
O	-1.98650400	-0.38191400	-0.67051100
C	-1.88031500	-5.30645300	-1.94235900
H	-0.18085100	-4.22240500	-2.72800100
H	-1.72064800	-3.66084300	-3.37625000
C	-1.24025900	-5.76284900	-0.62226400

H	-2.95538900	-5.13691700	-1.78839900
H	-1.79508600	-6.09226900	-2.70376600
H	-1.75612600	-6.65423700	-0.24140500
H	-0.19698000	-6.04947200	-0.80371300
H	-0.77555200	-4.95835300	1.34910800
H	-2.31914700	-4.41323100	0.68550100
C	4.83792900	-1.93588200	1.15403100
C	5.35126800	-1.49768500	-0.08276100
H	6.33117200	-1.05408400	-0.05100400
C	4.79775800	-1.67573000	-1.36137700
N	3.63142600	-2.42540700	1.37237900
N	3.57876600	-2.11296200	-1.64213600
C	5.84012900	-1.86703700	2.32154400
C	5.74640700	-1.31160400	-2.52033400
F	6.20659900	-3.10947400	2.71980100
F	5.32415700	-1.24135100	3.39519100
F	6.98241900	-1.21879600	2.00639000
C	3.16769800	-2.55517600	-2.94786100
C	3.41556200	-3.90789300	-3.30277400
C	2.40840300	-1.71302100	-3.78775500
C	2.91399800	-4.38162100	-4.51860800
C	1.91733400	-2.24081400	-4.99262400
C	2.16771000	-3.55705700	-5.36227100
H	3.09750400	-5.41080400	-4.80947700
H	1.32643800	-1.60505500	-5.64671800
H	1.77926200	-3.94586100	-6.30025800
C	2.09246700	-0.27105600	-3.42740000
H	1.02247400	-0.18961700	-3.18729700
H	2.62749800	0.00687200	-2.51676000
C	4.19026000	-4.81146700	-2.35788000
H	5.20489100	-4.41324900	-2.23259800
H	3.73084300	-4.74399300	-1.36395500
C	-3.86949500	2.73094800	1.24596900
C	-4.38359900	3.11292700	-0.00600000
H	-5.41021700	3.43627900	-0.00918500
C	-3.69885200	3.24618900	-1.22842100
C	-4.51282500	3.94547200	-2.33830500
C	-4.82042000	2.98416700	2.43279500
N	-2.67080400	2.22133000	1.48596600
C	-1.73920400	3.23677500	-2.67854300
C	-1.67863000	2.37944300	-3.79723300
C	-0.99593000	4.44416600	-2.63255000
C	-0.87893200	2.76791600	-4.88339200
C	-0.21914700	4.78698900	-3.74310800
C	-0.15995900	3.95800900	-4.86426200
H	-0.82214700	2.12409800	-5.75626600
H	0.35001000	5.71065400	-3.73559500
H	0.45008700	4.24061000	-5.71835100
C	-2.42860400	1.05777400	-3.85357700
H	-1.70865400	0.23775400	-3.71569000
H	-3.12363900	0.99444300	-3.01406900
C	-1.04754700	5.32488900	-1.39392800
H	-0.72127200	4.73015700	-0.52935500
H	-2.09117700	5.58691200	-1.18478400
F	-6.06362800	3.33380900	2.04671200
F	-4.95134200	1.88403700	3.20500500
F	-4.36838600	3.98019400	3.22554700
O	-4.14097400	-0.90099000	-0.81298800
C	-5.17915400	-1.84222000	-1.26611600
H	-4.89722400	-2.82645200	-0.90544000

C	-5.27469000	-1.79397200	-2.78502100
H	-4.34222300	-2.13072900	-3.24582800
H	-6.08237900	-2.44633900	-3.13128500
H	-5.49724500	-0.77236400	-3.10355700
O	2.55784600	1.05355800	0.51991700
C	2.95945900	2.41750600	0.79141300
H	2.68766700	3.03728900	-0.06156400
C	2.31113400	2.96815100	2.06252300
H	1.22527100	2.98028800	1.96247900
H	2.58968700	2.35690000	2.92462500
H	2.65654900	3.99371300	2.23492700
C	-2.10409500	2.09233800	2.80656500
C	-2.10441300	0.82916100	3.44273000
C	-1.43801500	3.20204900	3.38231900
C	-1.43178900	0.69998500	4.66483900
C	-0.78215200	3.01797800	4.60711400
C	-0.77544500	1.78163600	5.24761700
H	-1.42388600	-0.26387300	5.16594900
H	-0.26140900	3.85681600	5.06048700
H	-0.25868500	1.66071300	6.19594500
C	3.23288100	-3.10806900	2.57714100
C	2.49739100	-2.41666900	3.56860300
C	3.43920600	-4.50677400	2.67195800
C	1.97134100	-3.14904400	4.64136800
C	2.89538900	-5.18973600	3.76762500
C	2.16203400	-4.52415900	4.74601400
H	1.39715300	-2.62965300	5.40402800
H	3.03852500	-6.26452600	3.84348300
H	1.73861300	-5.07416100	5.58272300
F	6.91203200	-0.77320600	-2.10662100
F	6.06643900	-2.38355400	-3.27795700
F	5.17945900	-0.39861600	-3.34377000
F	-5.77651100	4.22836500	-1.96629700
F	-4.60115200	3.17005100	-3.43953900
F	-3.95151400	5.11552200	-2.71315500
C	-2.80490900	-0.37937100	2.84269600
H	-2.04643200	-1.08077000	2.46531600
H	-3.39280100	-0.07167800	1.97535700
C	-3.72198700	-1.12856500	3.82248000
H	-4.22952400	-1.95259700	3.30726400
H	-3.16512800	-1.56122900	4.66062600
H	-4.48690800	-0.46227900	4.23585800
C	-1.36812200	4.56111000	2.70036200
H	-0.35197200	4.69661200	2.30205200
H	-2.03264500	4.58207500	1.83463200
C	-1.69780500	5.75807900	3.60628400
H	-0.99199100	5.85443700	4.43824000
H	-1.65081800	6.68863500	3.02801900
H	-2.70468900	5.67192700	4.02735100
C	4.29043700	-6.28557400	-2.75798400
H	4.82475600	-6.42035900	-3.70587100
H	4.84122000	-6.83942600	-1.98894300
H	3.30208600	-6.74970900	-2.85730900
C	2.42114100	0.73838400	-4.53912500
H	1.85034400	0.54005500	-5.45284400
H	2.17467400	1.75515300	-4.21580700
H	3.48466900	0.70945300	-4.79748100
C	2.25311800	-0.91822300	3.50174000
H	1.19187700	-0.73958300	3.27461600
H	2.81869400	-0.48174700	2.67731300

C	2.60770600	-0.17250600	4.79872900
H	2.41680600	0.90037500	4.68409600
H	2.01450100	-0.51882200	5.65230200
H	3.66550500	-0.30300300	5.05084900
C	4.18512800	-5.29968000	1.61021600
H	3.46069700	-5.93101400	1.07554200
H	4.60208300	-4.62349000	0.86197400
C	5.30994600	-6.19679700	2.15191400
H	4.93355100	-6.95769400	2.84450600
H	5.80392300	-6.72160000	1.32510000
H	6.06715800	-5.60731900	2.67911900
C	4.48049700	2.34516900	1.03975400
O	4.89876000	1.45096600	1.77171500
C	-6.47855900	-1.30274200	-0.62576200
O	-6.77386400	-0.13678400	-0.88995200
C	-3.20080100	0.81663400	-5.16027700
H	-2.53600000	0.76022900	-6.02902000
H	-3.74687300	-0.13237300	-5.10651900
H	-3.92727600	1.61523700	-5.34396100
C	-0.22789300	6.61654700	-1.44683700
H	-0.34282400	7.16447000	-0.50459700
H	0.84149900	6.42233200	-1.58805900
H	-0.56120300	7.27726600	-2.25573400
N	5.29251700	3.37186600	0.58375400
Si	5.03374500	4.17483900	-1.01816000
Si	6.74462900	3.59945500	1.67111200
C	7.48319400	5.31836000	1.37840000
H	6.72454300	6.10334000	1.27124900
H	8.07898600	5.57128700	2.26637800
H	8.15518700	5.36978100	0.51711400
C	8.07100600	2.29873700	1.35315800
H	8.96958300	2.51706800	1.94624000
H	7.71873300	1.29820400	1.62257700
H	8.37111900	2.28045400	0.29752800
C	6.17492200	3.60330600	3.47234900
H	5.78312800	2.63795600	3.80104400
H	7.02791200	3.86186800	4.11444900
H	5.40195200	4.36441000	3.64187300
C	4.32895800	2.91884900	-2.24072000
H	3.30372500	2.59859900	-2.03379900
H	4.32813200	3.37528800	-3.23937600
H	4.95727300	2.02159800	-2.29446800
C	6.67639200	4.73547200	-1.75927600
H	6.50982700	4.89228600	-2.83380500
H	7.04541600	5.67898500	-1.34845300
H	7.46772700	3.98265000	-1.66451500
C	3.89073600	5.66583300	-0.83592900
H	4.30951600	6.40648700	-0.14277200
H	3.75619400	6.16101300	-1.80696900
H	2.89768700	5.38689500	-0.46368800
N	-7.25132600	-2.09256200	0.19898400
Si	-7.06759500	-3.89858400	0.33872100
Si	-8.53270800	-1.05348600	1.02619400
C	-5.62871400	-4.29063300	1.49397800
H	-5.47162300	-5.37584000	1.55413500
H	-4.68442700	-3.83769700	1.16964700
H	-5.83897000	-3.93176200	2.50947900
C	-8.62855800	-4.71932400	1.00423800
H	-8.51050900	-5.79629700	0.82172500
H	-8.77982500	-4.58842400	2.07806600

H	-9.53917600	-4.40445600	0.48192700
C	-6.82916200	-4.69012500	-1.36574700
H	-7.59727600	-4.35013600	-2.07203900
H	-5.85097200	-4.54381400	-1.83292800
H	-6.96288100	-5.77359100	-1.24432800
C	-9.30014200	-1.97512300	2.48920000
H	-9.85017800	-1.22110900	3.06960100
H	-10.01840300	-2.74979200	2.20993100
H	-8.55858400	-2.41561500	3.16634700
C	-9.90935600	-0.64638800	-0.19667900
H	-10.69102600	-0.05401200	0.29786600
H	-9.53674900	-0.07047100	-1.04948600
H	-10.38396900	-1.55851400	-0.58088300
C	-7.74377400	0.48023200	1.79259100
H	-6.78321100	0.23833100	2.26251400
H	-7.56760500	1.27252700	1.06352200
H	-8.40042400	0.87073500	2.58144200

IM4

Zn	2.09933200	-0.07587500	0.62683200
F	5.53626300	-1.05847700	-2.78153100
F	6.64255000	-1.07520600	-0.91081500
F	6.63139600	0.69567900	-2.14874700
F	3.55391600	4.48471400	0.64807200
F	4.78730600	4.20061400	-1.10482800
F	2.65332300	4.45545200	-1.32957000
N	3.76751300	-0.71212900	-0.43690000
N	2.27980400	1.90589800	0.14358100
C	4.59429400	0.17734400	-0.95892200
C	4.45354600	1.57903800	-0.92141000
C	3.39157700	2.35302300	-0.42134100
C	5.85775800	-0.31394700	-1.70192800
C	3.59797500	3.87841700	-0.55814600
C	3.94206100	-2.13817600	-0.52872100
C	3.32281900	-2.83331500	-1.59264100
C	3.43853900	-4.22873100	-1.61985700
C	4.11967100	-4.91370000	-0.61532200
C	4.68191300	-4.21356400	0.45055400
C	4.59623700	-2.81782700	0.52413900
C	2.53162400	-2.07190700	-2.64487800
C	1.87254500	-2.91798000	-3.73704500
C	5.15819400	-2.03972500	1.70330200
C	5.79945400	-2.87159900	2.81675400
C	1.18845700	2.74191300	0.56937000
C	1.10655100	3.10845700	1.93152100
C	-0.00179400	3.85641700	2.34635600
C	-1.00619600	4.20729300	1.44602200
C	-0.93181900	3.79220000	0.11727700
C	0.15491300	3.04062100	-0.34688200
C	2.19171200	2.66625500	2.89962400
C	1.95861100	2.99692400	4.37522800
C	0.22573700	2.52480300	-1.77577400
C	-1.00612500	2.78263500	-2.64640100
H	5.26406900	2.13597700	-1.35812000
H	2.98489500	-4.78832400	-2.43117500
H	4.19934100	-5.99711300	-0.65516000
H	5.18803300	-4.76170900	1.23828100
H	3.18342500	-1.33010800	-3.11984700
H	1.75237800	-1.49063000	-2.13231900
H	1.15667800	-3.63718100	-3.32226000

H	2.61150400	-3.47563300	-4.32449100
H	1.32448300	-2.26679900	-4.42746100
H	5.89274500	-1.31331300	1.33748300
H	4.34486200	-1.44197800	2.13743300
H	5.08743900	-3.57630400	3.26169300
H	6.15290600	-2.20939300	3.61535200
H	6.66246600	-3.44337200	2.45572900
H	-0.08606700	4.16203500	3.38406400
H	-1.85922100	4.78959000	1.78474400
H	-1.73649300	4.04773000	-0.56402200
H	3.15108000	3.09400300	2.58444700
H	2.31647100	1.57705900	2.79906900
H	1.03216100	2.54825600	4.75191900
H	1.90670900	4.07825400	4.54773800
H	2.78653900	2.60600700	4.97746800
H	0.41377800	1.44273700	-1.74216400
H	1.10383400	2.95365900	-2.27219500
H	-1.90753200	2.33101600	-2.21689300
H	-0.85447800	2.34423100	-3.63942400
H	-1.19450500	3.85381200	-2.78467500
C	-2.48713500	-2.04916200	1.60125700
C	-1.41066300	-3.09561200	1.27046200
O	-0.20456300	-2.75597000	1.97226100
O	-3.64032900	-2.42428900	1.01497800
C	-1.79738200	-4.50263900	1.71672500
H	-1.22698600	-3.06679400	0.19293100
H	-1.99575700	-4.52990800	2.79359600
H	-0.98007700	-5.19545400	1.49420500
O	-2.30408600	-1.08250300	2.30247500
C	-4.87200900	-1.66953900	1.10912700
H	-5.61748300	-2.42340900	0.85776300
C	0.56044700	-1.77696300	1.46871900
O	1.56658200	-1.43302800	2.16582400
O	0.30908800	-1.24978300	0.34266400
H	-2.69229200	-4.83357800	1.18468000
C	-5.20311200	-1.12890000	2.50481500
H	-6.24902400	-0.80656300	2.51317900
H	-5.08624700	-1.92457300	3.24832900
H	-4.56496400	-0.29047800	2.78198500
C	-4.87685900	-0.53844500	0.06214500
O	-3.82397100	0.01103500	-0.23579400
N	-6.12139800	-0.11624900	-0.40382400
Si	-6.17263600	1.67158600	-0.74535500
Si	-7.36156400	-1.32425000	-0.93107300
C	-5.23523800	2.58221300	0.61697300
H	-5.63348300	2.32993900	1.60846300
H	-4.16265900	2.37322300	0.61842800
H	-5.37229600	3.66349700	0.47968800
C	-7.96299700	2.27503700	-0.62859500
H	-7.93736500	3.35818300	-0.44605100
H	-8.54411400	2.11708000	-1.54155600
H	-8.50864400	1.82312200	0.20896700
C	-5.48233800	2.07895500	-2.45225300
H	-5.52905400	3.16064000	-2.63786600
H	-4.43641700	1.76549100	-2.54071900
H	-6.05107900	1.58371300	-3.24935500
C	-6.46645100	-2.75668000	-1.78390000
H	-7.20243500	-3.50879300	-2.09854000
H	-5.95880200	-2.39834400	-2.68890700
H	-5.71824000	-3.27127900	-1.17141000

C	-8.51808600	-0.58817400	-2.22660500
H	-9.29204400	0.05880600	-1.80379600
H	-7.99378900	-0.03527500	-3.01423000
H	-9.03032900	-1.43039600	-2.71239700
C	-8.41590000	-1.93237900	0.51404200
H	-7.85468100	-2.51663300	1.25229500
H	-8.88763600	-1.09312900	1.04090100
H	-9.22193700	-2.57485700	0.13400200

IM5

N	-1.52457600	-0.77854300	0.02458300
O	-0.11911200	1.93237300	1.45209100
C	0.45112900	3.07529700	1.63188000
O	1.13529000	3.44289100	2.56615300
C	1.32444000	-1.99734600	-0.07168600
C	0.06599500	-2.62946100	-0.05555300
H	0.09462600	-3.70490100	-0.07459300
C	-1.22309800	-2.06670700	-0.01321100
C	-2.37011600	-3.10337600	-0.01775600
C	2.52045000	-2.97774500	-0.10444800
N	1.56316800	-0.69481000	-0.06288500
C	-2.86317400	-0.25028800	0.05869200
C	-3.48583200	0.10910000	-1.15939600
C	-3.45285800	0.04026100	1.31083000
C	-4.75055400	0.70825100	-1.10006300
C	-4.71944500	0.63854800	1.31412100
C	-5.36783300	0.96197100	0.12339300
H	-5.25878900	0.98225100	-2.01872300
H	-5.20342900	0.86137500	2.25920000
H	-6.35121100	1.42438700	0.14925300
C	-2.77438200	-0.13052400	-2.48256100
H	-1.78978700	0.35890600	-2.44259000
H	-2.55705900	-1.19944800	-2.58511400
C	-2.70603300	-0.26706000	2.59957800
H	-1.73891600	0.25251700	2.56805500
H	-2.46488200	-1.33548800	2.62801300
F	2.14008300	-4.27071700	-0.10114900
F	3.27391900	-2.80285400	-1.21113700
F	3.32986100	-2.81378400	0.96206200
Zn	-0.02386900	0.63261300	-0.06601100
C	-3.50405800	0.34704300	-3.74030700
H	-2.89116000	0.13800300	-4.62428200
H	-4.46329400	-0.16610500	-3.87385700
H	-3.69751700	1.42592800	-3.71885800
C	-3.42330400	0.10838100	3.89888500
H	-2.79160300	-0.15189600	4.75567200
H	-3.63101000	1.18327200	3.95679200
H	-4.37328000	-0.42707100	4.01330000
C	2.88008400	-0.11068300	-0.07296200
C	3.46053500	0.24878700	-1.31111600
C	3.48944200	0.21861600	1.15989700
C	4.70675200	0.88760500	-1.29190600
C	4.73584400	0.85609300	1.12302800
C	5.34495900	1.17957500	-0.08789800
H	5.18250000	1.16490600	-2.22679400
H	5.23444300	1.11083800	2.05222900
H	6.31299400	1.67390800	-0.09287400
C	2.78449900	-0.09192200	2.47139000
H	1.81287300	0.42048400	2.46977800
H	2.55373700	-1.16230700	2.50922100

C	2.72545900	-0.03386400	-2.61249200
H	1.72796500	0.42600400	-2.55268500
H	2.53894400	-1.11067400	-2.69510600
C	3.40929200	0.44805300	-3.89398600
H	2.78308700	0.20531900	-4.75994100
H	3.56733400	1.53276500	-3.89138900
H	4.38138300	-0.03570300	-4.04366000
C	3.53670800	0.29326900	3.74784400
H	3.73030500	1.37066700	3.79835800
H	2.93428500	0.02596000	4.62345200
H	4.49626900	-0.23073900	3.83275800
F	-1.93003900	-4.37656600	-0.04682800
F	-3.17007300	-2.94943900	-1.09516100
F	-3.15044300	-2.99199100	1.07698300
O	0.24999100	4.03042100	0.61447700
C	-0.78886900	3.84391300	-0.32401500
H	-1.67808900	3.41172200	0.14622400
C	-1.08682200	5.17641800	-0.99500900
H	-0.19150900	5.58574900	-1.47132400
H	-1.87068000	5.05474700	-1.74870100
H	-1.43751000	5.88119200	-0.23462800
C	-0.30334900	2.77518000	-1.36961700
O	-0.09742600	2.92835800	-2.52460100

IM6

N	1.34842200	1.24283100	-0.30166300
C	-1.32883200	1.31274200	-1.79503600
C	-0.10567800	1.90601200	-2.14004800
H	-0.09049200	2.45506300	-3.06630700
C	1.06695100	1.98459900	-1.35666100
C	2.01978600	3.11670800	-1.79841700
C	-2.46383100	1.58082500	-2.81106100
N	-1.57219300	0.55758100	-0.72808400
C	2.46562400	1.49994200	0.57197200
C	3.65313400	0.73735100	0.41073400
C	2.33487700	2.41604800	1.64163300
C	4.67595200	0.88860500	1.35162500
C	3.38936900	2.52049500	2.56451200
C	4.54655200	1.76413100	2.43073300
H	5.59177900	0.31795500	1.24104100
H	3.29272200	3.20832900	3.40027400
H	5.35039600	1.85833700	3.15638300
C	3.80985500	-0.19300700	-0.78015800
H	3.02585200	-0.96065400	-0.74259200
H	3.60969700	0.37797000	-1.69485600
C	1.09602300	3.27226300	1.85274200
H	0.54017400	2.88704900	2.71932900
H	0.42531600	3.17610900	0.99792500
F	-2.00170600	2.05886000	-3.98652700
F	-3.12337400	0.43675100	-3.10186200
F	-3.38662000	2.46797700	-2.37803500
Zn	0.16297100	-0.61080300	-0.05268600
C	5.17321900	-0.87539100	-0.92307100
H	5.18713300	-1.48834100	-1.83109700
H	5.98855900	-0.14649200	-1.00455900
H	5.39643300	-1.53673500	-0.07749100
C	1.38784200	4.76368900	2.08839300
H	0.44840100	5.32585900	2.15178500
H	1.93404500	4.93435600	3.02226100
H	1.98058600	5.18523500	1.27054300

C	-2.90417500	0.42516100	-0.20835400
C	-3.58227100	-0.81655800	-0.27562500
C	-3.48981100	1.53425900	0.46104900
C	-4.85765600	-0.91416400	0.29612700
C	-4.77177800	1.38542000	1.00540400
C	-5.45725700	0.17616700	0.92195200
H	-5.39531700	-1.85494300	0.24373300
H	-5.23782900	2.22415700	1.51234100
H	-6.45160400	0.08069900	1.35087500
C	-2.73721100	2.84933000	0.60733100
H	-1.67761700	2.62296800	0.76614700
H	-2.77226000	3.40013500	-0.34019700
C	-2.96036900	-2.00216000	-0.99113800
H	-1.89595000	-2.06406900	-0.73409900
H	-2.97846000	-1.80697000	-2.07175200
C	-3.60944700	-3.36328100	-0.72064300
H	-3.03615100	-4.15359800	-1.21681000
H	-3.63640100	-3.59359600	0.35106800
H	-4.63531000	-3.41683300	-1.10316900
C	-3.22115900	3.78382200	1.72209300
H	-3.23174000	3.28723500	2.69989200
H	-2.55247600	4.64959800	1.79283400
H	-4.22874000	4.17025500	1.53190300
F	1.80010700	3.51000900	-3.07103100
F	3.32208400	2.77896800	-1.73066800
F	1.84896900	4.21064900	-1.01890300
O	-0.39855000	-0.73085300	1.94213600
C	0.26208300	-0.31460200	3.20267600
C	-1.05153800	0.23745700	2.83237700
H	-1.08233900	1.23389700	2.40184200
H	1.14012500	0.29493700	3.00880300
C	-2.31126800	-0.22741800	3.52274900
C	0.39166700	-1.37993200	4.27715500
C	-0.86768900	-1.51178300	5.15048400
C	-2.14149000	-1.54238300	4.29883700
H	-3.12400600	-0.29771400	2.79259000
H	-2.58571700	0.57668600	4.22096700
H	-3.02270500	-1.69722900	4.93224600
H	-2.10157900	-2.38834200	3.60104600
H	-0.92151700	-0.66129600	5.84495200
H	-0.78937400	-2.41655000	5.76436200
H	1.26252000	-1.13384000	4.89572600
H	0.61454200	-2.33610400	3.79255300
N	0.84038000	-2.42522200	-0.70849200
Si	0.85952300	-2.81338800	-2.40409800
Si	1.26618400	-3.58734400	0.51377700
C	-0.26220200	-4.17842800	1.48298400
H	-0.89989100	-4.79944500	0.83889200
H	0.01193000	-4.78967100	2.35441200
H	-0.87045200	-3.33994200	1.83834500
C	2.09607400	-5.18534300	-0.11336200
H	3.08003600	-5.00066200	-0.56035900
H	2.25520900	-5.84983700	0.74836200
H	1.49562200	-5.74416800	-0.84057700
C	2.58173900	-3.28790900	-3.07318900
H	2.94143500	-4.25054800	-2.69254500
H	2.54944600	-3.36633000	-4.16930700
H	3.33667900	-2.53176100	-2.82302800
C	0.31572100	-1.35373500	-3.48985200
H	0.95702000	-0.47233100	-3.36978000

H	0.37662500	-1.65311600	-4.54551300
H	-0.71879800	-1.04316100	-3.30539800
C	-0.30564900	-4.24410500	-2.88867200
H	-1.35841400	-3.94941400	-2.79446200
H	-0.14308100	-4.53390700	-3.93670800
H	-0.16129900	-5.14349700	-2.27774600
C	2.55573900	-2.87438700	1.72240700
H	3.53049000	-2.80855900	1.22033100
H	2.31797400	-1.87045200	2.09056500
H	2.68935300	-3.52347100	2.59880800

IM7

O	0.22919100	1.94475000	1.48605800
O	1.14744500	1.79423400	-0.53414000
C	0.91752100	2.43494100	0.53411900
Zn	-0.03704100	0.17780200	0.41062300
N	-2.02041700	-0.10480200	-0.09308300
N	0.62275000	-1.71712500	0.03687800
C	-2.40689400	-1.28938500	-0.53499300
C	-2.89369700	1.02397000	0.09649200
C	-0.23793600	-2.62675500	-0.40028400
C	-1.60527700	-2.44099900	-0.67407100
C	-3.88161500	-1.48704900	-0.95485300
C	-3.50920100	1.20402100	1.35637700
C	-2.98780700	1.99657100	-0.92433200
C	0.26366900	-4.07056800	-0.62524000
H	-2.11982300	-3.31293100	-1.03877700
C	-4.28807800	2.35180800	1.54791900
C	-3.29128100	0.18892000	2.46767000
C	-3.78036200	3.12564900	-0.68265600
C	-2.21826100	1.81902500	-2.22416800
F	-0.69649600	-4.89835900	-1.08244200
F	1.27105400	-4.12171700	-1.52127400
F	0.71978700	-4.60781300	0.52686700
H	-4.78045100	2.51306100	2.50117300
C	-4.43352200	3.29899200	0.53617300
H	-3.67028600	-0.78749300	2.14445400
H	-2.20856700	0.04885800	2.60004100
H	-3.88355200	3.88287300	-1.45278200
H	-2.48551800	0.85475600	-2.67089500
H	-1.14777900	1.74411100	-1.98434400
H	-5.04401500	4.18256400	0.70407200
O	1.38790800	3.67788000	0.71611500
C	2.22944200	4.20699800	-0.32737400
C	2.02810500	-1.96347400	0.24213100
C	2.92577000	-1.68543300	-0.81877700
C	2.49040100	-2.35545100	1.51417000
C	4.29400400	-1.85950100	-0.58406700
C	3.87158700	-2.51955900	1.69706900
C	4.76752500	-2.28101000	0.66055200
H	5.00211700	-1.66786300	-1.38356900
H	4.23702900	-2.84106200	2.66985700
H	5.83426700	-2.41903300	0.81704700
C	1.56266100	-2.56305700	2.69598200
H	1.89750600	-3.44561700	3.25502900
H	0.54666300	-2.77944300	2.35711700
C	1.53632200	-1.35540900	3.65042100
H	1.18541000	-0.44588500	3.14574700
H	0.86781700	-1.54715700	4.49833500
H	2.53499500	-1.14295200	4.04884100

C	2.39559700	-1.21085000	-2.16260000
H	1.74080800	-0.34691800	-1.99137500
H	1.74802800	-1.98992200	-2.58350500
C	3.44642000	-0.82469200	-3.20634700
H	2.94759500	-0.48739000	-4.12205000
H	4.08485400	-0.00460700	-2.85729600
H	4.09168100	-1.66933100	-3.47470600
C	2.50379000	5.66509000	0.02758900
H	3.12862800	6.12232600	-0.74545000
H	1.56058800	6.21669900	0.08692100
H	3.01882200	5.74089200	0.99074200
C	3.54060200	3.43231600	-0.47130800
H	1.71107000	4.13197900	-1.28571000
O	4.19350200	3.44368700	-1.49442300
O	3.90803800	2.82073000	0.66238300
C	5.16142100	2.10749700	0.61395100
H	5.10321000	1.28404100	-0.10217500
H	5.97567400	2.78172500	0.33632700
H	5.31393800	1.71949100	1.62141400
F	-4.13409600	-2.72468600	-1.42505700
F	-4.72741200	-1.28931500	0.07844500
F	-4.23384300	-0.62529400	-1.93181600
C	-3.90842000	0.53074600	3.82612100
H	-3.66680900	-0.25626100	4.54961600
H	-3.52354000	1.47713600	4.22336300
H	-5.00079800	0.60442200	3.77238000
C	-2.40619400	2.91755400	-3.27363000
H	-1.80865400	2.68480800	-4.16231700
H	-3.45204600	3.00511400	-3.59086800
H	-2.08134700	3.89740900	-2.90459400

IM8

O	1.23526600	-0.16836500	1.82597000
O	-1.02986600	0.01459000	1.73689100
O	0.44044700	-0.10352800	-0.93213400
O	-1.14810700	-0.46191100	-2.42430400
C	0.05456700	-0.30493200	-2.14964200
C	0.07860500	-0.12458200	2.32652600
Zn	2.23191500	0.14480100	0.09581100
N	3.98651100	-1.00847700	0.11939700
N	3.21394000	1.98807900	0.10495700
C	5.16657300	-0.41919300	-0.01035700
C	3.84769100	-2.43953100	0.25568800
C	4.53049100	2.04366700	-0.02608000
C	5.42150800	0.95910100	-0.10611900
C	6.44278900	-1.29127400	-0.08864700
C	3.78638200	-2.98882500	1.56108200
C	3.69036500	-3.24584900	-0.89252000
C	5.22362400	3.42442600	-0.12108300
H	6.45629700	1.22550400	-0.22741000
C	3.59754500	-4.36877700	1.68697400
C	3.94131400	-2.08986200	2.77761400
C	3.50256300	-4.62466600	-0.70980600
C	3.68777500	-2.65960500	-2.29583000
F	6.56579100	3.33403600	-0.22385700
F	4.80532000	4.10743600	-1.20823900
F	4.97848300	4.19341200	0.95937200
H	3.55759300	-4.81607400	2.67449600
C	3.46270900	-5.18483100	0.56308500
H	4.91600400	-1.58917400	2.72410300

H	3.19326400	-1.29041100	2.71629500
H	3.38991200	-5.26581600	-1.57898700
H	3.32496600	-6.25653900	0.68293400
Zn	-1.71835400	-0.24028000	-0.16703600
N	-3.49509900	0.80335200	-0.53907700
N	-2.68687600	-2.10780500	-0.12748800
C	-4.37278400	0.17591400	-1.31088600
C	-3.69438400	2.15535200	-0.07666300
C	-3.73375500	-2.24362400	-0.92377400
C	-4.43273000	-1.20490100	-1.56951400
C	-5.47005800	0.99825500	-2.02215900
C	-4.51190000	2.36720200	1.06398000
C	-3.00970100	3.22437200	-0.69109000
C	-4.29137800	-3.65455300	-1.20631300
H	-5.18893400	-1.51597300	-2.26928300
C	-4.64408000	3.67152500	1.55178600
C	-5.20394900	1.19846400	1.74799400
C	-3.16414900	4.51112500	-0.15266300
C	-2.11440100	3.02174000	-1.89939700
F	-5.29603100	-3.65483800	-2.10611900
F	-3.33538900	-4.46853000	-1.70236300
F	-4.77654900	-4.23955100	-0.08949900
H	-5.27802100	3.85957200	2.41196100
C	-3.97455000	4.73943100	0.95288200
H	-5.72608400	0.59409300	0.99958500
H	-4.43245600	0.53870100	2.16673100
H	-2.64176100	5.34362500	-0.61504000
H	-1.06837300	3.13349600	-1.58211800
H	-4.08644500	5.74458900	1.35154900
O	0.08292700	-0.27355000	3.67058400
C	-1.15326000	-0.17240700	4.38495700
O	1.03549600	-0.34407500	-3.06188500
C	0.67935500	-0.57278500	-4.44905900
H	1.63187800	-0.41133900	-4.96506800
C	0.20663700	-1.99695900	-4.71182100
C	-0.24734900	0.54941600	-4.93418700
H	-0.77122100	-2.18991400	-4.26782200
H	0.14054800	-2.16374300	-5.79030900
H	0.93735300	-2.70231700	-4.30388900
C	-2.16317600	-3.17199600	0.69186200
C	-1.04513100	-3.91863700	0.26484500
C	-2.71933900	-3.36036500	1.98373200
C	-0.49453200	-4.85746800	1.15135900
C	-2.14153700	-4.31690400	2.82386500
C	-1.03317200	-5.06041400	2.41622700
H	0.37503300	-5.42911600	0.84094100
H	-2.55631900	-4.48180100	3.81277000
H	-0.59175400	-5.79249800	3.08769200
C	-0.41725500	-3.73387900	-1.10620500
H	0.56308500	-3.25284700	-0.98226800
H	-1.02412700	-3.04678800	-1.69853700
C	-0.22054100	-5.03962700	-1.89379100
H	0.20276800	-4.82569500	-2.88262600
H	0.46477600	-5.72568400	-1.38541200
H	-1.17094900	-5.56249300	-2.04038200
C	-6.20072300	1.55470000	2.85449700
H	-5.72113500	2.06754400	3.69564000
H	-7.00814100	2.19659000	2.48234500
H	-6.65886400	0.63929800	3.24642300
C	-3.90208900	-2.51991000	2.43421400

H	-3.62386500	-1.46253100	2.34072100
H	-4.73181700	-2.66073000	1.73206200
C	-4.41836700	-2.77931600	3.85178000
H	-3.64906100	-2.60072500	4.61239900
H	-5.25821000	-2.10898200	4.06748600
H	-4.77782200	-3.80796000	3.97322100
F	-6.19487800	0.26545500	-2.89316000
F	-6.35174900	1.54255200	-1.15590500
F	-4.92933600	2.00955600	-2.73504600
C	2.39823700	3.16972800	0.25618100
C	1.83845900	3.78860100	-0.88136900
C	2.10867300	3.61868400	1.56867400
C	0.99459800	4.89157700	-0.67829700
C	1.25852600	4.71918900	1.71401400
C	0.70618300	5.35468600	0.60157500
H	0.55904300	5.39180300	-1.53828900
H	1.02275000	5.08659000	2.70705600
H	0.04931600	6.21008500	0.73649100
C	2.72540000	2.91917100	2.77043000
H	3.81201300	2.87578300	2.63354200
H	2.38823800	1.87456000	2.77780500
C	2.42998500	3.54156100	4.13754800
H	1.36076900	3.51722300	4.36961700
H	2.95083400	2.97395700	4.91776600
H	2.77703200	4.58030000	4.19749100
C	2.10155700	3.28026800	-2.29016700
H	1.23632300	2.69638300	-2.63130200
H	2.94349300	2.58407000	-2.27701900
C	2.38514200	4.37314600	-3.33183800
H	2.61150100	3.91352000	-4.30132600
H	1.52622300	5.03615900	-3.48162100
H	3.24143400	4.99142200	-3.04084800
H	-2.20991200	1.99968200	-2.26913100
C	-2.37816000	3.99443200	-3.05984600
H	-3.41772000	3.93068000	-3.40036900
H	-2.18346900	5.03614600	-2.78099700
H	-1.72502300	3.74421700	-3.90192300
C	-0.93170100	-0.82673100	5.74714300
H	-1.85186300	-0.79052800	6.33615600
H	-0.64241200	-1.87280600	5.60828200
H	-0.13814100	-0.31314000	6.30025300
C	-1.53917300	1.30272400	4.51913400
H	-1.94431700	-0.68858000	3.83626000
O	-0.86072500	2.23949000	4.15846600
O	-2.73515500	1.41716600	5.11813800
C	-3.18866400	2.76648000	5.36001300
H	-2.48347300	3.29402300	6.00800200
H	-3.29514100	3.30857500	4.41756400
H	-4.15353500	2.66515300	5.85738000
O	-0.22689000	1.67979500	-4.49381100
O	-1.00453700	0.14696600	-5.95932900
C	-1.85384600	1.15285200	-6.55426300
H	-1.25604400	1.99338200	-6.91542500
H	-2.35329500	0.65451900	-7.38535000
H	-2.58755900	1.50721500	-5.82616700
F	7.57545700	-0.56277300	-0.16430500
F	6.57936400	-2.09098900	0.98873600
F	6.42859900	-2.08410900	-1.18269000
H	4.09664000	-1.64732100	-2.27304900
C	3.81684900	-2.77428000	4.14136100

H	3.93365000	-2.03019500	4.93754600
H	2.83624100	-3.24690500	4.27240300
H	4.58601700	-3.54138700	4.29102400
H	2.64558500	-2.54830600	-2.62643400
C	4.45401200	-3.47653000	-3.34647900
H	4.00609200	-4.46141800	-3.51697800
H	4.45137500	-2.94698600	-4.30675500
H	5.49680700	-3.62842000	-3.04757000

IM9

O	3.08094600	-0.21638000	0.35203300
O	1.37465500	-1.20113700	-0.77056100
C	2.58052200	-1.12262700	-0.31624600
Zn	-0.11466500	-0.10382500	-0.04420600
N	-0.35001200	1.93630900	-0.24632800
N	-2.00153900	-0.51214900	-0.79560800
C	-1.25643800	2.43859000	-1.06226500
C	0.55743500	2.71341400	0.54965200
C	-2.61591400	0.37401600	-1.56366800
C	-2.24330700	1.71503800	-1.75895400
C	-1.29369800	3.96567400	-1.27264700
C	0.16622900	3.07688000	1.85625600
C	1.86350700	2.93311900	0.06675500
C	-3.89530500	-0.05646000	-2.31285000
H	-2.84401900	2.27946600	-2.45172900
C	1.10095300	3.74469500	2.65601200
C	-1.21770200	2.69961200	2.35480600
C	2.76320700	3.60387300	0.90381600
C	2.25069500	2.42528900	-1.30946800
F	-4.30359500	0.85529900	-3.21911300
F	-3.70649000	-1.21023700	-2.98779500
F	-4.93251400	-0.25487400	-1.46893700
H	0.83140900	4.04825900	3.66243800
C	2.38425600	4.01598000	2.18067500
H	-1.97187100	3.20637600	1.74152000
H	-1.36163600	1.62963800	2.16354000
H	3.77558100	3.79403000	0.56306900
H	1.71746600	3.01048800	-2.06870100
H	1.87715500	1.39974800	-1.41222200
H	3.09798000	4.53449900	2.81594200
O	3.30140900	-2.23523400	-0.65390500
C	4.64205700	-2.27196300	-0.15717800
C	-2.60114200	-1.75131100	-0.38911800
C	-2.19692300	-2.95239300	-1.00835700
C	-3.47774700	-1.73789700	0.71903100
C	-2.74172400	-4.15116500	-0.53067500
C	-3.99733900	-2.96123100	1.15908800
C	-3.64164200	-4.15666700	0.53487200
H	-2.46097000	-5.09172800	-0.99282700
H	-4.67962600	-2.98531400	2.00239000
H	-4.05524500	-5.09720500	0.88969000
C	-3.79062400	-0.42418400	1.41541300
H	-4.31383500	0.23961000	0.71843400
H	-2.83924200	0.07768300	1.62805900
C	-4.60863000	-0.52323900	2.70430200
H	-4.12197700	-1.16146500	3.45157900
H	-4.72879400	0.47332500	3.14439200
H	-5.61100500	-0.92763700	2.52133700
C	-1.19449500	-2.90814500	-2.14704200
H	-0.28212000	-2.41561900	-1.78876900

H	-1.58833200	-2.25525700	-2.93440300
C	-0.81224700	-4.25851900	-2.75582100
H	-0.08308100	-4.10902500	-3.56008000
H	-0.35376600	-4.92216400	-2.01289400
H	-1.67953800	-4.77583500	-3.18344700
C	5.17839600	-3.67108400	-0.44712400
H	6.20218100	-3.76578100	-0.07234900
H	4.54949200	-4.41647800	0.04968100
H	5.17366400	-3.86819400	-1.52418300
C	5.55312200	-1.22703600	-0.79770000
H	4.64751900	-2.06966800	0.91726600
O	6.56709800	-0.82722600	-0.26179300
O	5.16512700	-0.88914200	-2.03571500
C	6.05819700	-0.00635700	-2.74426300
H	6.21456600	0.91957200	-2.18688600
H	7.02219400	-0.49741000	-2.90944900
H	5.57147400	0.19995500	-3.69794000
F	-2.20500900	4.34993600	-2.18895600
F	-1.60199000	4.60781200	-0.12392000
F	-0.10272000	4.44490200	-1.68876000
C	-1.50160200	2.98063700	3.83136600
H	-2.50565400	2.62538900	4.09066000
H	-0.78623800	2.46882000	4.48662500
H	-1.45952800	4.05183900	4.06069500
C	3.74687000	2.42130500	-1.62112700
H	3.91373500	1.99089000	-2.61431400
H	4.17317700	3.43160100	-1.62404200
H	4.28980000	1.81128500	-0.89297100
O	-0.41941500	-0.61100300	1.96289000
C	-0.81205600	-1.66454200	2.89812200
C	0.26200200	-0.71906100	3.26181500
C	1.72048500	-1.11717100	3.21388700
C	-0.49584800	-3.07815600	2.48495600
C	1.94062800	-2.62881700	3.00417700
H	2.19572300	-0.54527600	2.40911800
H	2.19170800	-0.79338900	4.14915500
C	0.95211800	-3.24415500	2.00371600
H	1.82657300	-3.14572700	3.96723100
H	2.97248700	-2.79834100	2.67432100
H	1.16565600	-4.31123300	1.87253700
H	1.06378600	-2.77983100	1.01921100
H	-1.20832900	-3.39252100	1.71535100
H	-0.67838400	-3.70830900	3.36697900
H	-1.80873600	-1.49017400	3.29756500
H	0.00394200	0.12653000	3.89660900

TS3

O	2.77990600	0.25621800	0.11377900
O	0.82594200	0.00907700	-0.99449200
C	1.99910800	0.44260400	-0.87265100
Zn	-0.45458500	-0.09010500	0.60121400
N	-1.76779400	1.46003800	0.28154300
N	-1.81372300	-1.50148400	-0.05020400
C	-3.06221200	1.26465600	0.11035800
C	-1.10484200	2.72970600	0.26268200
C	-3.09335700	-1.23681000	-0.20940900
C	-3.70514000	0.02341400	-0.05550300
C	-3.98432300	2.49714900	0.06827200
C	-0.74220000	3.32137000	1.49233000
C	-0.66263600	3.24447400	-0.97645900

C	-4.02430000	-2.38264600	-0.63836900
H	-4.77784200	0.04893600	-0.15208900
C	0.01310300	4.49959300	1.45631800
C	-1.15035200	2.64931100	2.79168500
C	0.10323100	4.41712600	-0.95950400
C	-0.96127700	2.48298900	-2.25623500
F	-5.32895300	-2.04208000	-0.62749400
F	-3.73687400	-2.79681800	-1.89296700
F	-3.89589200	-3.45501100	0.17389500
H	0.29384300	4.98918900	2.38303100
C	0.42664200	5.04773500	0.24213900
H	-2.24099900	2.54166700	2.80904200
H	-0.75177600	1.62401000	2.78638400
H	0.45591100	4.84277000	-1.89328100
H	-2.04681300	2.38804000	-2.37231500
H	-0.58296700	1.46224600	-2.13059000
H	1.01641800	5.96094200	0.23300900
O	2.44450500	1.18082200	-1.90868000
C	3.80953100	1.64818000	-1.87163700
C	-1.15936500	-2.72731400	-0.39627000
C	-0.68141600	-2.90817500	-1.71232000
C	-0.83651900	-3.62884100	0.64535500
C	0.07736500	-4.05694000	-1.98030100
C	-0.07166100	-4.75594200	0.32787300
C	0.37602700	-4.97487800	-0.97682200
H	0.44697800	-4.22777300	-2.98712900
H	0.18135100	-5.47213500	1.10293500
H	0.96684400	-5.85807000	-1.20660100
C	-1.30074200	-3.32540700	2.05828900
H	-2.39207600	-3.21817400	2.05322600
H	-0.90500500	-2.33859500	2.33708400
C	-0.89815200	-4.34203400	3.12815000
H	-1.30722000	-5.33861700	2.92250300
H	0.19176900	-4.43617200	3.20985600
H	-1.27574100	-4.02213900	4.10593900
C	-0.96235500	-1.88805100	-2.80221300
H	-1.26447000	-0.94762300	-2.33464000
H	-1.82424100	-2.22376300	-3.39436600
C	0.22093300	-1.60755900	-3.73774100
H	-0.03681500	-0.79647100	-4.42970000
H	1.10113700	-1.29449800	-3.16830600
H	0.49012000	-2.48043400	-4.34314100
C	3.99484100	2.79024200	-0.88022600
H	3.91517400	2.43796700	0.14973100
H	4.97496200	3.25311200	-1.02278000
H	3.22041200	3.54323400	-1.05814100
C	4.75180800	0.44710400	-1.71388500
H	3.96827200	2.02066900	-2.88964000
O	4.50723900	-0.66394800	-2.13707700
O	5.90124400	0.79797900	-1.12320000
C	6.89264600	-0.24637100	-1.01327400
H	6.50293900	-1.08561500	-0.43226400
H	7.18891000	-0.59593000	-2.00628800
H	7.74007400	0.20999800	-0.50092900
F	-5.29362400	2.17944100	0.01097500
F	-3.82038300	3.26572500	1.16799500
F	-3.72632100	3.27964000	-1.00307300
C	-0.68638200	3.33694800	4.07699800
H	-1.02453100	2.76369700	4.94767900
H	0.40694900	3.40317400	4.12721100

H	-1.09235600	4.35158600	4.16815200
C	-0.37336400	3.07367100	-3.53844500
H	-0.64054900	2.44177500	-4.39339500
H	-0.75072900	4.08350100	-3.73973400
H	0.72087200	3.11959500	-3.49090100
O	0.56248100	-0.49149100	2.26079800
C	2.42128400	-1.54332500	1.07760000
C	1.79351200	-1.08459700	2.34532400
C	2.78769100	-0.27677300	3.20496700
C	3.81818600	-2.05217500	1.05397900
C	4.15941100	-0.95687700	3.32075500
H	2.88398900	0.70779800	2.73232000
H	2.33405900	-0.12764000	4.19048700
C	4.76906100	-1.22869800	1.93865200
H	4.05402000	-1.90557700	3.86678000
H	4.83708200	-0.32746500	3.91038300
H	5.72402800	-1.75811800	2.03165800
H	4.97054100	-0.27824500	1.43159700
H	4.16222400	-2.11589600	0.01756300
H	3.74747900	-3.08899600	1.42545700
H	1.70869800	-2.10147600	2.82542000
H	1.74240300	-1.90571300	0.30722700

IM10

O	-0.62924400	-0.14003000	2.09654200
C	-1.72312000	-0.92954900	2.42239500
C	-2.56730200	-1.36526600	1.21201600
C	-1.32630800	-2.20402400	3.20216200
H	-2.40615700	-0.34617000	3.07159500
C	-3.78961100	-2.19904300	1.58932400
H	-1.94331000	-1.90241900	0.49012800
C	-2.53302000	-3.06140300	3.61058200
H	-0.65038700	-2.79791500	2.56972500
H	-0.74802800	-1.89173700	4.08025700
C	-3.37022100	-3.44612600	2.38263000
H	-4.33602500	-2.47593200	0.68023000
H	-4.46226600	-1.58147200	2.19955300
H	-2.19642100	-3.96325600	4.13762900
H	-3.16132000	-2.50022300	4.31752600
H	-4.26500200	-4.00616800	2.68056600
H	-2.78239000	-4.11071700	1.73352300
O	-3.10187600	-0.17518400	0.51663600
C	-2.43284800	0.36947400	-0.47382900
O	-1.28632400	0.09400200	-0.83659500
Zn	0.41262900	-0.10747500	0.48973900
N	1.46087600	1.68880300	0.18144100
N	1.81809700	-1.28271300	-0.49582500
C	2.69361000	1.67585400	-0.29098600
C	2.98887300	-0.78473100	-0.86360500
C	1.47269600	-2.67679600	-0.57249700
C	3.40582400	0.55367600	-0.76069100
C	3.47947600	3.00240000	-0.37886000
C	4.05151400	-1.73025300	-1.46894200
C	1.71194300	-3.49855700	0.55504100
C	0.77343800	-3.15499700	-1.70507600
H	4.40581800	0.75353100	-1.10381400
F	3.50355400	3.64750600	0.80639900
F	2.93282800	3.84275200	-1.28409400
F	4.76709600	2.83148500	-0.74377500
C	1.28444500	-4.83152600	0.50064200

C	2.38897000	-2.92407700	1.79081700
C	0.36662100	-4.49576000	-1.70780200
C	0.46925500	-2.22184300	-2.86702100
C	0.62499200	-5.33007200	-0.62166700
H	1.46575700	-5.48768000	1.34556200
H	3.35777200	-2.50017800	1.50532400
H	1.79381800	-2.07186200	2.14927700
H	-0.16202300	-4.89303100	-2.56805500
H	-0.05316000	-1.33974100	-2.47593800
H	1.41294100	-1.84204500	-3.27455900
H	0.30277800	-6.36800800	-0.64559800
O	-3.09482200	1.32414500	-1.12211300
C	-4.50104600	1.54134300	-0.86783200
H	-4.66746200	1.64255500	0.20712500
C	-4.87546000	2.82937900	-1.59256400
H	-4.71642700	2.72970100	-2.67115500
H	-5.92720900	3.06338100	-1.40882600
H	-4.26163800	3.65339100	-1.21711000
C	0.75472000	2.88740200	0.55378600
C	0.69728800	3.23673000	1.92661700
C	0.02503500	3.60488800	-0.42017100
C	-0.07623800	4.34121600	2.29619000
C	-0.74361900	4.69915500	0.00693300
C	-0.79302700	5.07045700	1.34610700
H	-0.12634800	4.63548400	3.33938900
H	-1.31481000	5.26302300	-0.72567300
H	-1.39288200	5.92322200	1.65436100
C	-0.35564100	-2.81644200	-4.01143800
H	-0.52454200	-2.05222700	-4.77865500
H	0.15495600	-3.65929000	-4.49225400
H	-1.33787100	-3.16526600	-3.67106300
C	2.60476700	-3.89392100	2.95542100
H	3.24434100	-4.73762800	2.67046400
H	3.09652000	-3.37106200	3.78360900
H	1.66016500	-4.29973600	3.33586700
C	1.44771400	2.40499800	2.95385100
H	1.02119600	1.39214000	2.94198800
H	2.49133000	2.30157600	2.63427600
C	1.42474800	2.92980100	4.39217600
H	0.40755400	2.96665300	4.79947600
H	2.01218200	2.26582700	5.03691700
H	1.85655300	3.93500300	4.46992700
C	0.00522100	3.20426600	-1.88803200
H	-0.95415000	2.71316700	-2.09736400
H	0.77032700	2.44900500	-2.07867500
C	0.19451900	4.36395200	-2.87806400
H	0.20981300	3.98018700	-3.90532800
H	-0.61659900	5.09788400	-2.81754600
H	1.13764500	4.89137100	-2.70021400
C	-5.28657500	0.33272900	-1.38665000
O	-4.80617800	-0.59074900	-2.00765500
F	5.17972900	-1.09034700	-1.83801200
F	4.42610800	-2.68781700	-0.59224900
F	3.59340400	-2.36020400	-2.57170100
O	-6.57940100	0.45514500	-1.06537700
C	-7.44965700	-0.60572400	-1.51906300
H	-7.14224800	-1.56077400	-1.08577400
H	-8.44570200	-0.33256200	-1.17043100
H	-7.43232800	-0.67305000	-2.60974600

TS4

O	-1.11800100	-0.45437900	1.51926000
C	-2.08611200	-1.48007000	1.58352600
C	-2.47879300	-2.01442200	0.20363900
C	-1.59383900	-2.65242400	2.45631700
H	-2.99129500	-1.05566900	2.04231600
C	-3.50406800	-3.14668300	0.27950000
H	-1.59096400	-2.33608500	-0.34795200
C	-2.61582400	-3.79287700	2.55398500
H	-0.65347000	-3.03202100	2.03488400
H	-1.36126800	-2.25624900	3.45099000
C	-2.99716300	-4.29980400	1.15788100
H	-3.72610700	-3.49635800	-0.73539700
H	-4.43610000	-2.74565000	0.69904200
H	-2.20520100	-4.61099500	3.15831200
H	-3.51753300	-3.43772600	3.07318900
H	-3.77163700	-5.07356400	1.22065200
H	-2.12042300	-4.76432100	0.68545800
O	-3.13203000	-0.95886500	-0.59533700
C	-2.41345900	-0.17371000	-1.36827000
O	-1.18141600	-0.13853700	-1.43185100
Zn	0.26486300	0.00398600	0.18641600
N	1.22512400	1.80593800	-0.20377700
N	1.81225000	-1.20923200	-0.54095700
C	2.21468400	1.81079700	-1.08729000
C	2.79063100	-0.66030900	-1.24005100
C	1.77968300	-2.59964000	-0.16850700
C	2.90885300	0.69830000	-1.59367300
C	2.70331700	3.16297600	-1.65638000
C	3.98677300	-1.53083900	-1.69125000
C	2.26527800	-2.96952000	1.10716800
C	1.14845400	-3.53380900	-1.02343100
H	3.70292600	0.92656300	-2.28305800
F	3.28862800	3.94452200	-0.72486600
F	1.67146300	3.86025200	-2.17728000
F	3.60393900	3.01850200	-2.65098800
C	2.16429300	-4.31427600	1.48660700
C	2.84657600	-1.91499600	2.03603800
C	1.07005300	-4.86575300	-0.59432100
C	0.57488300	-3.09310300	-2.36209400
C	1.58027100	-5.25713900	0.64254800
H	2.54167200	-4.62857700	2.45405800
H	3.63869800	-1.37164400	1.50878700
H	2.06622100	-1.16767200	2.24334500
H	0.60543600	-5.60798600	-1.23515400
H	-0.03164500	-2.19375000	-2.20286900
H	1.39526900	-2.77066500	-3.01345500
H	1.51369700	-6.29671500	0.95304900
C	-0.90318400	0.48879400	3.17120800
O	-1.95947100	0.45202200	3.72170800
O	0.24532500	0.82148200	3.11960400
O	-3.11427000	0.61157600	-2.17668000
C	-4.56697400	0.64294400	-2.16797900
H	-4.77533000	1.47736400	-2.84572400
C	-5.19628600	-0.62083300	-2.74335900
H	-4.71115200	-0.86370000	-3.69403200
H	-5.11211600	-1.47398000	-2.06830000
H	-6.25531600	-0.43489100	-2.94008300
F	4.67261100	-1.97851900	-0.61522200
F	3.61798900	-2.61357500	-2.40528000

F	4.86774100	-0.85656600	-2.45714400
C	0.80338600	3.00006900	0.49398400
C	1.53629500	3.39065200	1.64452200
C	-0.36660500	3.68360700	0.10389600
C	1.08275100	4.49297200	2.37451000
C	-0.78777900	4.77342600	0.88204400
C	-0.07247000	5.18126000	2.00156500
H	1.62820200	4.81260300	3.25622200
H	-1.69315000	5.30468700	0.60057500
H	-0.41433900	6.02906700	2.59007200
C	3.40126700	-2.42120300	3.36993800
H	4.21800100	-3.13854200	3.22627200
H	3.79730100	-1.57822100	3.94727100
H	2.62891600	-2.90412400	3.97967000
C	-0.26169600	-4.13319100	-3.11284100
H	-0.65513000	-3.69209600	-4.03588200
H	0.32948600	-5.01165000	-3.39622700
H	-1.11638000	-4.48119600	-2.51992300
C	-1.18700800	3.27422100	-1.10630900
H	-2.13398400	2.84010000	-0.75983000
H	-0.67211200	2.48050700	-1.65024200
C	-1.50457300	4.42129100	-2.07971800
H	-2.07107500	4.03845300	-2.93752000
H	-2.11034100	5.20462700	-1.61062300
H	-0.58998700	4.88827600	-2.46020900
C	2.76778400	2.60831800	2.07248000
H	2.49301400	1.54888800	2.12829800
H	3.53090100	2.67713600	1.28794900
C	3.40259900	3.02328100	3.40234100
H	2.69683900	2.93223200	4.23600500
H	4.25946500	2.37508000	3.61998900
H	3.77003000	4.05608300	3.38016800
C	-5.06530400	1.09136300	-0.78819900
O	-4.38346400	1.66871600	0.03115300
O	-6.36788400	0.82677800	-0.64760600
C	-6.97730000	1.28882400	0.58001000
H	-6.89035500	2.37502300	0.66248800
H	-8.02431100	0.99347600	0.51156600
H	-6.50085300	0.81448800	1.44128700

IM11

O	-2.07950500	-0.69832000	1.78768700
C	-3.49677400	-0.57735500	1.59220400
C	-3.73119200	-0.13425000	0.14583100
C	-4.18069000	-1.91967400	1.86349100
H	-3.87402100	0.18824900	2.27691500
C	-5.21224700	-0.06619100	-0.21067900
H	-3.18278900	-0.78410100	-0.53935800
C	-5.67594200	-1.86556500	1.51420900
H	-3.68673600	-2.69647400	1.26635300
H	-4.03118600	-2.17748200	2.91826000
C	-5.88922400	-1.41986200	0.06021200
H	-5.31987600	0.22482600	-1.26179400
H	-5.68754100	0.71487400	0.39690400
H	-6.12835600	-2.85051900	1.67962100
H	-6.18679400	-1.16446200	2.18914800
H	-6.95897300	-1.33965700	-0.16516200
H	-5.47634800	-2.17810100	-0.61970400
O	-3.19921600	1.23240900	-0.01849000
C	-1.93333600	1.43062200	-0.32636300

O	-1.11313600	0.55794200	-0.62717500
Zn	0.51598100	-0.23895200	0.53791400
N	2.35154400	0.68642300	0.14629300
N	0.98747200	-2.06987500	-0.29183000
C	3.35638600	-0.05092800	-0.29353000
C	2.24914500	-2.32550300	-0.61366900
C	-0.07693700	-3.02901300	-0.44158600
C	3.32947700	-1.42701200	-0.59772000
C	4.72442200	0.62077300	-0.55136700
C	2.63287000	-3.75372600	-1.06935500
C	-0.47278200	-3.79426800	0.67840000
C	-0.77531400	-3.08953100	-1.67006500
H	4.27437200	-1.84488900	-0.89743300
F	5.19116300	1.26337300	0.53854100
F	4.63465900	1.52780900	-1.54830100
F	5.68343300	-0.25495800	-0.91463000
C	-1.54193900	-4.68530400	0.52007400
C	0.23905400	-3.62297200	2.01104200
C	-1.84276000	-3.99111000	-1.77414000
C	-0.37877800	-2.18139200	-2.82457300
C	-2.21556900	-4.79237100	-0.69600600
H	-1.85529400	-5.30100500	1.35666200
H	0.15983700	-2.56877700	2.31202800
H	1.31040800	-3.80668300	1.87167700
H	-2.38880700	-4.07007000	-2.70847900
H	-0.34953900	-1.14806600	-2.45587400
H	0.64936100	-2.41148600	-3.12617200
H	-3.03969600	-5.49365800	-0.80014300
C	-1.43824700	0.24555000	2.59059100
O	-2.05153700	0.90660200	3.41491900
O	-0.17535000	0.28542600	2.32365500
O	-1.56651500	2.70344300	-0.30919400
C	-2.52627300	3.73964500	0.04462400
H	-3.01779100	3.46007600	0.97814400
C	-1.72797200	5.02532000	0.22011800
H	-1.22511500	5.30409000	-0.71099500
H	-2.40704200	5.83147600	0.51228900
H	-0.97848600	4.89410200	1.00523900
C	2.45279800	2.10077400	0.41025300
C	2.72768200	2.51877100	1.73681700
C	2.16011700	3.02904600	-0.61152000
C	2.73875500	3.89072200	2.00584300
C	2.18345400	4.39412400	-0.28665200
C	2.47343800	4.82508700	1.00340600
H	2.95478100	4.23767400	3.01082300
H	1.96384300	5.12657600	-1.05843900
H	2.48792600	5.88747800	1.23355500
C	-1.27495000	-2.23715400	-4.06462600
H	-0.91013400	-1.52632600	-4.81484300
H	-1.27669400	-3.23125400	-4.52662600
H	-2.31312900	-1.97085000	-3.83263400
C	-0.26602700	-4.49556600	3.16275700
H	-0.16119300	-5.56460800	2.94294200
H	0.31559800	-4.28478300	4.06728300
H	-1.31926900	-4.29814100	3.39374800
C	1.77419200	2.59747400	-2.01819100
H	0.68941300	2.73197100	-2.13148500
H	1.95619100	1.52741600	-2.14160300
C	2.48805000	3.35442300	-3.14847300
H	2.17529900	2.95699200	-4.12154800

H	2.25422900	4.42460400	-3.14359900
H	3.57538100	3.24810800	-3.07326300
C	2.99729800	1.48902000	2.82262600
H	2.12313600	0.82978600	2.89568400
H	3.82978800	0.84938900	2.50646800
C	3.30771300	2.04343700	4.21550900
H	2.47584800	2.63517900	4.61487700
H	3.48518500	1.21440600	4.91016800
H	4.20474800	2.67421900	4.21708400
C	-3.60939000	3.91081000	-1.02054600
O	-4.64658600	4.49491100	-0.78940500
O	-3.25759300	3.40550600	-2.20771600
C	-4.22236200	3.56877300	-3.27124400
H	-3.76727100	3.10845600	-4.14827800
H	-5.15776000	3.06425900	-3.01635200
H	-4.41350300	4.62944100	-3.45143700
F	3.95540500	-3.89918700	-1.28792500
F	2.01678400	-4.10050600	-2.21970600
F	2.29789500	-4.67615600	-0.14239700

TS5

Zn	-2.40110400	0.32851600	-0.05825500
Zn	2.21444300	-0.34772400	-0.25327200
N	4.04660800	-0.37574300	0.61384300
O	-0.72676100	-0.73015300	-0.02016100
C	-0.15981900	-0.97828600	1.07884400
O	1.08632400	-1.09254400	1.23396100
O	1.12783400	3.26415700	-1.90138300
C	0.75088900	2.11395500	-1.25205800
O	-2.55692600	0.98696300	-1.93076700
C	-2.62213400	0.14121600	-3.13422600
C	-1.38023400	0.97024500	-2.79551700
H	-2.58832200	-0.91498300	-2.87245800
C	-1.17204100	2.19190300	-3.68862000
C	-3.66642600	0.51918400	-4.14809000
O	1.68123700	1.49891300	-0.61424500
C	-2.00488500	2.19698600	-4.97722400
H	-1.42126400	3.07451900	-3.09394000
H	-0.10610200	2.27441700	-3.91548200
C	-3.48568400	1.94855100	-4.67358200
H	-1.64612000	1.42081700	-5.66934200
H	-1.86646700	3.16046900	-5.48384000
H	-4.10516300	2.09585800	-5.56642300
H	-3.83047700	2.67060300	-3.92047600
H	-4.67008500	0.35910800	-3.73938200
H	-3.55312800	-0.19326900	-4.97810300
C	-4.52752500	-0.78791100	1.59440600
C	-4.29467200	0.20765400	2.55839200
H	-4.82188200	0.10251000	3.49134100
C	-3.52843700	1.37589400	2.40223300
N	-3.96878500	-0.86303600	0.40110100
N	-2.73573400	1.66692100	1.38741000
C	-3.62540100	2.38339900	3.55815700
C	3.90881200	-2.06743900	-1.91206500
C	5.04159400	-1.69710900	-1.16911700

H	5.98236600	-2.09812800	-1.50555200
C	6.45593300	-0.86806500	0.70222000
C	4.16425800	-3.13666900	-2.99254500
F	7.44988900	-1.37152800	-0.05778900
F	6.78445400	0.41409100	0.96741200
F	6.48187900	-1.54285000	1.87255400
N	2.67117200	-1.63348100	-1.73616100
C	1.54358200	-2.13812200	-2.47194900
C	0.80989700	-3.22295800	-1.95448000
C	1.13830500	-1.44415500	-3.63329000
C	-0.33703000	-3.62700100	-2.65345500
C	-0.00969300	-1.88771700	-4.29736300
C	-0.74396500	-2.97152700	-3.81198700
H	-0.92332100	-4.46017300	-2.27864100
H	-0.34545200	-1.37870500	-5.19447800
H	-1.64239900	-3.29466900	-4.33098400
C	1.20859000	-3.91062300	-0.66091900
H	2.20293900	-3.57617100	-0.35658600
H	0.53319100	-3.58342400	0.13858600
C	1.93346900	-0.23692300	-4.09990400
H	2.99867400	-0.48658700	-4.09221200
H	1.82272900	0.55957300	-3.34945500
C	-5.54421300	-1.87185100	1.99335700
C	-4.38294900	-1.76988900	-0.63139000
C	-3.69043500	-2.98053600	-0.82005800
C	-5.38375100	-1.32939700	-1.52761100
C	-4.02955800	-3.75819500	-1.93764900
C	-5.69385900	-2.14400600	-2.62028700
C	-5.01877800	-3.34888400	-2.82837400
H	-3.51030400	-4.69609500	-2.11075700
H	-6.46038000	-1.83490900	-3.32324600
H	-5.26587000	-3.96679100	-3.68795300
C	-6.04312300	0.01914900	-1.29945900
H	-6.40619100	0.06884600	-0.26735000
H	-5.26459200	0.79171900	-1.36832200
C	-2.58264000	-3.40923100	0.12163000
H	-2.62102100	-2.81861100	1.03647100
H	-1.62411100	-3.15456500	-0.34189400
F	-2.41871400	2.53473100	4.15429900
F	-4.48609300	2.00523900	4.52452000
F	-4.02483800	3.60015600	3.13558800
C	5.07538900	-0.95480300	0.02475600
O	-0.97430000	-1.09860500	2.14730400
C	-0.37888300	-1.39325400	3.42039500
O	-0.43513400	1.78538600	-1.39847200
C	-2.59282400	-4.89701600	0.49048100
H	-2.42488400	-5.54499300	-0.37754600
H	-1.79932700	-5.09713300	1.21675200
H	-3.55268100	-5.18184000	0.93829100
C	-7.19515900	0.37856900	-2.23925500
H	-6.87648000	0.43382600	-3.28638300
H	-8.00938200	-0.35294900	-2.17389800

H	-7.60236100	1.35904900	-1.96714200
F	-6.63149400	-1.85568900	1.19116500
F	-4.99681500	-3.10402900	1.90596400
F	-5.99254900	-1.73733200	3.25826200
C	-2.11567400	2.94553800	1.16273200
C	-2.81144400	3.86808000	0.35038800
C	-0.79147300	3.16883900	1.57555300
C	-2.15801900	5.04945800	-0.01138400
C	-0.17231300	4.35889500	1.17480200
C	-0.84398500	5.29134100	0.39226000
H	-2.66665600	5.77760600	-0.63539700
H	0.86330200	4.53869900	1.44200300
H	-0.32741500	6.18861000	0.06728500
C	-4.21226000	3.52747800	-0.12229600
H	-4.19266800	2.50804800	-0.52587700
H	-4.88128600	3.48051400	0.74779000
C	-0.01221700	2.13728200	2.36489500
H	-0.67328000	1.31294000	2.63233900
H	0.76303100	1.71594900	1.71260300
C	0.64498200	2.68571400	3.63858300
H	1.15043000	1.88082500	4.18287100
H	1.40019900	3.44511900	3.41021900
H	-0.09940400	3.13872800	4.30115700
C	-4.81211100	4.45707800	-1.17754300
H	-4.17797300	4.50596200	-2.07100400
H	-5.79687200	4.08616800	-1.48506800
H	-4.94471400	5.47810700	-0.80091200
H	0.52281500	-0.78896800	3.55545100
C	0.01665600	-2.86979500	3.44345800
O	0.65116200	-3.16386900	4.58630700
O	-0.22296800	-3.67012900	2.56439200
C	-1.41858900	-1.06100200	4.48459500
H	-1.67605600	0.00040100	4.43201900
H	-2.32761600	-1.65124700	4.33198200
H	-1.01289500	-1.27865500	5.47599700
C	4.09045000	0.16762500	1.94339500
C	3.86156300	-0.70038600	3.03677400
C	4.22350300	1.55919500	2.11673700
C	3.78478000	-0.13516300	4.31533700
C	4.14203500	2.07557400	3.41646200
C	3.92523300	1.23993900	4.50825900
H	3.61312900	-0.77514300	5.17484100
H	4.24171400	3.14702000	3.56817100
H	3.85832000	1.65723100	5.50967500
C	4.44939300	2.49556800	0.94550900
H	4.52102700	1.91649000	0.02230600
H	3.56324900	3.13261900	0.83260500
C	5.69748700	3.38006200	1.08967600
H	5.85393200	3.95811900	0.17366300
H	5.60171400	4.08698100	1.92142000
H	6.59108000	2.77408100	1.26708100
C	3.67324900	-2.19416800	2.82713500

H	2.61881900	-2.37688300	2.58852800
H	4.22681200	-2.51393600	1.94206300
C	4.10266400	-3.07336200	4.00600400
H	3.47143100	-2.92274500	4.88737200
H	4.03183000	-4.13145900	3.73005200
H	5.14110800	-2.86737700	4.29182800
C	2.90155800	4.79186400	-1.30615900
O	2.17896700	5.44015600	-0.58204600
O	4.19892500	5.08572000	-1.52491600
C	4.68947700	6.26300500	-0.85016900
H	4.15414700	7.15089600	-1.19893000
H	4.56766000	6.16735300	0.23167000
H	5.74628200	6.33158700	-1.10990000
C	2.50994400	3.55151300	-2.10906200
H	3.12307200	2.72134200	-1.75130800
C	2.72386500	3.76294100	-3.60886800
H	2.10076500	4.58704800	-3.97228600
H	3.77210300	3.99058000	-3.81956100
H	2.44449800	2.85184100	-4.14578100
F	5.46952800	-3.44470200	-3.13309000
F	3.52424500	-4.28542100	-2.67951600
F	3.72990700	-2.75106900	-4.21102300
C	1.19484800	-5.44375500	-0.72087800
H	0.19468900	-5.83871300	-0.92920700
H	1.87398400	-5.81452500	-1.49652800
H	1.51467700	-5.85809500	0.24264800
C	1.57016800	0.30370100	-5.48375200
H	0.53814600	0.66423500	-5.53187000
H	2.22559200	1.14205100	-5.74417900
H	1.69402100	-0.46812800	-6.25277000
C	1.02125100	-4.55123500	4.75386300
H	0.12487600	-5.17668600	4.79202400
H	1.66062400	-4.87878900	3.93137100
H	1.55923800	-4.59891600	5.70033700
H	-0.58783200	0.27531100	-2.57510000

References

1. Boulding, N. A.; Millican, J. M.; Hutchings, L. R., Understanding copolymerisation kinetics for the design of functional copolymers via free radical polymerisation. *Polymer Chemistry* **2019,** *10* (41), 5665-5675.
2. Tang, J.; Li, M.; Wang, X.; Tao, Y., Switchable Polymerization Organocatalysis: From Monomer Mixtures to Block Copolymers. *Angewandte Chemie International Edition* **2022,** *n/a* (n/a), e202115465.
3. Kissling, S.; Lehenmeier, M. W.; Altenbuchner, P. T.; Kronast, A.; Reiter, M.; Deglmann, P.; Seemann, U. B.; Rieger, B., Dinuclear zinc catalysts with unprecedented activities for the copolymerization of cyclohexene oxide and CO2. *Chemical Communications* **2015,** *51* (22), 4579-4582.
4. Moore, D. R.; Cheng, M.; Lobkovsky, E. B.; Coates, G. W., Mechanism of the Alternating Copolymerization of Epoxides and CO2 Using β-Diiminate Zinc Catalysts: Evidence for a Bimetallic Epoxide Enchainment. *Journal of the American Chemical Society* **2003,** *125* (39), 11911-11924.
5. Wang, R.; Zhang, J.; Yin, Q.; Xu, Y.; Cheng, J.; Tong, R., Controlled Ring-Opening Polymerization of O-Carboxyanhydrides Using a β-Diiminate Zinc Catalyst. *Angewandte Chemie International Edition* **2016,** *55* (42), 13010-13014.
6. Wang, X.; Chin, A. L.; Zhou, J.; Wang, H.; Tong, R., Resilient Poly(α-hydroxy acids) with Improved Strength and Ductility via Scalable Stereosequence-Controlled Polymerization. *Journal of the American Chemical Society* **2021,** *143* (40), 16813-16823.
7. Jeske, R. C.; Rowley, J. M.; Coates, G. W., Pre-Rate-Determining Selectivity in the Terpolymerization of Epoxides, Cyclic Anhydrides, and CO2: A One-Step Route to Diblock Copolymers. *Angewandte Chemie International Edition* **2008,** *47* (32), 6041-6044.
8. Romain, C.; Zhu, Y.; Dingwall, P.; Paul, S.; Rzepa, H. S.; Buchard, A.; Williams, C. K., Chemoselective Polymerizations from Mixtures of Epoxide, Lactone, Anhydride, and Carbon Dioxide. *Journal of the American Chemical Society* **2016,** *138* (12), 4120-4131.
9. Stößer, T.; Sulley, G. S.; Gregory, G. L.; Williams, C. K., Easy access to oxygenated block polymers via switchable catalysis. *Nature Communications* **2019,** *10* (1), 2668.
10. Deacy, A. C.; Gregory, G. L.; Sulley, G. S.; Chen, T. T. D.; Williams, C. K., Sequence Control from Mixtures: Switchable Polymerization Catalysis and Future Materials Applications. *Journal of the American Chemical Society* **2021,** *143* (27), 10021-10040.
11. McGraw, M. L.; Clarke, R. W.; Chen, E. Y. X., Synchronous Control of Chain Length/Sequence/Topology for Precision Synthesis of Cyclic Block Copolymers from Monomer Mixtures. *Journal of the American Chemical Society* **2021,** *143* (9), 3318-3322.
12. McGraw, M. L.; Clarke, R. W.; Chen, E. Y. X., Compounded Sequence Control in Polymerization of One-Pot Mixtures of Highly Reactive Acrylates by Differentiating Lewis Pairs. *Journal of the American Chemical Society* **2020,** *142* (13), 5969-5973.

13. Raman, S. K.; Raja, R.; Arnold, P. L.; Davidson, M. G.; Williams, C. K., Waste not, want not: CO2 (re)cycling into block polymers. *Chemical Communications* **2019,** *55* (51), 7315-7318.
14. Walsh, D. J.; Lau, S. H.; Hyatt, M. G.; Guironnet, D., Kinetic Study of Living Ring-Opening Metathesis Polymerization with Third-Generation Grubbs Catalysts. *Journal of the American Chemical Society* **2017,** *139* (39), 13644-13647.
15. Yoder, C. H.; Copenhafer, W. C.; DuBeshter, B., Structure of trimethylsilyl amides. *Journal of the American Chemical Society* **1974,** *96* (13), 4283-4286.
16. Evans, W. J.; Johnston, M. A.; Fujimoto, C. H.; Greaves, J., Utility of Electrospray Mass Spectrometry for the Characterization of Air-Sensitive Organolanthanides and Related Species1. *Organometallics* **2000,** *19* (21), 4258-4265.
17. Biernesser, A. B.; Delle Chiaie, K. R.; Curley, J. B.; Byers, J. A., Block Copolymerization of Lactide and an Epoxide Facilitated by a Redox Switchable Iron-Based Catalyst. **2016,** *55* (17), 5251-5254.
18. Reiter, M.; Vagin, S.; Kronast, A.; Jandl, C.; Rieger, B., A Lewis acid β-diiminato-zinc-complex as all-rounder for co- and terpolymerisation of various epoxides with carbon dioxide. *Chemical Science* **2017,** *8* (3), 1876-1882.
19. Guerin, W.; Diallo, A. K.; Kirilov, E.; Helou, M.; Slawinski, M.; Brusson, J.-M.; Carpentier, J.-F.; Guillaume, S. M., Enantiopure Isotactic PCHC Synthesized by Ring-Opening Polymerization of Cyclohexene Carbonate. *Macromolecules* **2014,** *47* (13), 4230-4235.
20. Becke, A. D., Density-functional exchange-energy approximation with correct asymptotic behavior. *Physical review. A, General physics* **1988,** *38* (6), 3098-3100.
21. Lee, C.; Yang, W.; Parr, R. G. J. P. r. B., Development of the Colle-Salvetti correlation-energy formula into a functional of the electron density. *Phys. Rev. B: Condens. Matter Mater. Phys.* **1988,** *37* (2), 785.
22. Roy, L. E.; Hay, P. J.; Martin, R. L., Revised Basis Sets for the LANL Effective Core Potentials. *Journal of Chemical Theory and Computation* **2008,** *4* (7), 1029-1031.
23. Grimme, S.; Antony, J.; Ehrlich, S.; Krieg, H., A consistent and accurate ab initio parametrization of density functional dispersion correction (DFT-D) for the 94 elements H-Pu. *The Journal of Chemical Physics* **2010,** *132* (15), 154104.
24. Frisch, M.; Trucks, G.; Schlegel, H.; Scuseria, G.; Robb, M.; Cheeseman, J.; Scalmani, G.; Barone, V.; Petersson, G.; Nakatsuji, H., Gaussian 16. Gaussian, Inc. Wallingford, CT: 2016.
25. Mardirossian, N.; Head-Gordon, M., ωB97M-V: A combinatorially optimized, range-separated hybrid, meta-GGA density functional with VV10 nonlocal correlation. **2016,** *144* (21), 214110.
26. Weigend, F.; Ahlrichs, R., Balanced basis sets of split valence, triple zeta valence and quadruple zeta valence quality for H to Rn: Design and assessment of accuracy. *Physical Chemistry Chemical Physics* **2005,** *7* (18), 3297-3305.
27. Neese, F., The ORCA program system. *WIREs Comput Mol Sci.* **2012,** *2* (1), 73-78.
28. Neese, F., Software update: The ORCA program system—Version 5.0. *WIREs Comput Mol Sci.* **2022,** *n/a* (n/a), e1606.
29. Marenich, A. V.; Cramer, C. J.; Truhlar, D. G., Universal Solvation Model Based on Solute Electron Density and on a Continuum Model of the Solvent Defined by the

Bulk Dielectric Constant and Atomic Surface Tensions. *The Journal of Physical Chemistry B* **2009,** *113* (18), 6378-6396.
30. Mardirossian, N.; Head-Gordon, M., Thirty years of density functional theory in computational chemistry: an overview and extensive assessment of 200 density functionals. *Molecular Physics* **2017,** *115* (19), 2315-2372.
31. Chan, B.; Gill, P. M. W.; Kimura, M., Assessment of DFT Methods for Transition Metals with the TMC151 Compilation of Data Sets and Comparison with Accuracies for Main-Group Chemistry. *Journal of Chemical Theory and Computation* **2019,** *15* (6), 3610-3622.
32. Legault, C., *CYLview, 1.0 b*. Université de Sherbrooke: 2009; Vol. 436, p 437.

CHAPTER 8

Mechanical and thermal properties of functionalized poly(ester-*b*-carbonates)

8.1 Introduction

Switchable / tandem copolymerization to synthesize sequence-defined copolymers has gained significant interest in commercial applications due to its ability to incorporate the distinct features of each segment inside the same molecule.[1] The physicochemical properties of the resulting sequence-controlled copolymers can be modified by adjusting the composition, molecular weight/molecular weight distribution, and structure of each segment. Therefore, sequence-controlled copolymers provide a platform for the production of a wide range of materials, with applications as innovative materials, in drug delivery, and in nanolithography, among others.[2] In chapter 5, we investigated the mechanical and thermal properties of functionalized poly(α-hydroxy acids).[3] The incorporation of the second block, polycarbonate, into poly(α-hydroxy acid) would undoubtedly alter the polymer backbone functionality and tune the properties of the resulting poly(ester-*b*-carbonate).[4] Such poly(ester-*b*-carbonate) with improved material properties synthesized by copolymerization of OCAs and epoxides would greatly expand the range of sustainable polymers. However, the previously reported copolymerization methods of OCAs and epoxides were unable to synthesize substantial high-molecular-weight poly(ester-*b*-carbonates) (<15 kDa);[5] hence, the mechanical properties of such poly(ester-*b*-carbonate) are undocumented.

In chapter 6, we identified a Zn complex that mediates copolymerization of OCAs and epoxides at room temperature to afford high-MW (>200 kDa) functionalized

poly(ester-*b*-carbonates) with narrow MW distributions (Đ < 1.1). This remarkably simple and scalable method allows us to investigate their valuable characteristics, and indeed such poly(ester-*b*-carbonates) have the great potential to substitute current non-degradable polyolefins.

8.2 Results and discussions

Having developed a scalable method for the synthesis of functionalized poly(ester-*b*-carbonates), we turned our attention to assessing their thermal and mechanical properties and exploring their potential applications. Predictably, the mechanical properties of these poly(ester-*b*-carbonates) were affected by their MWs. For instance, high-MW poly(L-**3**-*b*-CHC) (M_n = 81.5 kDa) exhibited better fracture stress (σ) and toughness than low-MW poly(L-**3**-*b*-CHC) (M_n = 33.4 kDa) (**Figure 8.1**), highlighting the importance of preparing high-MW copolymers.

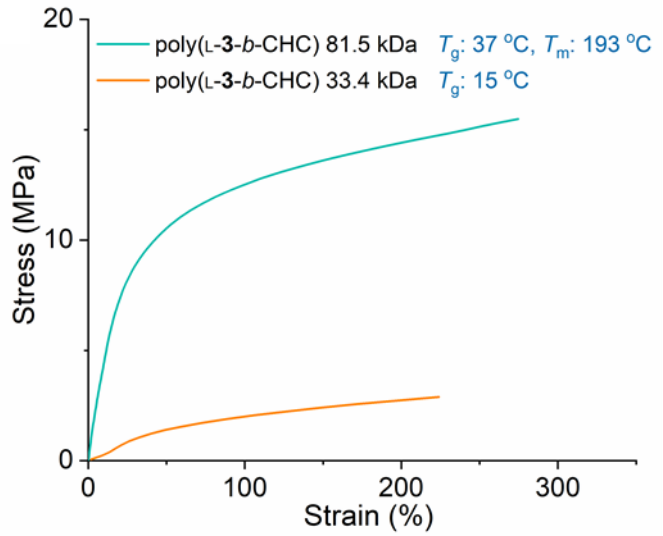

Figure 8.1 Representative stress-strain curves of uniaxial tensile tests of poly(L-**3**-*b*-CHC) with different molecular weights.

8.2.1 Mechanical properties of poly(L-1-*b*-carbonate) and poly(L-4-*b*-carbonate)

The homopolymers poly(CHC), poly(VCHC), and poly(lactic acid) (poly(L-**4**), PLA) are brittle, with σ values of 25–50 MPa and fracture strain (ε) values of less than 15% (**Figure 8.2**; **Table 8.1**, entries 1–3). Although the block copolymers poly(L-**4**-*b*-CHC) (entry 5), poly(L-**1**-*b*-CHC), and poly(L-**1**-*b*-VCHC) (**Figure 8.2**, entry 4 and 6) were also brittle, poly(L-**4**-*b*-VCHC)—a combination of two brittle polymers—exhibited significantly improved ductility, with an ε of 41.2%, which is 3.6 and 13.3 times the respective values for poly(L-**4**) and poly(VCHC), with little decrease in the tensile stress (σ = 44.8 MPa, entry 7; **Figure 8.2**). In addition, the tetrablock copolymer poly(L-**4**-*b*-VCHC-*b*-L-**2**-*b*-CHC) showed better ductility (ε = 67.4 %) than poly(L-**4**-*b*-VCHC) and had a σ of 33.0 MPa (entry 8; **Figure 8.2**). These mechanical properties are comparable to those of commodity polyolefins such as polypropylene (σ = 32.4 MPa, ε = 10.2%; entry 9; **Figure 8.2**). Both poly(L-**4**-*b*-VCHC) and poly(L-**4**-*b*-VCHC-*b*-L-**2**-*b*-CHC) had high glass transition temperatures (T_g ~ 102-103 °C); the values were higher than those of the common polyesters PLA (T_g ~ 50 °C),[6] poly(ethylene terephthalate) (T_g ~ 80 °C),[7] and poly(3-hydroxybutyrate) (T_g ~ 5 °C).[8] The melting temperatures (T_m) were around 165 °C, which is comparable to that of PLA (161 °C) (**Table 8.1**, compare entries 5 and 7 with entry 3; **Figure 8.3**). Additionally, poly(L-**4**-*b*-VCHC) exhibited excellent thermal stability, as indicated by thermogravimetric analysis; the degradation temperature at 5% mass loss ($T_{d,5\%}$) was 257 °C (**Figure 8.4**).

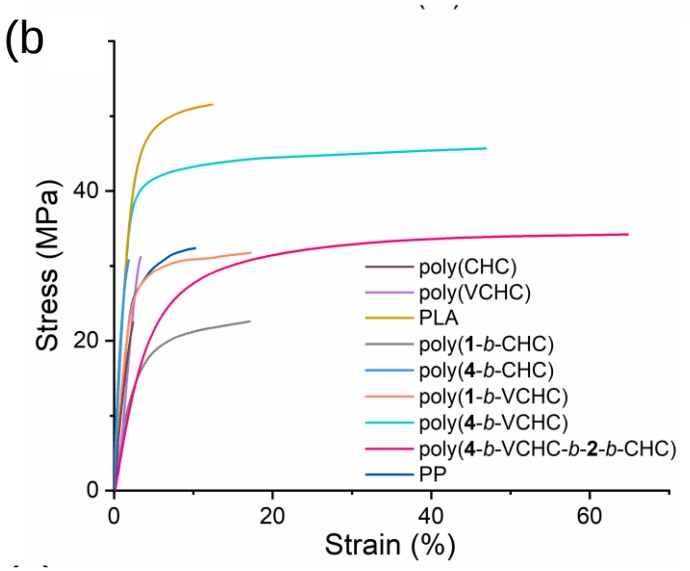

Figure 8.2 Various poly(ester-*b*-carbonates) compared with brittle polypropylene (PP), PCHC, PVCHC, and poly(lactic acid) (PLA), showing the block poly(ester-*b*-carbonates) could improve the ductility and keep the strength close to the polycarbonates.

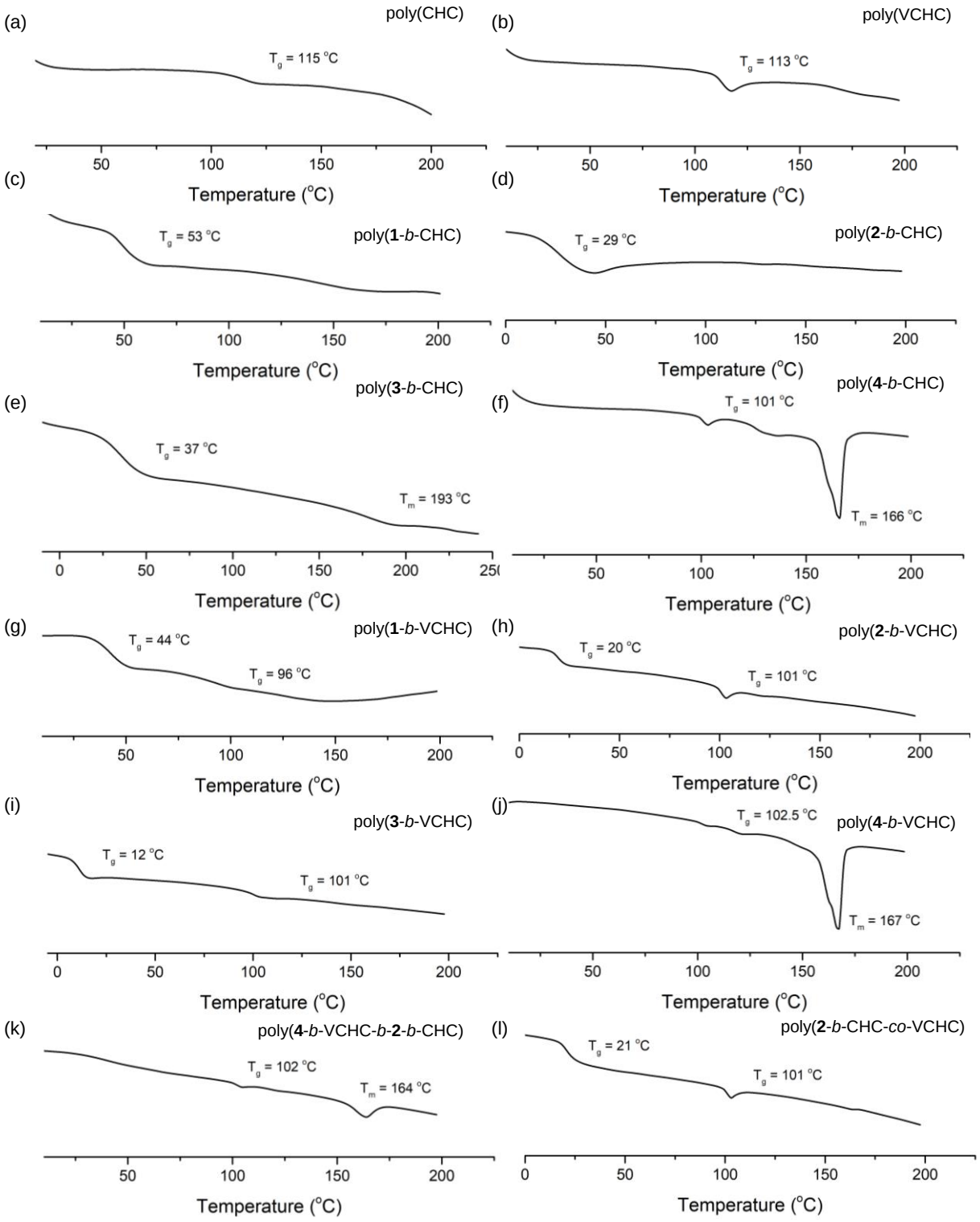

Figure 8.3 DSC measurements of T_gs and T_ms of various copolymers.

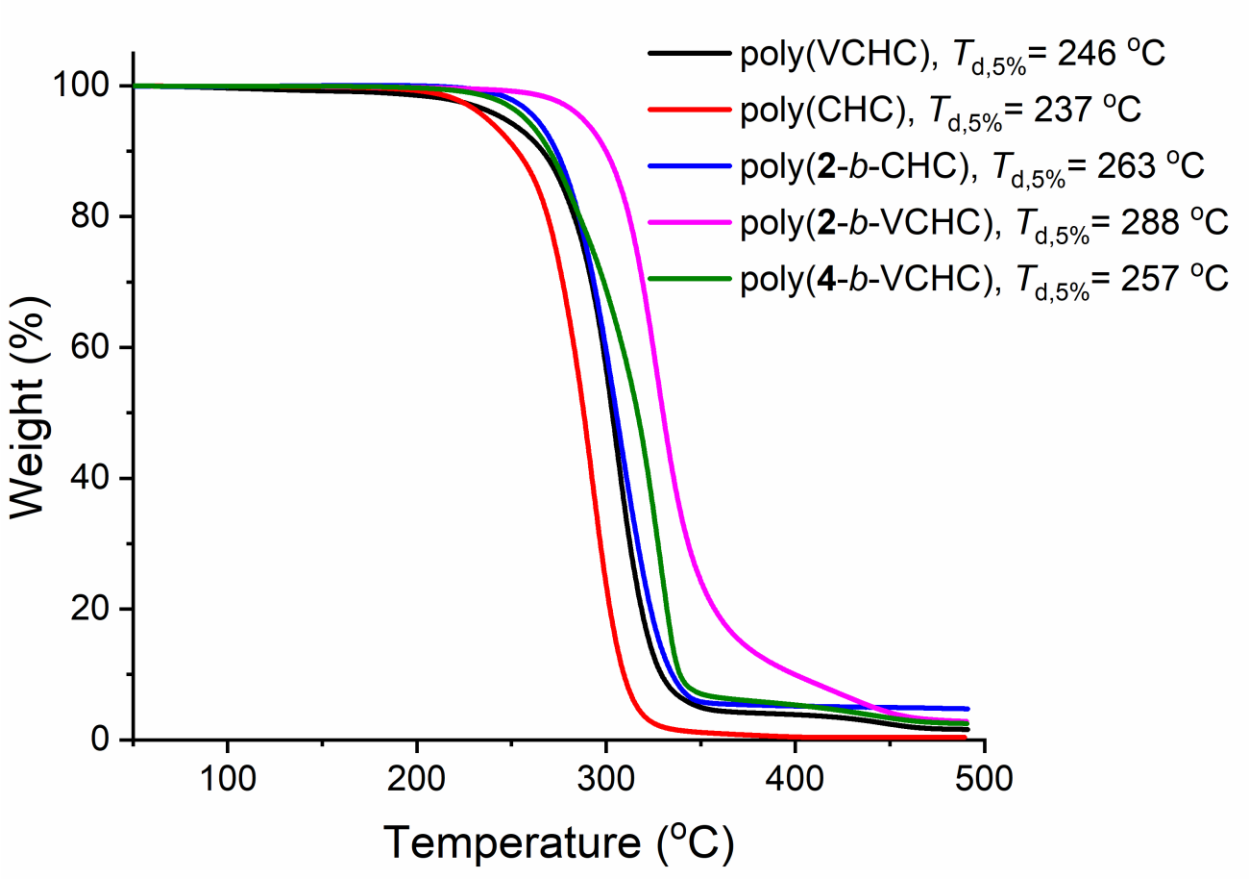

Figure 8.4 Thermogravimetric analysis (TGA) tests of various copolymers. All showed the onset thermal degradation temperatures ($T_{d,\ 5\%}$) higher than 230 °C.

Table 8.1 Thermal and mechanical properties of various poly(ester-*b*-carbonates)[a]

Entry	polymer	M_n (kDa) [b]	$Đ$ [b]	T_g / T_m (°C) [c]	E_y (MPa) [d]	σ (MPa) [d]	ε (%) [d]
1	poly(CHC)	42.9	1.06	115 / -	1007.9 ± 222.6	21.3 ± 1.4	4.0 ± 1.3
2	poly(VCHC)	105.8	1.01	113 / -	1489.9 ± 424.9	28.9 ± 2.1	3.1 ± 0.8
3	PLLA	247.7	1.04	- / 161	1303.1 ± 306.1	49.3 ± 3.3	11.5 ± 4.4
4	poly(**1**-*b*-CHC)	69.3	1.01	53 / -	725.6 ± 186.6	23.2 ± 1.5	15.6 ± 8.7
5	poly(**4**-*b*-CHC)	103.6	1.05	101 /166	2740.8 ± 617.9	32.5 ± 2.9	2.6 ± 1.1
6	poly(**1**-*b*-VCHC)	318.2	1.01	44, 96 / -	1516.5 ± 179.5	30.2 ± 3.9	14.8 ± 6.3
7	poly(**4**-*b*-VCHC)	404.2	1.03	102.5 / 167	1550.0 ± 408.0	44.8 ± 1.6	41.2 ± 17.3
8	poly(**4**-*b*-VCHC-*b*-**2**-*b*-CHC)	176.3	1.04	102 / 164	628.8 ± 19.6	33.0 ± 1.1	67.4 ± 8.6
9	PP [e]	/	/	/	1152.6 ± 262.7	32.4 ± 0.3	10.2 ± 1.9

[a] Abbreviations: M_n, number-average molecular weight; $Đ$, molecular weight distribution; T_g, glass transition temperature; T_m, melting temperature; E_y, Young's modulus; σ, fracture stress; ε, fracture strain; *b*, block. For all mechanical tests, n = 4-5, and data are presented as mean ± standard deviation.

[b] Determined by GPC.

[c] Determined by DSC. See Figure 8.3.

[d] Determined by stress-strain tests. See Figure 8.2.

[e] Commercially PP film from Braskem prepared by hot pressing. Our values are similar to other PP films reported in the literature.[9]

8.2.2 Mechanical properties of poly(L-2-*b*-carbonate) and poly(L-3-*b*-carbonate)

Next, we prepared toughened elastomers using our functionalized poly(ester-*b*-carbonates). Copolymers comprising elastic (soft) and glassy (hard) blocks usually exhibit characteristics of thermoplastic elastomers,[10] and this combination is the basis for the commercially successful non-degradable poly(styrene)–poly(diene) copolymers.[11] Because the brittleness of aliphatic polycarbonates such as poly(CHC) and poly(VCHC) has hampered their utility, we hypothesized that including ductile and soft blocks such as poly(L-**2**) (**Table 8.2**, entry 3) would afford a strong, ductile copolymer. Indeed, poly(L-**2**-*b*-CHC) (74.0 kDa) displayed a σ of 21.4 MPa and an ε of 376.7%, and poly(L-**2**-*b*-VCHC) (204.2 kDa) was even stronger and more ductile, with a σ of 25.0 MPa and an ε of 406.8% (**Figure 8.5**; entries 4 and 6). The addition of the soft poly(L-**3**) to poly(CHC) and poly(VCHC) also improved ductility, giving copolymers with ε values of 255.2% and 293.0%, respectively, and σ values of less than 20 MPa (entries 5 and 7). The modulus of toughness and ductility values of both poly(L-**2**-*b*-CHC) and poly(L-**2**-*b*-VCHC) were markedly better than those of LDPE (**Figure 8.5**; comparing entries 4 and 6 with entry 8 in Table 8.2) and our previously reported polyesters.[3] In addition, thermogravimetric analysis of poly(L-**2**-*b*-CHC) and poly(L-**2**-*b*-VCHC) showed that both copolymers had excellent thermal stabilities, with $T_{d,5\%}$ values of 263 and 288 °C, respectively (**Figure 8.4**). Notably, poly(L-**2**-*b*-CHC) showed a T_g of 29 °C with shape-memory recovery at room temperature (**Figures 8.3 and 8.6**; entry 3). In contrast, poly(L-**2**-*b*-VCHC), which had two T_g values (20 and 101 °C), underwent considerable strain hardening with visible white striations, resulting in unrecoverable plastic deformation (**Figure 8.6**; **Table 8.2**, entry 5).

Table 8.2 Thermal and mechanical properties of various poly(ester-*b*-carbonates)[a]

Entry	polymer	M_n (kDa) [b]	$Đ$ [b]	T_g / T_m (°C) [c]	E_y (MPa) [d]	σ (MPa) [d]	ε (%) [d]
1	poly(CHC)	42.9	1.06	115 / -	1007.9 ± 222.6	21.3 ± 1.4	4.0 ± 1.3
2	poly(VCHC)	105.8	1.01	113 / -	1489.9 ± 424.9	28.9 ± 2.1	3.1 ± 0.8
3	poly(**2**)	45.8	1.01	10 / -	2.1 ± 1.1	0.1 ± 0.04	1307.3 ± 7.9
4	poly(**2**-*b*-CHC)	74.0	1.01	29 / -	135.1 ± 38.1	21.4 ± 1.1	376.7 ± 75.3
5	poly(**3**-*b*-CHC)	81.5	1.01	37 / 193	76.1 ± 24.3	15.3 ± 1.9	255.2 ± 36.9
6	poly(**2**-*b*-VCHC)	204.2	1.01	20, 101/ -	369.8 ± 37.2	25.0 ± 2.2	406.8 ± 27.1
7	poly(**3**-*b*-VCHC)	64.8	1.01	12, 101 / -	116.9 ± 10.8	10.7 ± 1.2	293.0 ± 26.9
8	LDPE[e]	/	/	/	160.3 ± 55.1	10.0 ± 0.2	311.6 ± 10.9

[a] Abbreviations: M_n, number-average molecular weight; $Đ$, molecular weight distribution; T_g, glass transition temperature; T_m, melting temperature; E_y, Young's modulus; σ, fracture stress; ε, fracture strain; *b*, block; LDPE, low-density polypropylene. For all mechanical tests, n = 4 or 5, and data are presented as means ± standard deviations. [b] Determined by size-exclusion chromatography. [c] Determined by differential scanning calorimetry. See Figure 8.3. [d] Determined by stress–strain tests. See Figure 8.5. [e] Commercially available films from McMaster-Carr.

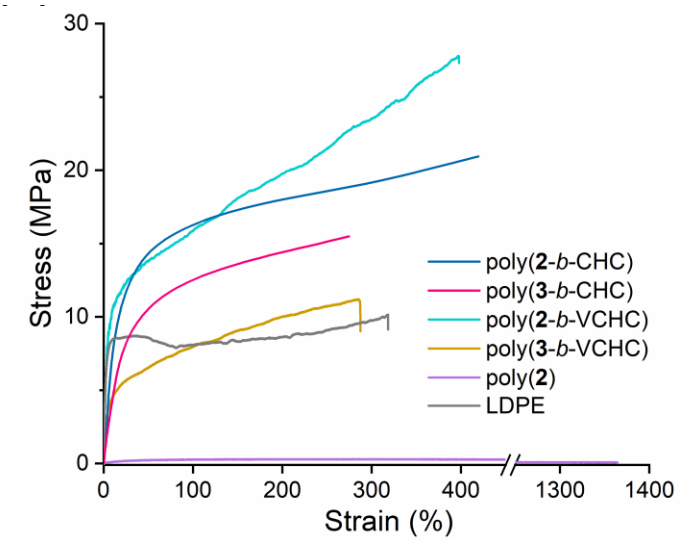

Figure 8.5 Various poly(ester-*b*-carbonates) compared with low-density polyethylene (LDPE) and poly(**2**) and poly(**3**), showing that poly(ester-*b*-carbonates) can be stronger and more ductile

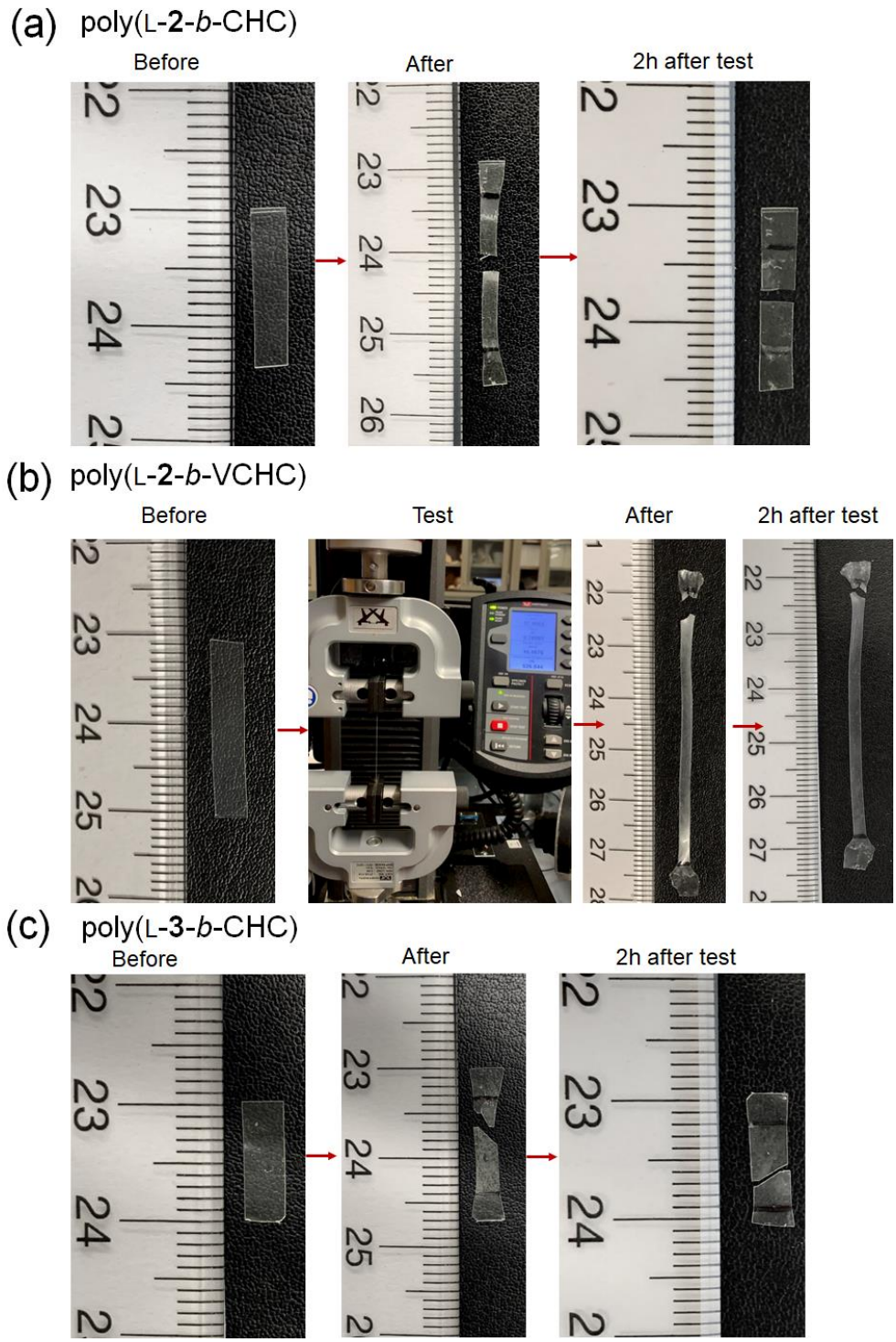

Figure 8.6 Shape recovery after the polymer fracture in stress-strain tests. Note that both poly(**2**-*b*-CHC) and poly(**3**-*b*-CHC) exhibited excellent shape recovery, while poly(**2**-*b*-VCHC) showed the strain-hardening effect during the stress-strain tensile test.

8.3 Materials and methods

8.3.1 Differential scanning calorimetry (DSC)

DSC measurements were performed on TA Instruments DSC Q2000 instrument equipped with photocalorimeter accessory and RCS90 cooling system. Polymer samples in crimped aluminum pans were analyzed under nitrogen at a heating rate of 10 °C/min from 0 to 200 °C. Glass transition temperature (T_g, defined as the inflection point based on ASTM method) and melting temperature (T_m, defined as the peak point) were obtained and reported from the second heating run.

8.3.2 Thermogravimetric analysis (TGA)

Polymer thermal degradation experiments were performed on TA Instrument Q50 thermogravimetric analyzer. Polymer samples were heated from 30 °C to 500 °C at 20 °C/min under nitrogen atmosphere.

8.3.3 Mechanical testing of polymers

Solvent-cast polyester sheets were prepared by pouring DCM solutions of the poly(ester-*co*-carbonates) (~200 mg/mL) into a polydimethylsiloxane mold. The solvent was slowly evaporated in the fume hood over 1-2 weeks, and DCM peak was no longer observed in ^{1}H NMR spectroscopy, confirming that the polyester sheets were sufficiently dry for mechanical tests. Tensile stress-strain testing was performed by an Instron 5966 universal testing system (10 kN load cell) or dynamic mechanical analyzer (DMA, Q800, TA instrument) on test specimens (10 mm × 4 mm × 0.2 mm, length × width × thickness) at 10 mm/min or 5 N/min extension rate, using the ASTM D882-18 standard, at ambient temperature (22 ^{o}C) and humidity (~ 16%). Modulus of toughness was calculated based on the integrated area under the tensile test curve. All values are reported as the average of three to five samples.

8.4 Conclusions

Our switchable/tandem copolymerization method provides access to new degradable polymers with a wide range of thermal and mechanical properties. The incorporation of the second block (polycarbonate) into the polyester block significantly tuned the mechanical and thermal properties of the resulting poly (ester-*b*-carbonate), compared with the materials properties of poly(α-hydroxy acids) reported in chapter 5. The obtained degradable poly(ester-*b*-carbonates) showed better toughness than their corresponding homopolymers and outperformed some commodity polyolefins, such as PP and LDPE.

References

1. Wang, X.; Tong, R., Facile Tandem Copolymerization of O-Carboxyanhydrides and Epoxides to Synthesize Functionalized Poly (ester-b-carbonates). *Journal of the American Chemical Society* **2022**.
2. Hu, C.; Pang, X.; Chen, X., Self-Switchable Polymerization: A Smart Approach to Sequence-Controlled Degradable Copolymers. *Macromolecules* **2022,** *55* (6), 1879-1893.
3. Wang, X.; Chin, A. L.; Zhou, J.; Wang, H.; Tong, R., Resilient Poly(α-hydroxy acids) with Improved Strength and Ductility via Scalable Stereosequence-Controlled Polymerization. *Journal of the American Chemical Society* **2021,** *143* (40), 16813-16823.
4. Raman, S. K.; Raja, R.; Arnold, P. L.; Davidson, M. G.; Williams, C. K., Waste not, want not: CO2 (re)cycling into block polymers. *Chemical Communications* **2019,** *55* (51), 7315-7318.
5. Tang, J.; Li, M.; Wang, X.; Tao, Y., Switchable Polymerization Organocatalysis: From Monomer Mixtures to Block Copolymers. *Angewandte Chemie International Edition* **2022,** *n/a* (n/a), e202115465.
6. Ovitt, T. M.; Coates, G. W., Stereochemistry of Lactide Polymerization with Chiral Catalysts: New Opportunities for Stereocontrol Using Polymer Exchange Mechanisms. *Journal of the American Chemical Society* **2002,** *124* (7), 1316-1326.
7. Paszkiewicz, S.; Szymczyk, A.; Pawlikowska, D.; Irska, I.; Taraghi, I.; Pilawka, R.; Gu, J.; Li, X.; Tu, Y.; Piesowicz, E., Synthesis and characterization of poly(ethylene terephthalate-co-1,4-cyclohexanedimethylene terephtlatate)-block-poly(tetramethylene oxide) copolymers. *RSC Advances* **2017,** *7* (66), 41745-41754.
8. Tang, X.; Westlie, A. H.; Watson, E. M.; Chen, E. Y.-X., Stereosequenced crystalline polyhydroxyalkanoates from diastereomeric monomer mixtures. *Science* **2019,** *366* (6466), 754-758.
9. Hasanpour, M.; Razavi Aghjeh, M. K.; mehrabi mazidi, M.; Afsari, B., Effect of morphology alteration on mechanical properties and fracture toughness of polypropylene/polyamide 6/ethylene polypropylene diene monomer graft maleic anhydride (PP/PA6/EPDM-g-MA) reactive ternary blends. *Polymer Bulletin* **2020,** *77*.
10. Bates, F. S.; Hillmyer, M. A.; Lodge, T. P.; Bates, C. M.; Delaney, K. T.; Fredrickson, G. H., Multiblock Polymers: Panacea or Pandora's Box? *Science* **2012,** *336* (6080), 434-440.
11. Handlin Jr., D. L.; Trenor, S.; Wright, K., Applications of Thermoplastic Elastomers Based on Styrenic Block Copolymers. In *Macromolecular Engineering*, 2007; pp 2001-2031.

CHAPTER 9

Summary and future work

9.1 Summary

The mainstream adoption of sustainable polyesters in plastics engineering has been stymied by a lack of general methods for preparing functionalized polyesters at scale and the consequent lack of information about their structure-property relationships, information that is necessary for the development of degradable alternatives to unsustainable polyolefins. Herein, one mechanism-inspired identification of a redox-active Mn complex that can be used for scalable synthesis of stereoregular polyesters with pendant functional groups by controlled ring-opening polymerization of *O*-carboxyanhydries (OCAs) and for elucidation of catalytic reaction pathways was described. This synthetic method is operationally simple and does not require external energy triggers compared to previously reported methods.[1-3] The method can be used to prepare homopolymers, block copolymers, stereoblock copolymers, and gradient copolymers; in particular, the gradient copolymer is tougher, more ductile, and more resilient than the corresponding block copolymers and homopolymers, and is comparable with some commodity polyolefins, such as low-density polyethylene (LDPE). The use of resulting degradable polyester elastomers for packaging, fiber, and biomedical applications can be foreseen.

Additionally, constructing sequence-controlled block copolymers from a mixture of co-monomers has been a long-standing challenge in polymer chemistry. The incorporation of functional-group-bearing OCAs into auto-switchable copolymerization reactions to synthesize poly(ester-*b*-carbonate) has been explored. However, these two

previously reported one-pot methods[4, 5] for switchable copolymerization gave polymers with low MWs (< 15 kDa) and broad MW distributions ($Đ$ ~ 1.2), and excess epoxide is required. A simple and high-performance Zn-mediated synthetic solution to this challenge has been presented herein with obvious advantages in terms of sustainability and ease of scale-up and with unique reaction kinetics that enables the perfectly clean switching of the polymerization mechanism during chain propagation. To our knowledge, the scalable synthesis of such high-MW functionalized poly(ester-*b*-carbonates) copolymers from equimolar mixtures of OCAs and epoxides using a single metal complex has never been achieved before. Notably, the mechanism in the first-stage polymerization, that is, ROP of OCA, likely proceeded via an activated-monomer pathway with zero-order reaction kinetics, as opposed to conventional metal-alkoxide-mediated chain propagation. The method described herein provides access to new degradable materials with a wide range of thermal and mechanical properties comparable to those of currently available non-degradable commodity polyolefins. Exploration of sequence-controlled copolymers by tandem/switchable copolymerization from mixed monomers would be one of the effective ways to develop new sustainable polymers with improved material properties in the future.[6]

9.2 Future work

9.2.1 Overview

Sequence-controlled polymerization is a powerful strategy that can produce copolymers with adjustable physicochemical properties and features by tuning the polymer's composition and sequence.[7] The copolymers could exhibit notable enhancements over pure homopolymers in terms of morphologies, and thermal and mechanical properties.[8] Recently, the emergence of auto-switchable / tandem copolymerization strategies in which a single catalyst is used to access and switch between catalytic cycles of ring-opening polymerization (ROP) and/or ring-opening copolymerization (ROCOP) has opened a realm of tandem catalysis processes for preparing sequence-controlled block copolymers from mixed comonomers.[9-14] In particular, the switchable / tandem copolymerization for the synthesis of poly(ester-*b*-carbonate) from mixed monomers has gained considerable interest due to the abundant variety of monomers and catalysts.[15]

9.2.2 The expansion of the monomer scope

Generally, switchable / tandem copolymerization requires different types of monomers to produce sequence-controlled block copolymers. So far, many pairs of monomers with switchable / tandem properties have been identified in the presence of appropriate catalysts (**Figure 9.1**). To prevent the formation of tapered microstructures during the switchable / tandem polymerization of mixed comonomers, the first monomer should be completely consumed before the second monomer initiates the reaction. Therefore, monomer pairs for switchable / tandem polymerization typically include a "strong" monomer and a "weak" monomer. As shown in **Figure 9.1b**, the possible

monomer reactivity followed the order: OCA > epoxides/cyclic anhydride > CO_2/epoxide > cyclic ester, which is extremely informative for the selection of possible monomer pairs. On the other hand, it's well known that distinct types of monomers would lead to dramatic changes in material properties. Therefore, expanding monomer types is intriguing and key to building diverse sequence-controlled block copolymers with unlimited functionality in the future. The representative monomer types are shown in **Figure 9.2**. Tandem / switchable copolymerization of mixed monomers is currently in its infancy. Both the expansion of monomer types and the search for new switch reactions will further enrich the variety of sustainable polymers and accelerate the development of tandem / switchable copolymerization. Moreover, the research path of selecting monomers with specific functional groups to synthesize polymers with corresponding materials properties is extremely promising.

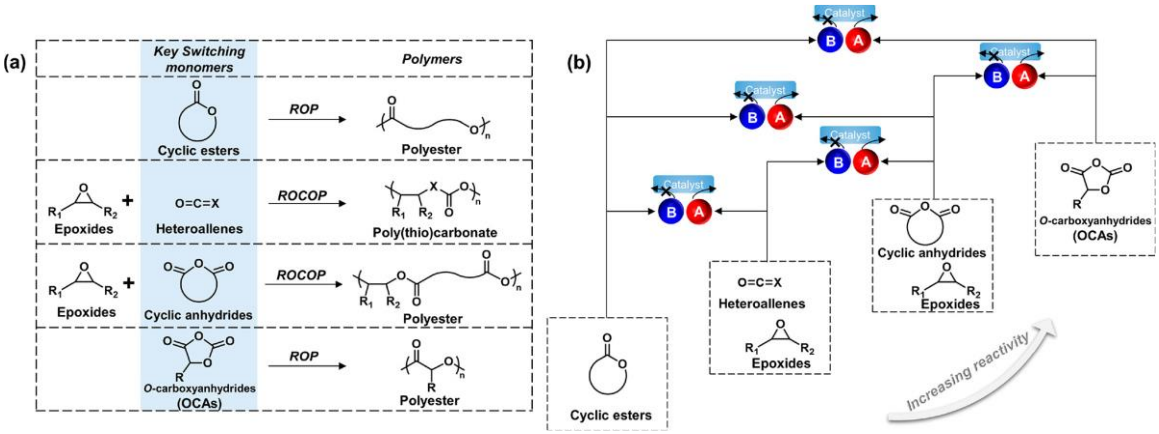

Figure 9.1 (a) Ring-opening (co)polymerizations and essential switching monomers. (b) Successful monomer pairs combined in self-switchable polymerization. (Reproduced from Macromolecules **2022**, *55* (6), 1879-1893.)

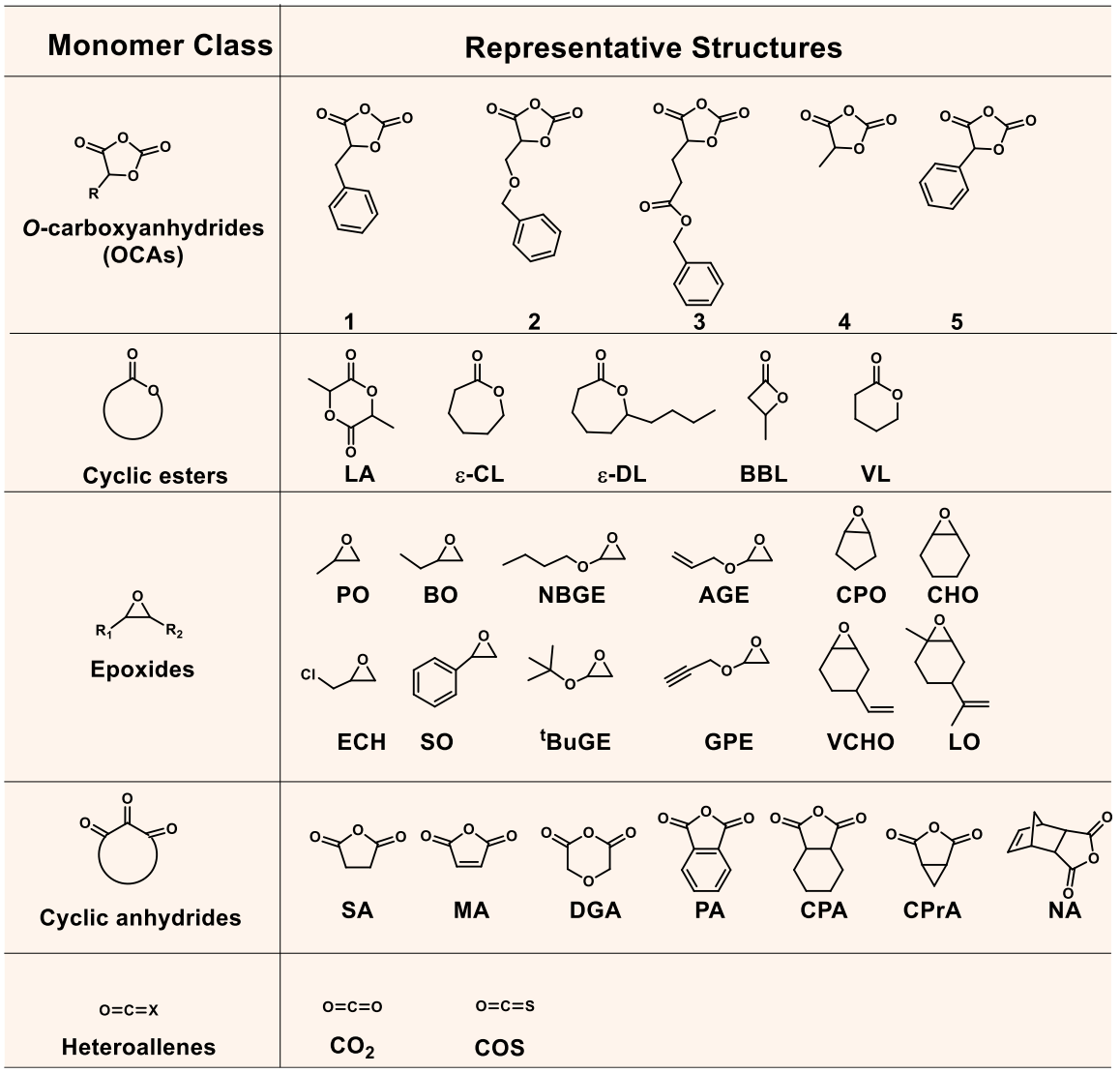

Figure 9.2 Representative monomers of different classes in self-switchable polymerization (LA, lactide; ε-CL, ε-caprolactone; ε-DL, ε-decalactone; BBL, β-butyrolactone; δ-VL, δ-valerolactone; PO, propylene oxide; BO, 1,2-butylene oxide; NBGE, n-butyl glycidyl ether; AGE, allyl glycidyl ether; ECH, epichlorohydrin; SO, styrene oxide; tBuGE, tert-butyl glycidyl ether; GPE, glycidyl propargyl ether; CPO, cyclopentene oxide; CHO, cyclohexene oxide; VCHO, vinyl cyclohexene oxide; LO, limonene oxide; SA, succinic anhydride; MA, maleic anhydride; DGA, diglycolide anhydride; PA, phthalic anhydride; CPA, cyclopentane-1,2-dicarboxylic acid anhydride; CPrA, cyclopropane-1,2-dicarboxylic acid anhydride; NA, norbornene anhydride).[16]

9.2.3 Developing new catalysts

To achieve sequence-controlled polymerization of mixed monomers, it is also essential to have a versatile catalyst that is active for distinct polymerization cycles. The currently representative catalytic systems are summarized in **Figure 9.3** for tandem / switchable copolymerization. It remains challenging to polymerize different types of monomers at sufficiently high rates throughout several cycles. Improving the performance of catalysts should concentrate on preserving their high tolerance and monomer scope while dramatically increasing rates and molar mass values and assuring operability at low catalyst loadings. In particular, efficient catalysts capable of producing high-molecular-weight sequence-controlled copolymers should be developed. It would allow us to examine the material properties of copolymers and further determine how material properties are dictated and controlled by parameters such as chain sequence order, length, and dispersity, which will empower future polymer design.

In addition, due to the complicated nature of many polymerization catalysts, the structure-activity relationships are often unpredictable. Therefore, the trial-and-error method that relies on a polymer chemist's experience, empirical data, and serendipity becomes the most common route to catalyst discovery, which can be both time and budget-consuming. Recently, a complementary approach has emerged in the chemistry community that applies data-driven methods, or so-called machine learning, to capture multi-dimensional structure-property relationships for catalysts.[17-23] Machine learning approaches can accept numerous reagent features and reaction conditions without recourse to a specific mechanistic hypothesis and evaluate functions with greater flexibility to match patterns in data.[24] In particular, the Bayesian optimization approach

uses parameter distributions reflecting the uncertainty of physical variables, which is opposed to conventional computationally-derived point values, and is thereby advantageous for uncertainty quantification in the exploration process.[25, 26] Such Bayesian optimization-based machine learning approach has been successfully applied in the enantioselective catalysts development and reaction yield prediction in organic chemistry.[24, 26-31] Thus, using machine learning to accelerate the discovery of catalysts for tandem/switchable polymerization can be foreseen.

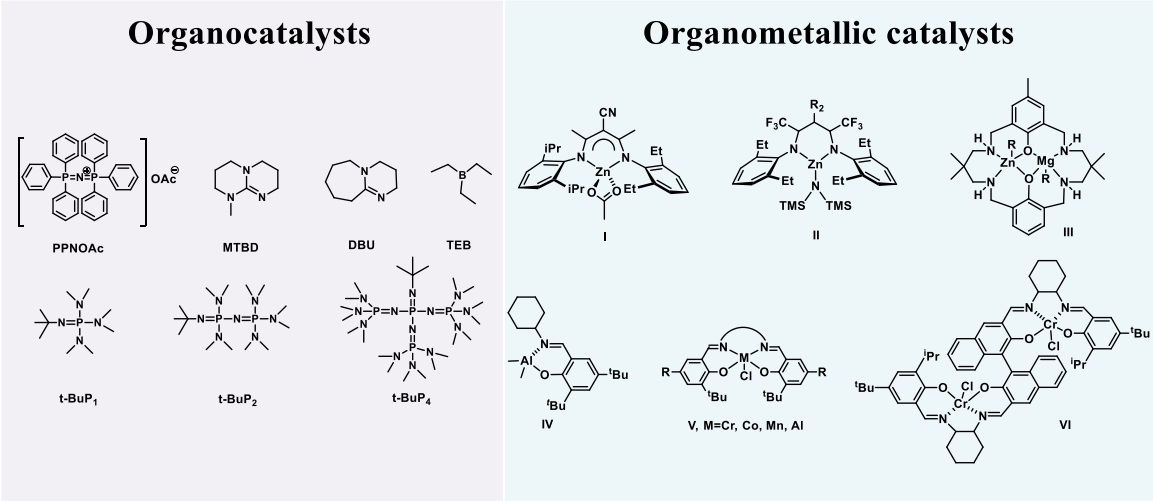

Figure 9.3 Representative catalysts for switchable/tandem copolymerization.

References

1. Zhong, Y.; Feng, Q.; Wang, X.; Chen, J.; Cai, W.; Tong, R., Functionalized Polyesters via Stereoselective Electrochemical Ring-Opening Polymerization of O-Carboxyanhydrides. *ACS Macro Letters* **2020,** *9* (8), 1114-1118.
2. Feng, Q.; Tong, R., Controlled photoredox ring-opening polymerization of O-carboxyanhydrides. *Journal of the American Chemical Society* **2017,** *139* (17), 6177-6182.
3. Zhong, Y.; Feng, Q.; Wang, X.; Yang, L.; Korovich, A. G.; Madsen, L. A.; Tong, R., Photocatalyst-independent photoredox ring-opening polymerization of O-carboxyanhydrides: stereocontrol and mechanism. *Chemical science* **2021,** *12* (10), 3702-3712.
4. Tang, J.; Li, M.; Wang, X.; Tao, Y., Switchable Polymerization Organocatalysis: From Monomer Mixtures to Block Copolymers. *Angewandte Chemie International Edition* **2022,** *61* (15), e202115465.
5. Raman, S. K.; Raja, R.; Arnold, P. L.; Davidson, M. G.; Williams, C. K., Waste not, want not: CO 2 (re) cycling into block polymers. *Chemical communications* **2019,** *55* (51), 7315-7318.
6. Tang, X.; Westlie, A. H.; Watson, E. M.; Chen, E. Y.-X., Stereosequenced crystalline polyhydroxyalkanoates from diastereomeric monomer mixtures. *Science* **2019,** *366* (6466), 754-758.
7. Pfeifer, S.; Lutz, J.-F., A facile procedure for controlling monomer sequence distribution in radical chain polymerizations. *Journal of the American Chemical Society* **2007,** *129* (31), 9542-9543.
8. Lutz, J.-F.; Ouchi, M.; Liu, D. R.; Sawamoto, M., Sequence-controlled polymers. *Science* **2013,** *341* (6146), 1238149.
9. Jeske, R. C.; Rowley, J. M.; Coates, G. W., Pre-Rate-Determining Selectivity in the Terpolymerization of Epoxides, Cyclic Anhydrides, and CO2: A One-Step Route to Diblock Copolymers. *Angew. Chem. Int. Ed.* **2008,** *47* (32), 6041-6044.
10. Romain, C.; Williams, C. K., Chemoselective Polymerization Control: From Mixed-Monomer Feedstock to Copolymers. *Angew. Chem. Int. Ed.* **2014,** *53* (6), 1607-1610.
11. Romain, C.; Zhu, Y.; Dingwall, P.; Paul, S.; Rzepa, H. S.; Buchard, A.; Williams, C. K., Chemoselective Polymerizations from Mixtures of Epoxide, Lactone, Anhydride, and Carbon Dioxide. *J. Am. Chem. Soc.* **2016,** *138* (12), 4120-4131.
12. Ji, H.-Y.; Wang, B.; Pan, L.; Li, Y.-S., One-Step Access to Sequence-Controlled Block Copolymers by Self-Switchable Organocatalytic Multicomponent Polymerization. *Angew. Chem. Int. Ed.* **2018,** *57* (51), 16888-16892.
13. Xu, J.; Wang, X.; Hadjichristidis, N., Diblock dialternating terpolymers by one-step/one-pot highly selective organocatalytic multimonomer polymerization. *Nat. Commun.* **2021,** *12* (1), 7124.
14. Zhang, Z.; Zeng, T.-Y.; Xia, L.; Hong, C.-Y.; Wu, D.-C.; You, Y.-Z., Synthesis of polymers with on-demand sequence structures via dually switchable and interconvertible polymerizations. *Nat. Commun.* **2018,** *9* (1), 2577.

15. Deacy, A. C.; Gregory, G. L.; Sulley, G. S.; Chen, T. T.; Williams, C. K., Sequence control from mixtures: switchable polymerization catalysis and future materials applications. *Journal of the American Chemical Society* **2021,** *143* (27), 10021-10040.
16. Hu, C.; Pang, X.; Chen, X., Self-Switchable Polymerization: A Smart Approach to Sequence-Controlled Degradable Copolymers. *Macromolecules* **2022,** *55* (6), 1879-1893.
17. Häse, F.; Roch, L. M.; Kreisbeck, C.; Aspuru-Guzik, A., Phoenics: A Bayesian Optimizer for Chemistry. *ACS Central Science* **2018,** *4* (9), 1134-1145.
18. Li, Z.; Wang, S.; Xin, H., Toward artificial intelligence in catalysis. *Nature Catalysis* **2018,** *1* (9), 641-642.
19. Tran, K.; Ulissi, Z. W., Active learning across intermetallics to guide discovery of electrocatalysts for CO2 reduction and H2 evolution. *Nature Catalysis* **2018,** *1* (9), 696-703.
20. Coley, C. W.; Eyke, N. S.; Jensen, K. F., Autonomous Discovery in the Chemical Sciences Part I: Progress. *Angewandte Chemie International Edition* **2020,** *59* (51), 22858-22893.
21. Chanussot, L.; Das, A.; Goyal, S.; Lavril, T.; Shuaibi, M.; Riviere, M.; Tran, K.; Heras-Domingo, J.; Ho, C.; Hu, W.; Palizhati, A.; Sriram, A.; Wood, B.; Yoon, J.; Parikh, D.; Zitnick, C. L.; Ulissi, Z., Open Catalyst 2020 (OC20) Dataset and Community Challenges. *ACS Catalysis* **2021,** *11* (10), 6059-6072.
22. Williams, W. L.; Zeng, L.; Gensch, T.; Sigman, M. S.; Doyle, A. G.; Anslyn, E. V., The Evolution of Data-Driven Modeling in Organic Chemistry. *ACS Central Science* **2021,** *7* (10), 1622-1637.
23. Kolluru, A.; Shuaibi, M.; Palizhati, A.; Shoghi, N.; Das, A.; Wood, B.; Zitnick, C. L.; Kitchin, J. R.; Ulissi, Z. W., Open Challenges in Developing Generalizable Large-Scale Machine-Learning Models for Catalyst Discovery. *ACS Catalysis* **2022,** *12* (14), 8572-8581.
24. Ahneman, D. T.; Estrada, J. G.; Lin, S.; Dreher, S. D.; Doyle, A. G., Predicting reaction performance in C–N cross-coupling using machine learning. *Science* **2018,** *360* (6385), 186-190.
25. Strieth-Kalthoff, F.; Sandfort, F.; Segler, M. H. S.; Glorius, F., Machine learning the ropes: principles, applications and directions in synthetic chemistry. *Chemical Society Reviews* **2020,** *49* (17), 6154-6168.
26. Shields, B. J.; Stevens, J.; Li, J.; Parasram, M.; Damani, F.; Alvarado, J. I. M.; Janey, J. M.; Adams, R. P.; Doyle, A. G., Bayesian reaction optimization as a tool for chemical synthesis. *Nature* **2021,** *590* (7844), 89-96.
27. Reker, D.; Hoyt, E. A.; Bernardes, G. J. L.; Rodrigues, T., Adaptive Optimization of Chemical Reactions with Minimal Experimental Information. *Cell Reports Physical Science* **2020,** *1* (11), 100247.
28. Żurański, A. M.; Martinez Alvarado, J. I.; Shields, B. J.; Doyle, A. G., Predicting Reaction Yields via Supervised Learning. *Accounts of Chemical Research* **2021,** *54* (8), 1856-1865.
29. Zahrt, A. F.; Henle, J. J.; Rose, B. T.; Wang, Y.; Darrow, W. T.; Denmark, S. E., Prediction of higher-selectivity catalysts by computer-driven workflow and machine learning. *Science* **2019,** *363* (6424), eaau5631.

30. Reid, J. P.; Sigman, M. S., Holistic prediction of enantioselectivity in asymmetric catalysis. *Nature* **2019,** *571* (7765), 343-348.
31. Hueffel, J. A.; Sperger, T.; Funes-Ardoiz, I.; Ward, J. S.; Rissanen, K.; Schoenebeck, F., Accelerated dinuclear palladium catalyst identification through unsupervised machine learning. *Science* **2021,** *374* (6571), 1134-1140